University of Zagreb

Faculty of Geodesy

Anja Batina

GEOSPATIAL MULTI-SENSOR APPROACH FOR LAKE WATER QUALITY MONITORING AND ASSESSMENT

DOCTORAL THESIS

Zagreb, 2026

University of Zagreb

Faculty of Geodesy

Anja Batina

GEOSPATIAL MULTI-SENSOR APPROACH FOR LAKE WATER QUALITY MONITORING AND ASSESSMENT

DOCTORAL THESIS

Mentors:
Assoc. Prof. Andrija Krtalić, PhD
Assoc. Prof. Ante Šiljeg, PhD

Zagreb, 2026

Sveučilište u Zagrebu

Geodetski fakultet

Anja Batina

GEOPROSTORNI VIŠESENZORSKI PRISTUP ZA PRAĆENJE I PROCJENU KAKVOĆE JEZERSKE VODE

DOKTORSKI RAD

Mentori:
izv. prof. dr. sc. Andrija Krtalić
izv. prof. dr. sc. Ante Šiljeg

Zagreb, 2026.

Declaration of Originality

UNIVERSITY OF ZAGREB
FACULTY OF GEODESY

Pursuant to Article 19 of the **Code of Ethics of the University of Zagreb** and Decision No. **1_349_11** of the Faculty Council of the Faculty of Geodesy, University of Zagreb, dated 26 October 2017 (Class: 643-03/16-07/03), the obligation to submit a **Declaration of Originality** for theses evaluated within the graduate study programme of Geodesy and Geoinformatics has been established, for the purpose of confirming that the thesis represents the original work of the student and that it does not contain sources other than those cited therein.

DECLARATION

I, **Anja Batina**, hereby declare that my thesis is the original result of my own work and that, in its preparation, I have not used any sources other than those cited in the thesis.

In Zagreb, on xxx	
	Signature of the student

Thesis Information

I. Author	
Name and surname:	Anja Batina
Date and place of birth:	August 23, 1991, Split, Croatia
Current employment:	Research assistant at the Center for Geospatial Technologies at the University of Zadar
II. Doctoral Dissertation	
Title:	Geospatial Multi-Sensor Approach for Lake Water Quality Monitoring and Assessment
Number of pages:	204
Number of figures:	34
Number of tables:	31
Number of bibliographic references:	352
Institution and place where the dissertation was prepared:	Faculty of Geodesy, University of Zagreb, Zagreb
Scientific area:	Technical Sciences
Scientific field:	Geodesy
Scientific branch:	Photogrammetry and Remote Sensing
Mentors:	Assoc. Prof. Andrija Krtalić, PhD Prof. Ante Šiljeg, PhD
Designation and serial number of the dissertation:	xxx
III. Evaluation and Defence	
Date of topic approval:	May 23, 2024
Date of the Faculty Council session at which the dissertation was approved:	June 27, 2024
Composition of the evaluation committee:	Assoc. Prof. Vesna Poslončec Petrić, PhD Assoc. Prof. Ivka Kljajić, PhD Assist. Prof. Ana Kuveždić Divjak, PhD Assoc. Prof. Monika Zovko, PhD Assoc. Prof. Ljiljana Šerić, PhD
Date of dissertation defence:	xxx, 2026
Composition of the defence committee:	xxx

Acknowledgements

Posveta

Abstract

Lake water quality monitoring in shallow and optically complex lake systems remains challenging due to strong spatial and temporal variability that cannot be adequately captured by conventional point-based *in situ* measurements. These challenges are further intensified by pressures related to climate change, eutrophication, land use dynamics, and hydromorphological variability, emphasising the need for integrated, spatially explicit, and scalable monitoring approaches. This doctoral dissertation addresses these challenges through the development and evaluation of an integrated geospatial framework that combines *in situ* measurements, Geographic Information Systems (GIS), satellite remote sensing, and machine learning (ML) to enable comprehensive lake water quality assessment. The research is structured as a cumulative thesis, with the results presented in four thematically and methodologically interconnected peer-reviewed scientific papers. Vrana Lake in Dalmatia, Croatia, the largest natural lake in the country, was selected as the study area because its shallow morphology, proximity to the sea, and pronounced anthropogenic pressures make it a representative example of a coastal shallow lake. The dissertation progresses from a comprehensive synthesis of contemporary remote sensing approaches for lake water quality monitoring, with particular emphasis on optically active parameters, methodological limitations, and the need for integration with *in situ* data and spatial modelling (Paper I). This theoretical and methodological foundation is followed by an empirical analysis of the spatial and seasonal variability of key water quality parameters, based on systematic *in situ* monitoring conducted over a 12-month period at a network of 20 sampling stations (Paper II). The analysis is further supported by long-term meteorological data, enabling the identification of dominant water quality parameters and key meteorological drivers influencing lake dynamics. GIS-based spatial interpolation transformed point-based observations into continuous water quality representations, which served as the empirical basis for subsequent spatial modelling. Building on these datasets, a GIS-based multicriteria decision analysis (GIS-MCDA) combined with the Fuzzy Analytic Hierarchy Process (F-AHP) was applied to assess eutrophication susceptibility and optimise the monitoring network (Paper III), resulting in spatially explicit water quality and eutrophication susceptibility maps, as well as a proposed optimised monitoring network. Based on the results of the GIS-MCDA, an integrated analytical workflow was developed to evaluate the suitability of Sentinel-2, Landsat 8-9, and PlanetScope satellite imagery for lake water quality monitoring (Paper IV). ML models were trained using both individual physicochemical parameters and a composite water quality index (WQI) derived from *in situ*, meteorological, and environmental data. Comparative analysis demonstrated that WQI-based ML models provide more stable, more accurate, and spatially more transferable results than models trained on individual parameters alone. The results confirm that integrating *in situ* observations, GIS-MCDA, satellite remote sensing, and ML significantly improves the accuracy, interpretability, and operational relevance of lake water quality assessment. The proposed framework is adaptable and transferable to other coastal shallow lakes, providing a robust methodological foundation for future scientific research and practical lake management under increasing environmental pressures.

Keywords: coastal shallow lakes; water quality index; GIS-based multicriteria decision analysis (GIS-MCDA); machine learning; satellite sensor; spatial interpolation; eutrophication susceptibility; environmental monitoring; Vrana Lake

Abstract in Croatian Language

Praćenje kakvoće vode u plitkim i optički složenim jezerskim sustavima predstavlja značajan znanstveni i operativni izazov, ponajprije zbog izražene prostorne i vremenske varijabilnosti koju konvencionalna točkasta *in situ* mjerenja ne mogu u potpunosti obuhvatiti. Ovi su izazovi dodatno naglašeni pritiscima uzrokovanima klimatskim promjenama, eutrofikacijom, promjenama u načinu korištenja zemljišta te hidromorfološkim varijacijama, što upućuje na potrebu za integriranim, prostorno eksplicitnim i skalabilnim pristupima praćenju kakvoće vode. U ovoj doktorskoj disertaciji navedeni se izazovi razmatraju kroz razvoj i evaluaciju integriranog geoprostornog okvira koji objedinjuje *in situ* mjerenja, geografske informacijske sustave (GIS), satelitska daljinska istraživanja i metode strojnog učenja u svrhu procjene kakvoće jezerske vode. Istraživanje je provedeno u okviru kumulativne disertacije, pri čemu su rezultati istraživanja predstavljeni u četiri tematski i metodološki povezana recenzirana znanstvena rada. Vransko jezero u Dalmaciji, najveće prirodno jezero u Republici Hrvatskoj, odabrano je kao područje istraživanja budući da zbog plitke morfologije, blizine mora i izraženih antropogenih utjecaja predstavlja reprezentativan primjer obalnog plitkog jezera. Disertacija započinje sveobuhvatnom sintezom suvremenih pristupa daljinskog istraživanja u praćenju kakvoće jezerskih voda, s posebnim naglaskom na optički aktivne parametre, ograničenja postojećih metoda te potrebu za njihovom integracijom s *in situ* podacima i prostornim modeliranjem (Rad I). Na toj se teorijskoj i metodološkoj osnovi nadovezuje empirijska analiza prostorne i sezonske varijabilnosti ključnih parametara kakvoće vode, temeljena na sustavnom *in situ* monitoringu provedenom tijekom dvanaest mjeseci na mreži od 20 mjernih postaja (Rad II). Analiza je dodatno pokrijepljena dugoročnim meteorološkim podacima, čime su identificirani dominantni parametri kakvoće vode i ključni meteorološki čimbenici koji utječu na dinamiku promatranog jezerskog sustava. Primjenom GIS-a provedena je prostorna interpolacija točkastih mjerenja, čime su dobiveni kontinuirani prikazi kakvoće vode koji predstavljaju empirijsku osnovu za daljnje prostorno modeliranje. Na temelju tih podloga provedena je višekriterijska GIS analiza u kombinaciji s Fuzzy analitičkim hijerarhijskim procesom, korištena za procjenu podložnosti eutrofikaciji i optimizaciju mreže monitoringa (Rad III). Rezultat su prostorno eksplicitne karte kakvoće vode i podložnosti eutrofikaciji, kao i prijedlog optimizirane mreže mjernih postaja. Na temelju rezultata višekriterijske GIS analize razvijen je integrirani analitički postupak za evaluaciju prikladnosti satelitskih snimaka Sentinel-2, Landsat 8-9 i PlanetScope za praćenje kakvoće jezerske vode (Rad IV). Modeli strojnog učenja trenirani su koristeći pojedinačne fizikalno-kemijske parametre te složeni indeks kakvoće vode izveden iz *in situ*, meteoroloških i okolišnih podataka. Usporedna analiza pokazala je da modeli temeljeni na indeksu kakvoće vode postižu stabilnije, točnije i prostorno primjenjivije rezultate u odnosu na modele trenirane isključivo na pojedinačnim parametrima. Rezultati disertacije potvrđuju da integracija *in situ* mjerenja, višekriterijske GIS analize, satelitskih daljinskih istraživanja i metoda strojnog učenja značajno unapređuje točnost, jasnoću interpretacije i operativnu primjenjivost procjene kakvoće jezerske vode. Predloženi okvir je prilagodljiv i prenosiv na druga obalna plitka jezera te predstavlja čvrstu metodološku osnovu za buduća znanstvena istraživanja i praktično upravljanje jezerima u uvjetima rastućih okolišnih pritisaka.

Ključne riječi: obalna plitka jezera; indeks kakvoće vode; višekriterijska GIS analiza; strojno učenje; satelitski senzori; prostorna interpolacija; podložnost eutrofikaciji; praćenje okoliša; Vransko jezero

Table of Contents

Declaration of Originality I

Thesis Information II

Acknowledgements III

Abstract I

Abstract in Croatian Language II

Table of Contents III

1. Introduction 1

1.1. Background and Problem Definition 1

1.2. Thesis Objectives and Hypotheses 3

1.3. Expected Scientific Contributions 5

1.4. Overview of the Included Scientific Papers 5

1.5. Chapter Summary 8

2. Integrating Remote Sensing Methods for Monitoring Lake Water Quality: A Comprehensive Review 9

2.1. Introduction 11

2.2. Bibliometric Analysis 12

2.3. Materials and Methods 15

2.3.1. Analytical Methods 15

2.3.2. Semi-Analytical Methods 16

2.3.3. Empirical Methods 16

2.3.4. Semi-Empirical Methods 17

2.3.5. Machine Learning (ML) Methods 17

2.4. Optically Active Water Quality Parameters 18

2.4.1. Chlorophyll-a (Chl-a) 19

2.4.2. Turbidity 22

2.4.3. Transparency (Secchi Disk Depth (SDD)) 24
2.4.4. Water Temperature (WT) 26
2.4.5. Salinity 27
2.4.6. Electrical Conductivity (EC) 28
2.5. Sensors for Assessing Water Quality Parameters 29
2.6. Discussion and Recommendations 32
2.7. Conclusion 38
3. Spatiotemporal Water Quality Analysis of Vrana Lake, Croatia 40
3.1. Introduction 42
3.2. Methods 43
3.2.1. Study Area and Monitoring 43
3.2.2. Data Collection 46
3.2.3. Data Analysis 49
3.3. Results 51
3.3.1. Temporal Trends of Meteorological Factors 51
3.3.2. Assessing Vertical and Temporal Variability in Water Column Data 52
3.3.3. Seasonal and Spatial Variations in Water Quality Parameters and Their Correlation With Meteorological Data 53
3.4. Discussion 58
3.4.1. Impact of Climate Change on Vrana Lake 58
3.4.2. Vertical Stratification and Water Quality Dynamics 58
3.4.3. Seasonal and Spatial Variations in Water Quality and Meteorological Influences 59
3.5. Conclusion 60
4. Enhancing Water Quality Monitoring in a Coastal Shallow Lake Using GIS and Multi-Criteria Decision Analysis 62
4.1. Introduction 64
4.2. Materials and Methods 66

4.2.1. Study Area 66
4.2.2. GIS Multi-Criteria Decision Analysis 67
4.2.3. Optimizing Monitoring Stations 77
4.3. Results and Discussion 78
4.3.1. Results for Selected Criteria According to Standardized Values 78
4.3.2. Results for Determined Criteria Weights 80
4.3.3. Results for Aggregated Criteria 82
4.3.4. Model Validation 83
4.3.5. Optimizing Monitoring Stations 85
4.3.6. Comparison With Similar Studies 87
4.4. Conclusions 88
5. SIGMaL: An Integrated Framework for Water Quality Monitoring in a Coastal Shallow Lake90
5.1. Introduction 92
5.2. Materials and Methods 94
5.2.1. Study Area 94
5.2.2. Data Collection 95
5.2.3. Satellite Data Acquisition and Preprocessing 97
5.2.4. Dataset Development 101
5.2.5. ML Framework 102
5.2.6. Workflow Overview 106
5.3. Results 107
5.3.1. Regression of In Situ Parameters 107
5.3.2. WQI CNN models 111
5.3.3. CNN-based Predictions of WQI 118
5.4. Discussion 120
5.4.1. Cross-Sensor Comparison 120

5.4.2. WQI Outperforms Modelling Individual Parameters 121
5.4.3. Spatial Predictions of WQI 122
5.4.4. Methodological Limitations and Future Work 123
5.5. Conclusions 124
6. Joint Discussion 125
7. Conclusion 129
Bibliography 133
Appendices 168
Appendix 1 168
Appendix 2 183
Appendix 3 195
List of Figures 197
List of Tables 200
CV 203
List of Papers Published in Scientific Journals 203
List of Papers Published in Scientific Conference Proceedings 203

1. Introduction

1.1. Background and Problem Definition

Lakes represent complex and highly dynamic aquatic ecosystems that provide essential ecological, economic, and social services, including freshwater supply, biodiversity conservation, fisheries, and recreation [1,2]. However, lake water quality is increasingly threatened by climate change, land cover-land use (LCLU) change, eutrophication, and hydrological alterations [3–5]. These pressures are particularly pronounced in shallow and coastal lakes, where limited depth, frequent water-column mixing, and hydrological connectivity with marine systems amplify the effects of meteorological forcing, nutrient loading, and salinity intrusion [6,7].

Conventional lake water quality monitoring relies primarily on *in situ* measurements and laboratory analyses [8]. Although such methods provide accurate point-based observations, they are constrained by high operational costs, limited spatial representativeness, and insufficient temporal resolution to capture rapid or heterogeneous changes across entire lake surfaces [9,10]. As a result, traditional monitoring approaches often fail to adequately describe spatial patterns, seasonal dynamics, and ecosystem-wide processes, especially in large or hydrologically complex lakes [7,9,11].

In response to these limitations, remote sensing has emerged as a powerful complementary tool for lake water quality monitoring [12,13]. Satellite and airborne sensors enable repeated, synoptic observations of inland waters, offering spatially continuous information over large areas and extended time periods [14–16]. Remote sensing techniques are particularly effective for monitoring optically active water quality parameters, such as chlorophyll-a (chl-a), turbidity, water temperature (WT), and electrical conductivity (EC) [13,17,18], while non-optical parameters, such as dissolved oxygen (DO), are commonly inferred indirectly through statistical and machine learning (ML)-based relationships [19,20]. When supported by *in situ* calibration and validation, remotely sensed data can significantly enhance the understanding of spatiotemporal water quality variability and support timely environmental decision-making [21,22]. The increasing availability of multi-sensor satellite data, including medium-resolution missions such as Landsat and Sentinel-2 and high-resolution commercial platforms, such as PlanetScope, further strengthens the potential for integrated lake monitoring. Comparative evaluation of different sensors is essential to identify their relative strengths and limitations for

specific water quality applications, particularly in shallow and optically complex lakes (with highly heterogeneous optical properties).

Despite substantial progress over recent decades, remote sensing of inland and coastal lake water quality remains challenging [23]. The optical complexity of inland waters, sensor-specific limitations, atmospheric effects, and strong seasonal variability often lead to site-specific models with limited transferability [16]. Moreover, many studies focus on single parameters or short time frames, which restricts their applicability for integrated ecosystem assessment and long-term monitoring [16,24]. These challenges highlight the need for comprehensive, integrative frameworks that combine remote sensing with robust *in situ* observations, spatial modelling, and advanced analytical methods.

Geographic Information Systems (GIS) provide an essential link between point-based measurements and spatially continuous representations of water quality [25]. Through spatial interpolation, multi-criteria decision analysis (MCDA), and raster-based modelling, GIS enables the integration of physicochemical parameters with hydrological, meteorological, and anthropogenic factors [24,26]. GIS-based approaches are particularly valuable in shallow lakes, where spatial gradients are often driven by wind exposure, inflows, land-based nutrient sources, and human activities. In particular, GIS multicriteria analysis enables the systematic evaluation of complex environmental interactions by combining primary water quality parameters with secondary variables such as meteorological conditions, hydrology, and LCLU characteristics [24,26]. By incorporating expert knowledge, environmental thresholds, and uncertainty analysis, GIS-MCDA provides transparent and interpretable decision-support tools for identifying vulnerable zones, supporting monitoring network design, facilitating targeted monitoring, and informing lake management strategies [22,27].

In parallel, ML techniques have opened new possibilities for joint analysis and integration of *in situ* observations, GIS-derived products, and satellite remote sensing data [28–30]. ML algorithms are capable of capturing complex, nonlinear relationships between spectral reflectance and water quality parameters that are difficult to model using traditional statistical approaches. ML algorithms can integrate spectral, spatial, and temporal information derived from satellite imagery with *in situ* observations to improve the estimation and prediction of water quality parameters [31]. Compared to analytical, semi-analytical, and empirical approaches, ML-based models have demonstrated superior performance in complex and heterogeneous aquatic environments [9]. Nevertheless, their successful application depends on the availability of high-quality training data, appropriate model selection, and robust validation procedures [13,32].

However, the effectiveness of ML approaches depends strongly on the quality, representativeness, and spatial density of training data [33]. In many lake systems, sparse monitoring networks limit model robustness and generalizability. Integrating GIS-based spatial modelling with ML offers a solution to this challenge by densifying training datasets and providing spatially continuous reference layers that better represent ecosystem variability.

This doctoral research addresses the need for an integrated, scalable, and transferable framework for lake water quality monitoring that systematically combines *in situ* measurements, remote sensing, GIS-based analysis, and ML within a single methodological approach. The research focuses on Vrana Lake in Dalmatia, the largest natural lake in Croatia, which is characterised by high ecological value, biodiversity, and increasing environmental pressures. Due to its shallow morphology and hydrological complexity, Vrana Lake represents an ideal case study for investigating spatiotemporal water quality dynamics and testing integrated monitoring approaches.

1.2. Thesis Objectives and Hypotheses

The primary objective of this doctoral dissertation is to develop and validate a novel integrated geospatial multi-sensor framework for lake water quality monitoring and assessment. This framework systematically combines *in situ* measurements, GIS-MCDA, satellite remote sensing, and ML to enable spatially continuous, robust, and operationally applicable water quality assessment in shallow and optically complex lake environments.

To achieve this primary objective, the dissertation addresses the following specific objectives:

1. To develop a novel methodological framework that integrates four approaches: *in situ* measurements, GIS-MCDA, satellite imagery, and ML to facilitate efficient lake water quality monitoring.
2. To assess the suitability of Sentinel-2/Landsat 8-9/PlanetScope satellite imagery for determining spatiotemporal water quality patterns, using Vrana Lake in Dalmatia as a case study.
3. To perform eutrophication susceptibility assessment using GIS multicriteria analysis by comparing primary (water quality parameters) and secondary parameters (meteorological, hydrological, and LCLU data).

Based on the defined objectives, the following hypotheses are formulated and tested in this dissertation:

H1: The accuracy of a model for lake water quality monitoring and assessment, derived based on integration of *in situ* measurements, GIS-MCDA, satellite imagery, and ML, will have AUC values above 0.8.

H2: PlanetScope satellite imagery will be the most suitable for monitoring water quality in Vrana Lake in Dalmatia compared to Sentinel-2 and Landsat 8-9 satellite imagery.

H3: The northeastern part of the lake will have the highest eutrophication susceptibility based on analysed primary (water quality parameters) and secondary parameters (meteorological, hydrological, and LCLU data) and GIS-MCDA.

The research hypotheses formulated are addressed through the following peer-reviewed scientific papers:

- Paper I – *Integrating Remote Sensing Methods for Monitoring Lake Water Quality: A Comprehensive Review*.
- Paper II – *Spatiotemporal Water Quality Analysis of Vrana Lake, Croatia*.
- Paper III – *Enhancing Water Quality Monitoring in a Coastal Shallow Lake Using GIS and Multi-Criteria Decision Analysis*.
- Paper IV – *SIGMaL: An Integrated Framework for Water Quality Monitoring in a Coastal Shallow Lake*.

The first research hypothesis (H1) is addressed primarily in Paper IV, which proposes and validates an integrated geospatial multi-sensor framework combining *in situ* measurements, GIS-MCDA, satellite imagery, and ML.

The second research hypothesis (H2) is addressed in Paper IV, which evaluates and compares the suitability of Sentinel-2, Landsat 8-9, and PlanetScope satellite imagery for monitoring spatiotemporal water quality patterns in Vrana Lake.

The third research hypothesis (H3) is addressed in Paper III, which develops a GIS-MCDA framework to assess spatial patterns of eutrophication susceptibility based on water quality, meteorological, hydrological, and LCLU parameters.

In addition, Paper II provides the empirical foundation for hypotheses testing by analysing the spatial and seasonal variability of *in situ* water quality parameters and their relationship with hydrological and meteorological drivers, while Paper I establishes the theoretical and methodological context by synthesising recent advances in remote sensing-based lake water quality monitoring.

1.3. Expected Scientific Contributions

This dissertation is expected to contribute to the scientific fields of geodesy and remote sensing, as well as to environmental sciences, hydrology, limnology, and geospatial data science, through the development of an integrated geospatial framework for lake water quality monitoring. The primary scientific contribution lies in the formulation of a novel methodological framework that systematically combines *in situ* measurements, GIS-MCDA, satellite imagery, and ML into a unified and efficient monitoring strategy. The dissertation further contributes methodologically by demonstrating how GIS-based raster densification can effectively bridge sparse *in situ* datasets and ML-based remote sensing models in data-limited lakes.

In addition, the research provides a comprehensive and innovative approach for assessing the applicability of multi-sensor satellite data in monitoring spatiotemporal water quality dynamics, particularly in shallow and optically complex lakes. The proposed framework is designed to be transferable and adaptable to different geographical regions and lake systems, thereby contributing to the advancement of scalable, interdisciplinary, and globally applicable coastal shallow lake water quality monitoring methodologies.

1.4. Overview of the Included Scientific Papers

This doctoral dissertation is based on four thematically and methodologically connected peer-reviewed scientific papers. Each paper addresses a specific component of the proposed geospatial multi-sensor framework for lake water quality monitoring and jointly contributes to testing the research hypotheses and enabling cross-paper methodological integration.

Paper I (*Integrating Remote Sensing Methods for Monitoring Lake Water Quality: A Comprehensive Review*) provides a critical synthesis of recent remote sensing approaches for lake water quality monitoring, with a particular focus on inland and coastal lake systems and their relevance for water management and decision-making. The paper explains the fundamental principles of remote sensing and reviews retrieval methods for water quality assessment in optically complex waterbodies. It addresses optically active parameters, including chl-a, turbidity, water transparency (Secchi disk depth), EC, surface salinity, and WT, and discusses their physical and biological relevance. The review further provides a comprehensive overview of satellite sensor characteristics, commonly used spectral bands, band combinations, and band equations for retrieving these parameters, together with key challenges related to sensor limitations and validation strategies. Particular emphasis is placed on the variability of water quality parameters and the need for comprehensive studies that

account for seasonal dynamics and longer temporal frameworks. In addition, the paper highlights key limitations of existing approaches, such as the predominance of single-parameter studies, short temporal coverage, and limited integration with *in situ* observations and spatial modelling. By identifying methodological gaps and outlining future research directions, including the integration of remote sensing with *in situ* measurements, hydrodynamic and computational modelling, optimization of sampling design, and the application of ML techniques, the paper establishes the theoretical and methodological foundation of the dissertation and motivates the development of integrated, multi-source, and spatially explicit monitoring frameworks.

Paper II (*Spatiotemporal Water Quality Analysis of Vrana Lake, Croatia*) investigates the spatial and seasonal variability of key water quality parameters based on systematic *in situ* measurements and environmental data, using Vrana Lake as a representative coastal shallow lake case study. The study is based on a structured monitoring grid of 20 sampling stations and monthly *in situ* measurements conducted over a 12-month period, capturing a set of physicochemical parameters including EC, turbidity, salinity, WT, DO, oxygen saturation, and chl-a. In addition to analysing current water quality conditions, the paper incorporates a long-term historical analysis of meteorological variables to contextualise observed water quality patterns within multi-decadal climatic variability. Relationships between water quality parameters, water level, and key meteorological drivers are analysed to assess both short-term dynamics and longer-term influences related to climate variability. Using GIS-based spatial interpolation, point-based measurements are transformed into spatially continuous water quality surfaces, enabling lake-wide assessment of spatial gradients. Multiple GIS interpolation methods are systematically evaluated using statistical performance metrics, and the most suitable approach is identified for modelling water quality distribution in the lake. The paper further presents the examination of vertical variability and temporal oscillations of selected parameters, demonstrating that the lake's shallow morphology allows reliable representation of water quality conditions using median values. By identifying the water quality and meteorological parameters with the strongest influence on lake dynamics, and subsequently using these parameters in combination with environmental variables as key inputs for the GIS-MCDA framework developed in Paper III, Paper II provides a robust empirical foundation and direct input for spatial decision-support modelling in Paper III.

Paper III (*Enhancing Water Quality Monitoring in a Coastal Shallow Lake Using GIS and Multi-Criteria Decision Analysis*) develops a GIS-based MCDA framework for spatial water quality and eutrophication susceptibility assessment, addressing water quality decline as a

critical issue in coastal shallow lake systems. Using Vrana Lake in Dalmatia, Croatia, as a case study, the paper explicitly considers the influence of seasonal water level fluctuations, salinization from the Adriatic Sea, and multiple anthropogenic and environmental pressures. Within this framework, a WQI raster is constructed based on a 12-month time series of *in situ* water quality measurements (EC, turbidity, WT, and DO), environmental variables (distance-based indicators of tributaries, nutrient runoff, and environmental pollution), and meteorological parameters (wind, precipitation, air temperature), providing a spatially continuous basis for eutrophication susceptibility assessment. Criteria standardisation and weighting are performed using a GIS-MCDA combined with the Fuzzy Analytical Hierarchy Process (F-AHP), enabling the systematic incorporation of expert knowledge. Model robustness is evaluated through sensitivity and uncertainty analysis based on Monte Carlo simulations. Beyond spatial susceptibility mapping, the paper addresses monitoring network optimisation by identifying areas where existing monitoring density is suboptimal and proposing an optimised network that ensures representative coverage of all water quality classes. The results reveal pronounced spatial heterogeneity in water quality, with lower quality and higher eutrophication susceptibility identified particularly in the northwestern and southern parts of the lake, influenced by anthropogenic activities and seawater intrusion. The GIS-MCDA-derived WQI raster produced in this paper serves as a spatially continuous reference layer and direct input for the ML-based analysis and sensor evaluation conducted in Paper IV.

Paper IV (*SIGMaL: An Integrated Framework for Water Quality Monitoring in a Coastal Shallow Lake*) addresses the need for monitoring approaches capable of capturing spatial and temporal variability in coastal lakes beyond the limitations of conventional *in situ* measurements. The paper presents the SIGMaL framework as a unified geospatial methodology that integrates *in situ* observations, GIS-MCDA-derived water quality information, satellite remote sensing, and ML for spatially continuous lake water quality assessment. Satellite reflectance data from Sentinel-2, Landsat 8-9, and PlanetScope are used to train regression models for individual physicochemical parameters, including EC, turbidity, WT, and DO. Subsequently, convolutional neural networks (CNNs) with spectral and temporal inputs are applied to classify WQI classes, enabling a comparative cross-sensor evaluation of their suitability for lake water quality monitoring. The trained models are further used to generate spatially continuous WQI maps for a subsequent monitoring period without concurrent *in situ* data, allowing assessment of model robustness and temporal transferability. Rather than fusing data from multiple sensors, the study focuses on comparative sensor evaluation, demonstrating that WQI-based models provide more stable and accurate results than models trained on

individual parameters. Paper IV thus represents the methodological culmination of the dissertation, demonstrating how the integration of *in situ* data, spatial modelling, and multi-sensor remote sensing can improve the accuracy, interpretability, and adaptability of water quality assessments in shallow and optically complex lakes.

1.5. Chapter Summary

The doctoral dissertation is structured into seven chapters, which together present a coherent progression from theoretical foundations to methodological development, empirical analysis, and integrated interpretation of results.

Chapter 1 introduces the scientific background and defines the research problem, outlining the research objectives, hypotheses, and expected scientific contributions. This chapter positions the dissertation within the broader context of integrated geospatial approaches to water quality monitoring.

Chapter 2, based on Paper I, provides a comprehensive review of remote sensing methods for lake water quality monitoring, with a particular focus on optically active parameters, satellite sensor characteristics, retrieval approaches, and current research challenges.

Chapter 3, corresponding to Paper II, analyses the spatiotemporal variability of lake water quality parameters based on *in situ* measurements and meteorological data, using Vrana Lake as a representative coastal shallow lake case study.

Chapter 4, based on Paper III, applies GIS-MCDA to assess eutrophication susceptibility by integrating primary water quality parameters with secondary meteorological, hydrological, and LCLU factors, resulting in spatially explicit water quality maps and decision-support outputs for monitoring network optimisation.

Chapter 5, corresponding to Paper IV, develops and evaluates ML models for integrated lake water quality monitoring through a comparative analysis of multisource satellite imagery, supported by *in situ* and GIS-derived data within a unified analytical framework.

Chapter 6 presents a joint discussion that synthesises and critically interprets the results obtained across Papers I-IV. The chapter highlights methodological interconnections and cross-paper knowledge transfer, evaluates the research hypotheses, and discusses the scientific and practical implications of the proposed geospatial multi-sensor approach.

Chapter 7 concludes the dissertation by summarising the main findings, emphasising the overall scientific contributions, and providing recommendations and directions for future research.

2. Integrating Remote Sensing Methods for Monitoring Lake Water Quality: A Comprehensive Review

This chapter has been published as: *Batina, A.; Krtalić, A. (2024): Integrating Remote Sensing Methods for Monitoring Lake Water Quality: A Comprehensive Review.* Hydrology*,* 11*(7), 92. doi: 10.3390/hydrology11070092.*

Conceptualization, A.B. and A.K.; methodology, A.B. and A.K.; validation, A.B. and A.K.; investigation, A.B.; resources, A.B. and A.K.; writing—original draft preparation, A.B.; writing—review and editing, A.B. and A.K.; visualization, A.B.; supervision, A.K.; project administration, A.B.; funding acquisition, A.K. All authors have read and agreed to the published version of the manuscript.

Abstract:

Remote sensing methods have the potential to improve lake water quality monitoring and decision-making in water management. This review discusses the use of remote sensing methods for monitoring and assessing water quality in lakes. It explains the principles of remote sensing and the different methods used for retrieving water quality parameters in complex waterbodies. The review highlights the importance of considering the variability of optically active parameters and the need for comprehensive studies that encompass different seasons and time frames. The paper addresses the specific physical and biological parameters that can be effectively estimated using remote sensing, such as chlorophyll-a, turbidity, water transparency (Secchi disk depth), electrical conductivity, surface salinity, and water temperature. It further provides a comprehensive summary of the bands, band combinations, and band equations commonly used for remote sensing of these parameters per satellite sensor. It also discusses the limitations of remote sensing methods and the challenges associated with satellite systems. The review recommends integrating remote sensing methods using *in situ* measurements and computer modelling to improve the understanding of water quality. It suggests future research directions, including the importance of optimizing grid selection and time frame for *in situ* measurements by combining hydrodynamic models with remote sensing retrieval methods, considering variability in water quality parameters when analysing satellite imagery, the development of advanced technologies, and the integration of machine learning algorithms for effective water quality problem-solving. The review concludes with a proposed workflow for monitoring and assessing water quality parameters in lakes using remote sensing methods.

Keywords: water quality monitoring; decision-making; optically active parameters; computer modelling; band combinations; sensors

2.1. Introduction

Lakes are important ecosystems that sustain a wide range of species and are essential for a variety of industries and human activities [34,35]. However, eutrophication, human exploitation, and climate change all have a negative impact on lake water quality and the general health of lake ecosystems [6,36–39]. To address this, remote sensing evolved as an effective method for monitoring and analysing worldwide water quality. This method, which collects spectrum data from aerial and satellite platforms, has been used since the 1970s to assess the physical, chemical, and biological characteristics of water quality.

Traditional methods of monitoring water quality through *in situ* measurements and laboratory analysis are time-consuming and costly, with limited geographical and temporal variability [40]. Remote sensing is a cost-effective and time-saving method that provides unique spatial information and data continuity for large-scale areas and inland waterbodies [16,21,41,42]. It can be combined with conventional methods to address the constraints of *in situ* methods [43]. Remote sensing methods and databases are highly useful for gathering data on lake ecological indicators, particularly in unstudied lakes with minimal *in situ* monitoring. Remote sensing, with sufficient *in situ* validation, may offer near-real-time information on lake changes, such as algae blooms or droughts. Interdisciplinary collaboration and validation may improve the accuracy and efficiency of remote sensing for waterbody evaluation and management [21], while requiring less time, effort, and money [22,44].

The conventional method for assessing water quality includes three types of parameters: (1) physical parameters such as water temperature (WT), transparency (Secchi disk depth (SDD)), salinity, turbidity, total suspended matter (TSM), coloured dissolved organic matters (CDOM), odour, and electrical conductivity (EC); (2) chemical parameters such as pH, dissolved oxygen (DO), chemical oxygen demand (COD), biochemical oxygen demand (BOD), total organic carbon (TOC), dissolved organic carbon (DOC), total nitrogen (TN), ammonia nitrogen (NH3-N), nitrate nitrogen (NO3-N), total phosphorus (TP), orthophosphate (PO4), heavy metal ions, and nonmetallic toxins; and (3) biological parameters such as chlorophyll-a (chl-a), total bacteria, and total coliforms. The analysed water quality parameters are divided into two groups using remote sensing methods. The initial categorization consists of parameters with active optical characteristics, including chl-a, TSM, and CDOM. These parameters affect the radioactive transfer process of waves by modifying the absorption of the spectrum. The second categorization includes parameters without defined optical properties, such as TN, TP, and DO. These parameters are commonly examined using statistical correlations with optically active

parameters [22]. The review covers six optically active water parameters, including chl-a, turbidity, SDD, WT, salinity, and EC.

This paper presents a comprehensive review of the current research status and developments in the use of remote sensing methods to monitor lake water quality. The review examines numerous research projects that evaluate water quality using remotely sensed data, emphasizing the potential use of these results for environmental researchers. It aims to offer a centralized resource for academics to obtain insights into present practices and suggest areas for improvement or future contributions. The review focuses on optically active physical and biological parameters that may be retrieved using satellite imagery, and it includes data from specialists in lake hydrology, biology, ecology, and chemistry. It also addresses the dependability of data representation by shifting from point to raster representation. The objectives of this paper are to (1) provide a bibliometric analysis, (2) provide insight into the current state of remote sensing methods for monitoring water quality in lakes, (3) summarize methods for retrieving water quality parameters based on remote sensing used in the literature, (4) provide a comprehensive summary of the bands, band combinations, and band equations commonly used for remote sensing of water quality parameters per satellite sensor, (5) address the importance of optimizing grid selection and time frame for *in situ* measurements, and (6) propose a workflow for monitoring and assessing water quality parameters in lakes using remote sensing methods. In addition, this review discusses the elements that influence the correlation between water quality parameters and satellite imagery, as well as possible solutions and limits to the challenges of remote sensing water quality assessment in lakes. Overall, this review adds new knowledge to the field and encourages further research and innovation in remote sensing methods for water quality monitoring.

2.2. Bibliometric Analysis

Long ago, remote sensing was acknowledged as a method for global tracking of inland water quality. Airborne and satellite spectral data collection has been used since the early 1970s to analyse a broad collection of water quality parameters [45] (Figure 2.1). Previous reviews [22,44,46–48] have offered excellent summaries of hundreds of publications presenting models for evaluating the biological, chemical, and physical properties of complex waterbodies published by scientists during the past 50 years. General trends in this sense were revealed after extensive bibliometric research of the Elsevier Scopus database (conducted in May 2024). Database titles, keywords, and abstracts from 1977 until 2023 for the terms ‘remote sensing’, ‘water quality’, and ‘lake’ in the English language were searched. The search found 29,901

unique publications published for terms ‘water quality’ and ‘lake’ and 1788 unique publications published for terms ‘remote sensing’, ‘water quality’, and ‘lake’. Globally, the number of publications employing remote sensing for lake water quality falls significantly behind those that do not, as shown in Figure 2.1.

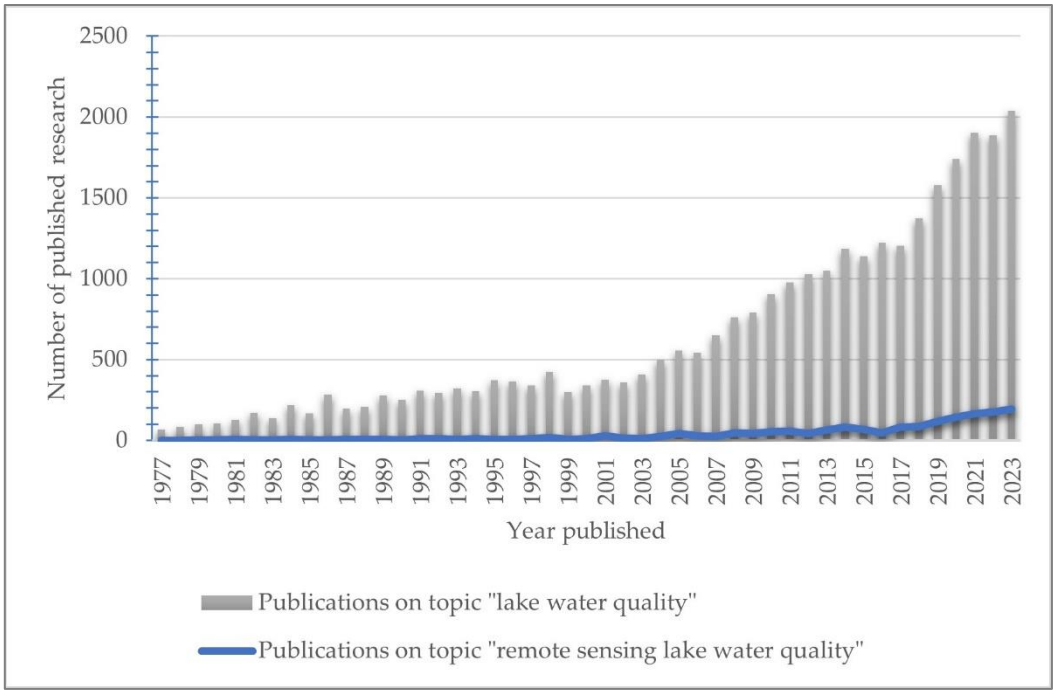

Figure 2.1. Number of publications retrieved from Elsevier Scopus on the search topic “(remote sensing) lake water quality”

Since the 1970s, papers describing the monitoring and assessment of water quality in lakes utilizing remote sensing methods have arisen (Figure 2.1). Publication numbers for the specific dataset follow a power law distribution, with a similar increase after 2008. The greatest increase in remote sensing studies from one year to the next happened after 2008, coinciding with the availability of free Landsat imagery. This conclusion is consistent with prior research indicating that the publication of the Landsat archive led to an increase in the frequency and scope of EO studies in different domains [49] and has resulted in a more comprehensive understanding of inland waterbodies to concentrate on demanding scientific problems and expanding research scales. Research on lakes based on remote sensing has seen a significant increase in publications in the past decade (2014–2023) compared to the previous 37 years (1977–2013). The majority of the publications in the bibliometric analysis were published in the United States and China, with the rest originating from various countries across Europe and from India, Canada, Japan, and Australia, as seen in Figure 2.2.

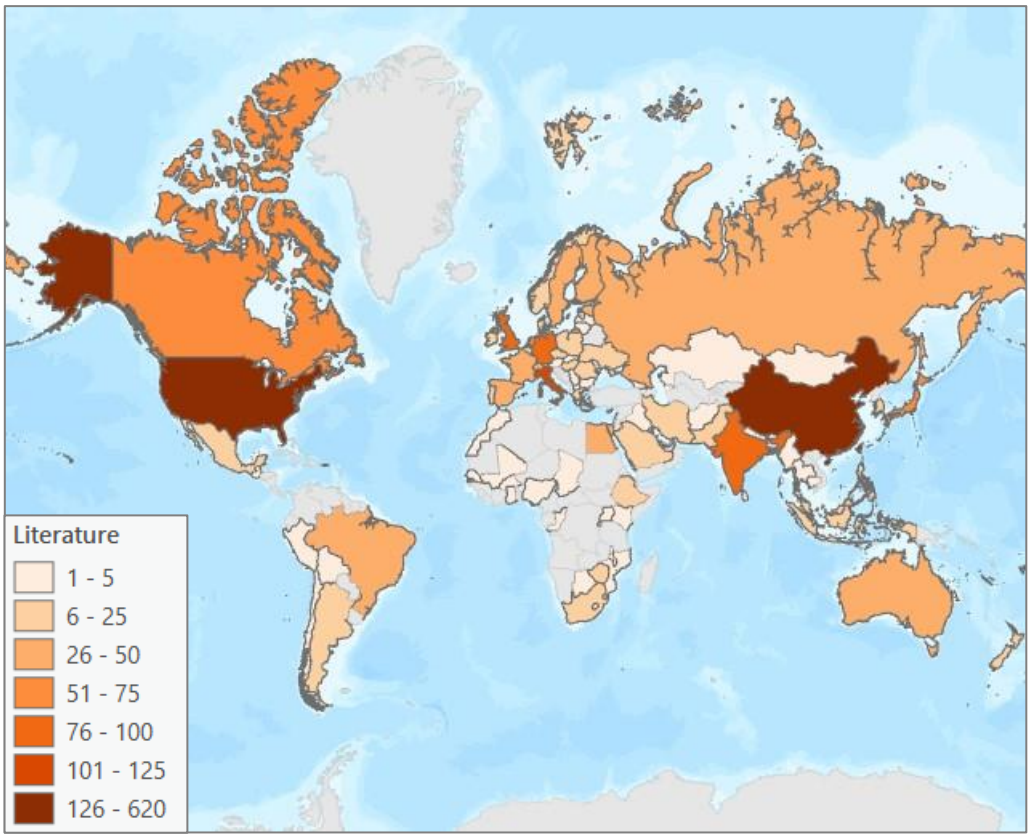

Figure 2.2. A map showing the literature count per country of origin based on the bibliometric analysis

The literature review suggests that the recent advancement in evaluating inland water quality through remote sensing initiatives can be attributed to the challenges associated with remote sensing of complex waterbodies and the limited availability of suitable sensors for this purpose (viz., hyperspectral airborne or space-borne remote sensing that captures extensive spatial and spectral information, especially in small lakes) [50]. This review uses the 'System A' lake typology of the WFD [51,52], which categorizes lakes based on four abiotic characteristics. The focus of the review is on categorizing lakes based on mean depth and surface area (Table 2.1). The complex bio-optical properties of a static waterbody (vegetation and pollutants) create problems in establishing an internal correlation between spectral responses and optically inactive water quality parameters. In tandem with the increase in remote sensing data accessibility during the past decade, *in situ* data accessible for model calibration and validation has increased. Modern databases offered by government agencies, nongovernmental organizations, and scholars provide a variety of freely accessible *in situ* data. In Europe, these include Eye on Water (www.eyeonwater.org (accessed on 16 October 2023)) and Seen-monitoring (www.seen-transparent.de (accessed on 16 October 2023)) [47]. These established databases can be enhanced with innovative datasets collected through citizen science activities.

In this way, data continuity is offered, resulting in cost and time savings for researchers, and a multitude of samples for calibration and validation of derived models.

Table 2.1. WFD lakes typology [51,52]

Lake Parameter	Value	Description
Depth	<3 m	Very shallow
	3-15 m	Shallow
	>15 m	Deep
Surface area	<1 km^2	Small
	1-10 km^2	Medium
	10-100 km^2	Large
	>100 km^2	Very large

2.3. Materials and Methods

The principle of using remote sensing methods to assess water quality involves creating models based on spectral responses and *in situ* measurements of water quality parameters. Locations of *in situ* measurements should consider hydrodynamic models and serve as a basis for comprehensive lake-wide analysis via remote sensing by choosing bands, band combinations, and band equations for retrieving optically active parameters. These models are calibrated and validated using *in situ* measurements and used for comprehensive analysis of water quality over a larger area and longer period [22]. Bio-optical methods use the correlation between a waterbody's optical properties and its optically active parameters to assess water quality. The performance of water quality retrieval models depends on spatial factors and the inherent optical properties of the region [46]. Optically active parameters interact with light and can be obtained through direct retrieval [53], while optically inactive parameters can be inferred from measurable water quality parameters [54].

There are five methods commonly used for monitoring and assessing water quality using remote sensing imagery: empirical, semi-empirical, semi-analytical, analytical, and machine learning (ML). Each method has its own characteristics and complexity.

2.3.1. Analytical Methods

Analytical models, also known as physical models, are used to determine spectral reflectance by analysing the optical properties of water and the atmosphere. These models are based on physics [47] and use inherent and apparent optical properties to model surface water reflectance and determine the concentration of constituents [44]. They link water quality parameters with

water-leaving radiance using radiation transmission theory [55]. The analytical method can identify all water parameters simultaneously, but it requires accurate measuring instruments and has high application costs [56]. Model development is challenging due to differences in spectral resolutions between satellite sensors and ground measurements. The analytical method is infrequently used for all water quality parameters [22] and requires theoretical breakthroughs to create more generalized models; nevertheless, it has good portability [56]. Studying the complex optical characteristics of water quality parameters can improve the accuracy of analytical methods [22].

2.3.2. Semi-Analytical Methods

Analytical and semi-analytical models are used to study the physics-based optical properties of water and the atmosphere [57]. Semi-analytical methods simplify analytical models and require statistical analysis [58]. Theoretical values are calculated by modelling the optical properties of a waterbody [57]. Some models are based on water column radiative transfer and use inversion and look-up tables to match spectral signatures and predict water quality parameters [59]. Semi-analytical models using *in situ* observations are common for remotely sensing inland water quality [46]. However, model development is challenging and requires knowledge of atmospheric correction and substantial *in situ* sampling [47]. These models have been successfully applied on broad spatiotemporal scales to retrieve optically active parameters, such as chl-a and SDD [22].

2.3.3. Empirical Methods

The empirical method is a statistical approach that uses regression analysis to establish relationships between water quality parameters and spectral response values [22,44]. This method is used to derive distinctive bands or band combinations and create a water quality inversion model [60]. Empirical methods include linear regression, band combination, and principal component analysis. However, these methods lack physical mechanisms and multitemporal validity, resulting in uncertainty and limited applicability. Inland waterbodies, which are optically complex, often require multivariate regression [13]. Empirical models also rely on *in situ* data and may be affected by changes in downwelling irradiance and water surface conditions [61]. Despite these drawbacks, the empirical method is preferred for its simplicity, low computational needs, and ability to account for specific waterbody properties [13,46]. It is commonly used to assess turbidity, chl-a, and trophic status [45].

2.3.4. Semi-Empirical Methods

Semi-empirical methods combine empirical and analytical methods to correlate water quality parameters with remote sensing data [56]. These methods involve statistical and measured spectral analysis to select characteristic bands and develop models [62]. They use physical and spectral data to create algorithms that correlate with measured parameters. However, their validity is limited to a specific range of optical water quality data [61]. Semi-empirical models do not model the inherent optical properties of waterbodies like semi-analytical models, but they improve the spectral properties of parameters and reduce noise. Physically based semi-empirical models are more generalizable but require sensors with properly positioned band centres and sufficient spectral resolution [47]. Spectral band ratios and shape algorithms are commonly used due to their generalizability and ease of implementation, although they assume consistent water and atmospheric conditions. Spectral band ratios and spectral shape methods are better for assessing regional water quality parameter distributions than precise estimates [13]. The temporal and spatial applicability of semi-empirical methods is limited by the availability of *in situ* measured data. These methods are often used to assess parameters such as chl-a, SDD, and turbidity [63–65].

2.3.5. Machine Learning (ML) Methods

The use of ML methods in remote sensing has been increasing [29,30]. ML methods, such as partial least squares regression (PLSR), support vector regression (SVR), artificial neural networks (ANN), deep neural networks (DNN), and convolutional neural networks (CNN), have shown promise in accurately estimating water quality parameters in remote sensing. Traditional ML algorithms like PLSR and SVR [66,67], and deep learning (DL)-based methods like ANN, DNN, and CNN [47] excel at solving complex nonlinear problems. ANN models require large training samples, while SVM models are suitable for small samples and nonlinearity [66]. CNN models are particularly effective for classifying hyperspectral images [68].

ML models are limited by the data used to train them and require distinct training and testing datasets. In order to ensure that representative samples of a data set are selected, a random split of 70% training data and 30% testing data should be used, according to Sagan et al. (2020) [13]. They can capture complex and nonlinear relationships between water quality parameters and remotely sensed reflectance when given appropriate inputs [47]. However, ML methods have downsides, such as the need for a lot of training data, the challenge of combining features from different spectral, spatial, and temporal information, and the potential for unexplained solutions

or ill-posed problems [33]. Despite these challenges, the use of ML in remote sensing for water quality estimation has become more popular due to algorithm development, sensor systems, computing power, and data accessibility [69]. DL methods have been found to outperform other remote sensing methods in estimating water quality parameters such as chl-a, turbidity, NO_3-N, and PO_4-P [13,17].

2.4. Optically Active Water Quality Parameters

Water molecules have properties such as scattering, reflecting, and absorbing the electromagnetic spectrum (Figure 2.3), which can create challenges for remote sensing in aquatic environments [70]. These properties limit optical remote sensing to the visible area of the electromagnetic spectrum [70], although the near infrared region can provide some information [43], especially in shallow water. Optically active parameters, such as chl-a, interact with light and modify radiation in the water column through absorption and scattering processes [54]. Remote sensing can accurately measure these parameters and other water quality parameters without the errors associated with *in situ* measurements. In optically shallow water, the reflected light also contains information about the bottom substrate and bathymetry [48]. The apparent optical properties depend on water quality and radiation geometry [71], and retrieval models can be built based on the interaction between inherent optical properties and remote sensing reflection. Remote sensing has been successful in measuring various optically active water quality parameters, including chl-a, SDD, turbidity, salinity, and WT [13,17,18,53,72,73], but there are challenges in estimating parameters with weak optical properties, such as pH, DO, nutrients, and heavy metals [13,60,73–75]. However, it is possible to estimate these parameters by establishing correlations with optically active parameters. The review emphasizes the importance of considering the variability of optically active biological (chl-a) and physical parameters (SDD, EC, turbidity, salinity, and WT), the correlation with satellite imagery, and the need for comprehensive studies that encompass different seasons and time frames to ensure accurate assessments and effective management of water resources.

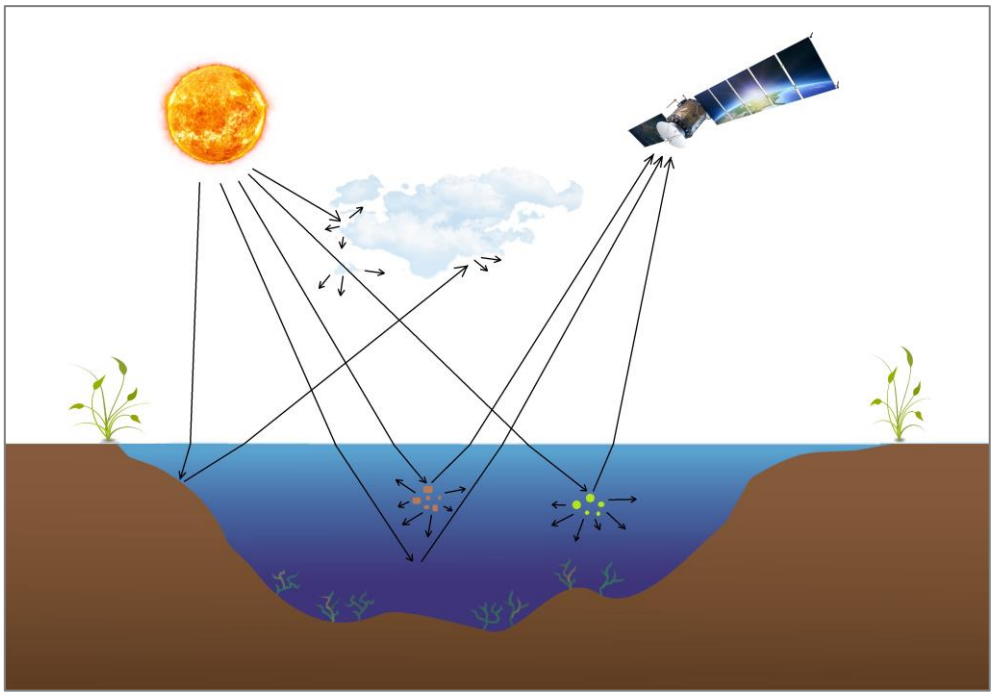

Figure 2.3. Schematic overview of the path of electromagnetic spectrum from the sun to a waterbody and a sensor

2.4.1. Chlorophyll-a (Chl-a)

Photosynthesis is a vital process for plants and other photosynthetic organisms, as it allows them to convert light energy into usable energy. Chlorophyll, specifically chl-a, is the most common pigment involved in photosynthesis [46]. It plays a crucial role in waterbody primary productivity, trophic status, and nutrient levels. However, excessive chl-a concentrations can lead to harmful algal blooms, particularly those caused by phycocyaninproducing cyanobacteria, which can be toxic to humans and wildlife [76]. The increase in harmful algal blooms worldwide is attributed to anthropogenic nutrient loading and climate change [77]. Therefore, it is important for local authorities to monitor and forecast these blooms.

Remote sensing methods, such as satellite and aerial imagery, can be used to assess chl-a concentrations in waterbodies. Due to sunlight-induced fluorescence, the chl-a spectrum peaks at 680 nm in oligotrophic to mesotrophic aquatic environments [78]. Narrow bands of imagery are needed for remote sensing chl-a concentration and its geographical and temporal fluctuations [79]. Table A1 lists selected remotely taken measurements of chl-a using various sensors and spectral bands, band ratios, and band combinations. As seen from Table A1, a conducted literature review showed Landsat-5 TM and Envisat MERIS as most suitable and popular for chl-a evaluation due to their easy accessibility, temporal coverage, and spatial resolution, making them a good choice.

Based on the summary given in Table A1 and Table A2, various methods, including analytical [80–83], semi-analytical [63,84–86], empirical [42,60,74,87–90], semi-empirical [91–93], ML [67,94], and NNs [53,90,95], have been employed to analyse remote sensing data and estimate chl-a concentrations in lakes. These methods utilize different approaches, such as measuring the optical properties of water, combining field and remote sensing data, establishing statistical relationships, and modelling complex relationships. The findings of Wu et al. (2009) [95] and Song et al. (2011) [90] demonstrated that NN models outperformed empirical models in utilizing spectral information and model reliance and highlighted the superior accuracy of utilizing NN models in water quality monitoring and management efforts compared to empirical regressions. The application of these methods has provided valuable insights into the dynamics and distribution of chl-a in different aquatic ecosystems, contributing to a better understanding of algal abundance and informing management strategies.

According to the outline provided in Table A2, waterbodies with a narrow range of measured chl-a values (chl-a concentrations between 0.01 and 11 µg/L) show a notable correlation with specific imagery from satellite and airborne sensors. Landsat-5 TM imagery revealed moderate correlations (R^2 = 0.513, 0.53, and 0.72) for a lake in Turkey [96] with *in situ* values ranging from 0.62 to 3.99 µg/L, a reservoir in Arkansas, USA [97], with *in situ* values ranging from 1.4 to 10 µg/L, and a lake in Italy [98] with *in situ* values ranging from 1.11 to 4.57 µg/L, respectively. There is a moderate correlation between MIVIS aerial hyperspectral imagery (R^2 = 0.71) for a lake in Italy [81] with *in situ* values ranging from 0.75 to 4.3 µg/L, and between EO Hyperion-1 satellite hyperspectral imagery (R^2 = 0.705) for a lake in Guatemala [91] with *in situ* values ranging from 1.01 to 10.91 µg/L. There is a strong correlation between a reservoir in Arkansas, USA [99] when compared using Landsat-5 TM (R^2 = 0.84) and *in situ* values ranging from 1 to 7 µg/L in four months throughout the year. A lake in Germany [93] correlates strongly with CASI and HyMap aerial hyperspectral imagery (R^2 = 0.89) with *in situ* values ranging from 1 to 3 µg/L collected from May to September.

Imagery from satellite and airborne sensors has shown a moderate to strong correlation with waterbodies with chl-a concentrations in the medium range of 0.07 and 40 µg/L. A moderate correlation has been discovered between chl-a and EO Hyperion-1 hyperspectral imagery (R^2 = 0.59) in a lake in Italy [80], with *in situ* values from 0.5 to 12 µg/L measured in one month. Terra MODIS imagery has a moderate correlation (R^2 = 0.632) for a lake in China [95] with chl-a *in situ* values from 5.2 to 33.9 µg/L during a 4-month study, and Landsat-5 TM imagery (R^2 = 0.72) for a lake in Italy [98] with *in situ* values from 4.63 to 11.35 µg/L measured in one month. Strong correlations were observed between Landsat-5 TM and lakes in Spain [100],

China [90], and Italy [101], with R^2 values of 0.82, 0.98, and 0.999, respectively. However, only four samples were used for the research of the lake in Italy [101], and *in situ* values ranged from 5.5 to 7.7 μg/L, while *in situ* values in the lake in Spain ranged from 0.4 to 20 μg/L in a 6-year study and *in situ* values in the lake in China ranged from 5 to 30 μg/L in one month.

A correlation has been found between imagery from satellite and airborne sensors and chl-a concentrations in waterbodies, which vary considerably in the wide range from 0.01 to 250 μg/L. A moderate correlation was observed between chl-a and Landsat-5 TM with a coefficient of correlation R^2 of 0.705 across 42 lakes in Michigan, USA [102]. The chl-a *in situ* values in Michigan lakes [102] varied from 0.2 to 87 μg/L over a period of six months. There is a strong correlation ($R^2 \geq 0.8$) between chl-a and several satellite and airborne imagery sources, such as Ikonos OSA, AISA, CASI, HyMap, PROBA-CHRIS, Landsat-7 ETM+, Envisat MERIS, Sentinel-2 MSI, and Sentinel-3 OLCI. This correlation was seen in 15 studies from Table A2 conducted across study periods ranging from one month to 13 years, with maximum chl-a levels reaching 120 μg/L.

Waterbodies with a very wide range of chl-a concentrations between 0.01 and 700 μg/L show a strong correlation with specific satellite images. A strong correlation ($R^2 = 0.85$) was discovered in a 3-year study, including 13 reservoirs in Oklahoma, USA [103]. The research used PlanetScope, Sentinel-2 MSI, and Landsat-8 OLI data in conjunction with chl-a *in situ* measurements ranging from 0.6 to 540 μg/L, where Sentinel-2 MSI showed the highest correlation with chl-a *in situ* values. A 6-year study conducted on nine waterbodies in the United States, Australia, and China [67] revealed a strong correlation ($R^2 = 0.91$) between Sentinel-3 OLCI images and *in situ* readings ranging from 2.8 to 285.5 μg/L. A 1-month study conducted on 15 lakes in Minnesota, USA [104], revealed a strong correlation ($R^2 = 0.99$) between chl-a concentrations ranging from 1.8 to 397 μg/L and Terra MODIS images.

The literature summarized in Table A2 provides information on the most commonly used sensors for assessing chl-a from satellite and airborne multispectral and hyperspectral imagery. The Landsat-5 TM sensor is frequently utilized and has an average R^2 value of 0.76 based on eight studies [90,96–102]. However, several other sensors have achieved better results for assessing chl-a. Satellite multispectral sensors such as Sentinel-3 OLCI and Ikonos OSA, satellite hyperspectral sensors such as Envisat MERIS and PROBA-CHRIS, and airborne hyperspectral sensors such as CASI, HyMap, and AISA have achieved the best R^2 values (>0.88) for assessing chl-a. Very shallow waterbodies (<3 m) have the highest R^2 values of 0.84 for retrieving chl-a from satellite and airborne imagery. The best results, with an R^2 value of 0.93, are achieved for medium-sized waterbodies (1–10 km^2). Additionally, studies lasting

longer than one year have achieved better results, with an R^2 value of 0.85. The most successful methods for retrieving chl-a from satellite and airborne imagery are empirical, NN, ML, and nonlinear regression, with R^2 values exceeding 0.93.

The most effective sensors for retrieving chl-a in small waterbodies (<1 km^2) are Landsat-5 TM, airborne hyperspectral CASI, and HyMap. For medium waterbodies (1–10 km^2), the most effective satellite sensor is hyperspectral Envisat MERIS. Ikonos OSA is the recommended multispectral sensor for large waterbodies (10–100 km^2), while multispectral Sentinel-3 OLCI and hyperspectral Envisat MERIS (satellite platforms) are most effective for very large waterbodies (>100 km^2), according to the literature in Table A2.

The most effective sensors for retrieving chl-a in very shallow waterbodies (<3 m) are multispectral Sentinel-3 OLCI, satellite hyperspectral Envisat MERIS, and airborne hyperspectral CASI and HyMap. In shallow waterbodies (3–15 m), the recommended satellite sensor is the hyperspectral Envisat MERIS. The most effective sensors for retrieving chl-a in deep waterbodies (>15 m) are multispectral Ikonos OSA, airborne hyperspectral CASI, and HyMap.

2.4.2. Turbidity

Turbidity is a measurement of the amount of suspended and dissolved particles in water that cause light to scatter [48]. High turbidity levels can reduce water transparency and carry contaminants and nutrients, impacting primary production, aquatic plant growth, and water quality in lakes [105]. Remote sensing is used to map turbidity concentrations and their variations over time and space. Various methods, including the empirical method [106–109], have been used to measure turbidity in lakes and reservoirs. Studies have shown that ML methods, such as NNs, can provide accurate predictions of turbidity concentrations [90,108]. Table A3 lists selected remotely taken measurements of turbidity using various sensors and spectral bands, band ratios, and band combinations. Integrating ML into turbidity concentration studies has the potential to enhance understanding of water quality dynamics in aquatic systems.

Waterbodies with turbidity levels in a narrow range from 0.1 to 20 NTU have a notable correlation with certain satellite images. Landsat-5 TM images showed a moderate correlation (R^2 = 0.537) for a lake in Tennessee, USA [102]. The *in situ* turbidity values in a lake in Tennessee, USA [102], vary from 4.1 to 20 NTU in one month.

Waterbodies with turbidity levels in the medium range of 0.1 to 100 NTU have a significant correlation with certain satellite images. There is a strong correlation between turbidity and Landsat-5 TM (R^2 = 0.822) in a lake in Turkey [96], with *in situ* values varying from 2.9 to

33.5 NTU during a 1-month period. There is a strong correlation between turbidity and PROBA-CHRIS ($R^2 = 0.9$) as well as turbidity and Landsat-5 TM/Landsat- 7 ETM+ ($R^2 = 0.85$) in a reservoir in Cyprus [110]. *In situ* turbidity levels ranged from 7.94 to 26.3 NTU during a period of six months (April–October 2010). The strongest correlation was identified between turbidity and Terra ASTER data for a lake in Egypt [106], with an R-squared value of 0.998, over the *in situ* range of 0–85 NTU measured during a 2-month period.

Waterbodies with turbidity levels in the wide range of 0.1 to 200 NTU exhibit a notable correlation with certain satellite images. Analysed Landsat-8 OLI data indicated a moderate correlation ($R^2 = 0.642$) for turbidity levels ranging from 13.5 to 117 NTU in a reservoir in Columbia [111] during a 1-month period. A strong correlation has been found between turbidity and Landsat-5 TM images for a lake in China [90] and a reservoir in China [112] ($R^2 = 0.98$ and 0.937, respectively). Research on a lake in China [90] spanned one month and measured *in situ* values between 5 and 180 NTU. Research conducted on a reservoir in China [112] consisted of two sessions within one month, revealing *in situ* values ranging from 2.13 to 142 NTU.

Waterbodies with turbidity levels in a very wide range from 0.1 to 1000 NTU exhibit a strong correlation with satellite imagery. Research conducted over 10 years throughout six summer sessions in New Zealand [107] found a significant association ($R^2 = 0.924$) between Landsat 7 ETM+ images and *in situ* values from 34 shallow lakes. *In situ* values ranged from 75 to 275 NTU. There is a strong correlation between turbidity and PlanetScope data ($R^2 = 0.79$) in a 3-year study of 13 reservoirs in Oklahoma, USA [103], where *in situ* turbidity levels ranged from 0 to 966 NTU.

The literature summarized in Table A4 provides information on the most commonly used sensors for assessing turbidity from satellite and airborne multispectral and hyperspectral imagery. The Landsat-5 TM sensor is frequently used and has an average R^2 value of 0.82 based on five studies. However, other satellite sensors such as Landsat-7 ETM+, Terra ASTER, and PROBA-CHRIS have achieved better results with R^2 values greater than 0.9 for assessing turbidity. Deep waterbodies (>15 m) have the highest R^2 values of 0.88 for retrieving turbidity from satellite and airborne imagery. Small-sized waterbodies (<1 km^2) achieve the best results with an R^2 value of 0.98. Studies lasting between two and six months have shown the best results, with an R^2 value greater than 0.87. The most effective methods for extracting turbidity from satellite and airborne images are empirical methods and NN ($R^2 > 0.85$).

According to the literature in Table A4, the most effective sensor for measuring turbidity in small (<1 km^2) and large (10–100 km^2) waterbodies is Landsat-5 TM. For very large waterbodies (>100 km^2), the recommended sensors are multispectral Landsat-5 TM, Landsat-7

ETM+, and hyperspectral PROBA-CHRIS. Multispectral Landsat-5 TM is also the most effective for measuring turbidity in very shallow (<3 m) and shallow (3–15 m) waterbodies, while the most effective sensor for retrieving turbidity in deep waterbodies (>15 m) is hyperspectral PROBA-CHRIS.

2.4.3. Transparency (Secchi Disk Depth (SDD))

Water transparency, which is a measure of the clarity of lake water, is an important indicator of water quality and the health of aquatic ecosystems [113]. It is commonly assessed using the Secchi disk [114], a white and black disk that is lowered into the water until it is no longer visible. However, this method is labour-intensive and limited in its ability to capture spatial variations in water clarity. Remote sensing methods, which use satellite data to estimate water transparency, offer a more efficient and comprehensive approach by approximating Secchi disk depth in water with an inverse variation of the diffuse attenuation coefficient (K_d). The diffuse attenuation coefficient of downwelling irradiance, which is frequently measured at 490 nm, shows the exponential drop in irradiance with increasing water depth [70].

These methods use semi-analytical, empirical [74,95,107,115], and ML models to correlate water reflectance with transparency in lakes [116]. DL algorithms, such as NNs, have also been used to improve the accuracy of water quality retrieval models [95]. Water clarity is often used as a proxy for the trophic state of a lake [117], indicating nutrient availability and chlorophyll concentrations. Turbidity and TSM levels in the water are inversely correlated with water clarity. Various spectral bands and ratios are used in remote sensing to measure water clarity, with wavelengths in the red spectrum being particularly [107]. Table A5 summarizes these findings. Landsat-5 TM and Envisat MERIS satellite systems have been found to be effective for evaluating water clarity due to their comparatively low cost, temporal coverage, spatial resolution, and data availability.

There is a significant correlation between satellite imagery and waterbodies, with SDD values in a narrow range of 0.1 and 2 m. An analysis of Landsat-5 TM data showed a moderate correlation ($R^2 = 0.588$) between SDD *in situ* values ranging from 0.16 to 0.33 m during a 1-month period on a lake in Tennessee, USA [102]. For a Chinese lake [95], Terra MODIS images revealed a moderate correlation ($R^2 = 0.628$) with in-situ SDD measurements ranging from 0.25 to 1.2 m over the course of four months. Using in-situ measurements ranging from 0.23 to 0.39 m over the course of a month, SDD and Envisat MERIS imagery of a South African lake [118] show a strong correlation with a R^2 value of 0.801. A month-long investigation on an Italian lake [98] found a strong correlation between SDD and Landsat-5 TM ($R^2 = 0.82$) with *in situ*

values ranging from 0.25 to 1 m. A 1-month study on three lakes in Brazil's Lower Amazon Floodplain [115] using SDD and PlanetScope imagery revealed a strong correlation (R^2 = 0.816) with *in situ* values ranging from 0.6 to 1.94 m.

Waterbodies exhibiting a medium range of SDD values between 0.1 and 3.75 m demonstrate a significant correlation with particular satellite images. A study conducted on 34 shallow lakes in New Zealand [107] identified a moderate correlation (R^2 = 0.67) between Landsat-7 ETM+ data and SDD *in situ* values varying from 0.05 to 3.04 m over the course of six summer sessions spanning ten years. SDD and identical satellite imagery have a strong correlation (R^2 = 0.8), as demonstrated by a study conducted for three months in the summer at a lake on the Canada–United States border [119] using *in situ* values ranging from 0.1 to 3 m. A strong correlation (R^2 = 0.82 and 0.929) was observed between SDD and Landsat-5 TM imagery for one lake in Italy [98] and one lake in Thailand [120], respectively. The 1-month study conducted in Italy [98] has measured *in situ* values from 3 to 3.75 m. For a study conducted in Thailand [120] over the course of three spring sessions in two months, the values ranged from 0.2 to 2.5 m.

Waterbodies exhibiting a wide range of SDD values between 0.1 and 15 m demonstrate a moderate-to-strong correlation with particular satellite images. A study conducted on a lake in Spain [100] identified a moderate correlation (R^2 = 0.63) between Landsat-5 TM data and SDD *in situ* values spanning a duration of six years, with values varying from 1.33 to 7.53 m. The correlation between SDD and Terra MODIS imagery is moderate (R^2 = 0.52), as demonstrated by a 1-month study involving 15 lakes in Minnesota, USA [104], with *in situ* values ranging from 0.2 to 6.1 m. In three years, Sentinel-2 MSI imagery revealed a strong correlation (R^2 = 0.8) between *in situ* SDD values ranging from 0.08 to 4 m for 13 reservoirs in Oklahoma, USA [103]. Multiple studies [99,101,121] have found a significant correlation (R^2 > 0.82) between SDD and Landsat-5 TM/Landsat-7 ETM+, with SDD *in situ* values varying from 0.02 to 6.8 m and study durations spanning from one month to two years. There is a strong correlation (R^2 = 0.95) between SDD and PROBA-CHRIS, with *in situ* values ranging from 0.1 to 6 m, according to a 1-month study of ten lakes in Poland [122]. A strong correlation (R^2 = 0.989) was observed between SDD and Ikonos OSA imagery and *in situ* values ranging from 0.8 to 6.5 m in a Turkish estuary during a 1-month study [123]. Two Finnish studies [64,124] demonstrate a strong correlation (R^2 > 0.86) between SDD and AISA imagery within the *in situ* range of 0.3 to 7 m. The literature summarized in Table A6 provides information on the most commonly used sensors for assessing SDD from satellite and airborne imagery. The Landsat-5 TM sensor is frequently used and has an average R^2 value of 0.8 based on seven studies. However, other satellite sensors such as Ikonos OSA, PROBA-CHRIS, and airborne AISA have achieved better

results with R^2 values greater than 0.87 for assessing SDD. Deep waterbodies (>15 m) have the highest R^2 values of 0.88 for retrieving SDD from satellite and airborne imagery. Large waterbodies (10–100 km^2) achieve the best results with an R^2 value of 0.92. Studies lasting between two and three months have shown the best results, with an R^2 value of 0.87. The most effective method for extracting SDD from satellite and airborne images is through empirical methods and multiple regression ($R^2 > 0.82$).

The literature in Table A6 suggests that the most effective sensor for measuring SDD in small (<1 km^2) and very large (>100 km^2) waterbodies is Landsat-5 TM. For large waterbodies (10–100 km^2), both multispectral Landsat-5 TM and Ikonos OSA are recommended. Hyperspectral Envisat MERIS is the recommended sensor for medium-sized waterbodies (1–10 km^2) and very shallow waterbodies (<3 m). Landsat-5 TM is most effective for assessing SDD in shallow waterbodies (3–15 m), while multispectral Landsat-5 and Ikonos OSA are most effective for assessing SDD in deep waterbodies (>15 m).

2.4.4. Water Temperature (WT)

WT is an important indicator of ecosystem health and water quality [44]. Accurate surface WT measurements are crucial for weather and climate research, and remote sensing can provide these measurements. However, measurements can be affected by factors like emissivity and atmospheric absorptions [125]. Infrared radiometers can provide surface WT measurements with a precision of around 0.5 °C, but optical remote sensing methods should be used to identify and mask clouds and fog. Passive microwave approaches can be used in cloudy locations with an accuracy limit of roughly 1.5–2 °C [126]. While passive microwave radiometers have lower accuracy and resolution compared to infrared radiometers, they are not affected by air and cloud influences [41]. Estimating primary production and phytoplankton growth rates can be performed using remote sensing and *in situ* measurements of WT [44]. WT also affects DO concentrations and the distribution of contaminants in the water. Remote sensing, combined with *in situ* measurements, can provide accurate data on temperature zones at a reasonable cost. Various studies have explored the challenges and benefits of using empirical methods [106,127] and numerical weather prediction models to estimate WT in different types of lakes. Following a conducted review of the literature, Table A7 summarizes how combinations of bands may be used to measure WT. The most commonly utilized instruments mounted on satellites used for remote sensing retrieval of WT are Landsat-8 TIRS and Terra MODIS.

A correlation has been observed between specific satellite imagery and waterbodies exhibiting WT concentrations that have narrow-range variability. An R-squared value of 0.535 indicates

a moderate correlation between WT and Terra ASTER for a lake in Egypt [106], where WT levels fluctuate between 29.7 and 31.2 °C over the course of two months.

Waterbodies characterized by wide range in WT levels demonstrate a significant correlation with satellite imagery. Over a 10-month period, Landsat-7 ETM+ and Landsat-5 TM satellite imagery established a strong correlation (R^2 = 0.921) with WT in multiple lakes located in northern Germany [128]. The *in situ* temperatures measured during this period varied between 2.5 and 21.5 °C. Based on 120 sessions over six years and *in situ* values spanning from 1 to 29 °C, a study on four lakes in Switzerland–France, Hungary, Sweden, and Finland [129] reveals a strong correlation (R^2 = 0.792) between WT and NOAA-9, -11, -12, -14, -16, -17, and-19 AVHRR. A strong correlation (R^2 = 0.92 and 0.9928, respectively) is observed between Terra MODIS and WT in two lakes in Sweden [130] and one lake in Iran [127]. The research in Sweden [130] spanned two years from April to October and utilized *in situ* temperatures varying from 1 to 22 °C. The Iranian study [127] spanned four years and utilized *in situ* temperatures ranging from 3.5 to 32 °C.

The literature summarized in Table A8 provides information on the most commonly used sensors for assessing WT from satellite imagery. The Terra MODIS sensor is frequently used and has an average R^2 value of 0.96 based on two studies, making it the most effective sensor for retrieving WT. Medium-sized waterbodies (1–10 km^2) have the highest R^2 value of 0.92 for retrieving WT from satellite imagery. Deep waterbodies (>15 m) achieve the best results with an R^2 value of 0.96. Studies lasting more than six months have shown the best results, with an R^2 value greater than 0.89. The most effective method for extracting WT from satellite images is through the empirical method, which has an R^2 value of 0.84.

The literature in Table A8 suggests that different sensors are recommended for assessing WT in different sizes and depths of waterbodies. For very large waterbodies (>100 km^2), Terra MODIS is considered the most effective sensor. For medium-sized waterbodies (1–10 km^2), multispectral Landsat-5 TM and Landsat-7 ETM+ are the recommended sensors. Landsat-7 ETM+ and Terra MODIS are the most effective for assessing WT in shallow (3–15 m) and deep waterbodies (>15 m).

2.4.5. Salinity

Salinity is an important parameter for brackish lakes but not relevant for freshwater lakes. It affects water density and currents, as well as the exchange of gases between air and water. Satellite measurements can be affected by a layer of fresh surface water on top of salty water. Salinity in inland waterbodies varies due to factors like precipitation, evaporation, river runoff,

and interactions with oceans [44]. Monthly salinity maps can help determine variations in freshwater input and outflow. Table A9 lists the band combinations needed to accurately measure salinity using optical sensors on satellites like Landsat-5 TM, Landsat-8 OLI, and Sentinel-2 MSI. Table A9 presents a concise overview of the studies conducted to assess salinity in shallow lakes through empirical [106], ML [131], and NN methods [132]. Indirect methods, such as brightness temperature, CDOM, and temperature profiles, are used to estimate salinity. Due to the lack of a direct colour signal from salinity, the colour signal can instead be estimated using relationships between salinity, WT, and brightness temperature [133] and between salinity and CDOM [134].

An R-squared value of 0.657 indicates a moderate correlation between Sentinel-2 MSI imagery and salinity for a hypersaline lake in Iran [131], where salinity values fluctuate between 30.7 and 36.1 over the course of three months (April, June, and July 2021). In April and June of 2019, a strong correlation ($R^2 = 0.94$) was identified between salinity measurements obtained from Sentinel-2 MSI in the same lake in Iran [132]. *In situ* values for this correlation varied from 6.5 to 32.

The literature on remote sensing-based salinity assessment in lakes is limited, with only two studies conducted on Urmia Lake, a very large and shallow waterbody. Both studies used the Sentinel-2 MSI sensor and found promising results, as highlighted in Table A10. The first study, which lasted for three months, used the ML method and achieved an R^2 value of 0.66. The second study, which lasted for two months, used the NN method and achieved a high R^2 value of 0.94.

2.4.6. Electrical Conductivity (EC)

The EC of water is a measure of its ability to conduct electricity and is influenced by the concentration of ions or salt in the water [135]. The standard unit of measurement for EC is microSiemens per centimetre (µS/cm). Higher salinity levels in water lead to a decrease in oxygen absorption. Changes in EC that occur rapidly can indicate water contamination. Anions like chloride, phosphate, and nitrate can increase EC when added to sewage discharge or agricultural runoff [135]. The combination of chemical and biological processes can cause changes in EC, and diurnal variations in EC have been observed during low-flow cycles [136]. Conductivity probes are used to measure EC in the laboratory or field, and some devices can also measure salinity. Correlations between EC and spectral measurements are challenging due to complex interactions with optically active water quality elements [13]. Table A11 lists selected remotely taken measurements of EC using various sensors and spectral bands and band

combinations. Landsat-8 OLI is commonly used for retrieving EC, either as a single band or in combination with other bands.

Waterbodies with EC in a narrow range from 0.01 to 4 mS/cm exhibit a moderate correlation with specific satellite images. An R-squared value of 0.699 indicates a moderate correlation between EC and Landsat-8 OLI imagery for a reservoir in Columbia [111] (EC values range from 0.54 to 1.82 mS/cm over one month) and an R-squared value of 0.615 for the same satellite imagery in a lake in Kashmir, India [109] (EC levels range from 0.01 to 0.3 mS/cm over one month).

Waterbodies with EC in the medium range of 40 to 60 mS/cm exhibit a strong correlation with specific satellite imagery. A strong correlation was identified between EC and Landsat-8 OLI in a lake in Egypt [137] over the course of one month, with *in situ* values varying from 42.86 to 52.55 mS/cm and coefficient of correlation $R^2 = 0.87$.

The literature summarized in Table A12 provides information on the most commonly used sensors for assessing EC from satellite imagery. The Landsat-8 OLI sensor is frequently used and has been found to be the most effective sensor for retrieving EC, with an average R^2 value of 0.73 based on three 1-month studies [109,111,137]. These studies were conducted on very large (>100 km^2) and shallow waterbodies (3–15 m). The most effective method for extracting EC is regression, which has an R^2 value of 0.87 [137].

2.5. Sensors for Assessing Water Quality Parameters

The complementary use of traditional *in situ* monitoring and remote sensing data/products maximizes strengths and minimizes existing weaknesses in lake monitoring. Satellite and airborne (aircraft and unmanned aerial vehicle (UAV)) remote sensing methods are important for evaluating the quality of inland waterbodies [44]. To monitor water quality over time, it is necessary to calibrate and validate satellite and airborne data using *in situ* measurements. Different types of sensors on UAVs, aircrafts, and satellites (Table 2.2) can analyse waterbody radiation at different wavelengths and scales. Multispectral and high-resolution remote sensing devices record reflected or emitted radiation in a few spectral bands that cover a considerable section of the electromagnetic spectrum for inland water quality monitoring [138–141]. Hyperspectral sensors measure continuously across the electromagnetic spectrum in up to 200 narrow spectral bands [142]. Due to their high spatial and spectral resolutions and simultaneous collection of narrower and contiguous bands, hyperspectral sensors can measure and monitor many water quality parameters in lakes [64,124,143]. Spaceborne sensors with visible, infrared, and microwave wavelengths can also monitor water quality. UAVs integrated with various

sensors are practical and efficient for water management and can accurately recover water quality parameters due to its higher spatial and spectral resolution for smaller waterbodies. Data fusion from multiple satellite sensors can provide higher spatial, temporal, and spectral resolution for water quality monitoring [144]. Atmospheric correction and addressing adjacency effects are important for post-processing remote sensing data. Atmospheric correction reduces atmospheric radiation error and improves the evaluation of water quality parameters [40]. UAVs with high-resolution sensors can measure water quality without atmospheric impacts [145]. Factors such as white caps, sun glare, wave motion, and vegetation density can affect remote sensing imagery processing [70]. Reflection and refraction can be limited by collecting data during calm conditions and using a nadir sensor setup [146]. Bathymetric data enhances water column correction by providing information on the depth of waterbodies.

Table 2.2. Overview of satellite and airborne sensors commonly used in aquatic environments

Satellite Sensor	Full Name of the Sensor	Platform	Sensor Type	Agency	Operational Years	Reference
AISA	Airborne Imaging Spectrometer for Applications	Airborne	Hyperspectral	Specim	-	[148]
CASI	Compact Airborne Spectrographic Imager	Airborne	Hyperspectral	Itres Research	-	[149]
Daedalus ATM	Airborne Thematic Mapper	Airborne	Multispectral	Daedalus Enterprises	-	[150]
HyMap	-	Airborne	Hyperspectral	NASA	-	[151]
HyperOCR	Ocean Colour Radiometer	Airborne	Hyperspectral	Sea-Bird	-	[152]
MIVIS	Multispectral Infrared and Visible Imaging Spectrometer	Airborne	Hyperspectral	Italian National Research Council	-	[153]
Envisat MERIS	Medium Resolution Imaging Spectrometer	Satellite	Hyperspectral	ESA	2002-2012	[154]
EO-1 Hyperion	-	Satellite	Hyperspectral	NASA	2000-2017	[155]

Ikonos OSA	Optical Sensor Assembly	Satellite	Multispectral	GeoEye	1999-2015	[156]
ISS HICO	Hyperspectral Imager for the Coastal Ocean	Satellite	Hyperspectral	NASA	2009-2014	
Landsat-5 MSS	Multi-Spectral Scanner	Satellite	Multispectral	NASA	1972-2011	[157]
Landsat-5 TM	Thematic Mapper	Satellite	Multispectral	NASA	1982-2011	[157]
Landsat-7 ETM+	Enhanced Thematic Mapper Plus	Satellite	Multispectral	NASA	1999-present	[158]
Landsat-8 OLI	Operational Land Imager	Satellite	Multispectral	NASA	2013-present	[159]
Landsat-8 TIRS	Thermal Infra-Red Sensor	Satellite	Multispectral	NASA	2013-present	[159]
NOAA AVHRR	Advanced Very High-Resolution Radiometer	Satellite	Radiometer	NOAA	1998-present	[160]
PlanetScope	-	Satellite	Multispectral	Planet	2014-present	[161]
PROBA-CHRIS	Compact High Resolution Imaging Spectrometer	Satellite	Hyperspectral	UKSA	2002-present	[162]
Sentinel-2 MSI	Multispectral Instrument	Satellite	Multispectral	ESA	2015-present	[163]
Sentinel-3 OLCI	Ocean and Land Colour Instrument	Satellite	Multispectral	ESA	2016-present	[164]
Terra ASTER	Advanced Spaceborne Thermal Emission and Reflection Radiometer	Satellite	Multispectral	NASA	2000-present	[165]
Terra MODIS	Moderate Resolution Imaging Spectroradiometer	Satellite	Multispectral	NASA	2000-present	[166]
WorldView-2	-	Satellite	Multispectral	DigitalGlobe	2010-present	[167]

The spatial, temporal, and spectral resolution limitations of numerous contemporary satellite and airborne sensors can restrict the use of remotely sensed data for evaluating water quality. Satellite sensors are preferable for large and very large waterbodies, while airborne and UAV sensors are effective in collecting frequent and wide-ranging data for small and medium-sized waterbodies [147]. Non-satellite remote sensing data is less affected by atmospheric conditions. The cost of hyperspectral or airborne data is one of the primary limitations of using these remote sensing methods for assessing water quality. UAV remote sensing data collection is challenging due to limitations in flight duration, weather conditions, and the data requirements for creating high-quality orthomosaic maps [147]. Remote sensing technologies, such as satellite and airborne sensors, are useful for collecting historical lake ecological indicator data in unstudied lakes without monitoring networks or data. The project budget, spatial and spectral resolution, and geographic coverage area determine the remote sensing platform. Table 2.2 includes regularly used satellite and airborne sensors in aquatic environments.

2.6. Discussion and Recommendations

This paper discusses the use of remote sensing methods for monitoring water quality in lakes. The paper focuses on three main areas: bibliometric analysis of published literature, methods for retrieving water quality using remote sensing, and exploring optically active water quality parameters that may be assessed using remote sensing.

The literature reviewed in this study provides information on the most commonly used sensors and methods for assessing various water quality parameters from satellite and airborne imagery. The Landsat-5 TM sensor is frequently utilized and has a consistently significant value of R^2 for all parameters, regardless of the waterbody size and depth. Different sensors and methods have achieved the best results for different parameters, with some sensors consistently performing well across multiple parameters. For small waterbodies, the most effective satellite sensor for chl-a, turbidity, and SDD retrieval is Landsat-5 TM. For chl-a retrieval from small and medium-sized waterbodies, the most effective airborne sensors are CASI and HyMap, whereas the most effective satellite sensor for recovering chl-a and SDD for medium waterbodies is MERIS. For large waterbodies, the most effective satellite sensor for assessing chl-a and SDD is the Ikonos OSA, while the Landsat-5 TM is the most effective sensor for retrieving turbidity and SDD. The most effective satellite sensors for chl-a retrieval from very large waterbodies are hyperspectral MERIS and multispectral Sentinel-3 OLCI. The most effective sensors for turbidity and SDD retrieval from very large waterbodies include multispectral Landsat-5 TM and Landsat-7 ETM+, and hyperspectral PROBA-CHRIS. For

very large waterbodies, the most effective sensor for retrieving WT is MODIS, for salinity is Sentinel-2 MSI, and for EC is Landsat-8 OLI.

The retrieval of water quality parameters using remote sensing can be achieved through various methods. One commonly used method is the analytical method, also known as the physical method, which is characterized by its theoretical analyses of spectral data. Statistical analyses are commonly used in empirical and semi-empirical methods, which are preferred due to their complexity. On the other hand, ML methods, which are empirical in nature, are known for their computational complexity and ability to manage nonlinear relationships. NNs are essential components of ML and have gained significant importance in solving different tasks in supervised ML [168]. The most successful methods for retrieving chl-a and turbidity from satellite and airborne imagery are the empirical and NN methods, with a high coefficient of correlation (R^2) value of 0.98. The most effective method for extracting salinity from satellite and airborne images is the NN method with a high correlation coefficient (R^2 = 0.94). Regression is the most effective algorithm for retrieving SDD and EC, while the empirical method is the most suitable for retrieving WT.

Satellite data is acknowledged as a useful tool for monitoring water quality parameters in lakes. Unlike *in situ* measurements, satellite imagery gathers water quality data simultaneously using a grid-based method. The concept of using remote sensing technology for water quality monitoring is based on the different spectral characteristics of pure water compared to contaminated or saturated water. The properties of individual water quality parameters are analysed in relation to their interaction with the spectrum to identify bands. These bands are combined to obtain the parameter's value and its distribution over the lake [44].

However, there are limitations to remote sensing methods, including spatial, temporal, and spectral resolutions of satellite systems, the optical complexity of inland waters, atmospheric and cloud interference, the need for proper calibration and validation with *in situ* measurements [44], errors in creating standard satellite products like atmospheric correction [169], and the cost of commercial satellite imagery or deploying aircrafts or UAVs for study purposes. Various satellite systems, such as Landsat, Sentinel-2, and Terra, are used in the literature to estimate water quality metrics, but for smaller lakes, the selection of available satellite sensors is limited. Satellites with spatial resolution like Terra MODIS (260 m, 500 m, and 1000 m), Envisat MERIS (260 m × 300 m), or OrbView-2 SeaWiFS (260 m, 500 m, and 1000 m) are not recommended due to their tendency to overgeneralize the state of the parameters. This especially applies to parts of smaller lakes with stronger external influences (the influence of ballast water or nutrients from agricultural land). For the purpose of determining amplitude

values on an annual level, bands with a higher spatial resolution can be used; however, if smaller changes in parameters are to be observed in shorter periods of time (day, week, month), it is necessary to provide bands with a better spatial resolution. UAVs with integrated sensors are effective for water management and can accurately measure water quality parameters in smaller waterbodies. Their higher spatial and spectral resolution makes them practical and efficient for this purpose. The selection of satellite and aerial images should depend on the dynamics of parameter changes within the lake and the lake's size, rather than just the availability of images. To conduct effective remote research, it is important to familiarize oneself with the lake and its environment, understand the seasonal cycle of submerged macrophytes and phytoplankton, identify external sources of water flow into the lake, consider meteorological conditions during specific times of the year (including water temperature, water levels, dry spells, and high-water periods following heavy rainfall prior to measurement), and understand agricultural practices around the lake. The correlation between satellite and airborne imagery and *in situ* values varies depending on the size and depth of the waterbodies. The research suggests that small waterbodies have the highest correlation for retrieving turbidity, medium waterbodies for chl-a and WT, large waterbodies for SDD, and very large waterbodies for salinity and EC. Deep waterbodies have the highest correlation for retrieving WT, turbidity, and SDD, while very shallow waterbodies have the highest correlation for assessing chl-a, and shallow waterbodies have the highest correlation for retrieving salinity and EC. Extensive temporal statistical analysis of *in situ* data (specific water quality parameters) along with meteorological and hydrological data (water level, lake depth, and dry and rainy periods) is recommended to identify correlations and mitigate negative effects. Modelling based on specific conditions can provide insight into the movement of parameter concentrations on the lake's surface. The development of ML and NN methods aligns well with this scenario, as it leverages the progress in computer technology and storage capacity to enhance productivity and retain data for future studies. In this way, a system is established that acquires and applies all acquired "knowledge" (representing stored results) for subsequent analyses.

The range of a specific parameter measured *in situ* inside the lake throughout the study duration and the length of the study (year, season, month, week, and day) are crucial pieces of information for estimating water quality parameters based on remote sensing. The time period with the highest correlation between satellite and airborne imagery and *in situ* values varies for different water quality parameters. The highest correlation between satellite and airborne imagery and *in situ* values for retrieving turbidity, SDD, and salinity is found within a time frame of 2–3 months. For EC, the highest correlation is achieved in studies lasting one month,

while for chl-a and WT, it takes studies lasting more than six months up to several years to obtain the highest correlation. When water quality measurements are determined annually (over twelve months), all influences on the lake (both internal and external) are averaged. The parameter values are observed throughout the year, but variations due to varied weather conditions (seasons and meteorological data) and other external parameters are not included. The purpose of a forecasting model is to predict extreme events that significantly impact the lake, such as heavy rainfall during intense agricultural activity or the intrusion of seawater during an extremely dry period, in order to minimize their impact on the lake's water quality. Following a thorough examination of how external influences impact internal parameters and the dispersion of water quality parameters in the lake, it is essential to choose suitable satellite or airborne data to achieve optimal outcomes. This pertains to the spatial resolution of imagery to represent the frequency of changes in water quality parameter values, the spectral bands of sensors for calculating optically active water quality parameters, and the temporal resolution of the system. Ensuring that *in situ* measurements are taken on the day of the satellite's overpassing (or in a window of a few days prior to or after the overpass) allows for conducting correlation analysis between the observed parameter values from *in situ* measurements and calculated parameter values from satellite data.

The synergy of computer resources, remote sensing methods and data, GIS multicriteria analysis, decision support systems, and ML methods enable a high-quality assessment of water quality parameters. The authors' knowledge collected in this review and previous general and specific knowledge about the considered problem and the field of remote sensing resulted in the creation of a framework for monitoring water quality parameters in the lake, supported by remote sensing methods (Figure 2.4).

The proposed working framework (Figure 2.4) includes three main components: (1) conducting a literature review to gain theoretical knowledge, (2) practical work involving data collection and analysis, and (3) analysing the results for decision-making. The theoretical part of the workflow includes the following:

(1) Conducting a thorough time analysis of the waterbody and its surroundings (for a period of 10 to 15 years, utilising meteorological and *in situ* data) under various conditions (dry period, rainfall period, etc.).
(2) Determining and evaluating all internal and external factors that may influence water quality.
(3) Referring to relevant scientific research.
(4) Determining which water quality parameters will be included in the study.

(5) Determining the study period based on historical analysis by recognizing various environmental scenarios such as seasons, dry period, and heavy rainfall. If a lake is susceptible to ice or snow, the study period should focus on the coldest months when the lake is affected by these conditions. Similarly, if a brackish lake experiences dry periods leading to increased salinity due to evaporation and low water influx, the study period should include this phenomenon.

(6) Analysing temporal statistical data and water quality parameter distribution throughout the waterbody, taking into account hydrological model of the lake's bathymetry and important tributaries, to determine the sampling grid and the quantity and locations of *in situ* measurement locations.

(7) Choosing the appropriate satellite or airborne sensor(s) for data collection based on spectral characteristics, number of bands, spatial resolution, time resolution (if the system is a satellite), lake size and depth, and chosen water quality parameters.

The operational features of the workflow can be determined by considering certain factors, as follows:

(1) *In situ* measurement collection is based on defined study period and sampling grid; data collection should occur on the day of the chosen sensor's overpassing or in a small window frame (± 4 days) around that day.

(2) *In situ* data should be analysed by removing outliers and normalizing the data. This is important in order to make the measured values for different parameters comparable, even if they are measured in different units (e.g., chl-a is usually measured in µg/L, while WT is measured in °C).

(3) A total of 30% of *in situ* measurements shall be utilized for validation purposes, while the remaining 70% shall be utilized to calibrate the calculated values of water quality parameters via the spectral band combinations of the chosen sensor(s).

(4) To ensure accurate remote sensing data, it is important to collect the data using a suitable satellite, aircraft, or UAV platform.

(5) All imagery should be resampled to the same spatial resolution and undergo necessary corrections such as geometric, radiometric, and atmospheric correction. Any obstructions like clouds, haze, or other obstacles covering water pixels on an image should be masked out. Satellite measurements use a grid-based method to gather water quality data simultaneously, so the reflectance values of different water sampling locations are extracted to analyse the spectral characteristics.

(6) Remote sensing technology is used to monitor water quality by analysing the interaction of water quality parameters with the spectrum and identifying specific bands. These bands are combined as single bands, band ratios, and band combinations to obtain the parameter's value and its distribution over the lake.

(7) A correlation analysis is performed between measured *in situ* data and band combinations from selected sensors. This analysis is conducted on a training dataset in order to determine the best method (e.g., analytical, empirical, or ML), which is the one with the highest correlation coefficient.

(8) The developed models are validated using 30% of *in situ* measurements as a testing dataset.

The final part of the workflow involves analysing the results for decision-making, as follows:

(1) Conducting spatiotemporal distribution analysis and generating accurate spatial distribution maps based on validation results.

(2) Optimizing sampling stations by using spatiotemporal analysis and GIS multicriteria analysis. This involves considering various influencing factors such as key water quality parameters, meteorological data, and environmental influences (e.g., distance to the tributaries and land cover-land use data).

(3) Creating a database of outputs for different lake environment scenarios, which can be used by ML methods to simulate and forecast lake behaviour in similar scenarios.

Recommendations to the authorities in charge of managing the lake how to improve lake resource management based on data collection, analysis, and modelling. Developed models can be used by local authorities to obtain surface water quality parameters of the lake during periods with similar weather conditions as the ones used for model generation. This approach offers reduced cost and time while maintaining reasonable accuracy.

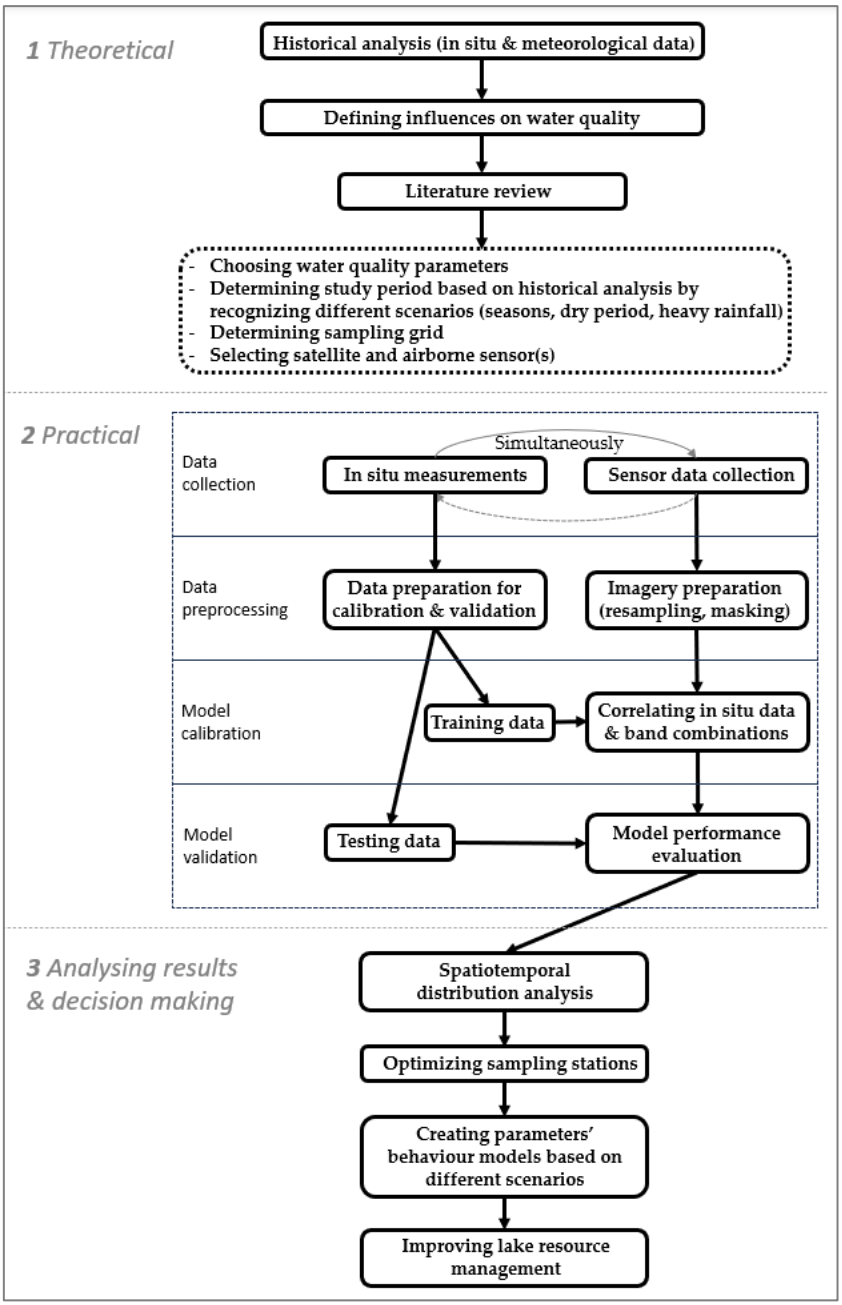

Figure 2.4. Workflow proposal for monitoring and assessment of water quality parameters in lakes using remote sensing methods

2.7. Conclusion

Conducting effective remote research on lakes requires a comprehensive understanding of the lake and its environment, including factors such as submerged macrophytes, phytoplankton, hydrology, bathymetry, meteorological conditions, and agricultural practices. Analysing year-round fluctuations from historical water quality data and categorizing data based on common criteria can help identify significant seasonal variations. The use of satellite and airborne imagery, along with *in situ* data and statistical analysis, can help identify correlations and

mitigate negative effects. Empirical methods are commonly used for monitoring and analysing water quality due to the complexity of analytical methods, but ML and NN methods show promise in simplifying and analysing large datasets with high accuracy. Modelling based on specific conditions can provide valuable insights into parameter concentrations on the lake's surface. By leveraging advancements in computer technology and storage capacity, a system can be established to acquire and apply knowledge for future analyses. Overall, remote research methods offer valuable insights into lake ecosystems and water quality.

The proposed workflow aims to provide guidance for effectively monitoring and managing the quality of lakes. It combines theoretical knowledge about the study area, practical work regrading data collection, and data analysis to provide a comprehensive approach to understanding and improving water quality. Furthermore, the framework includes conducting thorough analysis, choosing appropriate sensors, and incorporating remote sensing technology to generate accurate water quality models and spatial distribution maps. The output generated by the workflow has multiple benefits, including scientific purposes, decision-making, and resource management. The proposed framework aims to enhance global water quality monitoring by integrating different data sources and methods to understand spatiotemporal water quality trends.

The review highlights the importance of integrating remote sensing methods using *in situ* measurements and computer modelling to improve the understanding of water quality. Future research should focus on (1) the development of advanced technologies, such as advanced algorithms, for in-depth statistical analyses of data (meteorological and measured *in situ* water quality parameters); (2) selection of a sampling grid of strategic *in situ* measurements (according to the distribution and concentration of a particular water quality parameter) and time period, (3) integration of very high resolution spectral data (the selection of spectral bands and increased use of hyperspectral sensors for estimating water quality parameters), and (4) integration of ML and NN algorithms for effective water quality problem solving (use of modern computer technologies in modelling different scenarios of impact on lake water). These technologies can enhance the ability to detect and respond promptly to water quality issues, optimize sampling locations and time frames, estimate optically inactive parameters indirectly, and facilitate real-time monitoring and timely response to potential risks or anomalies. Additionally, ML and NN algorithms can provide valuable insights and predictive models for future water resource management, especially in dynamic and ever-changing water systems.

3. Spatiotemporal Water Quality Analysis of Vrana Lake, Croatia

This chapter has been published as: *Batina, A.; Cukrov, N.; Ćuže Denona, M. (2025). Spatiotemporal water quality analysis of Vrana Lake, Croatia.* Open Geosciences, 17*(1); 20250817. doi: 10.1515/geo-2025-0817*.

Conceptualization, A.B., N.C., and M.Ć.D.; methodology, A.B., N.C., and M.Ć.D.; validation, N.C. and M.Ć.D.; investigation, A.B.; resources, A.B., N.C., and M.Ć.D.; data curation, A.B., N.C., and M.Ć.D.; formal analysis, A.B.; writing—original draft preparation, A.B.; writing—review and editing, A.B., N.C., and M.Ć.D.; visualization, A.B.; supervision, N.C.; project administration, A.B.; funding acquisition, N.C. All authors have read and agreed to the published version of the manuscript.

Abstract: The comprehensive analysis of spatiotemporal variations in water quality is crucial for ecosystem management. This study analyses and maps spatiotemporal variations in water quality at Vrana Lake, a coastal shallow lake in Dalmatia, Croatia. We established a monitoring grid of 20 stations and conducted monthly *in situ* measurements of seven water quality parameters from July 2023 to June 2024 using multiparameter probe. We measured electrical conductivity, turbidity, salinity, water temperature, dissolved oxygen, oxygen saturation, and chlorophyll-a. We analysed the correlation between these parameters, water level, and meteorological factors over a year and the impact of climate change over the 34 years. Additionally, we evaluated 15 geographic information system (GIS) spatial interpolation methods for mapping the distribution of water quality parameters, using root mean square error (RMSE) and mean error (ME) metrics. The vertical stratification analysis revealed that the lake's shallow nature allows effective assessment through median values. Key findings highlighted that air temperature, precipitation, and wind significantly affect water quality dynamics. The Simple Kriging – Trend emerged as the best GIS spatial interpolation method for modelling water quality parameters. Overall, this study enhances the understanding of water quality variations and their implications for ecosystem health in coastal shallow lakes.

Keywords: climate change, coastal shallow lake, distribution map, ecosystem management, GIS spatial interpolation, *in situ* measurements, meteorological factors, monitoring grid, Simple Kriging – Trend, vertical stratification

3.1. Introduction

Water quality monitoring is a vital segment of effective management and preservation of water ecosystems [170], particularly in the context of climate change threats to lake ecosystems [5]. The intergovernmental panel on climate change (IPCC) [171] anticipates that rising global temperatures and extreme weather events, such as heavy precipitation, will affect coastal ecosystems and increase local flooding. Climatic factors, such as precipitation (PP), air temperature (AT), wind speed (WS), and sunshine hours (SH), are expected to significantly influence lake water quality [172], with warmer temperatures and heavy rainfall contributing to nutrient release and pollution [173]. The ongoing issue of eutrophication in lakes has prompted extensive research into the interplay between climate change and water quality [172–174].

Numerous models and methods have been developed to evaluate spatial and seasonal variations in water quality parameters. Commonly used methods include water quality index [175–177] and tropic state index [173], alongside multivariate statistical analysis like principal components analysis [178] and cluster analysis [179]. Moreover, advancements in data mining [180] and machine learning methods [172,181] have proven effective in modelling water quality parameters and identifying pollution sources. Utilizing spatial data science and geographic information system (GIS) is essential for addressing pressing issues such as climate change, as geospatial methods play a crucial role in comprehending complex environmental challenges and monitoring [182,183].

The need for a robust and optimized monitoring network is emphasized to monitor water quality trends and inform environmental management strategies [27,178,179]. Recent studies also highlight the significance of understanding vertical variability in water quality parameters, which can be influenced by factors such as nutrients level, light penetration, and temperature gradients within lakes [170,184,185].

GIS-based spatial interpolation methods are used to estimate water quality parameters in locations lacking direct measurements. Frequently used methods are inverse distance weighted [186,187], universal Kriging, and ordinary Kriging methods [188,189]. In addition to water quality studies, GIS software has been extensively applied in broader geographic analyses. For instance, Vujović et al. (2024) [190] used ArcGIS and QGIS to analyse geomorphometry in the Ibar River basin, while Oseke et al. (2021) [191] applied GIS and a water quality index to assess reservoirs affected by water diversion. Aleksova et al. (2023) [192] modelled erosion and mass movements in North Macedonia using GIS-based multi-hazard assessments, and Durlević

(2021) [193] evaluated flood and landslide susceptibility in Serbia's Mlava River Basin using similar tools. Recent studies have focused on comparison between different GIS spatial interpolation methods for groundwater levels [194] and sediment distribution in coastal areas [195]. However, there is a lack of studies comprehensively evaluating the effectiveness of different GIS spatial interpolation methods specifically for lake water quality assessment. The study by Ouabo et al. (2020) [196] emphasizes the importance of selecting suitable interpolation methods, particularly considering the non-normal distribution of water quality parameters, to avoid biased results [197].

This study is part of a broader research initiative aimed at enhancing lake water quality monitoring and assessment through the integration of *in situ* measurements, GIS multicriteria analysis, satellite imagery, and machine learning. In the initial phase of the research initiative, Batina and Krtalić (2024) [9] established a comprehensive framework that includes a theoretical analysis of lake dynamics, operational data collection, and spatiotemporal distribution analysis. Building on that work, in this study, we aimed to investigate the seasonal and spatial variations in water quality parameters in Vrana Lake in Dalmatia, Croatia, where eutrophication issues, exacerbated by nutrient influx, have led to phytoplankton and cyanobacteria growth, causing the extinction of macrophytes [198]. A study by Trbojević et al. (2022) [199] indicates macrophytes absence in 2020 and 2021 in the lake, with chlorophyll-a (Chl-a) concentration serving as a key indicator of this ecological change [5].

In this study, we aim to investigate the seasonal and spatial variability of water quality parameters in Vrana Lake, Croatia, and to analyse their correlation with water level (WL) and meteorological factors over a 12-month monitoring period. Additionally, we assess the long-term impact of climate change on the lake ecosystem using 34 years of historical WL and meteorological data spanning from 1990 to 2023. A key objective is to evaluate and identify the most suitable GIS spatial interpolation method for accurately mapping the distribution of water quality parameters. This research is significant for advancing lake monitoring practices, supporting adaptive management strategies in response to climate change, and providing a foundation for future studies utilizing GIS multicriteria analysis, remote sensing, and machine learning.

3.2. Methods

3.2.1. Study Area and Monitoring

Vrana Lake, located in Dalmatia near the eastern Adriatic coastline, is the largest natural lake in Croatia (Figure 3.1A), covering an area of approximately 30 km^2 [200], and is situated

between 43°51′–43°57′N latitude and 15°30′–15°39′E longitude (WGS84 coordinate system). Its ecological characteristics and biodiversity have led to its protection as a nature park. The lake is characterized by shallow water that fluctuates seasonally, with higher levels in winter and spring (highest mean WL was 1.28m above sea level (MASL) from 1990 to 2023) and lower levels in summer and autumn (lowest mean WL was 0.41 MASL from 1990 to 2023), based on data provided by the Croatian Meteorological and Hydrological Service (DHMZ) and visualized in Figure 3.2. The lake's shallowness and geolocation make it particularly susceptible to wind influences that promote water column mixing [201]. In May 2023, heavy rainfall resulted in unusually high WL in subsequent months (Figure 3.2), highlighting the importance of considering meteorological and WL data in understanding water quality [202].

Several factors contribute to the WL dynamics of Vrana Lake, including its connections to the Adriatic Sea, freshwater tributaries, brackish submerged groundwater discharge in the lake, underground karst fissures, and evaporation. During periods when WL drops below sea level, the lake's salinity increases significantly due to the seawater influx through the artificial Prosika canal (Figure 3.1A). Additionally, the lake is affected by underground karst fissures along its western edge and the Jugovir brackish submerged groundwater discharge in the southern part, especially during strong south winds and high tides [203]. On the other hand, freshwater from surrounding karst fields and springs enters the lake through the Kotarka channel and the Lateral channel in the northern part (Figure 3.1A). Rainwater runoff from the northern and eastern hills is another significant source of water [198].

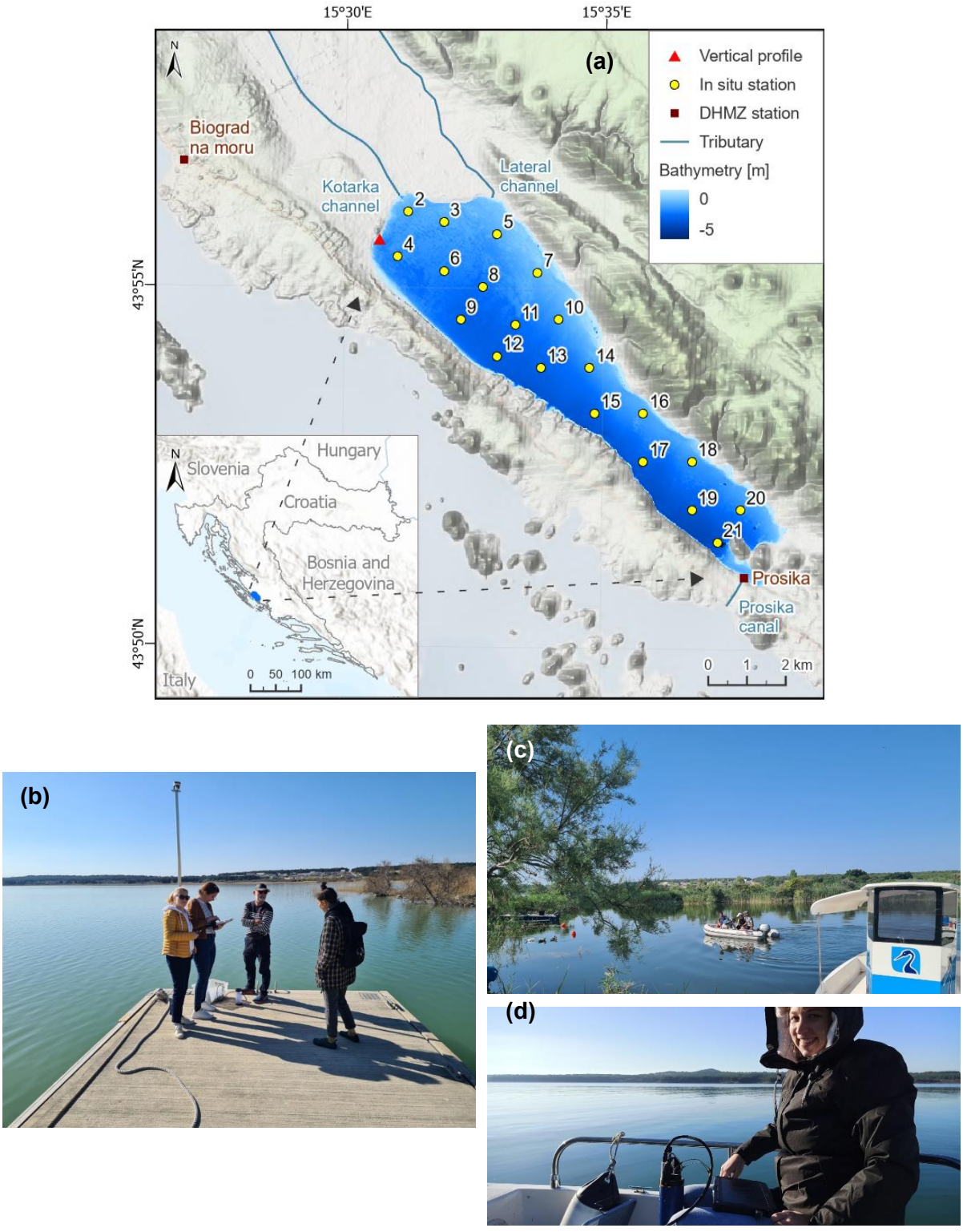

Figure 3.1. An overview of (a) Vrana Lake position and in situ *stations, (b) preparation for measuring vertical profiles, and (c) and (d)* in situ *monitoring*

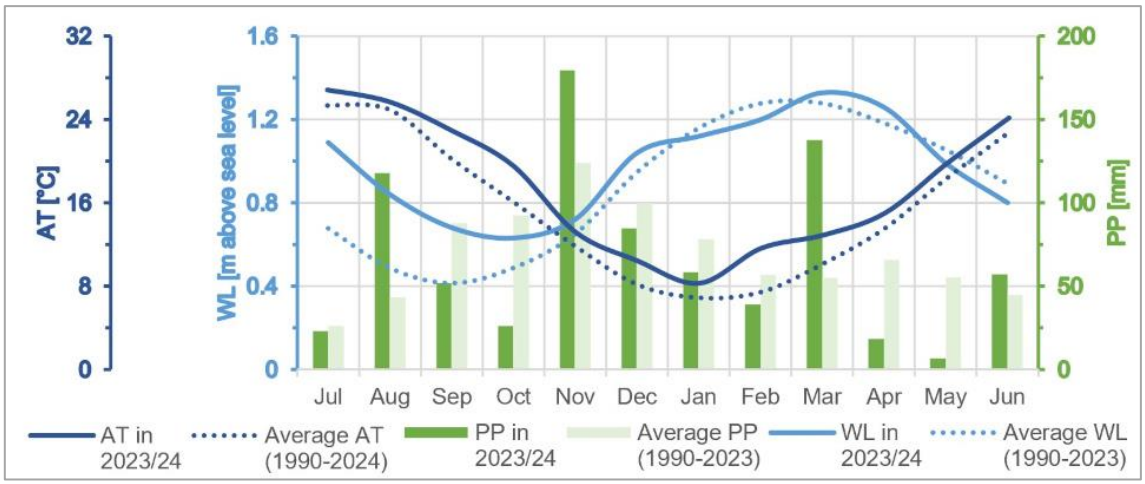

Figure 3.2. Comparison of AT, PP, and WL data for the research period of 2023/24 against historical averages

3.2.2. Data Collection

In this study, we developed a comprehensive monitoring grid of 20 *in situ* stations for monthly *in situ* measurements of seven water quality parameters, including electrical conductivity (EC), turbidity, salinity, water temperature (WT), dissolved oxygen (DO), oxygen saturation (SO), and Chl-a, from July 2023 to June 2024 [204]. Furthermore, we analysed correlations between these parameters, WL, and six meteorological factors, such as AT, WS, PP, SH, relative humidity (RH), and atmospheric pressure (AP), in a 12-month period to understand their influence on lake ecosystem health. Additionally, we built upon the work of Rubinić and Katalinić (2014) [205] by analysing 34 years of WL and meteorological data (1990–2023), including AT and PP, to evaluate the more recent impact of climate change on the lake. Finally, we evaluated 15 GIS spatial interpolation methods to determine the best method for mapping water quality parameters, using cross-validation, root mean square error (RMSE), and mean error (ME). The flowchart is shown in Figure 3.3.

The lake's ecological health is further impacted by anthropogenic influence from its tributaries [206] and influx of seawater via the Prosika canal, particularly during low WLs. To address these ecological concerns, we developed a new comprehensive monitoring grid designed to provide sufficient data for remote sensing and machine learning applications in subsequent research. Previously, monitoring efforts were limited to one station by the Water Institute Josip Juraj Strossmayer and three stations by the Public Institution Vransko Jezero Nature Park. We incorporated these existing stations and added new ones to ensure comprehensive spatial coverage. The 20 monitoring stations were strategically positioned (Figure 3.1A), considering lake's characteristics, existing monitoring stations, the time required to complete the

measurements by a vessel, and the hydrological model, including the lake's bathymetry, tributaries, and connection to the sea [176].

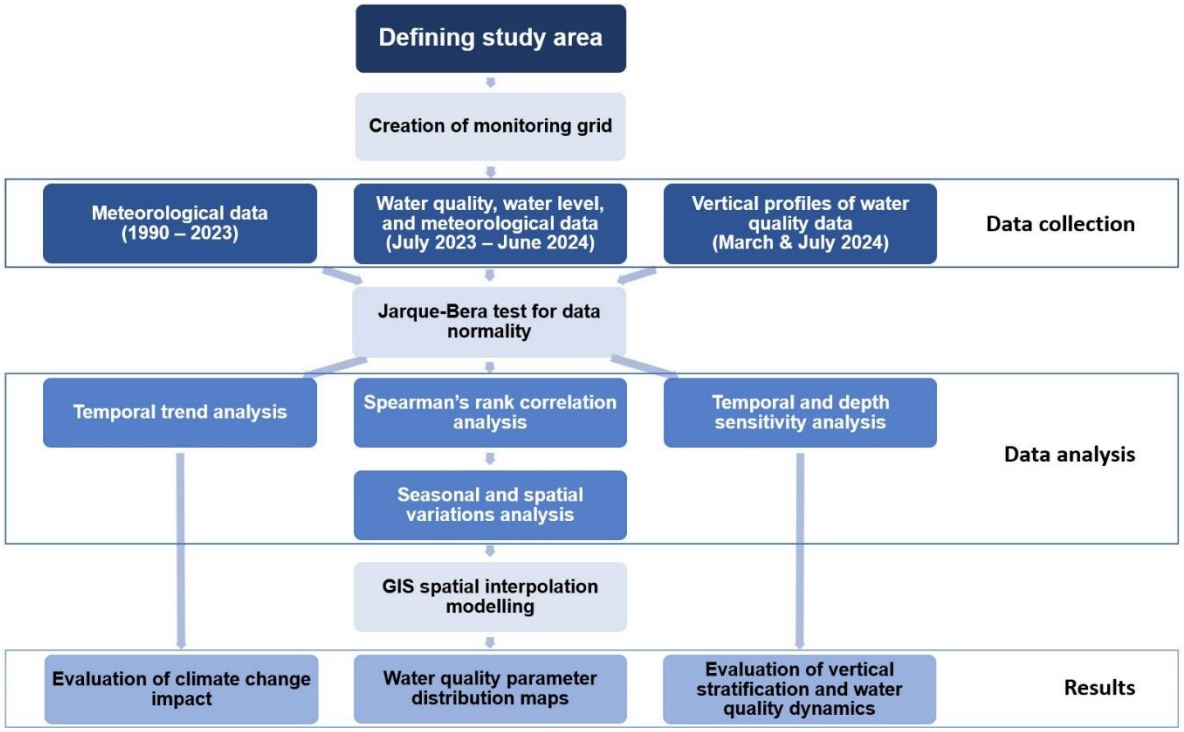

Figure 3.3. Flowchart illustrating the study's methodology

We delineated the lake boundary using PlanetScope satellite imagery [207] and the Normalized Difference Water Index [208], focusing on the month of October 2023, when the WL was at its lowest during our year-long research period (Figure 3.2).

DHMZ provided historical monthly data on average AT and total PP from 1990 to 2023 for the Biograd na Moru station (43°56′44.5″N, 15°26′52.8″E, WGS84), along with average WL data from the Prosika station (43°51′0.3″N, 15°37′45.3″E, WGS84) (Figure 3.1A, Table A13). Additionally, they supplied daily meteorological data from the Biograd na Moru and Zadar stations, as well as WL data from the Prosika station, for our research period from July 2023 to June 2024 (Table 3.1 and Table A14). We analysed meteorological andWL parameters for each measurement day, except for PP, which we assessed based on the amount from 3 days prior. We adopted this methodology because we aimed to conduct *in situ* measurements on sunny, non-cloudy days, and we plan to integrate satellite data for specific measurement dates in our future research.

Researchers from Ruđer Bošković Institute collected *in situ* data on seven physicochemical and biological parameters in the lake (Table 3.1). Using the YSI EXO2 (YSI, USA) multiparameter probe, the team collected vertical profiles on a monthly basis from July 2023 to June 2024

(Figure 3.1C and Figure 3.1D). These measurements were conducted between 8:00 and 13:00 at 20 designated monitoring stations (Table A15). Salinity is determined automatically from the sonde conductivity and temperature readings according to algorithms found in Standard Methods for the Examination of Water and Wastewater [209]. The use of the practical salinity scale results in values that are unitless, since the measurements are carried out in reference to the conductivity of standard water at 15°C [210]. Optical sensors in probes are increasingly important for real-time water quality assessment in environmental applications [211]. Due to poor weather conditions, we had to postpone our fieldwork scheduled for November 2023 to December 4th, and we conducted the December survey on the 19th, while all other measurements were conducted in their respective months.

Table 3.1. Summary of the dataset and probe specifications

Type	**Parameter**	**Abbr-eviation**	**Unit**	**YSI EXO2** [210]	
				Range	**Accuracy**
Water quality parameters	Chlorophyll-a	Chl-a	µg/L	0-400 µg/L	—
	Electrical conductivity	EC	dS/m	0-100 dS/m	±0.5% of reading or 0.001 dS/m
	Turbidity	—	FNU	0-999 FNU	0.3 FNU or ±2% of reading
	Salinity	—	—	0-42	±0.1
	Water temperature	WT	°C	-5 to 35°C	±0.01°C
	Dissolved oxygen	DO	mg/L	0-20 mg/L	±1% of reading or 0.1 mg/L
	Oxygen saturation	SO	%	0-200%	±1% of reading or 1% air sat.
				Meteorological station	
Meteorological parameters	Air temperature	AT	°C	Biograd na Moru	
	Wind speed	WS	Beaufort number	Biograd na Moru	
	Relative humidity	RH	%	Biograd na Moru	
	Atmospheric pressure	AP	hPa	Zadar	
	Amount of precipitation	PP	mm	Biograd na Moru	
	Sunshine hours	SH	h	Zadar	
—	Water level	WL	m	Prosika	

3.2.3. Data Analysis

3.2.3.1. Analysis of Meteorological and Water Quality Parameters

We used the Jarque–Bera test to assess the normality of historical monthly meteorological data, as well as meteorological and WL data for the research period [179]. The test evaluates whether sample data exhibit skewness and kurtosis consistent with a normal distribution, with p-values interpreted against a significance threshold of 0.05. For variables that did not meet the normality assumption, a cube root transformation was applied in Excel to normalize the data.

Furthermore, we used the Jarque–Bera test to assess the normality of raw water quality parameters such as Chl-a, EC, turbidity, salinity, WT, DO, and SO [179]. To address deviations from normality, we applied logarithmic, square root, cube root, and Box-Cox transformation using Esri ArcGIS Pro 3.2.

3.2.3.2. Vertical Profiles and Temporal Sensitivity

We conducted two separate measurements in March and July 2024 to analyse the temporal and depth sensitivity of seven physicochemical and biological parameters (EC, turbidity, salinity, WT, DO, SO, and Chl-a) at a single station (Figure 3.1A – point marked as "Vertical profile," Figure 3.1B). We measured vertical profiles every 30 min using the multiparameter probe, with the March measurement occurring from 9:30 to 12:30 and the July measurement from 11:00 to 13:30. We analysed and visualized the data using Microsoft Excel, finding patterns in vertical stratification and mixing within the water column.

3.2.3.3. Correlation Between Water Quality and Meteorological Parameters

We performed Spearman's rank correlation analysis to explore the relationships between meteorological and water quality parameters. This non-parametric test helped us to evaluate correlations among variables with non-normal distributions [179]. We calculated the median values for monthly water quality data from all relevant monitoring stations, as shown in Table A15, and then subjected these values to Spearman's rank correlation analysis using Excel. We analysed meteorological and WL data for each measurement day, while PP was analysed based on the total amount over the three days leading up to each measurement day.

3.2.3.4. GIS Spatial Interpolation Methods and Spatial Resolution

We classified the GIS spatial interpolation methods into two categories in our research: deterministic and geostatistical. Deterministic methods rely on mathematical functions, while geostatistical methods utilize statistical and mathematical algorithms [212]. Since our analysis

involved non-normally distributed data collected over several months, we focused on interpolation methods that do not require normal distribution, excluding Radial Basis Function due to its inability to handle coincident measurements.

We evaluated 15 GIS spatial interpolation methods (5 deterministic and 10 geostatistical) in Esri ArcGIS Pro 3.2 using the *Exploratory Interpolation* tool. The methods were ranked based on cross-validation, RMSE, and ME, to create accurate spatial distribution maps of water quality parameters [186], which are vital for GIS-based multicriteria assessments of water quality in subsequent research. These methods included Simple Kriging (SK) – Default, SK – Optimized, SK – Trend, SK – Trend and transformation, Ordinary Kriging – Default, Ordinary Kriging – Optimized, Universal Kriging – Default, Universal Kriging – Optimized, Empirical Bayesian Kriging (EBK) – Default, EBK – Advanced, Kernel (Local Polynomial Interpolation), Inverse Distance Weighted – Default, Inverse Distance Weighted – Optimized, Global Polynomial Interpolation – Second order, and Global Polynomial Interpolation – Third order (Table 3.2). Additional information about these methods can be found in "Exploratory Interpolation (Geostatistical Analyst)" [213]. Our objective was to determine the best interpolation method for Vrana Lake using *in situ* data for each parameter.

Table 3.2. List of GIS interpolation methods

Grouping of interpolation method	GIS spatial interpolation method
Geostatistical	EBK – Advanced
	EBK – Default
	Ordinary Kriging – Default
	Ordinary Kriging – Optimized
	SK – Default
	SK – Optimized
	SK – Trend
	SK – Trend and transformation
	Universal Kriging – Default
	Universal Kriging – Optimized
Deterministic	Global Polynomial Interpolation – Second order
	Global Polynomial Interpolation – Third order
	Inverse Distance Weighted – Default
	Inverse Distance Weighted – Optimized
	Kernel (Local Polynomial Interpolation)

We ranked results using two criteria: lowest RMSE and ME closest to zero. There metrics, implemented in the *Exploratory Interpolation* tool in ArcGIS Pro 3.2, are widely recognized in similar studies [188,195]. RMSE measures the average deviation between predicted and measured values, with a smaller value indicating higher prediction accuracy [214]. RMSE is mathematically expressed by the formula [214]:

$$\mathrm{RMSE} = \sqrt{\frac{\sum_{i=1}^{n}(\hat{z}(s_i)-z(s_i))^2}{n}} \quad (3.1)$$

where $\hat{z}(s_i)$ is the predicted value for the i^{th} observation, $z(s_i)$ is the actual value for the i^{th} observation, and n is the number of observations.

ME is the average of cross-validation errors, ideally close to zero. It indicates model bias: a positive ME suggests overprediction, while a negative ME indicates underprediction [214]. ME is mathematically expressed by the formula [214]:

$$\mathrm{ME} = \frac{\sum_{i=1}^{n}(\hat{z}(s_i)-z(s_i))}{n} \quad (3.2)$$

where $\hat{z}(s_i)$ is the predicted value for the i^{th} observation, $z(s_i)$ is the actual value for the i^{th} observation, and n is the number of observations.

Grid resolution is a popular format for spatial modelling due to its ideal properties, such as an orthogonal matrix and fixed resolution [215]. The placement of monitoring stations in the lake is not strictly based on a grid system, but rather on a more random distribution with uneven distance between monitoring stations due to the existing monitoring stations and the lake's characteristics. The formula for calculating the coarsest legible grid resolution for spatial modelling based on random sampling is [215]:

$$p = 0.25 * \sqrt{\frac{A}{N}} \quad (3.3)$$

where A is the surface of the study area in m^2 and N is the total number of observations.

3.3. Results

3.3.1. Temporal Trends of Meteorological Factors

The Jarque–Bera test confirmed that all historical monthly meteorological data exhibited a normal distribution annually, with p-values consistently exceeding the significance level of 0.05. Consequently, we used mean values to derive key annual metrics.

The WL values were historically low in 1990, 2008, and 2012, with measurements of 0.28, 0.32, and 0.31m, respectively (Table A13, Figure 3.4). These low WL values corresponded with low PP levels in 1989, 2007, and 2011, measured at 555.50, 516.30, and 435.90 mm, respectively (Table A13, Figure 3.4). The analysis of WL and PP historical data over 34 years

revealed an increasing WL trend of 3.12mmper year and an increasing PP trend of 2.28mm per year (Table A13, Figure 3.4). Average AT increased by 1.54°C during the same period, with a yearly increase trend of 0.05°C since 1990 (Table A13, Figure 3.4).

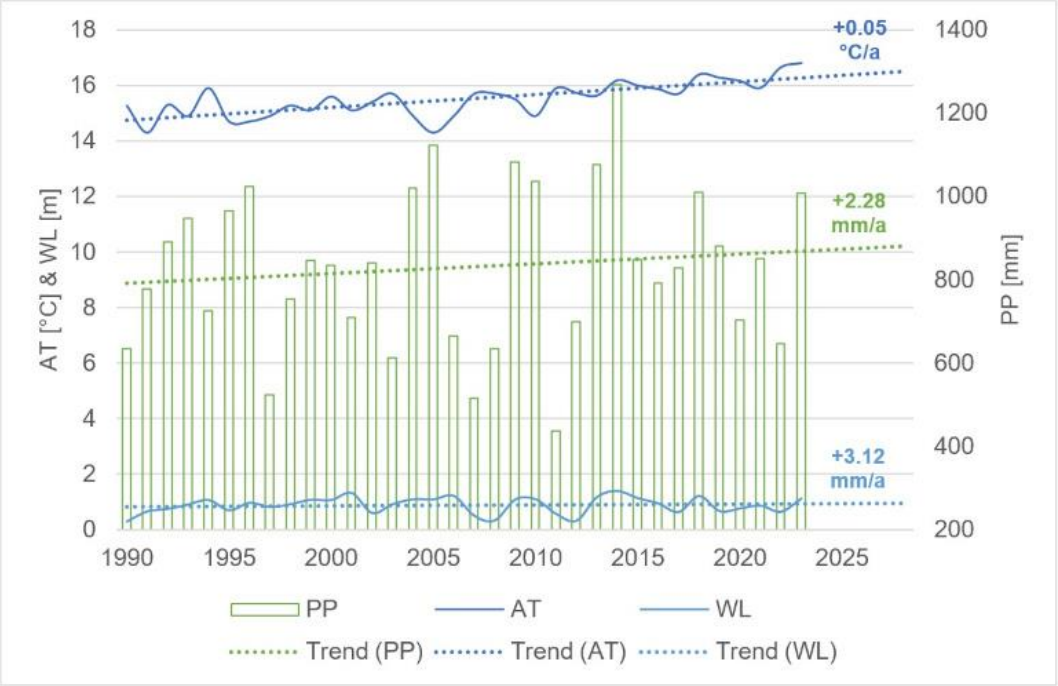

Figure 3.4. Annual average and trends of AT, PP, and WL during 1990-2023

During our research period, elevated WL prevented significant interchange between sea and lake water, with the lowest monthly average measured at 0.69 MASL (Figure 3.2). WL values were higher than historical averages due to heavy rainfall in May 2023 and subsequently dropped below historic averages in January and February 2024, which we attributed to lower monthly PP at the end of 2023 and the beginning of 2024. This downward trend continued into early spring 2024, leading to further decreases in WL during May and June. Throughout the research, average monthly AT remained consistently higher than historic averages (Figure 3.2).

3.3.2. Assessing Vertical and Temporal Variability in Water Column Data

We collected vertical profiles at the northern lake station (Figure 3.1A – point marked as "Vertical profile" at 15°30′40″E, and 43°55′41″N, WGS84) on March 15th and July 19th, 2024. On March 15th, we measured a water depth of 2.95m with a WL of 1.41 MASL, while on July 19th, the depth decreased to 2.12m with a WL of 0.58 MASL (Figure A1). We also observed the temporal sensitivity of parameters at the same monitoring site at 30 min intervals (Figure A2). Despite the difference in water depth and time frame of the two measurements, we found that the readings from both dates were comparable in relative units, indicating temporal sensitivity with change per hour and vertical variability with change per meter.

We observed that salinity and EC remained stable across all depths and time throughout our campaigns, with negligible differences of ≤0.01 in their respective units between the lowest and highest values for each parameter. We observed a slight increase in DO over time, with rates of 0.04 mg/L per hour in March and 0.12 mg/L per hour in July, while depth had little effect on it (decrease of 0.02mg/L per meter in March and decrease of 0.07 mg/L per meter in July). WT and SO decreased with depth, showing a decrease of 0.44°C per meter for WT and 1.11% per meter for SO in March and a decrease of 0.17°C per meter for WT and 1.15% per meter for SO in July. However, both parameters increased over time due to changes in AT, with an increase of 0.31°C per hour for WT and 1.20% per hour for SO in March and increase of 0.21°C per hour for WT and 1.73% per hour for SO in July. We also recorded fluctuations in Chl-a and turbidity, with Chl-a increasing by 0.45 µg/L per meter in March and 0.35 µg/L per meter in July. Turbidity experienced an increase of 0.52 FNU per meter in March and 0.49 FNU per meter in July, with gradual decline over time (decrease of 0.10 FNU per hour in March and 0.03 FNU per hour in July).

3.3.3. Seasonal and Spatial Variations in Water Quality Parameters and Their Correlation With Meteorological Data

During the research period, all meteorological and WL data, except PP, exhibited normal distribution based on the Jarque–Bera test (Table A14). We transformed the PP variable using a cube root to achieve a normality. All water quality parameters had *p*-values below the 0.05 significance threshold, indicating non-normal distribution. While various transformations yielded marginal improvements, only the Chl-a parameter gained normal distribution following a square root transformation. Due to the predominance of non-normal distributions, we conducted our analysis of monthly water quality data using median values. We employed the median absolute deviation (MAD) to assess variation, as it is less sensitive to outliers compared to standard deviation [197]. Table A15 presents a comprehensive overview of the data distribution, presenting mean and median values alongside standard deviation and MAD. Our calculations were based on a maximum of 20 monitoring stations in the lake per date, and the quantity of measured data stations per date varied (Table A15).

We observed that Chl-a varied from 0.15 µg/L in April 2023 to 2.39 µg/L in November 2023, with a mean value of 0.94 ± 0.39 µg/L and median value of 0.90 ± 0.24 µg/L (Table A15). The range of Chl-a levels was 2.24 µg/L, with the maximum and minimum values differing almost 2.5 times the median. In June 2024, we measured the lowest EC value of 2.66 dS/m, which peaked in November 2023 at 4.80 dS/m, showing a gradual decrease by the end of our research

period (Table A15, Figure 3.5). The mean and median EC measurements were 3.96 ± 0.65 dS/m and 4.19 ± 0.49 dS/ m, respectively, with a range differing by 2.14 dS/m. This range represents 45 and 51% of the highest value and median value, respectively. The mean and median *in situ* values for salinity were 2.10 ± 0.36 and 2.22 ± 0.28, respectively, with values ranging from 1.37 in June 2024 to 2.58 in November 2023 (Table A15, Figure 3.5). The salinity values showed a 1.21 variation, accounting for 47 and 55% of the highest and median values, respectively.

We measured the turbidity levels ranging from 0.73 FNU in July 2023 to 15.93 FNU in August 2023, with a mean value of 5.76 ± 3.96 FNU and median value of 3.85 ± 1.63 FNU. Over this 12-month period, we observed a range of turbidity values of 15.20 FNU, which accounts for 95% of the maximum value and 395% of the median value. In July 2023, we measured the highest WT (30.22°C), which declined to 4.47°C in January 2024, with a mean of 16.98 ± 7.87°C and a median of 17.16 ± 7.33°C. The WT data exhibited a fluctuation of 25.75°C, representing 85 and 150% of the maximum and median values, respectively.

We observed that DO levels ranged from 7.60 mg/L in August 2023 to 12.60 mg/L in January 2024, with a mean value of 10.33 ± 1.15 mg/L and a median of 10.35 ± 0.85 mg/L. During this period, DO values fluctuated within a range of 5 mg/L, which represented 40 and 48% of the maximum and median values, respectively. We observed that SO decreased to 93.46% in December 2023 after reaching a high of 143.28% in July 2023. A mean of SO is 106.70 ± 8.85% and a median is 103.64 ± 4.95%, while the SO values ranged from 49.82%, which is equivalent to 35% of the highest value and 48% of the median value.

Spearman's correlation analysis revealed that the daily vertical movement of phytoplankton (Figure A1), influenced by factors like SH, WS, water column mixing, and PP, leads to changes in Chl-a concentrations (Figure 3.6A). Notably, we observed higher Chl-a levels in November compared to July (Figure 3.5), but we found no significant correlation between Chl-a and DO levels (Figure 3.6B), likely due to unpredictable fluctuations from factors such as the absence of macrophytes and phytoplankton accumulation. Our study revealed that EC, salinity, and turbidity significantly impact the Chl-a values across the lake (Figure 3.6B). We found that factors such as WT, total dissolved solids, PP, flooding, evaporation, and water flow have an impact on EC and salinity levels. Increased water volume and level can reduce EC and salinity (Figure 3.6A).

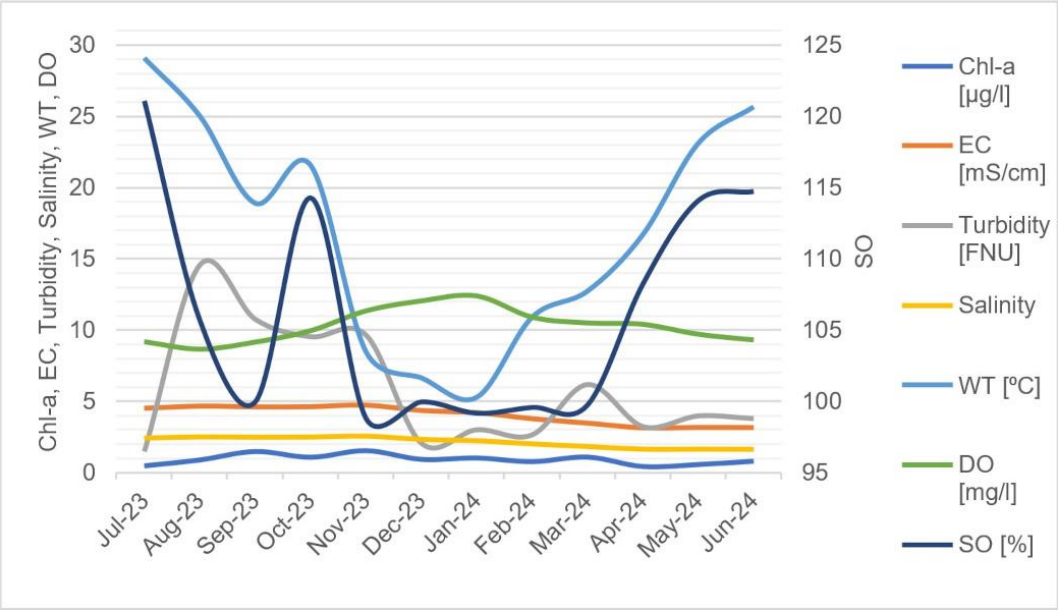

Figure 3.5. Median values of water quality parameters from the dataset (Chl-a, EC, turbidity, salinity, WT, DO, SO)

We found that turbidity can lead to increased WT and decreased DO levels (Figure 3.6B). We recognized that factors such as PP and WS can further impact turbidity by increasing stream volume and resuspending settled sediments (Figure 3.6A). Turbidity will often spike annually due to spring rains (Figure 3.5) and snowmelt. Sunlight and AT primarily influence WT in Vrana Lake (Figure 3.6A). We measured higher WT during summer, autumn, and spring, and lower temperatures during colder months (Figure 3.5). Warmer waters have higher EC, but colder waters can hold more DO and have lower levels of SO (Figure 3.6B).

Aeration sources such as wind, AT (Figure 3.6A), photosynthetic activity, and oxygen consumption by aquatic organisms influence the levels of DO in waterbodies. DO levels can vary based on WT (Figure 3.6B), water pressure, and salinity, with fluctuations occurring due to microbial breakdown and limited air contact. DO levels are higher in winter and lower in summer (Figure 3.5). SO levels are around or slightly exceeded 100% throughout the year (Table A15 and Figure 3.5).

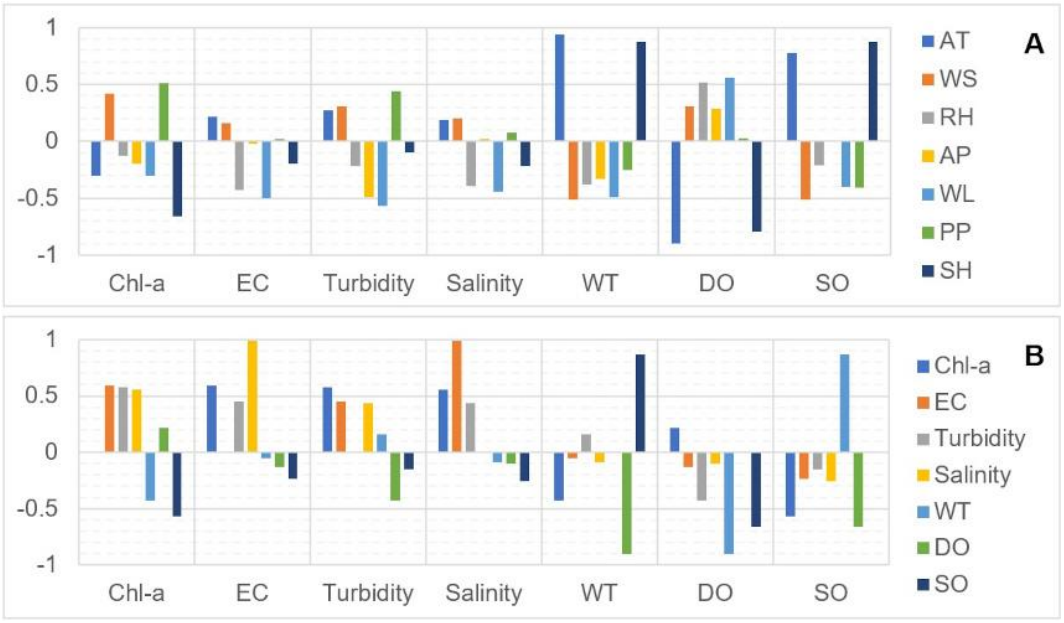

Figure 3.6. Spearman's coefficient of determination between: (a) WL, meteorological (AT, WS, RH, AP, PP, SH), and water quality parameters (Chl-a, EC, turbidity, salinity, WT, DO, SO) and (b) in-between water quality parameters (Chl-a, EC, turbidity, salinity, WT, DO, SO)

3.3.3.1. Spatial Distribution

According to Eq. 3.3, we found that the coarsest grid resolution is approximately 300m when considering 20 unevenly distributed monitoring stations in an area of approximately 30 km^2. The comparison of 15 GIS spatial interpolation methods revealed that the Global Polynomial Interpolation – Second order method achieved the lowest RMSE for Chl-a, while SK – Optimized achieved the lowest RMSE for EC, salinity, DO, and SO (Table A16, Figure A3). EBK – Advanced had the lowest RMSE for turbidity, and SK – Default had the lowest RMSE for WT (Table A16). Generally, Kriging methods outperformed deterministic interpolation methods regarding RMSE values, with EBK – Advanced and all SK methods ranking in the top five for average rank across all parameters. Overall, SK – Optimized ranked as the best for lowest RMSE using Eq. 3.1 across all parameters (Table A17). We calculated ME values using Eq. 3.2, and both Inverse Distance Weighted methods and EBK – Default consistently scored 0, indicating the highest accuracy (Table A16). However, when we considered the ranking of all GIS spatial interpolation methods, we found that SK – Trend emerged as the most suitable method for modelling all parameters (Table A17). We used this method to create distribution maps demonstrating the variability of water quality parameters (Figure 3.7).

We observed that Chl-a concentrations peak in the northwestern region of the lake, particularly near the Kotarka channel, which serves as the main freshwater tributary (Figure 3.7A).

Conversely, we found that the eastern part of the lake, being the shallowest (Figure 3.1A), consistently maintained lower Chl-a levels throughout the year (Figure 3.7A). Turbidity was the highest in the northwestern part of the lake, near the Kotarka channel, while the southeastern part exhibited the lowest turbidity levels (Figure 3.7C).

There was a strong correlation between EC and salinity in the lake, with both parameters exhibiting similar distribution patterns. The southern region, connected to the sea through the Prosika canal, experienced seawater intrusion, especially during warmer months with lower WL. This resulted in higher EC and salinity in the south and lower EC levels in the north (Figure 3.7B and D).

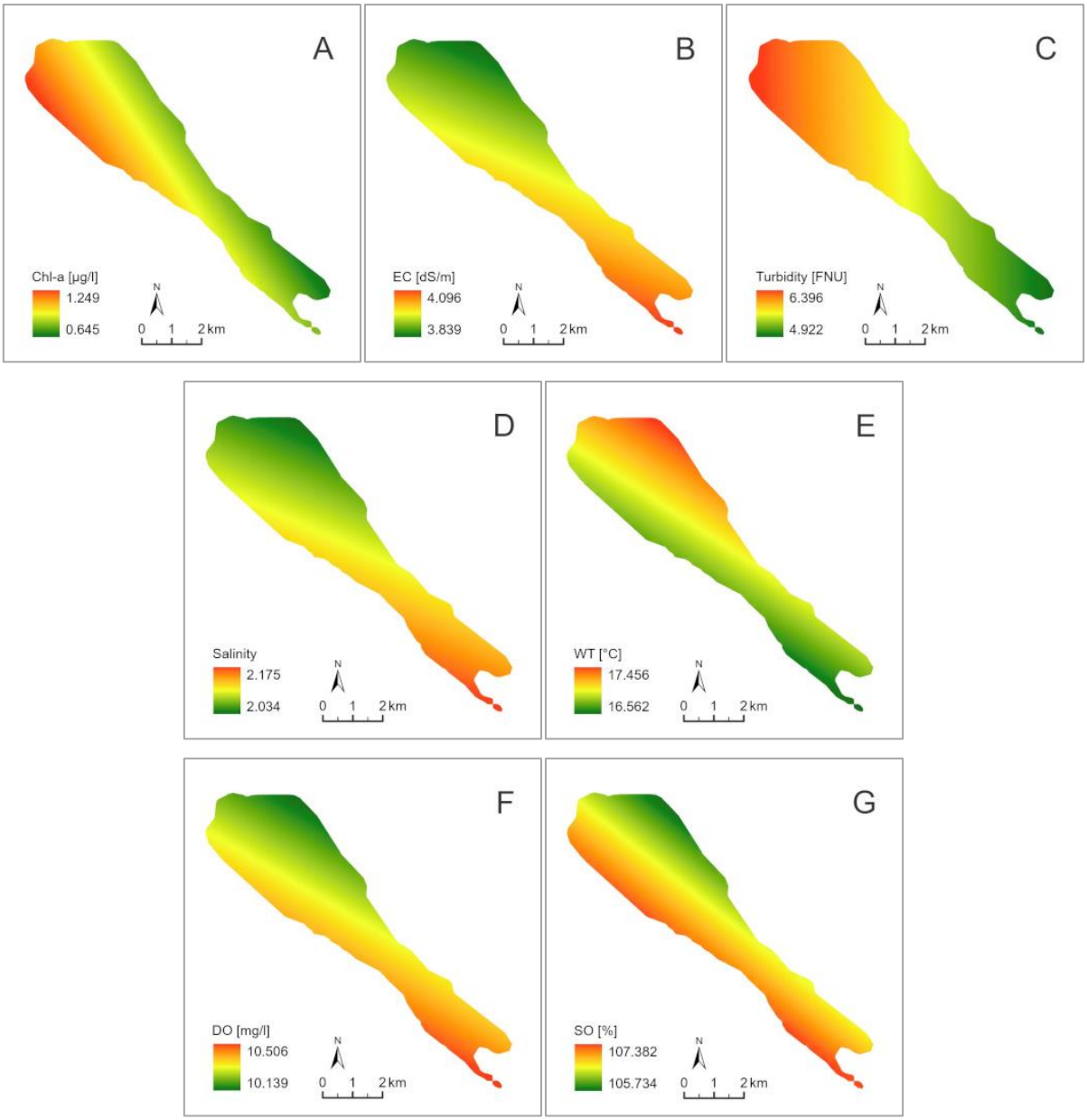

Figure 3.7. SK – Trend interpolation showing parameter distributions: (a) Chl-a, (b) EC, (c) turbidity, (d) salinity, (e) WT, (f) DO, and (g) SO

We monitored the lake in a counterclockwise direction, starting at station 4 and ending at station 2 (Figure 3.1A), which took us approximately 3 h. During this process, WT and SO levels gradually increased, influenced by AT (Figure A2). This resulted in higher WT at later monitoring stations and in shallower areas on the northern and eastern sides of the lake (Figure 3.7E). DO levels were highest in the southern, deepest part of the lake near the Prosika canal and lowest in the northern area near the freshwater tributary Lateral channel (Figure 3.7F). Similarly, SO levels were highest in the deep western part of the lake and lowest in the shallow northeastern region (Figure 3.7G).

3.4. Discussion

3.4.1. Impact of Climate Change on Vrana Lake

Historical data indicate rising global temperatures and extreme weather events, including heavy precipitation. Our study confirms the growing trend of overall AT from the early 1990s till 2020s (2.11°C in 34 years) anticipated by IPCC [171], impacting ecosystems and affecting lake water quality. PP levels exhibit significant variability from average values, reflecting the occurrence of extreme weather events throughout the years, such as drought years and flooding years. Rising WL trend may be influenced by the Adriatic Sea's mean sea level rise of +2.6mm/year from 1993 to 2019, as reported by Pandžić et al. (2024) [216]. Given Vrana Lake's connection to the sea through the Prosika canal, it is especially vulnerable to sea-level changes – a trend also observed in other coastal lakes, such as those in the Netherlands [217]. Our trend analysis, based on the work of Rubinić and Katalinić (2014) [205], which covers the period from 1961 to 2010, indicates a similar increase in AT and lake WL.

3.4.2. Vertical Stratification and Water Quality Dynamics

Vertical profiles revealed a very well-mixed water column with minimal or no stratification. This aligns with findings by Holgerson et al. (2022) [218], who reported that shallow lakes over 4 ha in surface tend to experience frequent mixing driven by wind and convection, preventing sustained stratification. In Vrana Lake, we measured slightly elevated Chl-a and turbidity at greater depths with lower light availability, a pattern also observed by Girdner et al. (2020) [219]. Similar to the observations in Lake Taihu [220] and Siombak Lake [221], where vertical WT differences were typically within 1°C and showed no significant variation in DO across the water column, we observed that Vrana Lake also exhibits very limited vertical WT gradients and minimal variations in DO, confirming its classification as a shallow, well-mixed system. Likewise, the stability of salinity throughout the water column mirrors observations in shallow

saline Lake Shunet in Russia [222], where salinity remains stable to depths of 5 m. Given the shallow nature of Vrana Lake, we find that vertical variations are not significant and can be disregarded, allowing us to use median values from vertical profiles as reference measures for each monitoring station.

3.4.3. Seasonal and Spatial Variations in Water Quality and Meteorological Influences

The spatial distribution of water quality parameters is important for understanding changes in water quality across a lake. Our findings indicate a slight increase in Chl-a concentrations outside the vegetation period, particularly during autumn and winter. This is consistent with a study by Kong et al. (2021) [223], in which it was found that phytoplankton growth in winter is particularly sensitive to light and temperature changes, making it vulnerable to the impacts of climate change.

According to the legislation in The Official Gazette [224], our 12-month study of Vrana Lake shows that it is mesotrophic (classified as "very good" based on eutrophication indicators for mean annual Chl-a values). This differs from the 2021 measurements from Hrvatske vode, which classified the lake as mesotrophic/eutrophic (classified as "good") [206]. We acknowledge that the reliability of Chl-a measurements in our study is uncertain due to the use of the multiparameter probe without spectrophotometric analysis of water samples. A study by Zolfaghari et al. (2020) [211] shows that the connections between sonde and laboratory measurements of Chl-a depend on the site and the methods used in the laboratory.

Salinity concentrations in Vrana Lake rise due to evaporation and the entry of seawater, particularly during the summer (Figure 3.5), as demonstrated by recent findings in another coastal lake in Croatia [225]. While the Lateral channel remains fresh, heavy rainfall can introduce slightly saline water into the Kotarka channel due to the spring from Vrana polje in the north [201]. Seasonal changes, such as reduced seawater influx during colder periods and potential salinity changes in the Kotarka channel, further affect water quality.

Turbidity levels in Vrana Lake are influenced by factors like nutrient and water flow from tributaries, with warmer months leading to increased turbidity due to lower WLs and active vegetation periods. Contributing sources include soil erosion, seasonal variations, local geology, and algal blooms, which can negatively impact water quality and aquatic life [226]. Additionally, higher turbidity level in the northwestern part of the lake may be linked to the anthropogenic influence, as reported by Silva et al. (2020) [227], including nearby road network and industries.

WT is affected by AT and SH, showing higher temperatures in shallow parts of the lake, as found by Anamunda and Lamtane (2022) [228]. WT variations have effect on the DO and SO levels, biological activities, and other parameters, as reported by Wang et al. (2024) [229] and Khouni et al. (2021) [186]. Areas with higher Chl-a concentrations generally have elevated DO levels, which inversely correlate with WT and AT, as found by Saturday et al. (2022) [230]. In shallow lakes like Vrana Lake, higher DO levels are typically associated with increased SO concentrations, and SO levels typically remain near 100% or slightly above, sustained by photosynthesis, aeration, and shallow mixing [231], as found by Allesson et al. (2022) [232].

3.5. Conclusion

Our study of Vrana Lake reveals significant impacts of climate change on water quality and ecosystem dynamics. Longterm trends show increasing AT, PP, and WL, suggesting a complex interaction influenced by rising sea levels from the Adriatic Sea. Due to the lake's shallow nature and minimal vertical stratification, median values from vertical profiles are sufficient for station-level monitoring.

We observed seasonal variability in turbidity, EC, and Chl-a, with a shift from mesotrophic/eutrophic to mesotrophic conditions, emphasizing the need for continuous monitoring. Additionally, we identify the SK – Trend method as the most effective GIS spatial interpolation method for modelling water quality parameters, based on RMSE and ME rankings.

Limitations of our study include exclusive use of the YSI EXO2 multiparameter probe and the absence of water sampling for laboratory analysis. In the absence of macrophytes, Chl-a measurements accuracy could be improved through spectrophotometry and phytoplankton identification. While we found turbidity to be a useful water quality indicator, incorporating a Secchi disk for assessing water clarity would have been advantageous. The expanded monitoring network supports subsequent remote sensing and machine learning analyses; however, selecting a subset of optimal stations based on GIS multicriteria analysis in future studies could improve cost-efficiency.

We recommend that future research on Vrana Lake addresses these limitations, identifies specific phytoplankton and macrophyte species, and prioritizes vertical stratification analysis and water quality dynamics before modelling water quality. Given the strong correlation between EC and salinity, and the fact that salinity is derived from EC measurements using the EXO2 probe, we recommend using EC as the primary parameter in similar studies.

Overall, our findings underscore the complex environmental interactions shaping Vrana Lake's ecosystem and the necessity for adaptive management in response to climate change. Our findings are particularly relevant to institutions responsible for monitoring Vrana Lake, including the Water Institute Josip Juraj Strossmayer and the Public Institution Vransko Jezero Nature Park. They may also benefit other authorities and researchers engaged in future studies on Lake Vrana and other coastal shallow lakes. Our research lays the groundwork for future studies using GIS multicriteria analysis, remote sensing, and machine learning to improve lake management and address ecological challenges.

4. Enhancing Water Quality Monitoring in a Coastal Shallow Lake Using GIS and Multi-Criteria Decision Analysis

This chapter has been published as: *Batina, A.; Šiljeg, A. (2025). Enhancing water quality monitoring in a coastal shallow lake using GIS and multi-criteria decision analysis.* Environmental and sustainability indicators*,* 28*, 100881. doi: 10.1016/j.indic.2025.100881*.
Conceptualization, A.B. and A.Š.; methodology, A.Š.; software, A.B.; validation, A.Š.; investigation, A.B.; resources, A.Š.; data curation, A.B.; formal analysis, A.B. and A.Š.; writing—original draft preparation, A.B.; writing—review and editing, A.Š.; visualization, A.B.; supervision, A.Š.; project administration, A.B.; funding acquisition, A.Š. All authors have read and agreed to the published version of the manuscript.

Abstract:

Water quality decline is a critical global issue affecting both aquatic ecosystems and human health. This study focuses on Vrana Lake, a coastal shallow lake in Dalmatia, Croatia, which is subject to seasonal water level fluctuations, salinization from the Adriatic Sea, and various anthropogenic and environmental pressures. To evaluate and improve water quality monitoring, a spatial assessment was conducted using a Geographic Information System-based Multi-Criteria Decision Analysis (GIS-MCDA) integrated with the Fuzzy Analytical Hierarchy Process (F-AHP). The analysis incorporated multiple criteria including electrical conductivity, turbidity, dissolved oxygen, water temperature, distance from water resources, distance from land nutrient runoff, distance from environmental pollutants, wind, precipitation, and air temperature, using data collected from July 2023 to June 2024. The methodology included standardization of criteria in GIS software, weighting through F-AHP, and a sensitivity analysis using 1000 Monte Carlo simulations to assess model robustness. Results revealed spatial variations in water quality, with lower quality observed in the northwestern and southern regions, influenced by anthropogenic activities and seawater intrusion. An optimized monitoring network of seven stations was developed based on Jenks natural breaks classification, ensuring comprehensive lake coverage and efficient representation of all water quality classes. Three existing stations and two from previous networks were incorporated into the new network, with two additional stations proposed to maintain consistent spatial distribution. This study provides an adaptable decision support framework for improving water quality monitoring and management in coastal shallow lakes, offering a strategic approach to early eutrophication warning systems and informed resource planning.

Keywords: ecosystem health, environmental decision support, eutrophication, Fuzzy AHP, Monte Carlo, spatial analysis

4.1. Introduction

The decline of water quality is a pressing global issue that impacts both aquatic ecosystems and human health [233], highlighting the need for improved evaluation methods for effective lake water quality management. The complexity of water quality assessment is influenced by various factors, such as ecosystem components, human activities, geographic location, and climate change [234]. Understanding the hydrodynamic processes and characteristics of lakes is crucial for effective management, especially as water levels fluctuate [24].

Shallow coastal lakes face salinization influenced by geomorphology, wind, tides, precipitation, and water discharge, with climate change exacerbating these issues [7]. During dry periods, these lakes also experience increased nutrient loading, which can modify natural eutrophication processes [235]. The development of various water quality assessment methods, including water quality indexes [236–238], multivariate statistical methods [237,239], and deep learning methods [240], reflects the concerns of decision-makers regarding the degradation and restoration of waterbodies.

The integration of multi-criteria decision analysis (MCDA) with geographic information systems (GIS) improves the evaluation of alternatives based on multiple criteria by combining spatial data and value judgments [24,241]. The GIS-MCDA method is favoured for its decision-making capabilities and ease of interpretation, though careful parameter selection is crucial to avoid misleading results [242,243]. The Analytical Hierarchy Process (AHP) method, and fuzzy set theory are most widely-used method used in water resource analysis [244], with integrated fuzzy AHP (F-AHP) allowing for better handling of uncertainty in evaluations [241]. Various MCDA methods, such as analytical network process (ANP) [245], multi-attribute utility theory (MAUT) [246], technique for order preference by similarity to ideal solution (TOPSIS) [246,247], and weighted product method (WPM) [247], are also employed in water resources planning. While GIS-MCDA integrated with F-AHP has been successfully applied to various waterbodies like watersheds, rivers, and river basins [248–250], to our best knowledge, this is the first published study on using GIS-MCDA with F-AHP to assess water quality in a coastal shallow lake.

Sensitivity analysis is a crucial aspect of model-based research, helping to measure the impact of uncertainties in input parameters on model outputs [251]. Different methods, such as local one-at-a-time method, global Monte Carlo-based analyses, variance decomposition (Sobol indices), and screening techniques (Morris method), are suited to varying levels of model

complexity and research objectives [252], with Monte Carlo being particularly robust for measuring uncertainty and providing probabilistic insights into decision reliability [251,253].

This study evaluates the water quality of Vrana Lake, a coastal shallow lake in Dalmatia, Croatia, which is affected by seasonal water level fluctuations, salinization from the Adriatic Sea, and various anthropogenic and environmental factors. The research employs a GIS-MCDA methodology combined with F-AHP to assess water quality over a year from July 2023 to June 2024, considering multiple factors such as electrical conductivity (EC), turbidity, dissolved oxygen (DO), water temperature (WT), distance from water resources, distance from land nutrient runoff, distance from environmental pollutants, wind, air temperature, and precipitation. The model's sensitivity is analysed through 1000 Monte Carlo simulations using Python 3.8 with random ±10 % to ±30 % noise to every comparison to account for variability in input parameters.

This study forms a part of broader PhD research project aimed at improving lake water quality monitoring by integrating *in situ* measurements, GIS-MCDA, satellite remote sensing, and machine learning methods. Building on the conceptual framework established by Batina and Krtalić (2024) [9], a monthly monitoring strategy was implemented over a 12-month period in Vrana Lake. This strategy was designed to balance scientific objectives with practical constraints, while supporting the spatiotemporal analysis described in Batina et al. (2025) [25]. This adopted approach ensured adequate seasonal coverage, which is essential for dynamic systems such as coastal shallow lakes. It also facilitates integration with Sentinel-2 and Landsat 8–9 imagery, whose revisit cycles (5 and 8 days, respectively) were considered to optimize alignment with *in situ* data and to reduce the impact of cloud cover in future remote sensing applications. The 12-month sampling campaign provided a realistic and manageable timeframe for doctoral-level research while offering sufficient data density to enable robust analysis. Similar approaches have been adopted in studies by Romero et al. (2002) [254], Umwali et al. (2021) [255], and Armstrong et al. (2022) [256], which confirm that monthly sampling is appropriate for capturing seasonal and spatial variability in shallow lake environments. In this study, annual averages were used within the GIS-MCDA framework to identify long-term spatial patterns [257,258] and to support monitoring network optimization. Seasonal trends were explored separately in the study conducted by Batina et al. (2025) [25]. Considering the limitations in available human and financial resources, the monitoring design represented a practical and scientifically sound compromise, ensuring data reliability, seasonal representation, and compatibility with remote sensing applications.

This study aims to: (1) model water quality in Vrana Lake, (2) identify areas susceptible to eutrophication, and (3) optimize monitoring stations to reduce costs and time associated with *in situ* measurements. By using Vrana Lake as a case study, the research seeks to develop a flexible decision support system adaptable and applicable to coastal shallow lakes globally.

4.2. Materials and Methods

4.2.1. Study Area

Vrana Lake, the largest natural lake in Croatia, covers approximately 30 km^2. It is recognized as a protected nature park due to its ecological importance and biodiversity [259]. The lake has an average water level of 0.82 m above sea level and depths ranging from 0.5 to 5 m [259], with seasonal water level fluctuations that peak at a mean of 1.26 m above sea level in winter and spring and drop to 0.40 m above sea level in summer and autumn [25]. The lake's bottom is located at 3.47 m below sea level [259]. Figure 4.1 shows an overview of the study area. Map lines delineate study area and do not necessarily depict accepted national boundaries.

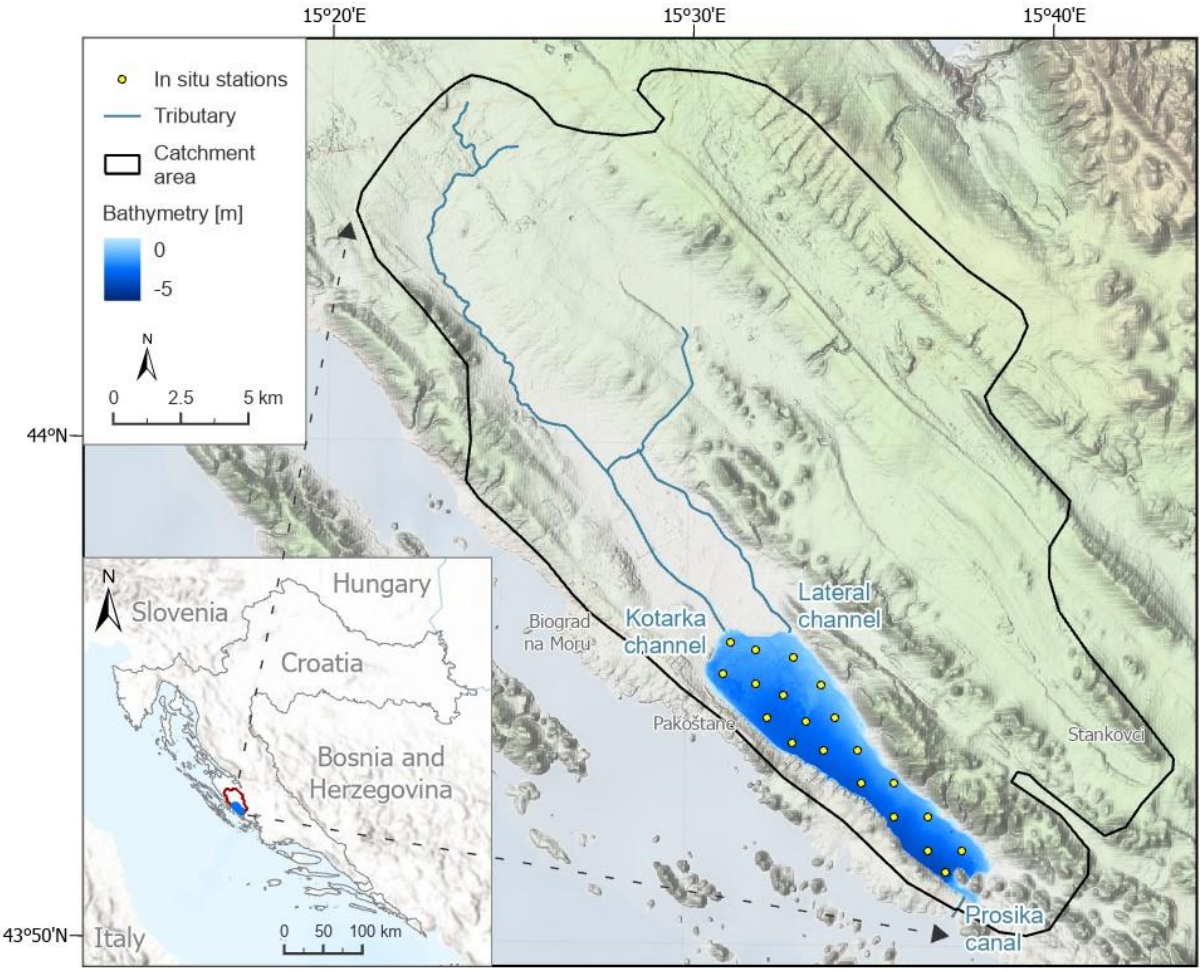

Figure 4.1. Overview of Vrana Lake's geospatial features and in situ *monitoring stations*

A previous study by Batina et al. (2025) [25] established a comprehensive monitoring grid to enhance data collection for water quality assessment, expanding the monitoring network from three to 20 monitoring stations within the lake. This study aims to optimize the monitoring network using GIS-MCDA, while considering the impact of climate, human activities, and pollution sources. Furthermore, the lake boundary was delineated using PlanetScope satellite imagery (3 m spatial resolution) [207] and the Normalized Difference Water Index (NDWI) [208] for each month of the 12-month research period to capture seasonal water level variations typical of shallow lakes, with October 2023 selected for presentation (Figure 4.1) as it represented the lowest recorded water level during the study period [25].

4.2.2. GIS Multi-Criteria Decision Analysis

This study employs GIS-MCDA integrated with F-AHP to model water quality in Vrana Lake, using triangular fuzzy elements for pairwise comparisons in online Fuzzy AHP software [241,260]. The analysis follows a six-step process, including (1) defining the problem and setting the goal, (2) selecting criteria, (3) standardizing criteria, (4) determining criteria weights, (5) aggregating criteria, and (6) model validation [261].

4.2.2.1. Defining the Problem and Setting the Goal

The goal of the GIS-MDCA is to model water quality in Vrana Lake, adhering to SMART (specific, measurable, achievable, relevant, and time-bound) criteria [242].

4.2.2.2. Selecting Criteria

The selected criteria for the analysis are based on the lake's characteristics, literature review according to the framework developed by Batina and Krtalić (2024) [9], and insights from the experts from the Ruđer Bošković Institute and Public Institution Vrana Lake Nature Park. Ten criteria were used for the GIS-MDCA: (C1) EC, (C2) turbidity, (C3) DO, (C4) WT, (C5) distance from water resources, (C6) distance from land nutrient runoff, (C7) distance from environmental pollutants, (C8) air temperature, (C9) wind, and (C10) precipitation. A detailed list of criteria and their reasoning is provided in Table 4.1.

Table 4.1. Summary of GIS-MCDA criteria with corresponding codes, formats, spatial resolutions, data sources, and membership functions

Code	Criteria	Reasoning	Data type	Data source	Literature
C1	EC	Evaluates water capacity to conduct electricity, indicating the levels of salinity and inorganic substances. High EC may indicate pollution or alterations in water chemistry, especially in coastal lakes.	Raster (300 m)	Batina et al. (2025) [25]	[262]
C2	Turbidity	Indicates water clarity by measuring the presence of suspended particles. High turbidity can hinder light penetration, impact the growth of aquatic plants and suggest potential contamination.	Raster (300 m)	Batina et al. (2025) [25]	[24]
C3	DO	Essential for the survival of aquatic species. Low levels can indicate pollution and lead to hypoxic conditions, harming aquatic life.	Raster (300 m)	Batina et al. (2025) [25]	[263,264]
C4	WT	Influences metabolic rates of aquatic life, solubility of gases, and chemical reaction rates in water. Temperature variations can disrupt aquatic ecosystems.	Raster (300 m)	Batina et al. (2025) [25]	[265]
C5	Distance from water resource	Proximity to water sources, such as tributaries, sea connections, and rainfall runoff, affects water availability and accessibility, influencing potential contamination risks.	Raster (1 m)	LiDAR DEM (*Flow accumulation* tool)	[266]

C6	Distance from land nutrient runoff	Areas closer to agricultural lands may experience higher nutrient runoff, leading to eutrophication and degraded water quality.	Vector (polygon)	Land cover/land use (LCLU) [267]	[257,266]
C7	Distance from environ-mental pollutants	Proximity to pollution sources, such as industrial sites and road network, increases the risk of nutrient export and contaminant entry into waterbodies, affecting water quality and ecosystem health.	Vector (point)	Environmental pollutant registry [268]	[269]
C8	Air tempera-ture	Affects WT, influencing DO levels, metabolic rates of aquatic life, and the overall health of the ecosystem.	Raster (20 km)	Copernicus Climate Change Service [270]	[271,272]
C9	Wind	Influences water mixing, aeration, and distribution of nutrients and pollutants, affecting water quality.	Raster (30 m)	Croatian Meteorological and Hydrologi-cal Service	[271]
C10	Precipitation	Affects water levels, introduces new pollutants through runoff, and influences nutrient loading in waterbodies. Heavy rainfall can lead to increased turbidity and pollutant concentrations.	Raster (20 km)	Copernicus Climate Change Service [270]	[266,272]

The analysis incorporates various criteria originating from different data types and sources. Grid resolution is crucial in spatial modelling, influencing mapping effectiveness and spatial variability representation [215]. The study utilizes water quality parameter distribution maps generated from 20 irregularly monitoring stations, calculating a grid resolution of approximately 300 m in a 30 km^2 lake area [25,215]. Raster data with a 300-m resolution generated from *in situ* measurements [204] using Simple Kriging – Trend interpolation method conducted by Batina et al. (2025) [25] was used for EC, Turbidity, DO, and WT. Additionally, a 1-m raster derived from a LiDAR Digital Elevation Model (DEM) was used in ArcGIS Pro 3.4.2 for accumulated flow analysis. The Flow Accumulation tool was applied to generate

surface flow paths, and the main points where flow enters the lake were identified. Based on these flow paths, distances from the flow entry points were calculated using Distance Accumulation tool [273] as distances from water resources. In addition, LCLU polygons adjacent to the lake shoreline were extracted, their areas calculated, and centroids along the lake boundary identified as representative nutrient runoff entry points. Distances from land nutrient runoff sources were calculated using Distance Accumulation tool using these nutrient runoff entry points derived from LCLU data. Environmental pollutants were obtained as vector points from an environmental pollutant registry, and meteorological factors such as air temperature and precipitation were obtained as ERA5 raster datasets with a spatial resolution of 20 km. Wind data were not extracted directly as raw measurements but were instead used to calculate a wind exposure index, based on data from the Croatian Meteorological and Hydrological Service, and applied to a 30-m resolution DEM to model its spatial influence on the lake environment. All raster maps are used in GIS-MCDA, resampled to consistent 300-m spatial resolution.

EC is an important indicator of water quality, with high levels indicating potential pollution or natural events that can harm freshwater organisms, particularly phytoplankton [274]. Eutrophication can cause phytoplankton blooms, but increased salinity can inhibit this process. EC is directly related to the electrolyte concentrations, with higher salinity leading to higher conductivity. In Vrana Lake, salinity rises due to evaporation and seawater intrusion, particularly in summer, with a study by Batina et al. (2025) [25] showing EC values ranging from 2.66 dS/m (salinity of 1.37) to 4.80 dS/m (salinity of 2.58) over a year. In a spatial distribution map of EC generated from 230 measurements collected during this 12-month research, mean values vary from 3.84 dS/m on north to 4.10 dS/m on south. Lower salinity and EC levels indicate better ecological health and water quality, as outlined in the Decree on Water Quality Standards [224].

Turbidity is one of the key indicators of water quality, influenced by factors such as salinity, soil erosion, rainfall runoff, and algal blooms, which can harm aquatic life and lead to increased WT and decreased DO levels [226]. Precipitation and wind can increase turbidity by resuspending sediments [25]. In Vrana Lake, turbidity levels fluctuate by location and season. A 12-month study by Batina et al. (2025) [25] measured turbidity values ranging from 0.73 FNU to 15.93 FNU, with the north area exhibiting the highest levels, while the southwestern region consistently shows the lowest turbidity. Furthermore, mean values from a spatial distribution map vary from 4.92 FNU in the southeast to 6.40 FNU in the northwest. Lower

turbidity levels, indicated by higher Secchi disk depth, reflect better ecological state and water quality, as outlined in the Decree on Water Quality Standards [224].

DO is a crucial parameter of water quality, as oxygen is vital for all aquatic life [224,231]. DO levels are influenced by factors such as wind, air temperature, WT, photosynthetic activity, and oxygen consumption by aquatic organisms [25]. Increased chlorophyll-a concentrations are associated with higher DO levels, while DO decreases with rising temperatures and salinity [231]. In warmer months, the southern area of the lake experiences lower DO due to increased salinity [25]. Extreme DO levels can harm aquatic life and overall water quality, and when levels drop below a certain threshold, fish mortality can rise [224,231]. A study by Batina et al. (2025) [25] found DO values ranging from 7.60 mg/L to 12.60 mg/L throughout the year, based on measurements taken in mornings on sunny days. Mean values from a spatial distribution map vary from 10.14 mg/L in the north to 10.51 mg/L in the south. All values above 6 mg/L indicate very good ecological state and water quality, as per the Decree on Water Quality Standards [224].

The WT in Vrana Lake is primarily influenced by sunlight and air temperature, with higher levels in warmer months and lower levels in winter [25]. In the 1-year study [25], the highest measured WT was 30.22 °C in July 2023, decreasing to 4.47 °C by January 2024, with mean values in a spatial distribution map varying between 16.56 and 17.46 °C. Variations in WT affect DO levels, with warmer waters typically posing more risks to aquatic life [275]. Higher temperatures promote eutrophication, indicating that cooler temperatures could enhance water quality, though this does not mean that ice represents the cleanest water. Lower WTs indicate a better ecological state and water quality, as indicated by the Decree on Water Quality Standards [224].

Tributaries play a crucial role in the hydrographic dynamics of the study area, enhancing water mixing and influencing salinity and ecosystem health. The influx of seawater also affects the lake's ecological health, especially during low water levels. Additionally, rainwater runoff can lead to nutrient release and eutrophication, especially during and after heavy rainfall [276]. A stream network was generated using a 1-m DEM to analyse water resource influx. The DEM was processed to eliminate artificial sinks while preserving natural ones. The stream network was calculated using Flow Accumulation tool in ArcGIS Pro 3.4.2. The impact of inlet points was evaluated based on stream length, with longer streams generally indicating greater influence, with the exception of Prosika canal which was assigned the highest influence category based on its documented influence on water quality in Vrana Lake, rather than its stream length. This assessment is ported by expert knowledge and previous research, including

recent studies by Batina et al. (2025) and Batina and Šiljeg (2025) [25,277], which highlight the measurable effect of saline inflow from the Prosika canal, especially during dry periods when the lake is most vulnerable. The Jenks classification method was employed to categorize the data into natural classes for better evaluation of stream influence. The main points where flow enters the lake were classified into five categories based on their stream length. To integrate this information into a spatial influence model, the Distance Accumulation tool in ArcGIS Pro was used, which calculates cost-weighted distances. In this model, stream length classes served as a cost surface, where longer streams were assigned higher costs (or weights), reflecting greater hydrological influence. The resulting cost-distance raster integrates both spatial proximity and the cumulative effect of upstream flow length, helping to identify and prioritize areas with potentially higher impacts on water quality. The resulting map shows high influence areas in the north from major freshwater tributaries and in the south from sea connection, with dense stream networks in the northeastern and southeastern regions due to hilly terrain facilitating rapid runoff (Figure 4.2A).

In this analysis, LCLU polygons adjacent to the lake shoreline were extracted from the LCLU dataset. These polygons were considered as areas most directly contributing to nutrient runoff into the lake. The area of each polygon was calculated, and centroids along the lake boundary were determined to serve as representative entry points for nutrient flow into the lake. To estimate nutrient input, the study by Ma et al. (2008) [278] was referenced, in which total nitrogen export values based on land cover types were provided, expressed in tons per square kilometre per year ($t/km^2/yr$). Based on these values, nitrogen export capacity for each polygon was calculated by combining the polygon's area with the relevant nitrogen export coefficient for its land cover class. The polygons were then categorized into five classes using the Jenks natural breaks classification method, allowing for clearer interpretation of spatial variation in nutrient pressure. In Figure 4.2B, the spatial distribution of nitrogen export capacity is illustrated, with values grouped into five classes ranging from low (0.11) to high (51.63). To incorporate this information into a spatial influence model, the Distance Accumulation tool in ArcGIS Pro was used. In this process, the nitrogen export classes were applied as a cost surface, with higher nitrogen export capacities being assigned greater weights. This allowed areas with higher nutrient export to be represented as having greater influence on the lake, effectively simulating the manner in which nutrient pressure is transmitted toward the shoreline. The resulting cost-distance raster reflects both spatial proximity and the magnitude of nutrient impact, allowing areas to be prioritized based on their potential to contribute to lake eutrophication.

The lake's catchment boundary was found not to fully align with the topographical and environmental influences affecting Vrana Lake. To account for important features located just outside the delineated catchment, such as streams and sources of environmental pollutants (e. g., roads on the western and southeastern sides of the lake), the analysis boundary was extended by 1 km beyond the official catchment. Through this buffer, areas that are technically outside the hydrological catchment but still exert a meaningful influence on lake water quality due to their proximity were included in the analysis. The resulting maps were then cropped to the lake's boundary to facilitate data aggregation with other clusters.

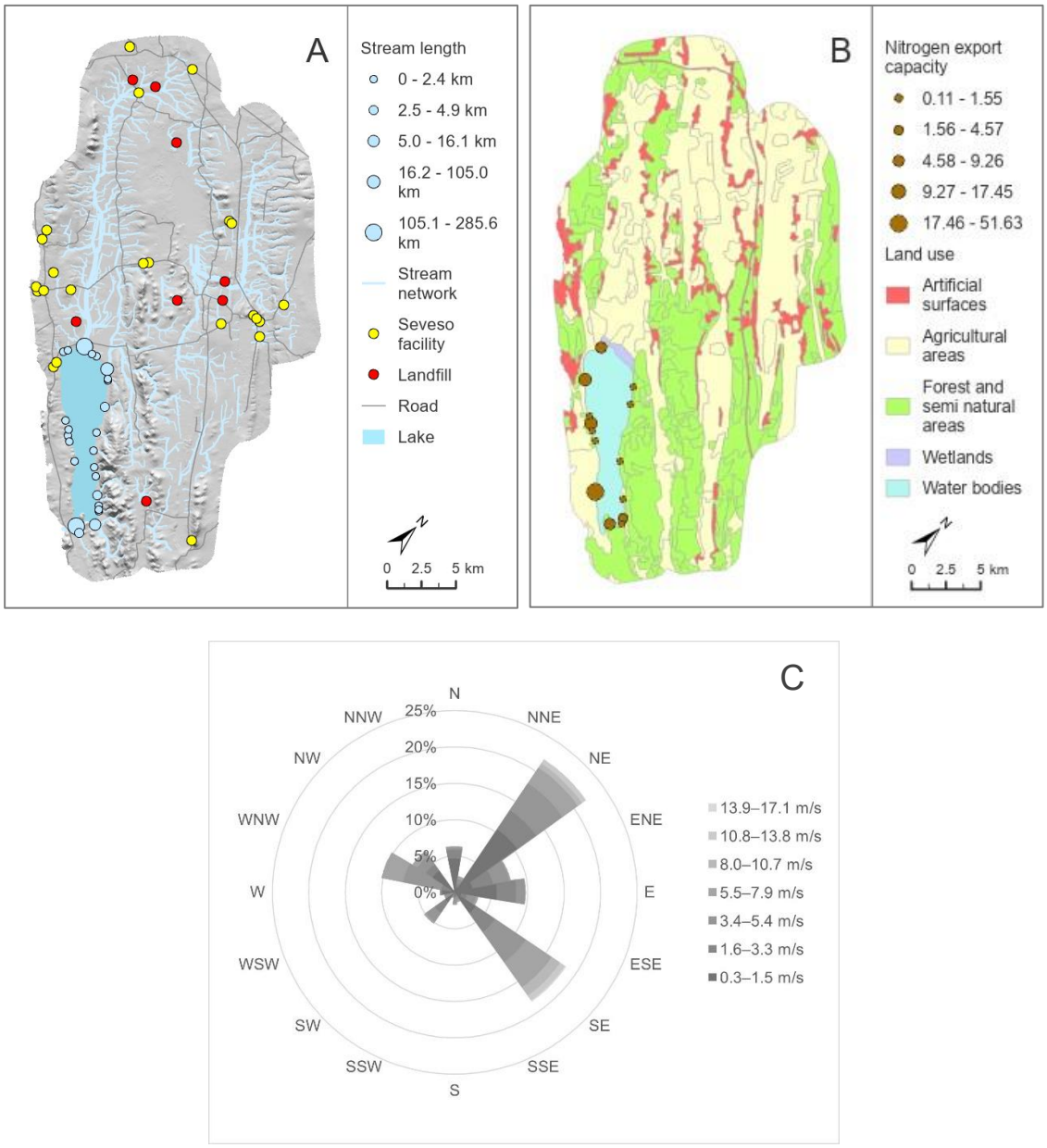

Figure 4.2. Maps of (a) stream lengths and environmental pollutants, (b) total nitrogen export capacity of land, and (c) wind rose

High nutrient concentrations from industrial and agricultural lands can lead to eutrophication, negatively affecting lake water quality [278]. The type of land cover influences nutrient runoff, with forests and natural grasslands reducing the amount of soil nitrogen that reaches lakes, while developed areas and agricultural fields contribute high levels of nitrogen [266,279]. Ma et al. (2008) [278] estimated total nitrogen export to lakes, revealing values of 4.10 t/km^2/yr for agricultural land, 0.80 for shrubland, 0.90 for grassland, 0.45 for forest, and 6.00 for developed areas, which are among the highest recorded in Europe and the United States. The Jenks classification method was used to categorize the nitrogen export capacity into natural classes for a better evaluation of its influence on the lake (Figure 4.2B). The map shows the spatial distribution, with values categorized into five classes, ranging from low (0.11) to high (51.63). The highest nitrogen export influences are observed along the southern and southwestern shore of the lake, corresponding primarily to areas adjacent to agricultural land.

Industrial activities and transportation network contribute to the degradation of the lake ecosystem, affect turbidity levels and promoting eutrophication [269]. Pollution hazards were calculated based on the probability of contamination and the volume of pollutants [268]. Key industrial activities and transport networks were identified as significant stressors in the Vrana Lake catchment, with pollution hazard values categorized using the Jenks classification method (Figure 4.2A). The map illustrates the proximity of Seveso facilities and landfills to the primary tributaries with increasing risk of pollutant transport toward the lake. Additionally, the road network may contribute to non-point source pollution through surface runoff, carrying pollutants such as heavy metals, oils, and sediments into the lake.

Air temperature variations impact water temperature and biochemical reactions rates, affecting water quality [280]. Air temperature data was collected from the Copernicus ERA5 hourly dataset, using the *in situ* measurement days specified in Batina et al. (2025) [25]. The second degree Inverse Distance Weighting interpolation method [281] was used to generate spatial distribution maps of air temperature and precipitation, utilizing meteorological data collected from an approximately 500 km^2 area surrounding the lake, since broader topographical data has significant influence on selected meteorological variables. Data was averaged to calculate a 12-month mean values, with maps cropped to the lake's boundary for data aggregation.

Wind influences in Vrana Lake promote water column mixing and deteriorate water quality [259]. Wind data from the Croatian Meteorological and Hydrological Service for Biograd na Moru station were subjected to a wind rose analysis, identifying significant winds such as bura (N-NE to E-NE) and jugo (E-SE to SS-E), particularly strong in winter (Figure 4.2C). The wind

exposure was assessed using the *Wind Effect (Windward/Leeward Index)* tool on Copernicus DEM in SAGA 9.6.0, calculating the mean wind effect index from predominant winds.
Precipitation can improve water quality by diluting chemical oxygen demand but excessive precipitation may lead to higher phosphorus release from sediments, negatively impacting water quality [280]. Precipitation data was gathered from the Copernicus ERA5 hourly dataset, using the *in situ* measurement days specified in Batina et al. (2025) [25]. Using ArcGIS Pro 3.4.2, the second-degree Inverse Distance Weighting interpolation method was used to average data for a 12-month mean value.

4.2.2.3. Standardizing Criteria

The important step in MCDA involves standardizing diverse datasets into comparable units. This study employs fuzzy logic for standardization, which is effective for data lacking precise boundaries, allowing for a range of membership rather than strict classifications. The selection of membership functions depends on the data's nature and expert input. Fuzzy logic is applied to standardize criteria based on a scale from 0 to 1, where 0 indicates the lowest water quality and 1 the highest. The standardization process incorporates various factors, including local features, expert opinions, relevant literature, and the Decree on Water Quality Standards [224]. The standardized values for each criterion are presented in Figure 4.3.
The standardization process was performed in ArcGIS Pro 3.4.2 software, applying linear fuzzy membership with monotonically decreasing values for parameters like EC, WT, turbidity, and meteorological parameters. Measured DO values were standardized using linear fuzzy membership with monotonically increasing values from 0 to 6 mg/L, whereas values greater than 6 mg/L have been standardized to 1, as their distribution range has no significant impact on water quality. Although DO does not directly influence the water quality in this study, it is still part of the GIS-MCDA analysis because it is recognized as a key factor in assessing water quality. Other criteria, such as distances from water resource, land nutrient runoff, and environmental pollutants were standardized using a combination of decision-maker method and linear fuzzy membership with monotonically increasing values.

4.2.2.4. Determining Criteria Weights

To accurately reflect the varying importance of different criteria in the analysis, appropriate weight coefficients must be assigned [282]. The F-AHP is employed to determine these weights through pairwise comparisons of triangular fuzzy elements, structured in a specific matrix $\tilde{A}$ format [283]:

$$\tilde{A} = \begin{bmatrix} a_{11}^L, a_{11}^M, a_{11}^U & \dots & a_{1n}^L, a_{1n}^M, a_{1n}^U \\ \vdots & \ddots & \vdots \\ a_{n1}^L, a_{n1}^M, a_{n1}^U & \dots & a_{nn}^L, a_{nn}^M, a_{nn}^U \end{bmatrix} \tag{4.1}$$

a_{ij}^L, a_{ij}^M, a_{ij}^U are real numbers such that $\frac{1}{\sigma} \leq a_{ij}^L \leq a_{ij}^M \leq a_{ij}^U \leq \sigma$ for a chosen $\sigma > 1$.

$\tilde{A}$ is reciprocal, if the following condition is satisfied [283]:

$\tilde{a}_{ij} = \left(a_{ij}^L, a_{ij}^M, a_{ij}^U\right)$ implies that $\tilde{a}_{ji} = \left(\frac{1}{a_{ij}^U}, \frac{1}{a_{ij}^M}, \frac{1}{a_{ij}^L}\right)$ (reciprocity) for all *i, j* = 1,2,…,*n*.

In addition to incorporating fuzzy triangular elements, another distinction from traditional AHP is that the preference intensities given by the expert are not restricted to a specific range $\left[\frac{1}{9}, 9\right]$; instead, they can be expressed more broadly $\left[\frac{1}{\sigma}, \sigma\right]$ for a selected value $\sigma > 1$. Fuzzy weights are obtained through the following method [283]:

$$w_k^L = C_{min} * \frac{\left(\prod_{j=1}^n a_{kj}^L\right)^{\frac{1}{n}}}{\sum_{i=1}^n \left(\prod_{j=1}^n a_{ij}^M\right)^{\frac{1}{n}}} \text{ where } C_{min} = \min_{i=1,\dots,n} \left\{ \frac{\left(\prod_{j=1}^n a_{ij}^M\right)^{\frac{1}{n}}}{\left(\prod_{j=1}^n a_{ij}^L\right)^{\frac{1}{n}}} \right\}, \tag{4.2}$$

$$w_k^M = \frac{\left(\prod_{j=1}^n a_{kj}^M\right)^{\frac{1}{n}}}{\sum_{i=1}^n \left(\prod_{j=1}^n a_{ij}^M\right)^{\frac{1}{n}}}, \tag{4.3}$$

$$w_k^U = C_{max} * \frac{\left(\prod_{j=1}^n a_{kj}^U\right)^{\frac{1}{n}}}{\sum_{i=1}^n \left(\prod_{j=1}^n a_{ij}^M\right)^{\frac{1}{n}}} \text{ where } C_{max} = \max_{i=1,\dots,n} \left\{ \frac{\left(\prod_{j=1}^n a_{ij}^M\right)^{\frac{1}{n}}}{\left(\prod_{j=1}^n a_{ij}^U\right)^{\frac{1}{n}}} \right\} \tag{4.4}$$

Matrix consistency refers to how logically coherent the pairwise comparisons are in a decision matrix. In F-AHP, consistency helps ensure that the priority weights derived from the matrix are reliable [283]. High inconsistency suggests that the judgments may need revision. The index below was utilized to evaluate the consistency of the matrix [283]:

$$NI_n^\sigma\left(\tilde{A}\right) = \gamma_n^\sigma * \max_{i,j} \left\{ max \left\{ \left| \frac{w_i^L}{w_j^U} - a_{ij}^L \right|, \left| \frac{w_i^M}{w_j^M} - a_{ij}^M \right|, \left| \frac{w_i^U}{w_j^L} - a_{ij}^U \right| \right\} \right\} \tag{4.5}$$

where w_k^L, w_k^M, w_k^U are given by Eq. 4.2-4.4 for all *k* = 1,2,…,*n*, and

$$\gamma_n^\sigma = \begin{cases} \frac{1}{max\left\{\sigma - \sigma^{\frac{2-2n}{n}},\ \sigma^2\left(\left(\frac{2}{n}\right)^{\frac{2}{n-2}} - \left(\frac{2}{n}\right)^{\frac{n}{n-2}}\right)\right\}} & \text{if } \sigma < \left(\frac{n}{2}\right)^{\frac{n}{n-2}} \\ \frac{1}{max\left\{\sigma - \sigma^{\frac{2-2n}{n}},\ \sigma^{\frac{2n-2}{n}} - \sigma\right\}} & \text{if } \sigma \geq \left(\frac{n}{2}\right)^{\frac{n}{n-2}} \end{cases} \tag{4.6}$$

The index values vary between 0 and 1, with 0 indicating that the matrix is entirely consistent.

4.2.2.5. Aggregating Criteria

The aggregation of the final water quality map involved using the weighted linear combination (WLC) [242,282] at 300 m resolution. This approach involves the integration of standardized values and weighting coefficients, with the analysis con ducted using a raster calculator in ArcGIS Pro 3.4.2 software based on the specified formula [282]:

$$\text{WQI} = \sum w_i x_i \tag{4.7}$$

where WQI is water quality index of the final water quality map, w_i is the weight coefficient of the criteria, and x_i is the value of the standardized criteria.

4.2.2.6. Model Validation

In the context of MCDA, sensitivity analysis is an essential tool for evaluating the stability of results against the subjectivity of decision-makers [282]. This research conducted a thorough sensitivity analysis of the F-AHP results. For each criterion, the mean rank and standard deviation of the rank were computed across 1000 Monte Carlo simulations to assess the central tendency and variability of their relative importance, with random ±10 % to ±30 % noise to every comparison to account for variability in input parameters [252]. The analysis included metrics such as Top 1 Probability (the frequency with which a criterion attained the highest rank), Top 3 Probability (the probability of a criterion ranking within the top three), and Bottom 3 Probability (the likelihood of a criterion being ranked among the three lowest). These rank-based metrics provided insights into the dominance and uncertainty associated with each criterion.

Furthermore, the frequency distributions of normalized weights were analysed to understand the consistency of priority values under uncertainty [284]. Visualizations, including ranking probabilities graph and histograms were generated to facilitate the interpretation of results. This multi-dimensional sensitivity analysis enabled a comprehensive understanding of the robustness of the prioritization process and highlighted criteria that were either consistently influential or highly sensitive to variations in input judgments.

4.2.3. Optimizing Monitoring Stations

The study also focused on optimizing monitoring stations for water quality assessment, utilizing the final water quality map. The objective was to enhance an early warning system for eutrophication susceptible areas by strategically placing monitoring stations in regions with lower water quality while maintaining comprehensive coverage of the lake, thereby allowing for more frequent monitoring of these potentially critical areas and to gather enough

information of lake water quality for future modelling. The water quality map was divided into seven classes using Jenks natural breaks classification. The Jenks Natural Breaks classification method works through Goodness of Variance Fit (GVF) optimization, a statistical approach that minimizes the squared deviations within each class while maximizing the deviations between class means [285,286]. This makes it particularly effective for detecting and illustrating significant pattern changes in complex environmental datasets. Its ability to group data based on inherent structure rather than arbitrary intervals ensures more meaningful classifications in spatial and ecological analysis [285].

Each monitoring station was assigned to one of the water quality classes while maintaining comprehensive coverage of the lake and, where possible, preserving existing *in situ* locations. Additionally, maintaining consistent distances between monitoring stations is essential for reducing spatial bias and ensuring comprehensive, representative coverage of the lake [287]. Even spacing improves the accuracy of spatial interpolation methods and supports the development of reliable predictive models for water quality trends [287]. The final placement of monitoring station was based on a combination of data analysis results and expert knowledge, ensuring both scientific principles and practical relevance in the network design. This strategic placement enhances the effectiveness of monitoring networks and strengthens early warning systems for detecting contamination.

4.3. Results and Discussion

The analysis aims to model water quality in Vrana Lake and to identify areas susceptible to eutrophication based on assessing water quality due to anthropogenic factors, climate change, and external pollution sources, while also optimizing the monitoring network based on modelled water quality using GIS-MDCA.

4.3.1. Results for Selected Criteria According to Standardized Values

The standardization process was performed in Esri ArcGIS Pro 3.4.2 software and the resulting maps with spatial resolution 300 m are shown in Figure 4.3.

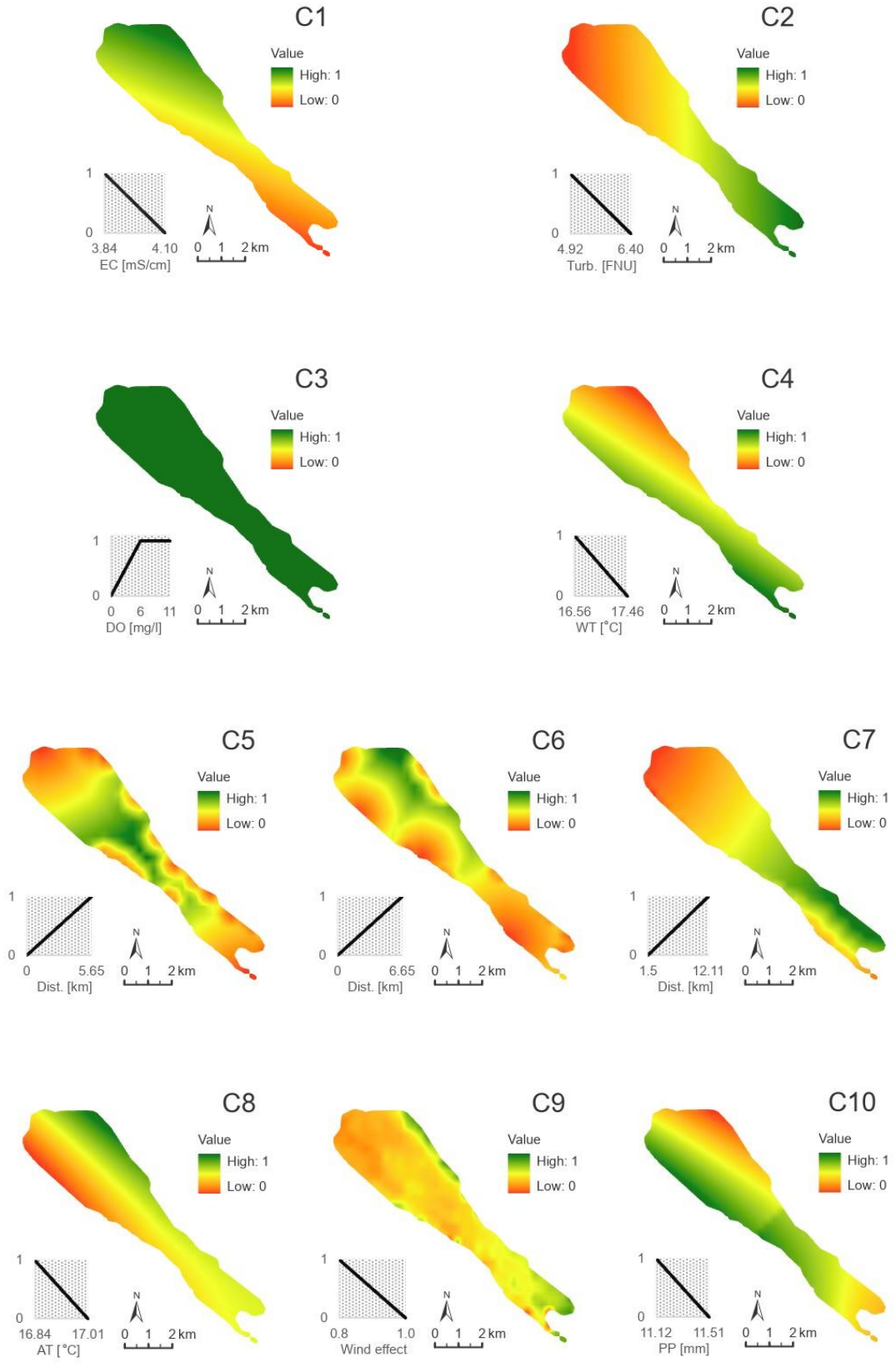

*Figure 4.3. Maps of standardized criteria and the aggregation per cluster. *Abbreviations alphabetically: AT – Air temperature, C1 – Electrical conductivity criterion, C2 – Turbidity*

criterion, C3 – Dissolved oxygen criterion, C4 – Water temperature criterion, C5 – Distance from water resource criterion, C6 – Distance from land nutrient runoff criterion, C7 – Distance from environmental pollutants criterion, C8 – Air temperature criterion, C9 - Wind criterion, C10 – Precipitation criterion, Dist. – Distance, PP – Precipitation, Turb. – Turbidity

Higher WT was measured in shallower regions on the northern and eastern sides of the lake, suggesting a lower water quality (Figure 4.3). The southern, deepest part of the lake near the Prosika canal measured the highest DO levels, while the northern area near the freshwater tributary Lateral channel had the lowest. However, all measured DO values are considered acceptable regarding their contribution to water quality, resulting in a water quality raster value of 1 for DO (Figure 4.3). Based on EC values, the southern part of the lake exhibits a lower water quality (Figure 4.3). This area, connected to the Adriatic Sea through the Prosika canal, experiences seawater intrusion during warmer months, leading to increased EC levels compared to the northern area. According to turbidity measurements, the northwestern part of the lake, near the Kotarka channel, has the highest turbidity and lowest water quality, whereas the southeastern part shows the lowest turbidity levels (Figure 4.3).

The standardization of distance from water resources indicates that areas with lowest water quality are located in the northern and southern part of the lake, as well as along the northeast shore, primarily due to tributaries, sea connection, and substantial rainwater runoff from sur rounding hilly terrains, respectively. In terms of distance from land nutrient runoff, the western part of the lake has lower water quality because of agricultural runoff from adjacent arable land (Figure 4.3). Additionally, the northern section is negatively impacted by anthropogenic pressures, including landfills, gas stations, and road networks (Figure 4.3).

Meteorological conditions impact water quality, with higher air temperature in the western part influenced by the Adriatic Sea, particularly during winter months, leading to a decline in water quality (Figure 4.3). Conversely, higher precipitation levels in the more continental areas of the lake contribute to water column mixing and decreased water quality (Figure 4.3). Additionally, wind patterns indicate that the eastern part of the lake is well-protected from strong predominant winds, while the central and northwestern areas are more exposed due to the sur rounding topographical features (Figure 4.3).

4.3.2. Results for Determined Criteria Weights

The F-AHP was conducted using online software Fuzzy AHP developed by Ryan and Nimick (2019) [241] by entering fuzzy numbers into the matrices, as shown in Table 4.2. The weighting

of the criteria, as well as their selection, was determined through a combination of the study area's specific characteristics, expert judgment, and a review of relevant literature. Particular emphasis was placed on physiochemical water quality parameters, reflecting the environmental conditions of the region. Additionally, a management-oriented perspective was rated, taking into account factors such as human activities, infrastructure, and regulatory frameworks. This integrated approach ensured a comprehensive evaluation that balances scientific data with practical, real-world considerations. The calculations were performed using Eq. 4.1-4.6. The inconsistency of the matrix based on the NI value of 0.176 is acceptable [260] (Table 4.3).

Table 4.2. F-AHP matrix using triangular fuzzy elements

F-AHP	C1	C2	C3	C4	C5	C6	C7	C8	C9	C10
C1	1	2 3 4	$\frac{1}{6}\frac{1}{5}\frac{1}{4}$	1	2 3 4	4 5 6	2 3 4	2 3 4	4 5 6	4 5 6
C2	$\frac{1}{4}\frac{1}{3}\frac{1}{2}$	1	$\frac{1}{8}\frac{1}{7}\frac{1}{6}$	$\frac{1}{4}\frac{1}{3}\frac{1}{2}$	2 3 4	4 5 6	2 3 4	2 3 4	4 5 6	4 5 6
C3	4 5 6	6 7 8	1	4 5 6	6 7 8	8 9 9	6 7 8	4 5 6	6 7 8	6 7 8
C4	1	2 3 4	$\frac{1}{6}\frac{1}{5}\frac{1}{4}$	1	2 3 4	4 5 6	2 3 4	2 3 4	4 5 6	4 5 6
C5	$\frac{1}{4}\frac{1}{3}\frac{1}{2}$	$\frac{1}{4}\frac{1}{3}\frac{1}{2}$	$\frac{1}{8}\frac{1}{7}\frac{1}{6}$	$\frac{1}{4}\frac{1}{3}\frac{1}{2}$	1	2 3 4	1	1	2 3 4	2 3 4
C6	$\frac{1}{6}\frac{1}{5}\frac{1}{4}$	$\frac{1}{6}\frac{1}{5}\frac{1}{4}$	$\frac{1}{9}\frac{1}{9}\frac{1}{8}$	$\frac{1}{6}\frac{1}{5}\frac{1}{4}$	$\frac{1}{4}\frac{1}{3}\frac{1}{2}$	1	$\frac{1}{4}\frac{1}{3}\frac{1}{2}$	$\frac{1}{4}\frac{1}{3}\frac{1}{2}$	1	1
C7	$\frac{1}{4}\frac{1}{3}\frac{1}{2}$	$\frac{1}{4}\frac{1}{3}\frac{1}{2}$	$\frac{1}{8}\frac{1}{7}\frac{1}{6}$	$\frac{1}{4}\frac{1}{3}\frac{1}{2}$	1	2 3 4	1	1	2 3 4	2 3 4
C8	$\frac{1}{4}\frac{1}{3}\frac{1}{2}$	$\frac{1}{4}\frac{1}{3}\frac{1}{2}$	$\frac{1}{6}\frac{1}{5}\frac{1}{4}$	$\frac{1}{4}\frac{1}{3}\frac{1}{2}$	1	2 3 4	1	1	2 3 4	2 3 4
C9	$\frac{1}{6}\frac{1}{5}\frac{1}{4}$	$\frac{1}{6}\frac{1}{5}\frac{1}{4}$	$\frac{1}{8}\frac{1}{7}\frac{1}{6}$	$\frac{1}{6}\frac{1}{5}\frac{1}{4}$	$\frac{1}{4}\frac{1}{3}\frac{1}{2}$	1	$\frac{1}{4}\frac{1}{3}\frac{1}{2}$	$\frac{1}{4}\frac{1}{3}\frac{1}{2}$	1	1
C10	$\frac{1}{6}\frac{1}{5}\frac{1}{4}$	$\frac{1}{6}\frac{1}{5}\frac{1}{4}$	$\frac{1}{8}\frac{1}{7}\frac{1}{6}$	$\frac{1}{6}\frac{1}{5}\frac{1}{4}$	$\frac{1}{4}\frac{1}{3}\frac{1}{2}$	1	$\frac{1}{4}\frac{1}{3}\frac{1}{2}$	$\frac{1}{4}\frac{1}{3}\frac{1}{2}$	1	1

(C1) EC, (C2) turbidity, (C3) DO, (C4) WT, (C5) distance from water resources, (C6) distance from land nutrient runoff, (C7) distance from environmental pollutants, (C8) air temperature, (C9) wind, and (C10) precipitation

Table 4.3. Criteria weighting and consistency

Criterion	Minimal weight coefficient	Mean weight coefficient	Maximum weight coefficient
EC	0.131	**0.146**	0.156
Turbidity	0.090	**0.101**	0.114
DO	0.358	**0.363**	0.363
WT	0.131	**0.146**	0.156
Distance from water resources	0.052	**0.056**	0.062
Distance from land nutrient runoff	0.024	**0.024**	0.026
Distance from environmental pollutants	0.052	**0.056**	0.062
Air temperature	0.053	**0.058**	0.065
Wind	0.025	**0.025**	0.027
Precipitation	0.025	**0.025**	0.027
Consistency (NI)	**0.176**		

4.3.3. Results for Aggregated Criteria

The development of a final water quality map involved the aggregation of criteria mean weight coefficients performed using the WLC in ArcGIS Pro 3.4.2. In the implementation of this method, each single aggregated raster model, represented as raster cells of 300 ×300 m, is multiplied by the weights shown in Table 4.3 using Eq. 4.7. Ultimately, a final multi-criteria model of water quality was created (Figure 4.4). The map employs a continuous colour gradient from green (high quality) to yellow (low quality) to visualize variations in water quality. Cell values range from 0.596 to 0.737, suggesting overall good water quality in the lake, although some areas show slightly poorer quality. The southeast-central part of the lake has the highest water quality, while the western parts show a decline in water quality based on factors such as anthropogenic influence and meteorological parameters. Human activities result in higher turbidity levels in the lake as a nutrient influx from surrounding land and nearby road network and industries influence water quality, while meteorological influence includes higher air temperature and wind in this region. The southern region near Prosika canal, despite being the deepest part with the lowest WT, exhibits slightly lower water quality, influenced primarily by seawater influx from the Adriatic Sea and environmental influences in terms of nutrient runoff and pollution from transportation network (Figure 4.4).

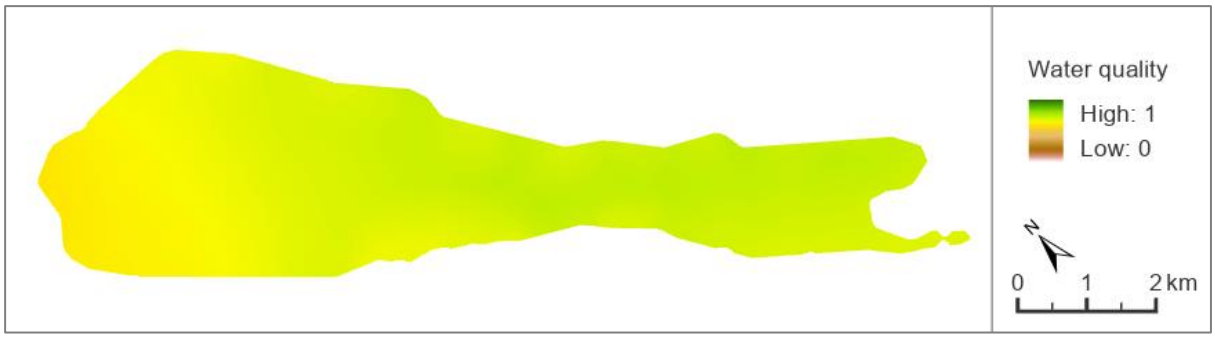

Figure 4.4. Aggregation of the final water quality map using weighted linear combination of all criteria (green colour represents higher water quality, while yellow and light orange represent lower water quality)

4.3.4. Model Validation

This study conducted an extensive sensitivity analysis of the F-AHP results through 1000 Monte Carlo simulations. Figure 4.5 shows histograms of normalized weights for each criterion derived from 1000 Monte Carlo simulations, highlighting the stability and variability of weight distributions under uncertainty, when compared to F-AHP weights provided in Table 4.3. Table 4.4 provides an overview of the conducted sensitivity analysis.

The decision model demonstrates remarkable stability, consistently ranking DO as the top criterion without exception (Table 4.4). EC and WT are in close competition for the second and third positions, with their rankings nearly evenly split. Turbidity consistently holds the fourth rank with no fluctuations. In contrast, criteria precipitation, wind, and distance from land nutrient runoff consistently rank among the bottom three, indicating their low importance. Middle-tier criteria, such as air temperature, distance from water resources, and distance from environmental pollutants show moderate variability.

Figure 4.6 shows violin plot of rank distributions based on 1000 Monte Carlo simulations. Narrow, concentrated violins around specific ranks indicate high rank stability, while wider shapes or multiple peaks suggest greater variability and sensitivity to input uncertainty. In Figure 4.6, DO shows the most concentrated violin shape at rank 1, indicating it was consistently identified as the most important criterion across almost all simulations. Similarly, turbidity shows stability at rank 4. EC and WT also demonstrate relatively stable ranks around the 2nd and 3rd rank, though with slightly more variability. Criteria such as distance to water resource, distance to land nutrient runoff, and distance to environmental pollutants exhibit broader or bimodal violin shapes, reflecting greater uncertainty in their rank positions, fluctuating mostly between mid-ranks (5th to 7th). Meanwhile, air temperature, wind, and precipitation have distributions concentrated towards bottom three ranks, suggesting they were

consistently considered less important, although slight spread indicates occasional shifts in perceived importance depending on input variation.

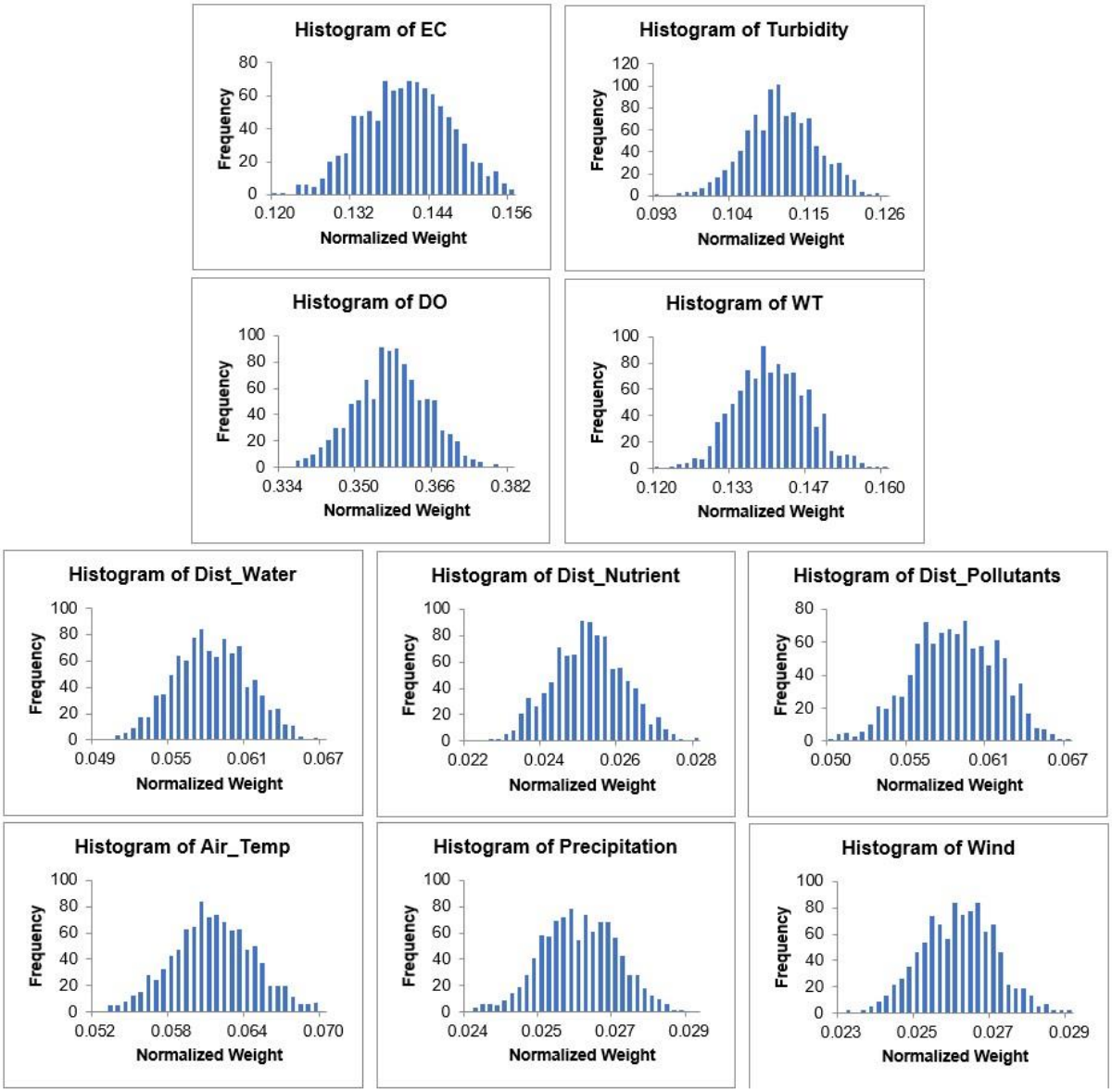

Figure 4.5. Histograms of normalized weights for each criterion based on 1000 Monte Carlo simulations

Table 4.4. Summary of mean ranks, standard deviations, and probabilities for the criteria based on 1000 Monte Carlo simulations

Criterion	Mean Rank	Std Dev of Rank	Top 1 Probability	Top 3 Probability	Bottom 3 Probability
DO	1	0	1 (100%)	1 (100%)	0
EC	2.48	0.50	0	1 (100%)	0
WT	2.52	0.50	0	1 (100%)	0
Turbidity	4	0	0	0	0
Air temperature	5.41	0.67	0	0	0
Distance from water resources	6.28	0.73	0	0	0
Distance from environmental pollutants	6.30	0.72	0	0	0
Precipitation	8.66	0.70	0	0	1 (100%)
Wind	8.67	0.70	0	0	1 (100%)
Distance from land nutrient runoff	9.66	0.60	0	0	1 (100%)

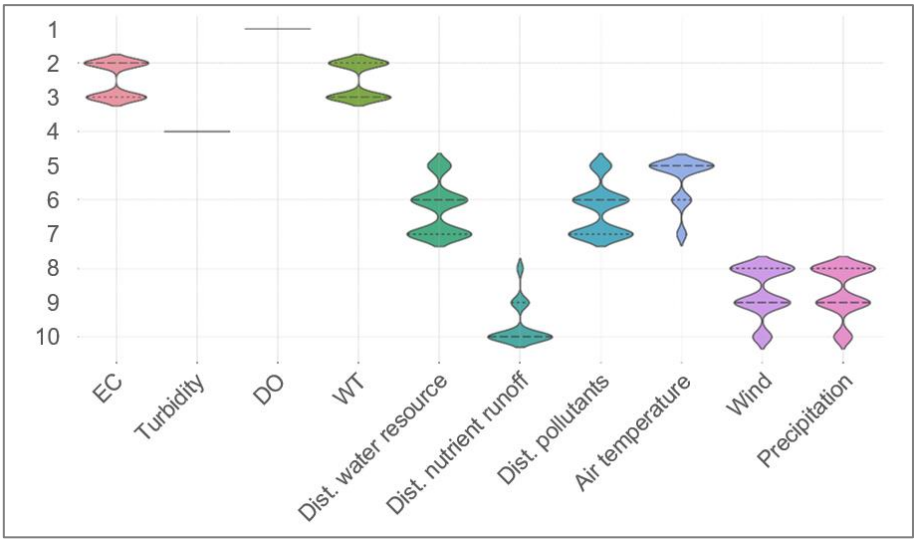

Figure 4.6. Violin plot of rank distributions based on 1000 Monte Carlo simulations

4.3.5. Optimizing Monitoring Stations

The study outlines a comprehensive approach to establishing an optimal monitoring network for monitoring water quality, consisting of seven strategically placed stations, each corresponding to a water quality class based on Jenks classification (Figure 4.7). Strategic positioning is crucial for effective contaminant detection and enhancing a eutrophication early

warning system, while also ensuring coverage across the lake for comprehensive monitoring of water quality. Continuous data collection from optimizing monitoring stations will aid in developing effective lake recovery and management plans to address potential water quality issues from unpredictable sources.

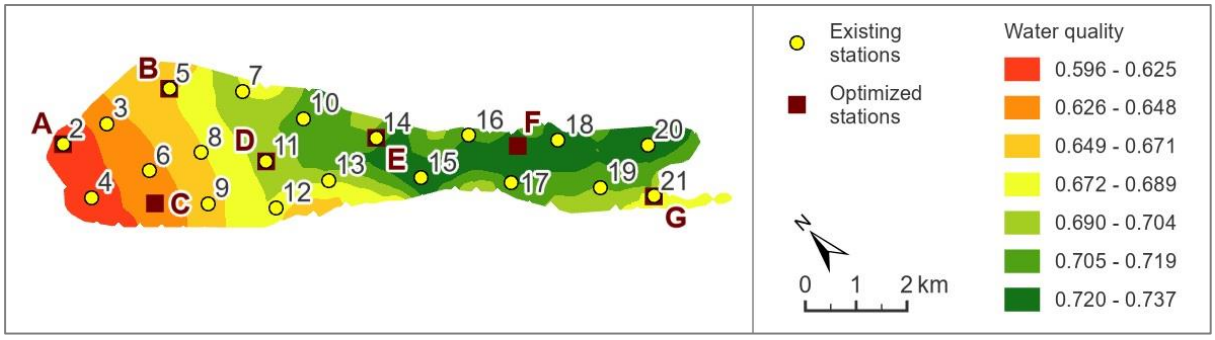

Figure 4.7. Map showing water quality regions, along with the locations of existing in situ *stations and optimized monitoring stations*

The water quality map in Figure 4.7 and graph in Figure 4.8 show four monitoring stations from the existing monitoring network in the central-southeast part of the lake in the class 1 (class with the highest water quality), four stations in the class 2, three stations per class 3 and 4, two stations per class 5, class 6, and class 7 (class with the highest water quality). The proposed optimized network of one station per Jenks water quality class is shown in Figure 4.7 and in graph in Figure 4.8, showing the distribution of these stations and the comprehensive coverage of the lake.

To enhance the effectiveness of the monitoring efforts, the optimized network incorporates three existing monitoring stations, specifically point 2, point 11, and point 21, which have been consistently utilized by the Public Institution Nature Park Vransko Jezero. These points from the existing network correspond to point A, D, and G in the optimized network, respectively (Figure 4.7). These stations are strategically positioned near the main freshwater tributary in the north, in the centre of the lake, and near the Prosika canal in the south, allowing for a comprehensive assessment of water quality in these critical areas. Additionally, two more station from the comprehensive network designed by Batina et al. (2025) [25] have been included in the optimized network; namely point 5 and point 14, corresponding to points B and E in the optimized network, respectively. Additional two new monitoring stations C and F have been placed to represent two remaining classes, ensuring they maintain approximately the same distances between neighbouring stations (Figure 4.7). The distances between point A-E are

around 2.2 km, and distance between points E-G are around 2.8 km, due to the lake's shape and the allocation of water quality classes.

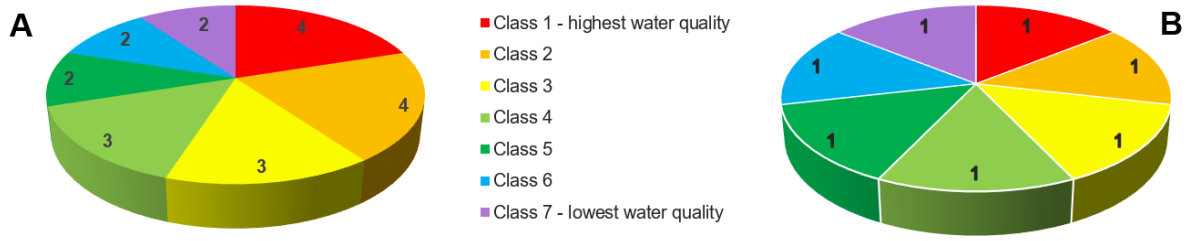

Figure 4.8. Allocation of monitoring stations per water quality class of (a) existing 20 in situ *stations and (b) optimized 7 stations*

4.3.6. Comparison With Similar Studies

To the best of authors' knowledge, no previous study has applied a GIS-MCDA framework integrated with the F-AHP to assess water quality in a coastal shallow lake. The methodology proposed in this research of combining F-AHP, water quality parameters, Monte Carlo sensitivity analysis, and optimized monitoring network design builds upon and extends several existing GIS-MCDA models through the inclusion of advanced spatial and decision-support components.

The use of spatial criteria for assessing water quality variability is conceptually supported by the study of Akar et al. (2024) [24], who implemented AHP within a GIS-MCDA framework to evaluate water quality in Turkish lakes. Similarly, the spatial detection of eutrophication-prone zones near inflows is in line with the findings of Chen et al. (2021) [258], who applied a multi-year water quality index approach in Erhai Lake to capture nutrient-related seasonal dynamics.

The integration of environmental indicators into hazard mapping follows the approach of Romanelli et al. (2013) [288], who developed a Lake Pollution Hazard Index for shallow lakes in Argentina. Additionally, the inclusion of anthropogenic stressors in multi-criteria assessments corresponds with the methodology of Avram et al. (2021) [269], who mapped lake degradation across Romania. The use of fuzzy logic in decision-making processes is consistent with the work of Ghosh and Gope (2021) [248], who applied F-AHP for watershed prioritization in data-scarce regions.

The monitoring network optimization developed in this study is further supported by the research of Lagogiannis et al. (2024) [249], who employed GIS-based fuzzy MCDA to design an automated water monitoring system, and by Theochari et al. (2021) [250], who combined MCDA and GIS to strategically position hydrometric and meteorological stations in complex

terrains. While previous studies confirm the value of spatial multi-criteria modelling, the present study advances the field by integrating *in situ* measurements, applying probabilistic sensitivity analysis, and designing a spatially balanced monitoring network specifically tailored to the environmental and hydrological characteristics of coastal shallow lakes.

4.4. Conclusions

This study demonstrated that the integration of GIS and MCDA, through the application of the F-AHP, provides an effective approach for evaluating the spatial distribution of water quality in coastal shallow lakes. By applying the developed model to the Vrana Lake, a comprehensive water quality map was generated, incorporating physicochemical parameters, the influence of environmental pollutants, topographic characteristics, land use, and meteorological conditions. One of the most significant findings was the identification of spatial heterogeneity in water quality, with lower quality observed in the northwestern and southern parts of the lake. These zones were identified as the most susceptible to eutrophication due to the combined impact of anthropogenic activities and seawater intrusion. To enable effective and timely monitoring of lake conditions, an optimized monitoring network consisting of seven strategically distributed stations was developed. This network ensures full spatial coverage and representation of all water quality classes, and provides a basis for early detection of eutrophication processes. Furthermore, the sensitivity analysis, conducted using 1000 Monte Carlo simulations, confirmed the stability of the developed decision model. The results indicated a high level of robustness, although a moderate degree of variability was observed among mid-ranking criteria, particularly between EC and WT.

Despite the achieved results, the study has several limitations. The most prominent limitation is the one-year monitoring period, which is insufficient for detecting long-term trends or rare extreme events. In addition, for certain criteria, high-resolution primary spatial data were unavailable, necessitating partial reliance on secondary sources and interpolation, which may affect the accuracy of the final outputs.

Future research will focus on extending the monitoring period to include multi-year datasets, with the aim of better understanding seasonal and interannual variations. The use of Real-Time Kinematic (RTK) drones is also planned, allowing for more precise, faster, and flexible water sampling, particularly in areas with limited accessibility. Beyond technological improvements, the study also aims to compare various methods for determining weighting coefficients, including objective techniques such as Entropy and CRITIC, as well as subjective methods based on the AHP, in order to enhance model transparency and reliability. The sensitivity

analysis will also be expanded through the application of additional methodological approaches, such as local sensitivity analysis, variance-based analysis, and scenario-based evaluation. These approaches will allow for a deeper understanding of the influence of individual criteria on the final model outcomes and support the adaptation of the model to specific management objectives.

Based on the results obtained, it can be concluded that the developed methodological framework has high applicability under real-world water resource management conditions. The application of this approach enables informed, data-driven decision-making, improvement of monitoring networks, and the development of strategies focused on the early detection of ecological risks. Ultimately, this approach contributes significantly to the sustainable management of water quality in coastal shallow lakes, particularly under increasing climatic and anthropogenic pressures.

5. SIGMaL: An Integrated Framework for Water Quality Monitoring in a Coastal Shallow Lake

This chapter has been published as: *Batina, A.; Šiljeg, A.; Krtalić, A.; Šerić, LJ. (2026). SIGMaL: An Integrated Framework for Water Quality Monitoring in a Coastal Shallow Lake.* Remote Sensing*,* 18*(2), 312. doi: 10.3390/rs18020312*.

Conceptualization, A.B., A.Š., L.Š. and A.K.; methodology, A.Š.; software, A.B. and L.Š.; validation, A.Š. and L.Š.; investigation, A.B. and L.Š.; resources, A.Š. and A.K.; data curation, A.B. and L.Š.; formal analysis, A.B., A.Š. and L.Š.; writing—original draft preparation, A.B.; writing—review and editing, A.Š. and A.K.; visualization, A.B. and L.Š.; supervision, A.Š., L.Š. and A.K.; project administration, A.B.; funding acquisition, A.Š. and A.K. All authors have read and agreed to the published version of the manuscript.

Abstract

Coastal lakes require monitoring approaches that capture spatial and temporal variability beyond the limits of conventional *in situ* measurements. In this study, a SIGMaL framework (Satellite–*In situ*–GIS-multicriteria decision analysis (MCDA)–Machine Learning (ML)) was developed, a unified methodology that integrates *in situ* monitoring, GIS MCDA-derived water quality index (WQI), satellite imagery, and ML models for comprehensive coastal lake water quality assessment. A WQI, derived from a 12-month series of *in situ* measurements and environmental parameters, was used alongside four physicochemical parameters measured by a multiparameter probe. First, satellite reflectance from each sensor was used to train a set of nine regression models for modelling electrical conductivity (EC), turbidity, water temperature (WT), and dissolved oxygen (DO). Second, convolutional neural networks (CNNs) with spectral and temporal inputs were trained to classify WQI classes, enabling a cross-sensor evaluation of their suitability for lake water quality monitoring. Third, the trained CNNs were applied to generate WQI maps for a subsequent 12-month period without *in situ* data. Across all analyses, WQI-based models provided more stable and accurate models than those trained on raw parameters. Sentinel- 2 achieved the most consistent WQI performance (AUC ≈ 1.00, R^2 ≈ 0.84), PlanetScope captured fine-scale spatial detail (R^2 ≈ 0.77), while Landsat 8–9 was most effective for WT but less reliable for multi-class WQI discrimination. Sentinel-2 is recommended as the primary satellite sensor for WQI mapping within the SIGMaL framework. These findings demonstrate the advantages of WQI-based modelling and highlight the potential of ML– remote sensing integration to support coastal lake water quality monitoring.

Keywords: convolutional neural networks; machine learning; satellite data; regression modelling; WQI assessment

5.1. Introduction

Freshwater and coastal lake ecosystems are globally vulnerable to accelerating pressures from climate change, land use transformations, and hydrological instability, making accurate and timely water quality monitoring increasingly essential [3,4,289,290]. Traditional *in situ* measurements remain the foundation of ecological assessment, yet their limited spatial and temporal coverage creates significant gaps in understanding ecosystem-wide dynamics, particularly in shallow coastal lakes where conditions can change rapidly [9].

Parallel advances in geospatial technologies, satellite remote sensing, and machine learning (ML) have created opportunities to bridge these gaps by integrating multi-source environmental information into coherent predictive frameworks [240]. Although many recent studies have explored remote sensing-based retrieval of single physicochemical parameters [16,24], inconsistencies in temporal matching, sparse *in situ* measurement networks, and spatial heterogeneity frequently constrain predictive robustness and limit operational use.

Vrana Lake in Dalmatia, Croatia, a shallow coastal freshwater system hydrologically connected to the Adriatic Sea, represents an ecologically sensitive environment where seawater intrusion, seasonal fluctuations, and nutrient inputs interact to shape water quality [25]. Previous research has characterized these dynamics [26,291,292], yet monitoring efforts remained spatially limited and did not fully capture system-wide variability [25]. To overcome this challenge, GIS-based multicriteria decision analysis (MCDA) has proven effective for synthesizing environmental factors into spatial models of water quality, enabling the identification of critical zones vulnerable to eutrophication and pollution pressures [26]. Similarly, satellite missions such as Landsat 8–9, Sentinel-2, and PlanetScope offer high-frequency, multispectral imagery that can be correlated with *in situ* data to map key water quality parameters across the entire lake surface [103].

These methods provide valuable complementary perspectives, but their full potential lies in their integration with advanced data-driven techniques. To ensure reliable temporal matching, water quality index (WQI) values were compared with satellite imagery acquired within a 10-day window from each field campaign. Previous studies have shown that a 1-day time window is ideal, with the possibility of extending up to 10 days if conditions do not significantly change [293,294], and further research has suggested that this window also depends on satellite resolution, where higher spatial, spectral, and radiometric resolution increases the reliability of extending the time window for pairing satellite and ground-based data [295]. A 10-day temporal tolerance was selected in this study to minimize the impact of cloud cover and to maximize the

availability of usable satellite scenes, while still maintaining ecological relevance in the comparison of *in situ* and remote sensing data, without major weather changes between the measurement day and satellite overpass. In practice, most satellite–*in situ* matchups occurred within 0–3 days of the field measurements.

Most remote sensing and ML studies addressing water quality rely on a direct comparison between raw *in situ* measurements and satellite imagery, with models trained to predict individual physicochemical parameters [296]. While effective for local analyses, this approach is often constrained by sparse monitoring networks and high spatial variability within inland waters, resulting in limited predictive robustness. In contrast, the present study emphasizes the use of an integrated WQI, generated through GIS-MCDA by Batina and Šiljeg (2025) [26], as the primary reference for model training (Figure A4). This index aggregates multiple parameters into a single, spatially continuous representation of water quality, thereby providing a more robust basis for predictive modelling. As a secondary comparison, ML models were also trained on raw *in situ* data, allowing the study to evaluate differences between the conventional approach and the proposed WQI-driven framework.

ML offers a powerful toolset for bridging the gap between point-based field data and spatially continuous remote sensing observations [296]. By leveraging statistical learning algorithms, ML can identify complex nonlinear relationships between spectral reflectance and water quality parameters [297], as well as classify ecological conditions into distinct quality classes. In the context of Vrana Lake, ML enables the combination of *in situ* measurements, raster-based GIS models, and satellite imagery into a unified monitoring framework, enhancing monitoring accuracy and supporting long-term ecological assessment in sensitive protected areas.

This study introduces SIGMaL, a unified framework for lake water quality monitoring that integrates satellite imagery, *in situ* measurements, GIS-MCDA, and ML into a single analytical pipeline. SIGMaL combines four complementary components: (i) a yearlong series of monthly *in situ* measurements of key physicochemical parameters; (ii) raster- based WQI derived from GIS-MCDA, providing spatially continuous water quality classes; (iii) multi-sensor satellite observations from Sentinel-2, Landsat 8–9, and PlanetScope (acquired and evaluated independently); and (iv) ML models, including convolutional neural networks (CNNs) for WQI classification, trained separately for each sensor to enable a fair cross-sensor comparison.

To overcome the spatial limitations of the 20 *in situ* monitoring stations, SIGMaL uses MCDA-derived raster densification, expanding the dataset to 318 samples that better represent lake water quality variability. Satellite reflectance data from each sensor were paired with these samples and used to train ML models under identical modelling settings, enabling systematic

comparison of spectral, spatial, and temporal performance across sensors. Designed as a modular, scalable, and reproducible workflow, SIGMaL enhances spatial and temporal coverage beyond conventional point-based monitoring and provides a robust basis for evaluating the suitability of different satellite platforms for coastal shallow lake environments. The framework supports improved ecological assessment and offers a transferable methodology for data-limited freshwater and coastal shallow lake systems.

In contrast to most lake studies in which ML is trained directly on raw *in situ* measurements [75,103,298,299], the GIS–MCDA WQI is adopted in this study as the primary modelling target. Two parallel strategies are employed: (A) CNN-based classification of WQI classes (principal track), and (B) regression on raw *in situ* parameters (comparison track). We hypothesize that (1) the WQI derived from GIS–MCDA provides a more stable modelling target than individual *in situ* parameters, and (2) the SIGMaL framework can accurately classify spatial water quality patterns across a complex coastal lake. The main findings indicate that the SIGMaL framework integrating *in situ* data, GIS–MCDA WQI, satellite imagery, and machine learning provides a more stable and spatially comprehensive approach to lake water quality monitoring than traditional parameter-based models, with Sentinel-2 offering the strongest overall performance and WQI-based CNNs consistently outperforming raw-parameter regression across all sensors.

5.2. Materials and Methods

5.2.1. Study Area

Vrana Lake, located in Dalmatia near the eastern Adriatic coast, is the largest natural freshwater lake in Croatia, covering an area of about 30 km^2 [200]. The lake extends between 43°51′–43°57′N and 15°30′–15°39′E (WGS84) (Figure 5.1). It is characterized by shallow water that undergoes strong seasonal fluctuations, with higher water levels in winter and spring, and lower levels in summer and autumn [201]. Due to its ecological importance and species richness, the lake and its surroundings are protected within the Vrana Lake Nature Park.

The lake's hydrological regime is influenced by multiple factors, including precipitation, tributary inflows, groundwater exchange, evaporation, and its artificial connection to the Adriatic Sea through the Prosika canal [25]. During periods of low water levels, seawater intrusion increases salinity, whereas freshwater inputs from surrounding karst fields and springs reduce salinity during wetter periods [203]. These dynamics, combined with wind-driven mixing, strongly affect the water quality and ecosystem health of the lake.

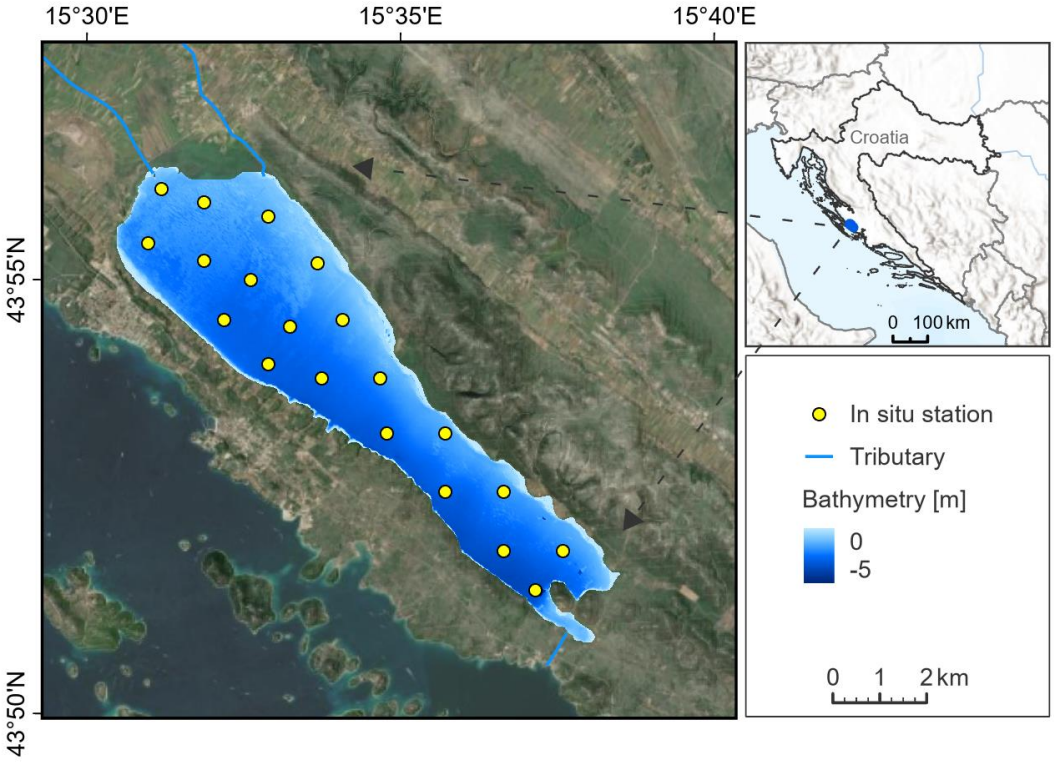

Figure 5.1. Vrana Lake with monitoring stations and main hydrological features

5.2.2. Data Collection

Field surveys were conducted on a monthly basis from July 2023 to June 2024. Measurements were performed in the morning hours (08:00–13:00 local time) to minimize diurnal variability in water temperature (WT), dissolved oxygen (DO), and chlorophyll-a concentrations. Measurement days were chosen to coincide with stable meteorological conditions, avoiding precipitation and strong winds that could compromise data comparability [25]. Each campaign was carried out by a team aboard a small research vessel using YSI EXO2 multiparameter probe (YSI Inc., Yellow Springs, OH, USA). The probe was calibrated before every campaign following manufacturer guidelines (explained in Section 5.2.2.2). Due to adverse weather conditions, the November 2023 survey was postponed and conducted on 4 December, while the regular December survey took place on 19 December [25]. All other campaigns were carried out as scheduled.

5.2.2.1. In Situ *Measurements*

Batina et al. (2025) [25] established a network of 20 fixed monitoring stations across the lake to ensure sufficient spatial coverage and representation of hydrological and ecological variability (Figure 5.1). Over the 12-month monitoring period, maximum of 20 stations was measured in each of the 12 campaigns, resulting in 230 valid station measurements per

parameter, as not all sites could be measured every month due to weather or equipment restraints.

Although several physicochemical and biological parameters were measured [25], this study includes DO, WT, turbidity, and electrical conductivity (EC), resulting in 230 observations for each of these four parameters over the one-year research period. The selection of these parameters is supported by a year-long multiparameter analysis and correlation study conducted in Vrana Lake [25], where they were identified as dominant drivers of lake water quality dynamics. Their selection was further supported by expert input from the Ruđer Bošković Institute and the Public Institution Vrana Lake Nature Park. Moreover, these parameters constitute the core physicochemical inputs of the GIS–MCDA-based WQI model, whose robustness was validated through sensitivity analysis and Monte Carlo simulations by Batina and Šiljeg (2025) [26] (Figure A4).

5.2.2.2. Multiparameter Probe

The YSI EXO2 multiparameter probe is designed to measure a wide range of physicochemical indicators, including WT, DO, EC, salinity, turbidity, and chlorophyll-a, with manufacturer-specified accuracies that vary by parameter (e.g., ±0.01 °C for WT, ±0.5% or 0.001 dS/m for EC, and ±1% or 0.1 mg/L for DO) [210]. Such precision makes the instrument highly suitable for ecological and hydrological monitoring; however, its reliability depends heavily on proper handling and routine calibration. Regular maintenance is essential to mitigate external influences such as sensor fouling, sediment deposition, or biological growth, which can compromise data quality. Calibration should be carried out using standard solutions of known conductivity, oxygen reference standards, and systematic cleaning of optical sensors to ensure that field measurements remain both accurate and reproducible [210].

The calibration procedure of the YSI EXO2 multiparameter probe was applied in accordance with the instructions provided in the official EXO User Manual [210] (Figure 5.2). Prior to each calibration step, the EXO calibration cup and sensors were rinsed two to three times with the appropriate standard for the parameter being adjusted, with the rinse solutions discarded and replaced with fresh calibration standard. When calibration standards were not used immediately, the sensors and cup were rinsed with deionized water and dried with a lint-free cloth before refilling. The calibration cup was filled to the recommended level to ensure that all sensors were fully submerged, while precautions were taken to avoid cross-contamination. Clean, dry probes were mounted on the sonde, and a calibration-dedicated guard was installed and tightened, and a separate guard was reserved for field deployments to maintain accuracy

and cleanliness. The sequence followed the prescribed order from the manual: verification of the temperature sensor against a certified reference thermometer, calibration of EC first, then pH and ORP, followed by turbidity, and finally the optical sensors such as DO and depth. This order reflects sensor interdependencies and is designed to minimize error propagation, ensuring that the EXO2 provides reliable and reproducible field measurements [210].

Figure 5.2. Calibration of the YSI EXO2 multiparameter probes

5.2.3. Satellite Data Acquisition and Preprocessing

This study used atmospherically corrected Level-2 (surface reflectance) imagery from Sentinel-2 MultiSpectral Instrument (MSI; European Space Agency, Paris, France), Landsat 8–9 Operational Land Imager (OLI)/Thermal Infrared Sensor (TIRS; National Aeronautics and Space Administration and U.S. Geological Survey, Washington, DC, USA), and PlanetScope SuperDove satellites (Planet Labs PBC, San Francisco, CA, USA). Sentinel- 2 images were obtained through the Copernicus Browser (European Space Agency, Paris, France), Landsat 8–9 through the USGS Earth Explorer (U.S. Geological Survey, Reston, VA, USA), and PlanetScope from Planet Explorer (Planet Labs PBC, San Francisco, CA, USA) [207]. Because the goal of the study was not to compare atmospheric correction algorithms, pre-processed Level-2 data were adopted to ensure consistency across sensors and to focus computational effort on the integration of remote sensing, GIS–MCDA, and ML.

Although employing pre-processed imagery simplifies the workflow, the authors are aware of potential limitations, especially over inland waters where atmospheric conditions, adjacency effects, aerosol variability, and water surface reflections complicate correction accuracy [300,301]. Previous research has shown the potential of advanced remote sensing and ML

approaches to enhance water quality monitoring when atmospheric corrections are adequately addressed [302]. Furthermore, Pan et al. (2022) [300] evaluated ten atmospheric correction algorithms over lakes and highlighted that adjacency effects near land and inconsistent aerosol modelling can reduce the fidelity of water reflectance retrievals. Similarly, Zhu and Xia (2023) [301] discuss that while atmospheric correction is generally beneficial for remote sensing inversion tasks, in large-scale statistical inference studies small residual atmospheric errors may have limited impact on performance when models rely on strong statistical correlations rather than pixel-level physical retrievals. Because the focus of this study is on the integrated WQI rather than individual water quality parameters, this approach was considered acceptable: it maintains consistency across Sentinel-2, Landsat 8–9, and PlanetScope datasets, and ensures that computational complexity is focused on the ML and MCDA integration stages rather than on refining atmospheric correction.

Moderate-resolution sensors such as Sentinel-2 (10–60 m, 5-day revisit) and Landsat 8–9 (30–100 m, 8-day aggregate revisit) have been widely used in water quality monitoring [103,303,304]. Recently, PlanetScope has emerged as a valuable alternative for small or narrow waterbodies due to its daily revisit and 3 m spatial resolution, despite its limited spectral depth relative to Sentinel-2 and Landsat (Table 5.1). The Landsat 8–9 collection includes OLI optical and TIRS thermal bands, with 30 m and 100 m reflectance and 15 m panchromatic resolution. Sentinel-2 MSI provides 13 spectral bands (10–60 m) in visible and near-infra red (NIR), including three Red-Edge bands critical for aquatic applications. PlanetScope Level-3B products consist of 8 spectral bands at 3 m resolution.

Field measurement dates were aligned with predicted Sentinel-2 and Landsat 8–9 overpasses, while PlanetScope was excluded from planning due to its daily revisit capability. Because Vrana Lake is shallow and highly exposed to wind, currents and waves can mix the entire water column, especially during strong Bora and Jugo events in winter and Maestral winds in summer, ensuring relatively uniform temperature and nutrient conditions [26]. Favourable meteorological conditions were therefore essential; satellite scenes had to be cloud-free and precipitation-free, and fieldwork had to be conducted under safe wind conditions for the vessel crew.

Table 5.2 summarizes the dates of *in situ* measurements alongside the closest available satellite acquisitions without clouds. As shown, satellite imagery did not always coincide with field measurements, and scenes from different sensors were often available on different days. Columns Max prior (days) and Max after (days) in

Table 5.2 indicate the maximum temporal offset between each *in situ* campaign and corresponding satellite scenes, illustrating, for example, that July measurements coincided with a Landsat 9 overpass and were preceded by Sentinel-2 and PlanetScope acquisitions by one day.

Table 5.1. Comparison of Sentinel-2 MSI, Landsat 8–9 OLI/TIRS, and PlanetScope sensor specifications

Category	**Sentinel-2 MSI**	**Landsat 8–9 OLI/TIRS**	**PlanetScope**
Spatial resolution	10–60 m	15 m (pan), 30–100 m	3 m
Temporal resolution	5 days	16 days (8-day combined)	Daily
Spectral resolution	13 bands	11 bands	8 bands
Bandwidth (nm)			
Coastal	B1: 433–453 (60 m)	B1: 433–453 (30 m)	B1: 431–452 (3 m)
Blue	B2: 460–525 (10 m)	B2: 450–515 (30 m)	B2: 465–515 (3 m)
Green I	-	-	B3: 513–549 (3 m)
Green	B3: 542–577 (10 m)	B3: 525–600 (30 m)	B4: 547–583 (3 m)
Yellow	-	-	B5: 600–620 (3 m)
Red	B4: 650–680 (10 m)	B4: 630–680 (30 m)	B6: 650–680 (3 m)
Red Edge 1	B5: 697–711 (20 m)	-	B7: 697–713 (3 m)
Red Edge 2	B6: 733–747 (20 m)	-	-
Red Edge 3	B7: 773–792 (20 m)	-	-
NIR (narrow)	B8: 780–885 (10 m)	-	-
NIR	B8A: 854–875 (20 m)	B5: 845–885 (30 m)	B8: 845–885 (3 m)
Water vapour	B9: 936–955 (60 m)	-	-
Cirrus	B10: 1359–1388 (60 m)	B9: 1360–1390 (30 m)	-
SWIR 1	B11: 1569–1659 (20 m)	B6: 1560–1660 (30 m)	-
SWIR 2	B12: 2115–2289 (20 m)	B7: 2100–2300 (30 m)	-
TIRS 1	-	B10: 10600–11200 (100 m)	-
TIRS 2	-	B11: 11500–12500 (100 m)	-
Panchromatic	-	B8: 500–680 (15 m)	-
Free Imagery	Unlimited	Unlimited	5,000 km^2/month (education) [207]

Table 5.2. Overview of dates of in situ *measurements, corresponding satellite acquisitions, temporal offsets, and number of measured stations*

***In Situ* Date**	**Sentinel-2**	**Landsat 8–9**	**PlanetScope**	**Max Prior (Days)**	**Max After (Days)**	**Stations Measured**
17 July 2023	16 Jul	17 Jul	16 Jul	–1	0	19
18 August 2023	20 Aug	18 Aug	18 Aug	0	2	20
27 September 2023	29 Sep	27 Sep	27 Sep	0	2	12
13 October 2023	09 Oct	05 Oct	16 Oct	–8	3	20
4 December 2023	23 Nov	08 Dec	08 Dec	–11	4	20
19 December 2023	18 Dec	16 Dec	19 Dec	–3	0	20
11 January 2024	12 Jan	09 Jan	11 Jan	–2	1	19
19 February 2024	21 Feb	18 Feb	20 Feb	–1	2	20
14 March 2024	12 Mar	13 Mar	14 Mar	–2	0	20
29 April 2024	21 Apr	30 Apr	30 Apr	–8	1	20
24 May 2024	24 May	01 Jun	18 May	–6	7	20
17 June 2024	15 Jun	17 Jun	17 Jun	–2	0	20
Extremes / Total	–	–	–	–11	7	230

Quantitative evidence of rapid temporal variability in Vrana Lake is provided by Batina et al. (2025) [25], who reported pronounced seasonal and intra-annual fluctuations in turbidity, EC, WT, and DO across monthly campaigns at 20 stations. That study further demonstrated that the lake behaves as a well-mixed shallow system with minimal vertical stratification but strong horizontal and temporal variability driven by meteorological forcing and seawater intrusion. Although maximum temporal offsets between satellite overpasses and *in situ* measurements reached up to 11 days, the majority of satellite–*in situ* matchups occurred within 0–3 days, with a mean offset of approximately 0.3 days, supporting the ecological relevance of the satellite-based analysis under typical conditions.

Although the monitoring network consisted of 20 fixed stations, the number of stations measured during each monthly campaign varied because adverse weather conditions or occasional equipment malfunction prevented safe access to all sites. The total number of valid measurements per month is visible in

Table 5.2.

5.2.4. Dataset Development

To strengthen the dataset for statistical analysis and ML applications, the original network of 20 *in situ* stations was densified to 318 points (Figure 5.3), corresponding to 318 pixels derived from the final water quality raster presented in Batina and Šiljeg (2025) [26]. Importantly, this procedure does not represent statistical resampling of point-based field observations, nor an attempt to create independent *in situ* measurements. Instead, the 318 samples serve as spatial reference points derived from a GIS–MCDA-based WQI surface. The rationale was that, instead of directly comparing maximum of 20 *in situ* measurements per parameter monthly with satellite imagery on a monthly basis, a larger number of measurements was required to ensure effective model training and testing.

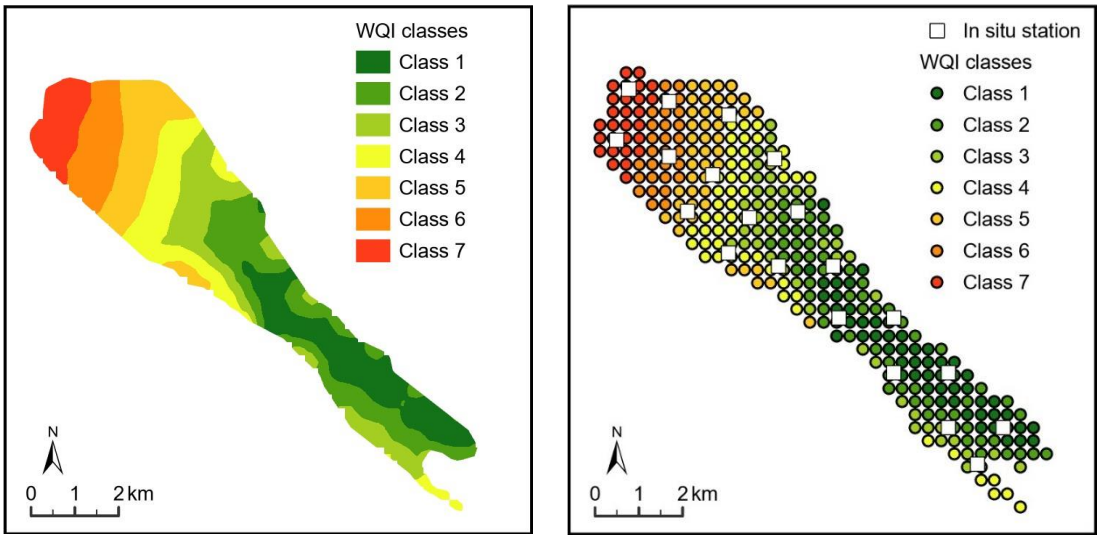

(a) (b)

Figure 5.3. Water quality raster of Vrana Lake derived from MCDA and its use for dataset densification. (a) Continuous raster surface classified into seven WQI classes. (b) Discretized raster with 318 extracted samples shown together with 20 in situ *monitoring stations*

The raster used for densification was generated by a MCDA approach, which aggregated multiple weighted criteria into a final water quality map using the Weighted Linear Combination (WLC) method [26]. The raster cells had a resolution of 300 × 300 m, each representing spatially explicit information on water quality across the lake. This rasterization provided a consistent framework for extracting 318 evenly distributed pixel values, which served as additional measurement points. By integrating these raster-derived points, the analysis was able to capture greater spatial variability and provide larger sample size to support robust ML model development. These raster-derived samples should therefore be interpreted as spatial representations of relative water quality patterns, not as statistically independent observations.

Accordingly, the ML models are trained to recognize relative spatial WQI patterns, emphasizing spatial differentiation across the lake.

A water quality raster of Vrana Lake was classified into seven discrete classes by Batina and Šiljeg (2025) [26], representing different levels of water quality across the lake surface. These classes provided a spatially explicit framework for distinguishing areas of higher and lower water quality, reflecting the heterogeneity of environmental conditions within the lake. The underlying raster values ranged from 0.596 (Class 7) to 0.737 (Class 1), indicating overall good water quality, but with detectable spatial variation that served as the basis for ranking and differentiating classes across the system.

In this study, the seven raster-derived classes were used as reference categories for ML, serving to identify which parts of the lake belong to each water quality class based on satellite imagery. To enable model training and testing, 318 raster cells (pixels) were extracted from the classified surface and used as measurement points, ensuring sufficient spatial coverage and dataset size for robust model development. The pixels were distributed across the classes as follows: Class 1—55 pixels, Class 2—64 pixels, Class 3—49 pixels, Class 4—48 pixels, Class 5—46 pixels, Class 6—29 pixels, and Class 7—27 pixels. This quantitative distribution ensured that all water quality categories were represented, allowing the ML models to be trained on the full spectrum of observed lake conditions and to capture subtle differences in relative water quality across the system.

The seven WQI classes are not intended to represent fine-scale or instantaneous water quality variability. Instead, they reflect integrated, lake-scale ecological conditions derived from annual averages and GIS-MCDA synthesis. Accordingly, the WQI serves as a spatial reference framework for identifying persistent patterns and relative gradients rather than micro-scale heterogeneity.

5.2.5. ML Framework

To model lake water quality, two modelling tracks were implemented: (A) regression of individual *in situ* parameters and (B) CNN-based WQI classification. Models were trained and evaluated separately for each satellite sensor (Sentinel-2, Landsat 8–9, PlanetScope) to allow a sensor-specific assessment of predictive capability under a consistent experimental design.

5.2.5.1. Regressors for Water Quality Parameters Modelling

In the task of water quality parameters modelling, a diverse set of regression algorithms was considered to balance linear baselines and nonlinear learners:

Linear Regression [305] is a fundamental supervised learning method that establishes a linear relationship between variables by fitting the best-fitting line to the observed data. The primary objective is to estimate model parameters that minimize the Sum of Squared Errors (SSE) between predicted and actual values. Implementing the algorithm involves key steps like data preprocessing, feature selection, model fitting using the least squares method, and subsequent evaluation and diagnosis.

Ridge Regression [306], also known as L2-regularized regression, is an advanced form of linear regression designed for situations where the dataset has many features relative to the number of data points or when features are highly correlated (multicollinearity). Its primary function is to prevent overfitting and improve the model's robustness. It achieves this by adding an L2 penalty term to the standard linear regression cost function.

Random Forest [307] is a ML technique that belongs to the ensemble family of algorithms, meaning it uses multiple models to get a better overall result. Its fundamental goal is to build a "forest" of many simple decision trees and combine their individual predictions to produce an outcome that is more accurate and less prone to errors than any single tree. Random Forest achieves this stability by purposefully introducing randomness; it trains each tree on a slightly different random subset of the data and features.

Gradient Boosting [308] is an ensemble method in ML that builds its predictive model as a series of sequential steps. It works by creating new, simple decision trees that are designed to fix the prediction errors of the trees that came before them. This process uses a gradient descent approach to gradually improve accuracy by minimizing a chosen measure of error. The technique is flexible and effective across various applications but does require careful setting of its parameters to achieve good performance.

The eXtreme Gradient Boosting (XGBoost) [309] is a highly efficient and scalable implementation of the gradient boosting framework, often favoured for its speed and performance in structured data competitions. It introduces several enhancements, such as regularization (L1 and L2) to prevent overfitting and parallel processing of the tree construction. Due to its advanced optimization and handling of missing values, it has become a leading choice for complex regression tasks.

The Support Vector Machine (SVM) [310] is a classification algorithm that works by finding the most distinct boundary to separate two classes of data. The main idea is to maximize the margin, which is the empty space between the separating line (hyperplane) and the closest data points from each class. These closest points are called support vectors because they are the only ones that "support" or define the final position of the boundary. By maximizing this gap, the

SVM creates a robust model that generalizes well and makes more reliable predictions on new, unseen data. For complex data that cannot be separated by a straight line, SVM uses the Kernel Trick. This mathematical technique allows the algorithm to effectively transform the data into a higher dimension where a straight separation is possible, enabling it to fit non-linear patterns. The Random Sample Consensus (RANSAC) algorithm [311] is an iterative algorithm that estimates model parameters by fitting candidate solutions to randomly selected data subsets and retaining the solution supported by the largest consensus set. Although robust to outliers, RANSAC is known to be computationally expensive and sensitive to noise and the correct selection of the true dimension.

K-Nearest Neighbours (KNN) Regression is a nonparametric and simple method highly valued for its effectiveness with complex data structures [312]. It works by predicting the value for a new data point based on the average (or a weighted average) of the k closest data points in the training set. While easy to implement, standard KNN regression is susceptible to overfitting and discontinuity in the fit. Methods like KNN are proposed to enhance its accuracy and robustness in big data applications by integrating techniques like kernel smoothing and bootstrap sampling.

Poisson Regression [313] is a generalized linear model for count data, using a log link, function to ensure non-negative predictions. This allows the model to correctly predict non-negative counts based on various input factors. Poisson regression was included to provide a statistical baseline for comparison across modelling approaches.

This extended set of models allowed for a comprehensive benchmarking of both classical statistical approaches and modern ensemble learners, ensuring that the analysis captured linear, nonlinear, and instance-based perspectives on the relationship between satellite reflectance and water quality parameters.

In situ parameter modelling was carried out using raw *in situ* measurements as regression targets using Python 3.12.4 (computer code is available, as stated in the section Data Availability Statement). Performance was quantified using the mean absolute error (MAE, Eq. 5.1), root mean square error (RMSE, Eq. 5.2), and the coefficient of determination (R^2, Eq. 5.3) [314].

$$\mathrm{MAE}(y, \hat{y}) = \frac{1}{N}\sum_{i=1}^{N}|y_i - \hat{y}_i|, \tag{5.1}$$

$$R\mathrm{MSE}(y, \hat{y}) = \sqrt{\frac{1}{N}\sum_{i=1}^{N}(y_i - \hat{y}_i)^2}, \tag{5.2}$$

$$\mathrm{R}^2(y, \hat{y}) = 1 - \frac{\sum_{i=1}^{N}(y_i - \hat{y}_i)^2}{\sum_{i=1}^{N}(y_i - \bar{y})^2}, \tag{5.3}$$

where $\hat{y}_i$ is the estimated value, y_i is the observed value, $\bar{y}$ is the mean of observed values, and N is the number of samples.

The R^2 quantifies the proportion of variance in the dependent variable that is explained by a regression model. Its values range from 1 (perfect prediction) to negative infinity. While values close to 1 indicate strong predictive performance, negative R^2 values occur when a model performs worse than a baseline predictor that simply returns the mean of the observed data [315]. Because R^2 is dependent on the variance of the underlying dataset, it is not directly comparable across datasets with different distributions. The score is undefined when the true target has zero variance; in such cases, implementations typically assign 1.0 for perfect predictions or 0.0 when predictions deviate from the constant target.

5.2.5.2. CNNs for WQI Assessment

To predict the WQI from satellite observations, the dataset of 318 raster-derived samples was randomly partitioned into two subsets: 80% for model training and 20% for independent testing, preserving the distribution of WQI classes using Python (computer code is available, as stated in the section Data Availability Statement).

The candidate models for WQI prediction were developed based on a one-dimensional (1D) CNN architecture. CNNs are a class of ML algorithms that combine convolutional layers with fully connected dense layers. The convolutional layers excel at extracting features from raw signals or imagery without requiring prior preprocessing, while the dense layers serve primarily for classification tasks. Given that WQI measurements were collected over a one-year period, each sampling point was represented by multiple satellite image snapshots spanning that time frame. Specifically, a single WQI value was predicted from a matrix consisting of 12 temporal snapshots for each spectral band, where the dimension is bands × 12 months, reflecting consistent temporal coverage used throughout the study.

The neural network architecture consisted of two convolutional layers, followed by normalization, pooling, and dense layers. Initially, the network was trained to learn spectral features by applying 1D convolutions in the spectral dimension, capturing spectral characteristics and their temporal variations. Subsequently, 1D convolutions were applied along the temporal dimension, enabling the model to identify significant feature dynamics over time for each spectral band separately. This two-folds convolution strategy allows us to effectively evaluate both spectral and temporal information in the satellite time series data contributions for the prediction accuracy of the WQI, aligning with common practices in deep learning for environmental and remote sensing applications.

For the WQI-based modelling, predicted classes were compared against reference labels derived from the classified MCDA raster. These accuracy metrics were used to quantitatively assess the performance of the classification models. Overall accuracy was evaluated using confusion matrices, where correct predictions correspond to the main diagonal and all misclassifications are treated equally, regardless of how close the predicted class is to the correct one [316]. Area under receiver operating characteristics (ROC) curve (AUC) [317] was used as the principal performance metric because, unlike accuracy, it evaluates the model based on the predicted probabilities of class membership, capturing how well the model ranks and separates water quality categories across all decision thresholds.

Generalization performance was assessed on the held-out 20% test subset. Testing was conducted independently for Sentinel-2, Landsat 8–9, and PlanetScope to ensure a fair, sensor-specific comparison under identical evaluation criteria.

5.2.6. Workflow Overview

The overall SIGMaL workflow (Figure 5.4) integrates four main components: (i) *in situ* water quality monitoring and probe calibration, (ii) GIS–MCDA and raster-based derivation of the WQI, (iii) satellite image acquisition and preprocessing, and (iv) ML model training, testing, and spatial prediction.

This stepwise design ensured consistency across heterogeneous data sources (*in situ* measurements, GIS–MCDA models, and satellite imagery) and facilitated reproducible ML experiments. The 80/20 split of raster-derived samples into training and testing subsets provided the foundation for robust model evaluation, while comparative benchmarking across algorithms and sensors allowed systematic identification of the most effective predictive approach.

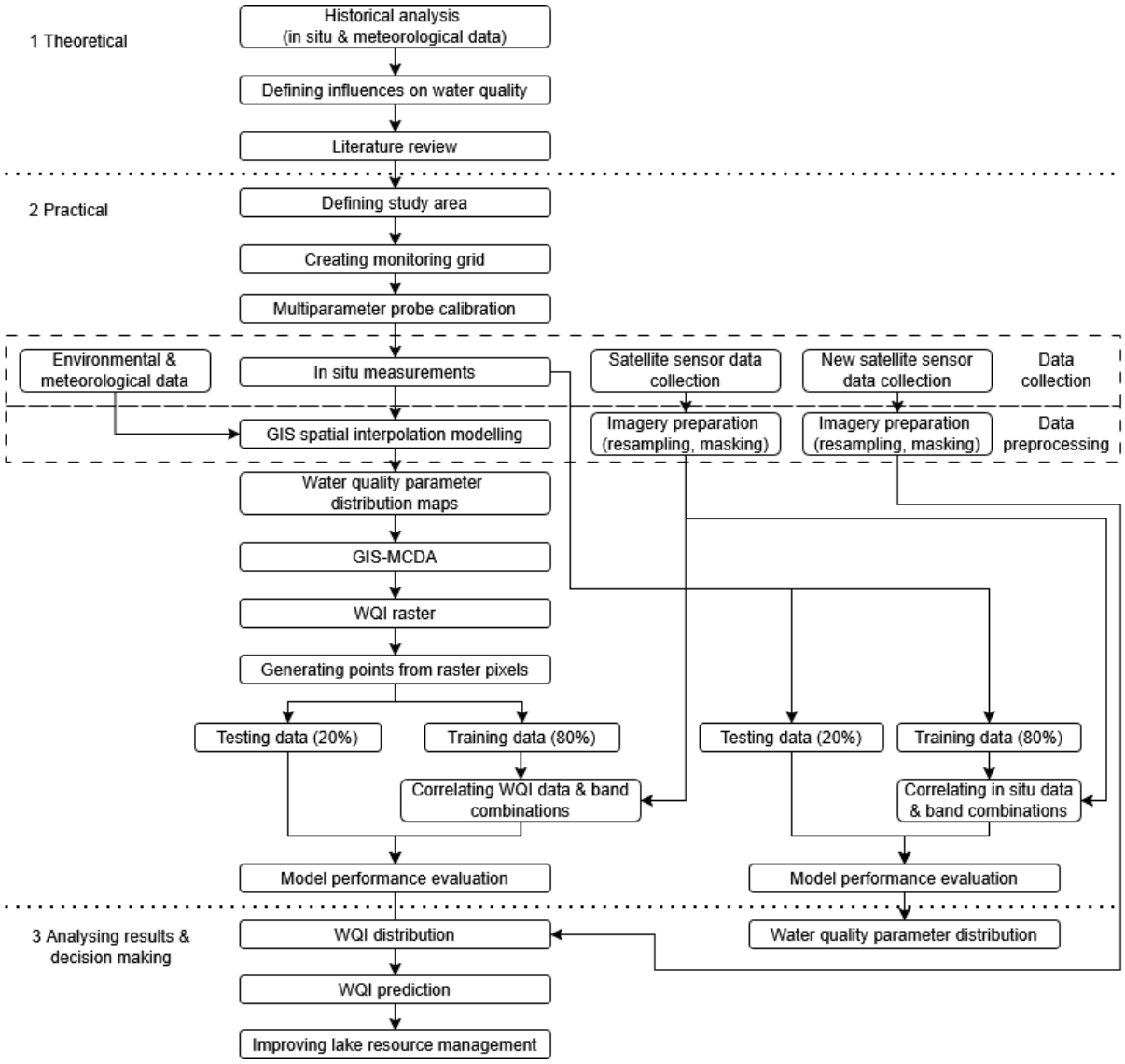

Figure 5.4. Integrated SIGMaL workflow combining in situ *data, GIS-MCDA, satellite imagery, and ML for WQI prediction*

5.3. Results

5.3.1. Regression of In Situ *Parameters*

5.3.1.1. Sentinel-2 Results

Across the Sentinel-2 dataset, ensemble methods outperformed linear and kernel-based approaches, with clear advantages in modelling nonlinear spectral–water quality relationships (Table 5.3). Gradient Boosting delivered the strongest overall performance for most variables, achieving the highest accuracy for WT (R^2 = 0.816, MAE = 15.218, RMSE = 25.675) and competitive fits for turbidity (R^2 = 0.765) and DO (R^2 = 0.682). For EC, Random Forest slightly outperformed Gradient Boosting, achieving the highest coefficient of determination (R^2 =

0.650) together with the lowest MAE (0.178) and a marginally lower RMSE (0.247) compared to Gradient Boosting (R^2 = 0.652, RMSE = 0.246, MAE = 0.185), indicating strong robustness to spectral heterogeneity and stable predictive performance.

Table 5.3. Benchmark results of regression models for each target variable for Sentinel-2

Model	EC			Turbidity			WT			DO		
	MAE	**RMSE**	**R²**	**MAE**	**RMSE**	**R²**	**MAE**	**RMSE**	**R²**	**MAE**	**RMSE**	**R²**
Linear Regression	0.284	0.360	0.258	10.047	11.941	0.470	29.859	37.166	0.615	0.706	0.837	0.591
Ridge Regression	0.388	0.417	0.001	13.806	16.597	–0.024	51.677	57.568	0.076	1.077	1.308	0.003
Random Forest	**0.178**	**0.247**	**0.650**	4.977	8.474	0.733	18.255	33.239	0.692	**0.450**	**0.740**	**0.680**
Gradient Boosting	0.185	0.246	0.652	4.524	7.947	0.765	**15.218**	**25.675**	**0.816**	0.531	0.738	0.682
XGBoost	0.195	0.308	0.457	3.956	8.241	0.748	15.899	29.560	0.756	0.511	0.790	0.637
SVM Regressor	0.212	0.291	0.516	11.691	16.693	–0.035	37.662	46.899	0.387	0.717	0.992	0.426
RANSAC Regressor	0.518	0.751	–2.235	13.751	22.137	–0.821	34.574	44.278	0.453	0.770	0.944	0.481
KNN Regressor	0.177	0.265	0.598	**4.889**	**7.228**	**0.806**	18.739	30.386	0.742	0.519	0.770	0.655
Poisson Regressor	0.390	0.417	0.000	13.937	16.732	–0.040	54.602	59.889	0.000	1.100	1.331	0.032

The KNN Regressor showed particularly strong behaviour for turbidity, achieving the highest R^2 across all models (0.806) and low MAE and RMSE values, suggesting that local neighbourhood patterns in reflectance strongly benefit turbidity estimation. Linear Regression produced moderate fits across all variables, while Ridge and Poisson regression models consistently resulted in near-zero or negative R^2 values, confirming their limited suitability for modelling nonlinear satellite reflectance–water quality relationships. SVM and RANSAC exhibited unstable performance, especially for turbidity and DO, with negative or low R^2, reflecting sensitivity to noise and high-variance spectral conditions.

5.3.1.2. Landsat 8–9 Results

For Landsat 8–9, ensemble tree-based models again provided superior performance relative to linear and kernel methods, with clearer separation among algorithms for individual water quality parameters (Table 5.4). Gradient Boosting achieved the best overall performance for EC, delivering the highest R^2 (0.728) and overall, the lowest MAE and RMSE among the tested learners. For turbidity, Random Forest achieved the best overall performance ($R^2 = 0.591$, MAE = 6.245), outperforming Gradient Boosting and XGBoost.

Table 5.4. Benchmark results of regression models for each target variable for Landsat 8–9

Model	EC			Turbidity			WT			DO		
	MAE	**RMSE**	**R²**	**MAE**	**RMSE**	**R²**	**MAE**	**RMSE**	**R²**	**MAE**	**RMSE**	**R²**
Linear Regression	0.227	0.272	0.576	10.097	13.961	0.276	6.887	8.233	0.981	0.476	0.576	0.807
Ridge Regression	0.379	0.404	0.061	13.784	16.378	0.003	9.224	12.439	0.957	0.522	0.616	0.779
Random Forest	0.168	0.262	0.605	**6.245**	**10.494**	**0.591**	**2.658**	**3.663**	**0.996**	**0.268**	**0.368**	**0.921**
Gradient Boosting	**0.148**	**0.218**	**0.728**	6.622	10.587	0.583	2.722	3.589	0.996	0.287	0.392	0.911
XGBoost	0.175	0.282	0.543	6.843	12.562	0.414	3.079	5.506	0.992	0.298	0.406	0.904
SVM Regressor	0.380	0.433	–0.076	13.495	19.497	–0.412	52.607	57.573	0.076	0.829	1.042	0.366
RANSAC Regressor	0.299	0.379	0.178	11.869	17.982	–0.202	6.922	8.260	0.981	0.623	1.159	0.217
KNN Regressor	0.211	0.326	0.389	7.763	13.064	0.366	4.308	6.871	0.987	0.365	0.519	0.843
Poisson Regressor	0.383	0.410	0.034	14.113	16.637	–0.029	13.073	16.727	0.922	0.529	0.624	0.773

WT prediction showed exceptionally strong accuracy across the board, with both Random Forest and Gradient Boosting achieving $R^2 = 0.996$ and very low error values (<4 °C RMSE). This indicates that Landsat's thermal bands (B10 and B11) provide highly stable temperature information for the study area. For DO, Random Forest outperformed all other models by a large margin ($R^2 = 0.921$, RMSE = 0.368), with Gradient Boosting performing similarly but

slightly weaker. Linear Regression provided moderate fits, while Ridge Regression suffered degraded performance for all variables except WT. Kernelbased SVM regression, Poisson regression, and RANSAC performed poorly, often yielding negative or near-zero R^2 values, highlighting their sensitivity to nonlinear and noisy spectral–ecological relationships.

5.3.1.3. PlanetScope Results

PlanetScope produced more variable model performance due to its limited spectral range and sensitivity to atmospheric and adjacency effects (Table 5.5). Nevertheless, several algorithms achieved strong predictive capability. The KNN Regressor was the strongest overall performer, delivering the highest R^2 values for EC (0.713), turbidity (0.661), and DO (0.613), indicating that PlanetScope's fine spatial resolution (3 m) enables effective exploitation of local spectral neighbourhoods despite the restricted spectral configuration.

Table 5.5. Benchmark results of regression models for each target variable for PlanetScope

Model	**EC**			**Turbidity**			**WT**			**DO**		
	MAE	**RMSE**	**R²**	**MAE**	**RMSE**	**R²**	**MAE**	**RMSE**	**R²**	**MAE**	**RMSE**	**R²**
Linear Regression	0.207	0.258	0.619	9.756	13.128	0.360	**26.530**	**33.612**	**0.685**	0.621	0.815	0.613
Ridge Regression	0.385	0.413	0.020	13.632	16.406	0.000	54.185	59.540	0.011	1.084	1.318	–0.012
Random Forest	0.185	0.271	0.578	7.264	11.810	0.482	26.112	40.752	0.537	0.612	0.890	0.538
Gradient Boosting	0.184	0.270	0.582	8.197	11.679	0.493	27.452	40.684	0.538	0.624	0.823	0.605
XGBoost	0.170	0.283	0.539	8.150	13.538	0.319	25.760	42.403	0.499	0.648	0.992	0.426
SVM Regressor	0.194	0.263	0.604	10.014	15.049	0.158	42.929	52.057	0.244	0.713	0.947	0.477
RANSAC Regressor	0.221	0.269	0.586	14.182	20.590	–0.575	32.051	43.412	0.474	0.779	0.987	0.432
KNN Regressor	**0.139**	**0.223**	**0.713**	**5.731**	**9.546**	**0.661**	25.088	39.978	0.554	**0.544**	**0.815**	**0.613**
Poisson Regressor	0.390	0.417	0.000	13.932	16.725	–0.039	54.877	60.116	–0.008	1.102	1.331	–0.033

For WT, Linear Regression surprisingly outperformed all nonlinear models (R^2 = 0.685), suggesting that under stable atmospheric conditions the reflectance–temperature relationship behaves more linearly than for other variables. Ensemble tree-based models such as Random Forest and Gradient Boosting produced moderate and consistent results across most parameters (R^2 between 0.48 and 0.60), confirming their robustness to noise but also highlighting the constraints imposed by PlanetScope's narrow spectral range. Ridge, Poisson, SVM, and RANSAC frequently yielded low or negative R^2, particularly for turbidity, where adjacency contamination and radiometric instability were most pronounced.

5.3.2. WQI CNN models

When using the integrated WQI derived from the GIS–MCDA raster, the problem was reformulated as a supervised classification task. The seven WQI classes served as categorical labels for model training and testing.

Classical classification algorithms are generally unsuitable for complex inputs such as time series of spectral vectors because they treat each feature independently and cannot capture the inherent spectral and temporal dependencies in the data. This results in suboptimal performance since these dependencies carry crucial information about the underlying processes. Moreover, the high dimensionality of such inputs significantly complicates the optimization process, especially when the number of training samples is limited. The large feature space can lead to overfitting and poor generalization, making convergence during training unlikely. In contrast, methods like CNNs are better suited to this type of data because they can learn local spectral features and temporal patterns through convolutional operations, preserving dependencies and reducing dimensional complexity via shared weights and pooling layers.

The following WQI results are produced by the CNN models; "spectral" refers to single-date band stacks, and "temporal" refers to band-wise concatenation of monthly windows.

Model evaluation was based on confusion matrices (Figure 5.5-Figure 5.10), with overall accuracy and AUC used as the principal metrics of predictive accuracy (Table 5.6). Figure 5.5-Figure 5.10 show confusion matrices illustrating the classification performance of WQI prediction models across the three satellite datasets (Sentinel-2, Landsat 8–9, and PlanetScope). Each figure contains four panels representing the training and test subsets for both spectral and temporal feature configurations.

The performance of ML models applied for WQI classification across Sentinel-2, Landsat 8–9, and PlanetScope datasets, using both spectral and temporal features, is listed in Table 5.6. Overall, the models based on spectral inputs consistently outperformed those relying on

temporal composites, indicating that spectral variability provides a more stable and discriminative basis for estimating integrated water quality conditions.

Table 5.6. Performance of ML models for WQI classification across satellite sensors, based on spectral and temporal analyses

Sensor	Analysis Type	Subset	AUC	Accuracy	R^2
Sentinel-2	Spectral	Train	1.00	0.73	0.89
		Test	**1.00**	**0.53**	**0.84**
	Temporal	Train	1.00	0.85	0.96
		Test	**0.99**	**0.53**	**0.82**
Landsat 8–9	Spectral	Train	0.98	0.80	0.93
		Test	0.97	0.53	0.51
	Temporal	Train	0.50	0.09	-3.41
		Test	0.50	0.08	-3.56
PlanetScope	Spectral	Train	1.00	0.81	0.91
		Test	0.97	0.42	0.77
	Temporal	Train	1.00	0.67	0.67
		Test	0.94	0.44	0.10

5.3.2.1. Sentinel-2 CNN Performance

In the spectral configuration, both the training and test confusion matrices (Figure 5.5) show a dominant diagonal, indicating generally correct class assignments. However, the model frequently confused neighbouring classes, mostly within the mid-range WQI categories (Classes 3–5). It is consistent with the moderate test accuracy of 0.53 and high AUC of 1.00 reported in Table 5.6. Misclassifications rarely extend far from the diagonal, suggesting that the model captured the overall ordinal structure of the WQI but struggled to resolve subtle class boundaries.

The temporal model exhibits even stronger diagonal structure. Training performance is notably higher (accuracy 0.85, AUC 1.00), and the test matrices show fewer off-diagonal entries than in the spectral case. Although test accuracy (0.53) matches that of the spectral model, the temporal model achieves higher test R^2 (0.82) and more concentrated diagonal predictions, indicating better preservation of ordinal class relationships. This suggests that temporal aggregation stabilized spectral variability and enhanced class separability, reducing confusion among adjacent WQI classes.

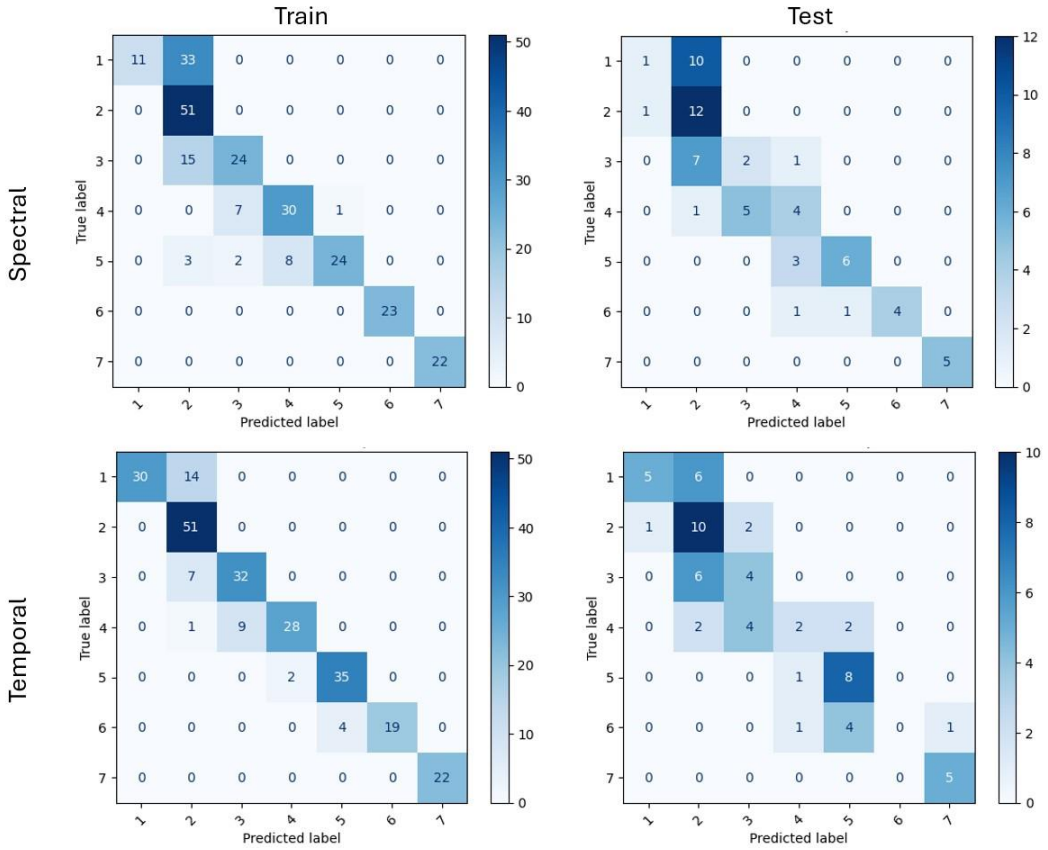

Figure 5.5. Confusion matrices showing WQI classification performance for Sentinel-2 spectral and temporal models

The learning curves for the Sentinel-2 spectral and temporal models are calculated (Figure 5.6). In both configurations, training accuracy increased steadily and reached values above 0.85, accompanied by a consistent decrease in training loss throughout the 500 epochs. Validation accuracy remained lower, fluctuating mostly between 0.45 and 0.60 in both cases, without a strong upward trend. Validation loss showed pronounced variability, including frequent spikes that increased in magnitude at later epochs. These patterns indicate that the model learned stable representations on the training data, while validation performance remained less consistent.

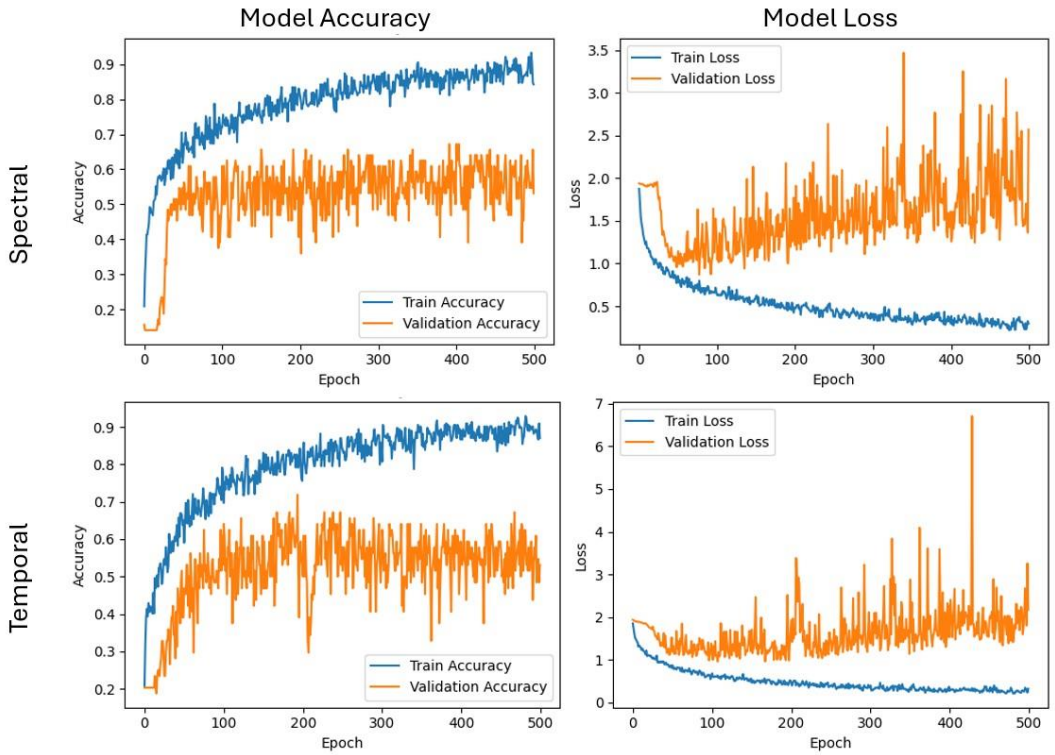

Figure 5.6. Training and validation accuracy and loss curves for the Sentinel-2 CNN spectral and temporal models

5.3.2.2. Landsat 8–9 CNN Performance

For Landsat 8–9 (Figure 5.7), the spectral model showed moderate classification capability, achieving high AUC values (0.98 train, 0.97 test) but only test accuracy of 0.53 (Table 5.6). The test confusion matrix confirms this mismatch: although the model correctly follows the overall WQI gradient, misclassifications remain frequent across several classes, including errors beyond neighbouring categories. This indicates that, despite good probabilistic separation reflected in the AUC, the spectral model struggled to assign discrete class labels with high reliability. It is likely a consequence of Landsat's coarser spatial resolution and fewer narrow spectral bands compared with Sentinel-2, limiting its ability to resolve subtle differences between adjacent WQI classes.

Temporal modelling resulted in severe degradation of performance. Both train and test AUC values collapsed to 0.50, with test accuracy decreasing to 0.08 and R^2 reaching −3.56, clearly indicating prediction collapse (Table 5.6). The temporal confusion matrices corroborate that nearly all samples were assigned to a single WQI class, with almost no differentiation across the seven classes. This behaviour suggests that temporal stacking introduced noise rather than informative temporal structure. The likely cause is Landsat's long revisit interval combined with inconsistent atmospheric and illumination conditions between acquisition dates, which

reduced temporal coherence and led the CNN to overfit the training set while failing entirely to generalize to unseen data.

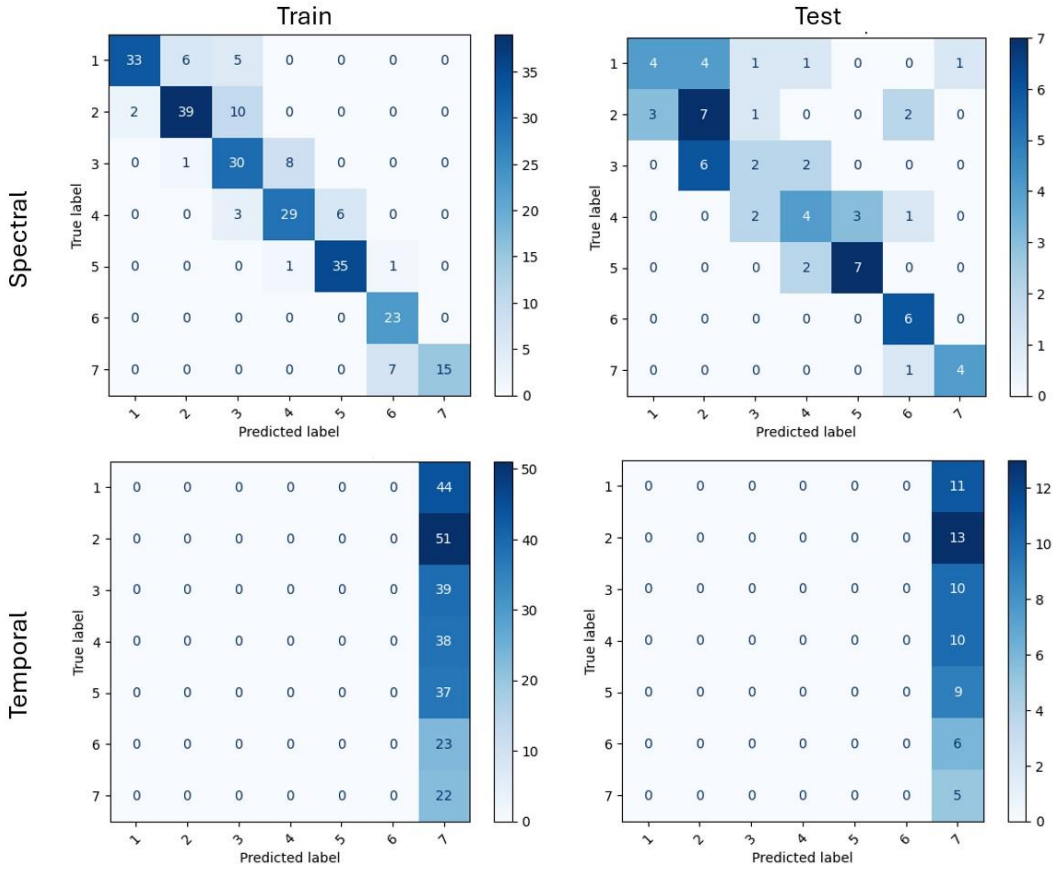

Figure 5.7. Confusion matrices showing WQI classification performance for Landsat 8–9 spectral and temporal models

The learning curves for the Landsat 8–9 temporal model are calculated (Figure 5.8). Training accuracy increased gradually to approximately 0.70, while training loss decreased smoothly over epochs. In contrast, validation accuracy remained low and highly variable, fluctuating mostly between 0.05 and 0.25 without a clear upward trend. Validation loss showed substantial instability, with frequent large spikes throughout training. These patterns indicate that, although the model fitted the training data, its performance on the validation set was inconsistent under the temporal configuration. Furthermore, the validation predictions tended to collapse into a single WQI class for extended periods during training, with the dominant predicted class shifting from epoch to epoch, reflecting unstable class separation under temporal inputs.

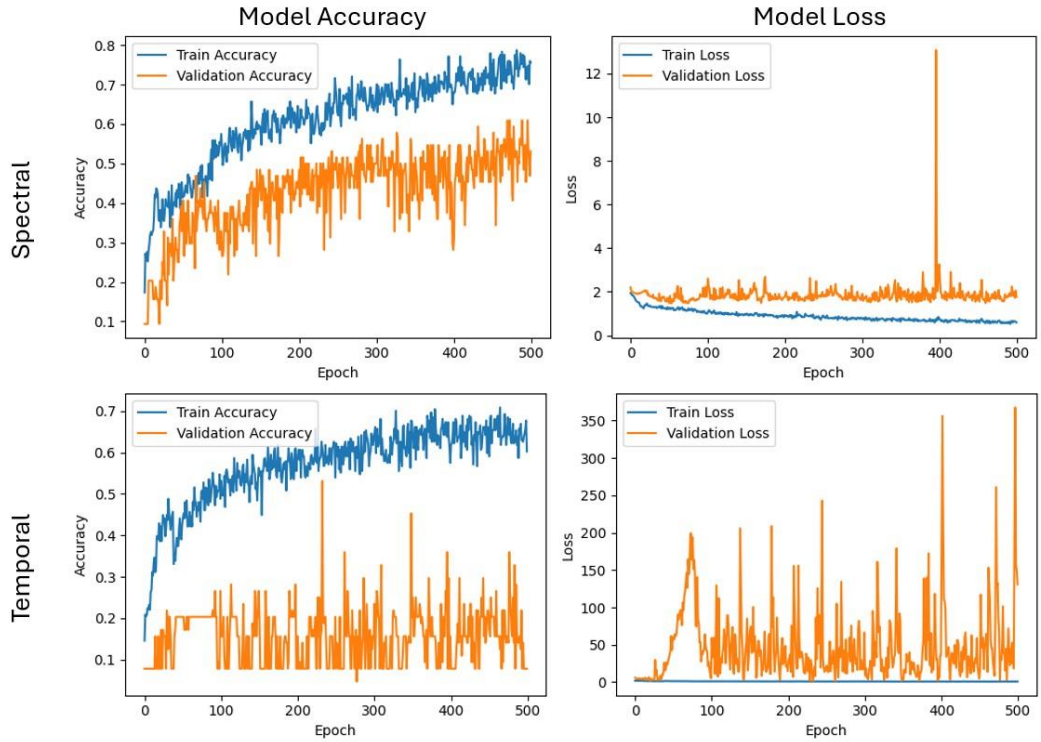

Figure 5.8. Training and validation accuracy and loss curves for the Landsat 8–9 CNN spectral and temporal models

5.3.2.3. PlanetScope CNN Performance

For PlanetScope (Figure 5.9), the spectral model showed strong classification ability, consistent with its test AUC of 0.97, accuracy of 0.42, and R^2 of 0.77 (Table 5.6). The spectral confusion matrices display a clear diagonal trend, with most predictions falling into the correct WQI class. Misclassifications occur primarily between adjacent classes (especially around Classes 2–3 and 4–5) which indicates that the model successfully captured the underlying ordinal gradient while occasionally struggling with fine boundary transitions. This behaviour aligns with the high spatial resolution of PlanetScope imagery (3 m), which enables discrimination of small-scale spatial patterns relevant to water quality.

The temporal model performed substantially worse, with a test AUC of 0.94, accuracy of 0.44, and a low R^2 of 0.10 (Table 5.6). The temporal confusion matrix reveals considerable class mixing: several classes show dispersion into multiple neighbouring categories, and true classes 3–5 exhibit notable overlap. Although diagonal structure is still present, class separability is reduced compared with the spectral model. This degradation likely reflects PlanetScope's limited spectral range combined with day-to-day variations in illumination and atmospheric conditions, which introduce noise into temporal features and reduce their predictive stability.

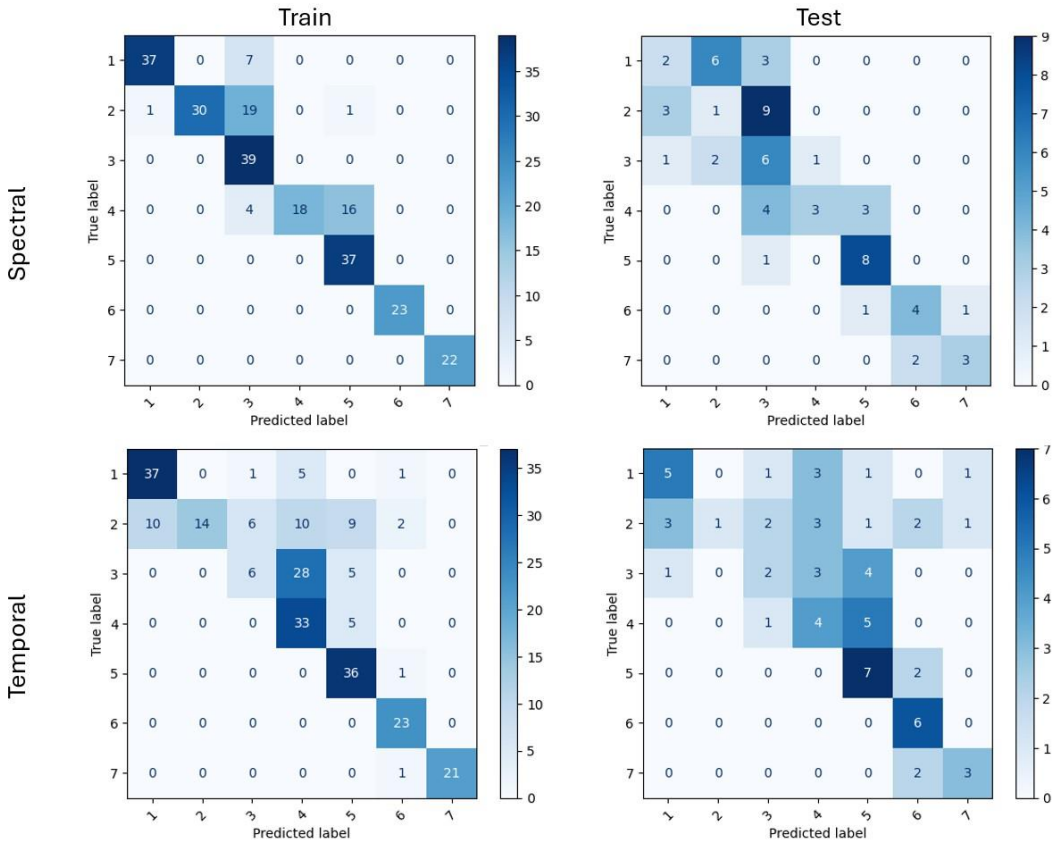

Figure 5.9. Confusion matrices showing WQI classification performance for PlanetScope spectral and temporal models

The learning curves for the PlanetScope spectral and temporal models are calculated (Figure 5.10). For both configurations, training accuracy increased steadily, reaching approximately 0.90, while training loss decreased smoothly across epochs. Validation accuracy remained notably lower, fluctuating mostly between 0.35 and 0.55 without a clear long-term upward trend. Validation loss exhibited substantial variability, with frequent spikes that persisted throughout training. Compared to the spectral configuration, the temporal model showed similar behaviour, with slightly larger oscillations in validation loss but comparable validation accuracy ranges. The curves indicate stable convergence on the training data but limited consistency in validation performance for both PlanetScope configurations.

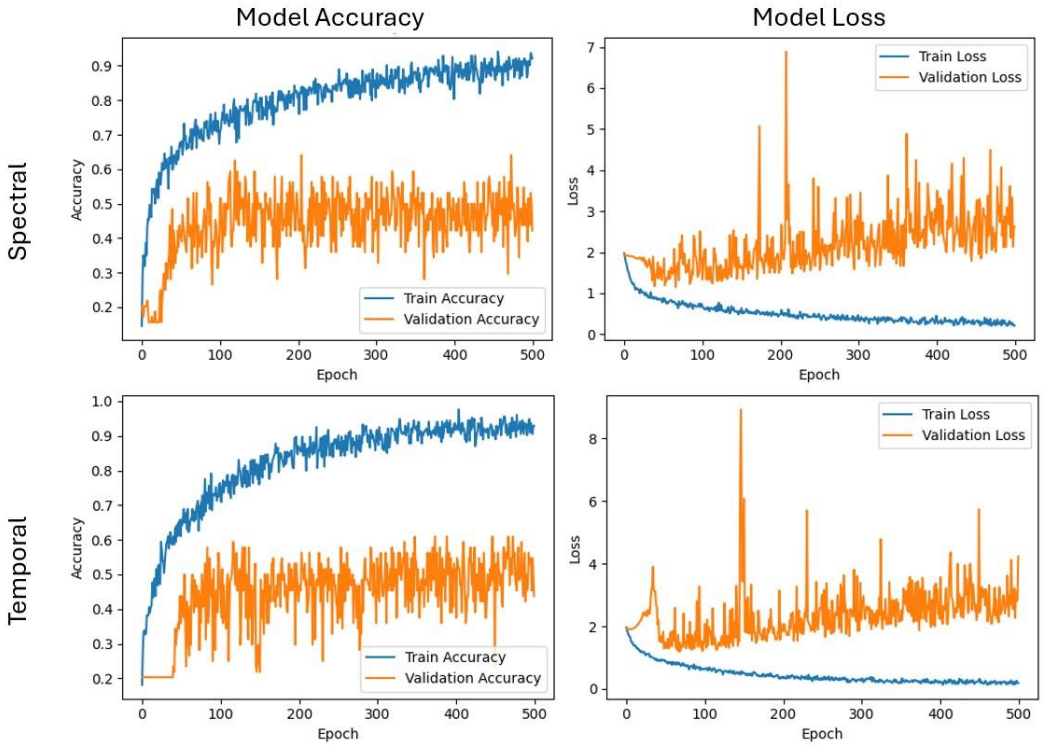

Figure 5.10. Training and validation accuracy and loss curves for the PlanetScope CNN spectral and temporal models

5.3.3. CNN-based Predictions of WQI

The CNN-based WQI prediction for the year following *in situ* monitoring period, generated separately for Sentinel-2, Landsat 8–9, and PlanetScope under spectral and temporal model configurations are calculated (Figure 5.11). Since no ground-truth data exist for this period, the maps represent forward predictions of spatial water quality patterns derived from the trained models.

Across all sensors, the maps in Figure 5.11 display a broadly consistent spatial structure: higher WQI classes (1–3) occur mainly in the western and central parts of Vrana Lake, while lower-quality classes (5–7) are more frequent along the eastern and southeastern margins. This gradient mirrors the dominant spatial trend captured during model training.

For Sentinel-2, the spectral model (top left) produces a smooth but spatially detailed gradient, with noticeable internal class transitions. In contrast, the temporal model (top right) yields a more uniform surface, with reduced fine-scale variability and more clustered class regions.

For Landsat 8–9, spectral predictions (middle left) exhibit stronger heterogeneity and a wider distribution of mid- to low-quality classes across the lake. The temporal model (middle right) produces highly homogenized outputs, with most pixels assigned to a narrow range of lower-quality classes, reflecting reduced class discrimination.

For PlanetScope, the spectral model (bottom left) generates the most spatially detailed output among all sensors, with well-defined class boundaries and visible local variation. The temporal model (bottom right) preserves the general lake-wide gradient but presents a smoother pattern with less within-lake differentiation.

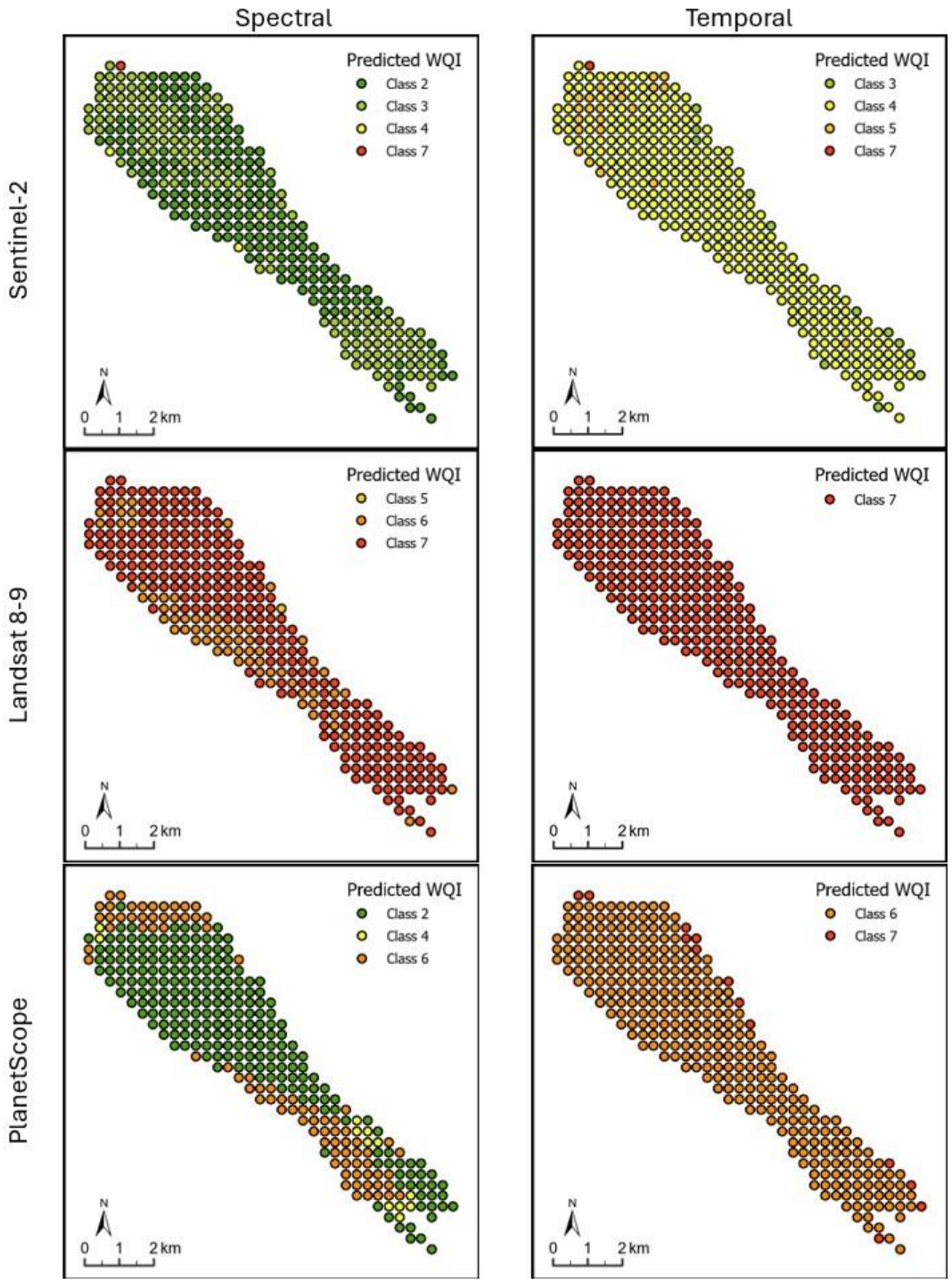

Figure 5.11. Predicted spatial distribution of WQI classes in Vrana Lake for the 12-month period following field measurements, based on CNN models using Sentinel-2, Landsat 8–9, and PlanetScope imagery under spectral and temporal modelling scenarios

5.4. Discussion

5.4.1. Cross-Sensor Comparison

Across all sensor–model configurations, Sentinel-2 demonstrated the strongest and most consistent performance for both regression of individual *in situ* parameters and CNN-based WQI classification. Its combination of dense visible and NIR spectral coverage and moderate spatial resolution allowed the models to capture both the optical complexity and spatial gradients of Vrana Lake. Ensemble regression models reached the highest R^2 values for EC, turbidity and DO, while CNN classification achieved AUC = 1.00 and stable WQI class separation. These findings align with recent studies by Pizani et al. (2020) [298] and Toming et al. (2016) [75] showing that Sentinel-2 reliably estimates water quality indicators across rivers, lakes and reservoirs. They highlight the suitability of Sentinel-2 as the primary remote-sensing component within the SIGMaL framework.

PlanetScope performed very well in tasks requiring fine spatial discrimination. Its spectral CNN model produced the most detailed WQI boundary delineation among all sensors, which is consistent with previous work showing that PlanetScope's 3 m resolution excels at mapping small-scale spatial heterogeneity despite its limited spectral range [299,318]. However, because it carries only a few broad multispectral bands, it is more susceptible to atmospheric variation and less robust when modelling temporally aggregated features. This behaviour is fully reflected in the SIGMaL experiments and matches patterns observed in earlier comparative water-quality study by Di Francesco et al. (2025) [319].

For Landsat 8–9 (OLI/TIRS), the results diverged between regression and classification tasks. *In situ* temperature regression achieved exceptionally high accuracy ($R^2 \approx 0.996$), consistent with many studies demonstrating that Landsat's thermal bands provide highly reliable surface water temperature retrievals [298,320]. In contrast, Landsat's CNN classification performance was modest in the spectral configuration (test accuracy = 0.53) and collapsed almost entirely in the temporal configuration (accuracy ≈ 0.08; strongly negative R^2). This behaviour reflects Landsat's coarser 30 m spatial resolution, lower revisit frequency, and fewer narrow spectral bands. These characteristics limit its ability to resolve the subtle water-quality gradients needed for seven-class WQI discrimination within the SIGMaL workflow. Similar shortcomings of Landsat relative to Sentinel-2 in inland waters have been observed broadly in recent comparisons by Deng et al. (2024), Pizani et al. (2020), and Parida et al. (2025) [296,298,299]. Across all sensors, spectral CNN models consistently outperformed temporal models [302]. Spectral snapshots preserve instantaneous optical conditions, whereas temporal composites

blend scenes captured under different illumination, atmospheric states, and hydrodynamic conditions, reducing contrast and adding noise. This aligns with recent studies by Deng et al. (2024), Pizani et al. (2020), and Toming et al. (2016) [75,296,298] emphasizing that, despite growing interest in temporal deep learning, snapshot-based spectral models remain more accurate for WQI estimation in optically complex inland waters.

An important explanatory factor in this study is the temporal offset between field surveys and satellite overpasses (

Table 5.2). Maximal offsets ranged from –11 to +7 days, especially problematic for Landsat. Vrana Lake is a shallow lake and strong Bora, Jugo or Maestral winds can change temperature and nutrient distributions within hours. Temporal inputs thus often combined reflectance measurements that possibly no longer corresponded to *in situ* water state. It weakens temporal coherence and degrading CNN performance across all temporal SIGMaL configurations, particularly for Landsat's already sparse revisit schedule.

Within this framework, satellite observations are essential because they provide spatially exhaustive, synoptic measurements that allow integrated WQI patterns to be mapped consistently across the entire lake surface. Repeated sampling of the same 20 *in situ* stations, even when combined with spatial interpolation, cannot provide sensor-comparable, wall-to-wall coverage or capture spatial organization at the resolution and extent enabled by satellite imagery. Satellite data are therefore not used to increase the number of independent observations, but to enable spatial generalization and pattern recognition beyond the discrete sampling network.

5.4.2. WQI Outperforms Modelling Individual Parameters

A central methodological finding is that using the integrated WQI as the modelling target substantially improved predictive stability relative to direct regression of raw physicochemical parameters. Within the SIGMaL framework, CNN classification produced clearer ordinal structure, more stable confusion matrices, and better cross-sensor consistency than parameter-specific models. This confirms that WQI acts as a noise-reduced, integrated ecological signal, smoothing short-term fluctuations and reducing the influence of measurement noise or parameter-specific anomalies.

Recent studies similarly show that ML/WQI models provide greater robustness and interpretability than models predicting individual parameters. For example, Wong et al. (2022) [321] demonstrated that WQI-based machine-learning models (particularly modified Random Forest) outperform raw parameter prediction by providing higher accuracy and more stable

explanatory structure. Pang et al. (2025) [32] showed that deep-learning approaches in remote sensing similarly benefit from using integrated indices such as WQI, which improve model robustness and cross-sensor transferability. The results of this study support these findings and show that WQI provides a superior modelling target within SIGMaL.

5.4.3. Spatial Predictions of WQI

CNN-based annual predictions for the post-monitoring period showed a consistent lake-wide west–east gradient across all sensors, with higher-quality classes (1–3) dominating the central and western areas and lower-quality classes (5–7) occurring more frequently along the eastern margins. This pattern matches field observations and known hydrodynamic processes in Vrana Lake, where nutrient inputs and restricted water exchange influence eastern basin conditions.

The Sentinel-2 and PlanetScope spectral models provided the clearest spatial structure. Sentinel-2 produced smooth, ecologically meaningful gradients, whereas PlanetScope highlighted small-scale shoreline and central-basin heterogeneities. Landsat 8–9 reproduced the general gradient but produced smoother, more spatially homogeneous maps consistent with its coarser spatial resolution. Temporal models, especially for Landsat and PlanetScope, yielded more uniform spatial fields and reduced internal variability, which is consistent with the confusion matrices and learning curves showing diminished class separability under temporal input conditions.

Visual differences among the WQI maps derived from Sentinel-2, Landsat 8–9, and PlanetScope do not contradict the relatively high quantitative performance metrics reported in Table 5.6. The WQI prediction is formulated as an ordinal classification problem, where classes represent ordered categories derived from continuous GIS–MCDA scores rather than exact spatial boundaries. High AUC and R^2 values therefore indicate consistent discrimination and correct ranking of relative water quality conditions, even when the spatial expression of class boundaries differs among sensors. These differences primarily reflect sensor-specific characteristics, including spatial resolution, spectral configuration, and revisit frequency, which influence the level of spatial detail and smoothness in the predicted maps. Consequently, the observed map discrepancies represent variations in spatial sensitivity rather than inconsistencies in model performance.

Finally, the one-year temporal offset between the *in situ*–based WQI modelling and satellite-based prediction may influence model accuracy due to potential domain shifts in key input parameters. Specifically, changes in the minimum and maximum values, distribution characteristics, or inter-parameter relationships driven by differing hydrological,

meteorological, or anthropogenic conditions could affect model generalization. Consequently, the spatial predictions presented here are interpreted as a scenario-based extrapolation of lake water quality patterns rather than a strict temporal validation.

5.4.4. Methodological Limitations and Future Work

Using Level-2 surface reflectance products (rather than performing atmospheric corrections based on date and lake specifications) likely introduced residual atmospheric and adjacency artefacts. Such effects can be significant in shallow, optically complex lakes. Although ML models are often robust to moderate atmospheric errors, employing algorithms tailored for inland waters (e.g., ACOLITE, iCOR, C2RCC) could further improve physical consistency in future work.

As shown in

Table 5.2, temporal offsets of up to 11 days were unavoidable due to cloud cover, satellite revisit constraints, and safety considerations for fieldwork. Because Vrana Lake mixes rapidly under strong wind conditions, water quality can change significantly within these time windows. Thus, “temporal” stacks often aggregated reflectance signals that no longer matched *in situ* conditions, explaining the instability and class-collapse seen especially in the Landsat temporal CNN models.

WQI simplifies ecological interpretation but conceals short-term or parameter-specific extremes (e.g., chlorophyll-a spikes). Future SIGMaL implementations should pair WQI-based classification with selective regression of critical parameters.

While promising, the results presented here reflect conditions in a single, moderately productive lake. The SIGMaL framework is designed to support spatial pattern recognition, comparative assessment, and monitoring prioritization, particularly in data-limited coastal lakes. It is not intended to replace *in situ* measurements or to provide fully quantitative water quality estimates that are directly transferable to other waterbodies without local calibration. Applying SIGMaL to other lakes will therefore require recalibration of the WQI, additional *in situ* sampling, and potentially model retraining to accommodate different optical environments.

Whitin this context, SIGMaL evaluates the ability of satellite sensors to reproduce the relative spatial organization of water quality across the lake, rather than fine-scale or instantaneous variability at individual locations. Nonetheless, the cross-sensor evaluation presented here provides a strong basis for generalizing the approach for shallow coastal lakes.

5.5. Conclusions

This study demonstrates that integrating *in situ* monitoring, GIS–MCDA, satellite remote sensing, and ML within the proposed SIGMaL framework provides a robust and scalable approach for assessing water quality in shallow and dynamic freshwater ecosystems such as Vrana Lake. Across all modelling approaches, WQI-based prediction consistently outperformed regression of individual physicochemical parameters, confirming that integrated ecological indices offer a more stable and noise-resistant modelling target for remote sensing applications.

Among the evaluated satellite systems, Sentinel-2 emerged as the most suitable sensor for integrated WQI mapping, combining the highest and most consistent classification performance (AUC ≈ 1.00, R^2 ≈ 0.84) with its rich visible and NIR spectral configuration. PlanetScope excelled in capturing fine-scale spatial variability (R^2 ≈ 0.77) due to its high spatial resolution. Landsat 8–9 performed best for WT retrieval but showed reduced capability for multi-class WQI discrimination, particularly in temporal CNN models, largely due to revisit limitations and temporal mismatches with field campaigns. Accordingly, Sentinel-2 is recommended as the primary sensor for operational WQI-based monitoring within the SIGMaL framework, with PlanetScope serving as a complementary data source for high-resolution spatial analyses and Landsat 8–9 supporting temperature-focused or long-term monitoring applications.

Temporal modelling was generally less effective than spectral modelling across all sensors, partly due to inconsistent overpass timing and rapid hydrodynamic changes in the lake, which weakened temporal coherence. Despite these challenges, CNN-based WQI predictions successfully reproduced the known west–east water quality gradient of Vrana Lake, demonstrating the ecological relevance of the integrated modelling framework.

The results of this study highlight that the SIGMaL framework offers a scalable, transferable, and operationally practical approach for water quality monitoring in coastal shallow lakes. Future work should expand the framework to multiple lakes, incorporate more advanced atmospheric correction, and explore hybrid approaches that pair WQI classification with parameter-specific retrievals.

6. Joint Discussion

The overarching objective of this dissertation was to develop and validate an integrated geospatial multi-sensor framework for lake water quality monitoring capable of overcoming the spatial, temporal, and methodological limitations of conventional point-based monitoring. The four papers collectively progress from theoretical synthesis (Paper I), through empirical characterisation of lake dynamics using *in situ* data (Paper II), spatial decision-support modelling (Paper III), and finally to full integration of satellite remote sensing and ML within the SIGMaL framework (Paper IV). This progression reflects a deliberate research design in which each study builds directly on the conceptual and empirical foundations established by the preceding ones.

Paper I establishes the conceptual and methodological foundation of the dissertation through a critical synthesis of recent advances in remote sensing of lake water quality [9]. The review demonstrates that, despite significant progress in sensor technology and retrieval algorithms, many studies remain limited by single-parameter approaches, short temporal coverage, and weak integration with *in situ* measurements. These limitations are widely reported in contemporary literature on inland water remote sensing, particularly for optically complex and shallow lakes [16,23].

A key conclusion of Paper I is that reliable lake water quality assessment cannot be achieved through remote sensing alone, but requires integration with *in situ* measurements, spatial modelling, and advanced analytical techniques. This conclusion directly motivated the methodological structure of the dissertation, in which remote sensing is treated not as an isolated tool, but as one component of a broader geospatial monitoring framework. Similar calls for integrated approaches have been emphasised in recent review studies addressing the limitations of purely data-driven or purely empirical remote sensing models [236,240].

Paper II provides the empirical backbone of the dissertation by analysing spatiotemporal variability of lake water quality parameters based on systematic *in situ* measurements in Vrana Lake [25]. In addition to descriptive analysis, Paper II performs the transformation of discrete point-based *in situ* measurements into spatially continuous datasets using established GIS interpolation methods, thereby enabling lake-wide representation of water quality patterns. This spatialisation step constitutes a critical methodological bridge between field measurements and subsequent spatial modelling.

The observed seasonal and spatial variability in parameters such as turbidity, EC, DO, and WT confirms that Vrana Lake exhibits characteristics typical of shallow coastal lakes, where

frequent mixing, meteorological forcing, and hydrological connectivity strongly influence water quality dynamics. The strong relationships identified between water quality parameters and meteorological and hydrological drivers are consistent with findings from other shallow and coastal lake systems, where wind forcing, precipitation, and water-level fluctuations play a dominant role [4,7]. Importantly, Paper II demonstrates that median or depth-integrated values can adequately represent the water column in such systems, thereby supporting the methodological feasibility of spatial upscaling and integration with satellite-derived surface observations.

Beyond their descriptive value, *in situ* data analysed in Paper II serve as essential input datasets for the GIS-MCDA framework developed in Paper III and for critical calibration and validation of subsequent ML-based models in Paper IV. This role aligns with best-practice recommendations in recent water quality monitoring literature, which emphasise that remote sensing and ML approaches must remain firmly anchored in high-quality *in situ* observations to ensure ecological interpretability and robustness [17,20].

Paper III represents a key methodological transition by combining the interpolated water quality rasters generated in Paper II with additional meteorological and environmental raster datasets within a GIS-MCDA framework [26]. Specifically, the GIS-MCDA model integrates primary water quality rasters (turbidity, EC, DO, and WT) with meteorological variables (air temperature, precipitation, and wind) and environmental factors, including distance from pollution sources, distance from inflows, and distance-based nitrogen input to the lake derived from LCLU data. By integrating these heterogeneous raster layers, the GIS-MCDA framework enables systematic assessment of eutrophication susceptibility across the entire lake surface. The results of Paper III reveal pronounced spatial heterogeneity in eutrophication susceptibility rather than a single dominant hotspot. While the northeastern part of the lake exhibits high eutrophication susceptibility due to nutrient inputs and hydrological conditions, lower water quality and increased susceptibility are observed in the northwestern and southern regions, influenced by anthropogenic activities and seawater intrusion. Comparable spatial patterns have been reported in recent GIS-MCDA-based studies of shallow and coastal lakes, where eutrophication risk reflects the combined effects of catchment pressure and hydrodynamic connectivity [22,24].

Sensitivity and uncertainty analyses performed in Paper III further demonstrate the robustness and transparency of the GIS-MCDA framework. This aspect is particularly important for environmental decision support, as it allows managers to evaluate the influence of individual criteria and weighting schemes. In addition, the GIS-MCDA-derived WQI raster provides a

spatially continuous reference layer that is subsequently used as an input for ML-based modelling in Paper IV, thereby addressing one of the most frequently cited limitations in lake monitoring studies: sparse and unevenly distributed *in situ* observations [240].

Paper IV represents the methodological culmination of the dissertation by integrating *in situ* measurements, GIS-derived WQI, multi-sensor satellite imagery, and ML within the SIGMaL framework [28]. Rather than fusing data from multiple satellite sensors, the study performs a comparative cross-sensor evaluation to assess the suitability of Sentinel-2, Landsat 8-9, and PlanetScope imagery for lake water quality monitoring.

Comparative evaluation of satellite sensors reveals distinct but complementary strengths. Sentinel-2 achieves the most consistent overall WQI performance (AUC ≈ 1.00, R^2 ≈ 0.84), making it the most reliable sensor for integrated WQI mapping. PlanetScope imagery captures fine-scale spatial variability (R^2 ≈ 0.77), which is particularly valuable in near-shore and heterogeneous environments, while Landsat 8-9 performs best for WT estimation but is less reliable for multi-class WQI discrimination. These findings indicate that initial expectations regarding sensor superiority were not confirmed, highlighting the importance of systematic sensor evaluation in operational monitoring contexts. Similar trade-offs between spatial resolution, spectral configuration, and radiometric stability have been highlighted in recent comparative studies of inland water remote sensing [14,16].

A central conceptual contribution of Paper IV is the demonstration that ML models trained on integrated, GIS-derived indices outperform models trained on individual water quality parameters. This finding supports emerging evidence that composite parameters reduce noise and enhance model generalisation in optically complex waters [236,240]. The SIGMaL framework therefore represents not only a technical integration of data sources, but also an adaptable and transferable analytical approach that supports ecosystem-level assessment through structured data integration.

When interpreted jointly, the results of Papers I–IV demonstrate the value of structured methodological integration. *In situ* measurements provide essential process-level understanding and calibration data; GIS-based spatial modelling enables lake-wide representation and decision-support functionality; and remote sensing combined with ML facilitates scalable and spatially continuous monitoring. These findings are consistent with broader limnological understanding of shallow and coastal lake systems [7] and support the general applicability of the proposed framework. The joint interpretation highlights how each methodological component compensates for the limitations of the others, resulting in a more comprehensive

and operationally relevant monitoring framework than any single approach could provide independently.

Recent studies have increasingly emphasised the need for integrated lake monitoring frameworks that combine remote sensing, spatial analysis, and data-driven modelling. Compared to approaches that rely solely on satellite-derived parameters or ML trained on limited *in situ* data, the framework proposed in this dissertation places stronger emphasis on spatial context and decision-support functionality. Similar integrated concepts have been proposed in recent literature, but often without explicit GIS-MCDA components or systematic sensor comparison [23,240]. In this respect, the SIGMaL framework extends existing approaches by explicitly integrating spatial decision-support modelling with ML and multi-sensor remote sensing. This integration allows not only accurate classification, but also improved interpretability of spatial patterns, which is essential for environmental management applications.

Effective lake water quality monitoring in shallow and optically complex systems requires a combination of empirical observation, spatial analysis, and data-driven modelling. The integrated workflow developed across the four papers demonstrates how geospatial methods can be systematically linked to support both scientific understanding and practical monitoring objectives, forming a cohesive basis for the conclusions presented in the final chapter.

7. Conclusion

This doctoral dissertation addressed the problem of lake water quality monitoring in shallow and optically complex lake systems, where conventional *in situ* monitoring is insufficient to capture spatial variability. The research was conducted through four interrelated scientific papers that collectively developed, tested, and evaluated an integrated geospatial approach combining *in situ* measurements, GIS-based spatial modelling, satellite remote sensing, and ML.

The dissertation was structured as a cumulative thesis, with each paper contributing a distinct methodological or empirical component and progressively building toward an integrated monitoring concept. The research objectives were achieved through systematic testing of the proposed methods using Vrana Lake in Dalmatia, Croatia as a representative coastal shallow lake case study.

The research hypotheses defined in Chapter 1 were evaluated based on the results obtained in Papers II–IV. Their confirmation status and interpretation are presented below.

H1: The accuracy of a model for lake water quality monitoring and assessment, derived based on integration of *in situ* measurements, GIS-MCDA, satellite imagery, and ML, will have AUC values above 0.8.

Hypothesis H1 was confirmed. This hypothesis was tested primarily in Paper IV, where an integrated analytical workflow was developed within the SIGMaL framework. The hypothesis was evaluated by testing ML models using satellite reflectance data from Sentinel-2, Landsat 8-9, and PlanetScope, supported by *in situ* measurements and GIS-MCDA-derived water quality information. CNNs were applied to classify WQI classes, and model performance was assessed using receiver operating characteristic analysis. Across sensors, the integrated modelling approach achieved AUC values exceeding 0.8, confirming that the combination of *in situ* data, GIS-based spatial modelling, satellite remote sensing, and ML significantly improves the accuracy and robustness of lake water quality assessment compared to traditional point-based approaches.

H2: PlanetScope satellite imagery will be the most suitable for monitoring water quality in Vrana Lake in Dalmatia compared to Sentinel-2 and Landsat 8-9 satellite imagery.

Hypothesis H2 was not confirmed. This hypothesis was tested in Paper IV through a comparative cross-sensor evaluation of Sentinel-2, Landsat 8-9, and PlanetScope imagery. Sensor suitability was assessed based on the performance of regression models for individual physicochemical parameters and CNN-based classification of WQI classes. Although PlanetScope imagery demonstrated strong capability in capturing fine-scale spatial variability due to its high spatial resolution, Sentinel-2 consistently achieved the highest overall classification accuracy and stability, with AUC values approaching 1.00 and high coefficient of determination values. The results indicate that higher spatial resolution alone does not guarantee superior monitoring performance. Consequently, Hypothesis H2 was rejected, and Sentinel-2 was identified as the most suitable sensor for operational water quality monitoring in Vrana Lake.

H3: The northeastern part of the lake will have the highest eutrophication susceptibility based on analysed primary (water quality parameters) and secondary parameters (meteorological, hydrological, and LCLU data) and GIS-MCDA.

Hypothesis H3 was not confirmed. This hypothesis was tested in Paper III using a GIS-MCDA framework combined with the F-AHP. The analysis integrated primary water quality parameters (EC, turbidity, WT, DO), meteorological variables, and environmental indicators derived from LCLU and distance-based metrics. The spatial eutrophication susceptibility assessment revealed pronounced heterogeneity across the lake rather than a single dominant hotspot. Elevated eutrophication susceptibility was identified particularly in the northwestern and southern parts of the lake, influenced by anthropogenic pressures and seawater intrusion, while the northeastern part did not consistently exhibit the highest susceptibility. Accordingly, Hypothesis H3 was rejected, highlighting the importance of spatially explicit modelling for understanding complex eutrophication patterns in coastal shallow lakes.

The primary scientific contribution of this dissertation is the development of an integrated and adaptable geospatial (SIGMaL) framework for lake water quality monitoring. The research demonstrates how GIS-based spatial modelling can effectively bridge sparse *in situ* observations and data-driven remote sensing models, enabling spatially continuous assessment in data-limited environments. Additional contributions include:

- design and implementation of a structured monitoring grid of 20 stations (providing spatially representative coverage of Vrana Lake and forming the empirical basis for *in*

situ measurements, spatial interpolation, GIS-MCDA modelling, and subsequent remote sensing and ML analyses),

- empirical characterization of spatiotemporal water quality dynamics in a coastal shallow lake (based on monthly *in situ* measurements of key physicochemical parameters over a 12-month period),
- impact of climate change over the 34 years on Vrana Lake (through long-term analysis of air temperature, precipitation, wind, and water level data and their relationships with observed water quality dynamics),
- systematic evaluation of GIS interpolation methods for water quality mapping (including comparison of multiple interpolation techniques using RMSE and ME metrics and identification of the most suitable method for spatial modelling),
- development of a GIS-MCDA-based monitoring network optimisation (resulting in an optimised network that ensures representative spatial coverage of all water quality classes),
- comparative evaluation of satellite sensors for operational lake monitoring (through cross-sensor analysis of Sentinel-2, Landsat 8-9, and PlanetScope imagery),
- comparative testing of ML models trained on individual physicochemical parameters and on a composite WQI (demonstrating the advantages of WQI-based modelling for stable, accurate, and transferable water quality assessment).

From a scientific perspective, the dissertation contributes to geodesy and geomatics, remote sensing, GIS science, hydrology, and limnology by demonstrating how geospatial methods can be systematically integrated into a unified monitoring framework. The research highlights the central role of GIS not only as a tool for visualisation, but as a methodological backbone for data integration, spatial reasoning, and decision support. From an applied perspective, the proposed framework offers a transferable and adaptable approach that can support lake management under increasing environmental pressures associated with climate change, land-use intensification, and anthropogenic impact. The proposed methodology enables more efficient allocation of monitoring resources, resulting in time- and cost-effective lake water quality assessment.

Despite the demonstrated advantages of the proposed approach, certain limitations remain. The research identified several limitations, including dependence on calibration data quality, challenges related to atmospheric correction in optically complex waters, and limited temporal coverage for long-term trend analysis. Furthermore, the accuracy of spatial interpolation and

ML models depends on the density and representativeness of *in situ* data. Future research should focus on longer time series, integration of higher-frequency observations, coupling with hydrodynamic models, and application of transfer learning techniques to improve spatial and temporal transferability.

This doctoral dissertation confirms that integrated geospatial multi-sensor approaches represent a significant advancement in lake water quality monitoring. By systematically integrating *in situ* measurements, spatial modelling, satellite remote sensing, and ML, the research provides a robust methodological foundation for future scientific studies and practical environmental management of shallow lake ecosystems.

Bibliography

1. Heino, J.; Alahuhta, J.; Bini, L.M.; Cai, Y.; Heiskanen, A.; Hellsten, S.; Kortelainen, P.; Kotamäki, N.; Tolonen, K.T.; Vihervaara, P.; et al. Lakes in the Era of Global Change: Moving beyond Single-lake Thinking in Maintaining Biodiversity and Ecosystem Services. *Biological Reviews* **2021**, *96*, 89–106, doi:10.1111/brv.12647.
2. Sterner, R.W.; Keeler, B.; Polasky, S.; Poudel, R.; Rhude, K.; Rogers, M. Ecosystem Services of Earth's Largest Freshwater Lakes. *Ecosystem Services* **2020**, *41*, 101046, doi:10.1016/j.ecoser.2019.101046.
3. Adjovu, G.E.; Stephen, H.; Ahmad, S. Spatial and Temporal Dynamics of Key Water Quality Parameters in a Thermal Stratified Lake Ecosystem: The Case Study of Lake Mead. *Earth* **2023**, *4*, 461–502, doi:10.3390/earth4030025.
4. Bănăduc, D.; Simić, V.; Cianfaglione, K.; Barinova, S.; Afanasyev, S.; Öktener, A.; McCall, G.; Simić, S.; Curtean-Bănăduc, A. Freshwater as a Sustainable Resource and Generator of Secondary Resources in the 21st Century: Stressors, Threats, Risks, Management and Protection Strategies, and Conservation Approaches. *IJERPH* **2022**, *19*, 16570, doi:10.3390/ijerph192416570.
5. Chen, F.; Li, S.; Song, K. Remote Sensing of Lake Chlorophyll-a in Qinghai-Tibet Plateau Responding to Climate Factors: Implications for Oligotrophic Lakes. *Ecol. Indic.* **2024**, *159*, 111674, doi:10.1016/j.ecolind.2024.111674.
6. Abell, J.M.; Özkundakci, D.; Hamilton, D.P.; Reeves, P. Restoring Shallow Lakes Impaired by Eutrophication: Approaches, Outcomes, and Challenges. *Crit Rev Environ Sci Technol* **2020**, *52*, 1199–1246, doi:10.1080/10643389.2020.1854564.
7. Jeppesen, E.; Brucet, S.; Naselli-Flores, L.; Papastergiadou, E.; Stefanidis, K.; Nõges, T.; Nõges, P.; Attayde, J.L.; Zohary, T.; Coppens, J.; et al. Ecological Impacts of Global Warming and Water Abstraction on Lakes and Reservoirs Due to Changes in Water Level and Related Changes in Salinity. *Hydrobiologia* **2015**, *750*, 201–227, doi:10.1007/s10750-014-2169-x.
8. O'Grady, J.; Zhang, D.; O'Connor, N.; Regan, F. A Comprehensive Review of Catchment Water Quality Monitoring Using a Tiered Framework of Integrated Sensing Technologies. *Science of The Total Environment* **2021**, *765*, 142766, doi:10.1016/j.scitotenv.2020.142766.

9. Batina, A.; Krtalić, A. Integrating Remote Sensing Methods for Monitoring Lake Water Quality: A Comprehensive Review. *Hydrol.* **2024**, *11*, 92, doi:10.3390/hydrology11070092.
10. Jan, F.; Min-Allah, N.; Düştegör, D. IoT Based Smart Water Quality Monitoring: Recent Techniques, Trends and Challenges for Domestic Applications. *Water* **2021**, *13*, 1729, doi:10.3390/w13131729.
11. Free, G.; Bresciani, M.; Trodd, W.; Tierney, D.; O'Boyle, S.; Plant, C.; Deakin, J. Estimation of Lake Ecological Quality from Sentinel-2 Remote Sensing Imagery. *Hydrobiologia* **2020**, *847*, 1423–1438, doi:10.1007/s10750-020-04197-y.
12. El Serafy, G.Y.H.; Schaeffer, B.A.; Neely, M.-B.; Spinosa, A.; Odermatt, D.; Weathers, K.C.; Baracchini, T.; Bouffard, D.; Carvalho, L.; Conmy, R.N.; et al. Integrating Inland and Coastal Water Quality Data for Actionable Knowledge. *Remote Sensing* **2021**, *13*, 2899, doi:10.3390/rs13152899.
13. Sagan, V.; Peterson, K.T.; Maimaitijiang, M.; Sidike, P.; Sloan, J.; Greeling, B.A.; Maalouf, S.; Adams, C. Monitoring Inland Water Quality Using Remote Sensing: Potential and Limitations of Spectral Indices, Bio-Optical Simulations, Machine Learning, and Cloud Computing. *Earth Sci Rev* **2020**, *205*, 103187, doi:10.1016/j.earscirev.2020.103187.
14. Cáceres-Merino, J.; Cuartero, A.; Torrecilla-Pinero, J.A. Finding Optimal Spatial Window: The Influence of Size on Remote-Sensing-Based Chl-a Prediction in Small Reservoirs. *IEEE J. Sel. Top. Appl. Earth Observations Remote Sensing* **2024**, *17*, 18769–18783, doi:10.1109/JSTARS.2024.3476970.
15. Sent, G.; Biguino, B.; Favareto, L.; Cruz, J.; Sá, C.; Dogliotti, A.I.; Palma, C.; Brotas, V.; Brito, A.C. Deriving Water Quality Parameters Using Sentinel-2 Imagery: A Case Study in the Sado Estuary, Portugal. *Remote Sensing* **2021**, *13*, 1043, doi:10.3390/rs13051043.
16. Xiong, Y.; Ran, Y.; Zhao, S.; Zhao, H.; Tian, Q. Remotely Assessing and Monitoring Coastal and Inland Water Quality in China: Progress, Challenges and Outlook. *Critical Reviews in Environmental Science and Technology* **2020**, *50*, 1266–1302, doi:10.1080/10643389.2019.1656511.
17. Pahlevan, N.; Smith, B.; Schalles, J.; Binding, C.; Cao, Z.; Ma, R.; Alikas, K.; Kangro, K.; Gurlin, D.; Hà, N.; et al. Seamless Retrievals of Chlorophyll-a from Sentinel-2 (MSI) and Sentinel-3 (OLCI) in Inland and Coastal Waters: A Machine-Learning Approach. *Remote Sens Environ* **2020**, *240*, 111604, doi:10.1016/j.rse.2019.111604.

18. Sharaf El Din, E.; Zhang, Y.; Suliman, A. Mapping Concentrations of Surface Water Quality Parameters Using a Novel Remote Sensing and Artificial Intelligence Framework. *Int J Remote Sens* **2017**, *38*, 1023–1042, doi:10.1080/01431161.2016.1275056.
19. Adjovu, G.E.; Stephen, H.; James, D.; Ahmad, S. Overview of the Application of Remote Sensing in Effective Monitoring of Water Quality Parameters. *Remote Sensing* **2023**, *15*, 1938, doi:10.3390/rs15071938.
20. Toming, K.; Liu, H.; Soomets, T.; Uuemaa, E.; Nõges, T.; Kutser, T. Estimation of the Biogeochemical and Physical Properties of Lakes Based on Remote Sensing and Artificial Intelligence Applications. *Remote Sensing* **2024**, *16*, 464, doi:10.3390/rs16030464.
21. Reyjol, Y.; Argillier, C.; Bonne, W.; Borja, A.; Buijse, A.D.; Cardoso, A.C.; Daufresne, M.; Kernan, M.; Ferreira, M.T.; Poikane, S.; et al. Assessing the Ecological Status in the Context of the European Water Framework Directive: Where Do We Go Now? *Sci. Total Environ.* **2014**, *497–498*, 332–344, doi:10.1016/j.scitotenv.2014.07.119.
22. Wang, X.; Yang, W. Water Quality Monitoring and Evaluation Using Remote Sensing Techniques in China: A Systematic Review. *ECOSYST HEALTH SUST* **2019**, *5*, 47–56, doi:10.1080/20964129.2019.1571443.
23. IOCCG *Earth Observations in Support of Global Water Quality Monitoring*; Greb, S., Dekker, A., Binding, C., Eds.; International Ocean Colour Coordinating Group: Dartmouth, Canada, 2018;
24. Akar, A.U.; Sisman, S.; Ulku, H.; Yel, E.; Yalpir, S. Evaluating Lake Water Quality with a GIS-Based MCDA Integrated Approach: A Case in Konya/Karapınar. *Environ Sci Pollut Res* **2024**, *31*, 19478–19499, doi:10.1007/s11356-024-32184-6.
25. Batina, A.; Cukrov, N.; Ćuže Denona, M. Spatiotemporal Water Quality Analysis of Vrana Lake, Croatia. *Open Geosciences* **2025**, *17*, 20250817, doi:10.1515/geo-2025-0817.
26. Batina, A.; Šiljeg, A. Enhancing Water Quality Monitoring in a Coastal Shallow Lake Using GIS and Multi-Criteria Decision Analysis. *Environmental and Sustainability Indicators* **2025**, *28*, 100881, doi:10.1016/j.indic.2025.100881.
27. Li, J.; Tian, L.; Wang, Y.; Jin, S.; Li, T.; Hou, X. Optimal Sampling Strategy of Water Quality Monitoring at High Dynamic Lakes: A Remote Sensing and Spatial Simulated Annealing Integrated Approach. *Science of The Total Environment* **2021**, *777*, 146113, doi:10.1016/j.scitotenv.2021.146113.

28. Batina, A.; Šiljeg, A.; Krtalić, A.; Šerić, L. SIGMaL: An Integrated Framework for Water Quality Monitoring in a Coastal Shallow Lake. *Remote Sensing* **2026**, *18*, 312, doi:10.3390/rs18020312.
29. Lei, L.; Pang, R.; Han, Z.; Wu, D.; Xie, B.; Su, Y. Current Applications and Future Impact of Machine Learning in Emerging Contaminants: A Review. *Critical Reviews in Environmental Science and Technology* **2023**, *53*, 1817–1835, doi:10.1080/10643389.2023.2190313.
30. Nguyen, X.C.; Bui, V.K.H.; Cho, K.H.; Hur, J. Practical Application of Machine Learning for Organic Matter and Harmful Algal Blooms in Freshwater Systems: A Review. *Critical Reviews in Environmental Science and Technology* **2024**, *54*, 953–975, doi:10.1080/10643389.2023.2285691.
31. Leggesse, E.S.; Zimale, F.A.; Sultan, D.; Enku, T.; Srinivasan, R.; Tilahun, S.A. Predicting Optical Water Quality Indicators from Remote Sensing Using Machine Learning Algorithms in Tropical Highlands of Ethiopia. *Hydrology* **2023**, *10*, 110, doi:10.3390/hydrology10050110.
32. Pang, Z.; Zhou, Z.; Fu, J.; Jiang, W.; Qin, X.; Sun, M. Deep Learning-Based Remote Sensing Retrieval of Inland Water Quality: A Review. *Journal of Hydrology: Regional Studies* **2025**, *61*, 102759, doi:10.1016/j.ejrh.2025.102759.
33. Ma, L.; Liu, Y.; Zhang, X.; Ye, Y.; Yin, G.; Johnson, B.A. Deep Learning in Remote Sensing Applications: A Meta-Analysis and Review. *ISPRS J. Photogramm. Remote Sens.* **2019**, *152*, 166–177, doi:10.1016/j.isprsjprs.2019.04.015.
34. Stendera, S.; Adrian, R.; Bonada, N.; Cañedo-Argüelles, M.; Hugueny, B.; Januschke, K.; Pletterbauer, F.; Hering, D. Drivers and Stressors of Freshwater Biodiversity Patterns across Different Ecosystems and Scales: A Review. *Hydrobiologia* **2012**, *696*, 1–28, doi:10.1007/s10750-012-1183-0.
35. Ho, L.T.; Goethals, P.L.M. Opportunities and Challenges for the Sustainability of Lakes and Reservoirs in Relation to the Sustainable Development Goals (SDGs). *Water* **2019**, *11*, 1462, doi:10.3390/w11071462.
36. Hering, D.; Borja, A.; Carstensen, J.; Carvalho, L.; Elliott, M.; Feld, C.K.; Heiskanen, A.-S.; Johnson, R.K.; Moe, J.; Pont, D.; et al. The European Water Framework Directive at the Age of 10: A Critical Review of the Achievements with Recommendations for the Future. *Sci. Total Environ.* **2010**, *408*, 4007–4019, doi:10.1016/j.scitotenv.2010.05.031.
37. Poikane, S.; Birk, S.; Böhmer, J.; Carvalho, L.; de Hoyos, C.; Gassner, H.; Hellsten, S.; Kelly, M.; Lyche Solheim, A.; Olin, M.; et al. A Hitchhiker's Guide to European Lake

Ecological Assessment and Intercalibration. *Ecol. Indic.* **2015**, *52*, 533–544, doi:10.1016/j.ecolind.2015.01.005.

38. Qu, J.; Fan, M. The Current State of Water Quality and Technology Development for Water Pollution Control in China. *Critical Reviews in Environmental Science and Technology* **2010**, *40*, 519–560, doi:10.1080/10643380802451953.
39. Trottet, A.; George, C.; Drillet, G.; Lauro, F.M. Aquaculture in Coastal Urbanized Areas: A Comparative Review of the Challenges Posed by Harmful Algal Blooms. *Critical Reviews in Environmental Science and Technology* **2021**, *52*, 2888–2929, doi:10.1080/10643389.2021.1897372.
40. Brivio, P.A.; Giardino, C.; Zilioli, E. Validation of Satellite Data for Quality Assurance in Lake Monitoring Applications. *Sci. Total Environ.* **2001**, *268*, 3–18, doi:10.1016/S0048-9697(00)00693-8.
41. Chang, N.-B.; Imen, S.; Vannah, B. Remote Sensing for Monitoring Surface Water Quality Status and Ecosystem State in Relation to the Nutrient Cycle: A 40-Year Perspective. *Crit Rev Environ Sci Technol* **2014**, *45*, 101–166, doi:10.1080/10643389.2013.829981.
42. El-Din, M.S.; Gaber, A.; Koch, M.; Ahmed, R.S.; Bahgat, I. Remote Sensing Application for Water Quality Assessment in Lake Timsah, Suez Canal, Egypt. *J. remote sens. technol.* **2013**, 61–74.
43. Visser, F.; Wallis, C.; Sinnott, A.M. Optical Remote Sensing of Submerged Aquatic Vegetation: Opportunities for Shallow Clearwater Streams. *Limnologica* **2013**, *43*, 388–398, doi:10.1016/j.limno.2013.05.005.
44. Gholizadeh, M.; Melesse, A.; Reddi, L. A Comprehensive Review on Water Quality Parameters Estimation Using Remote Sensing Techniques. *Sensors* **2016**, *16*, 1298, doi:10.3390/s16081298.
45. Scarpace, F.; Holmquist, K.; Fisher, L. Landsat Analysis of Lake Quality. *Photogramm Eng Remote Sensing* **1979**, *45*, 623–633.
46. Matthews, M.W. A Current Review of Empirical Procedures of Remote Sensing in Inland and Near-Coastal Transitional Waters. *Int J Remote Sens* **2011**, *32*, 6855–6899, doi:10.1080/01431161.2010.512947.
47. Topp, S.N.; Pavelsky, T.M.; Jensen, D.; Simard, M.; Ross, M.R.V. Research Trends in the Use of Remote Sensing for Inland Water Quality Science: Moving towards Multidisciplinary Applications. *Water* **2020**, *12*, 169, doi:10.3390/w12010169.

48. Dörnhöfer, K.; Oppelt, N. Remote Sensing for Lake Research and Monitoring – Recent Advances. *Ecol. Indic.* **2016**, *64*, 105–122, doi:10.1016/j.ecolind.2015.12.009.
49. Wulder, M.A.; Masek, J.G.; Cohen, W.B.; Loveland, T.R.; Woodcock, C.E. Opening the Archive: How Free Data Has Enabled the Science and Monitoring Promise of Landsat. *Remote Sens Environ* **2012**, *122*, 2–10, doi:10.1016/j.rse.2012.01.010.
50. Hestir, E.L.; Brando, V.E.; Bresciani, M.; Giardino, C.; Matta, E.; Villa, P.; Dekker, A.G. Measuring Freshwater Aquatic Ecosystems: The Need for a Hyperspectral Global Mapping Satellite Mission. *Remote Sens Environ* **2015**, *167*, 181–195, doi:10.1016/j.rse.2015.05.023.
51. European Communities *River and Lakes: Typology, Reference Conditions and Classification Systems*; OPOCE: Luxembourg, 2003;
52. CEN Water Quality - Guidance Standard on Assessing the Hydromorphological Features of Lakes 2010.
53. Palmer, S.C.J.; Hunter, P.D.; Lankester, T.; Hubbard, S.; Spyrakos, E.; N. Tyler, A.; Présing, M.; Horváth, H.; Lamb, A.; Balzter, H.; et al. Validation of Envisat MERIS Algorithms for Chlorophyll Retrieval in a Large, Turbid and Optically-Complex Shallow Lake. *Remote Sens Environ* **2015**, *157*, 158–169, doi:10.1016/j.rse.2014.07.024.
54. Ritchie, J.C.; Zimba, P.V.; Everitt, J.H. Remote Sensing Techniques to Assess Water Quality. *Photogramm Eng Remote Sensing* **2003**, *69*, 695–704, doi:10.14358/PERS.69.6.695.
55. Wu, G. Retrieval of Suspended Sediment Concentration in the Yangtze Estuary and Its Spatiotemporal Dynamics Analysis Based on GOCI Image Data. Master's Thesis, University of Twente: Enschede, The Netherlands, 2015.
56. Yang, H.; Kong, J.; Hu, H.; Du, Y.; Gao, M.; Chen, F. A Review of Remote Sensing for Water Quality Retrieval: Progress and Challenges. *Remote Sens.* **2022**, *14*, 1770, doi:10.3390/rs14081770.
57. IOCCG *Remote Sensing of Ocean Colour in Coastal, and Other Optically-Complex, Waters*; Sathyendranath, S., Ed.; Reports of the International Ocean Colour Coordinating Group (IOCCG); International Ocean Colour Coordinating Group (IOCCG): Dartmouth, NS, Canada, 2000;
58. Chen, Y.; Zheng, G.; Wang, X.; Chen, X. Retrieval of Chlorophyll-a Concentration with Multi-Sensor Data by GSM01 Merging Algorithm. *Journal of Geo-Information Science* **2013**, *15*, 911–917.

59. Gege, P. WASI-2D: A Software Tool for Regionally Optimized Analysis of Imaging Spectrometer Data from Deep and Shallow Waters. *Comput Geosci* **2014**, *62*, 208–215, doi:10.1016/j.cageo.2013.07.022.
60. Qi, L.; Hu, C.; Duan, H.; Barnes, B.; Ma, R. An EOF-Based Algorithm to Estimate Chlorophyll a Concentrations in Taihu Lake from MODIS Land-Band Measurements: Implications for near Real-Time Applications and Forecasting Models. *Remote Sens.* **2014**, *6*, 10694–10715, doi:10.3390/rs61110694.
61. Dekker, A.G.; Zamurović-Nenad, Ž.; Hoogenboom, H.J.; Peters, S.W.M. Remote Sensing, Ecological Water Quality Modelling and in Situ Measurements: A Case Study in Shallow Lakes. *Hydrol Sci J* **1996**, *41*, 531–547, doi:10.1080/02626669609491524.
62. Feng, L.; Hu, C.; Han, X.; Chen, X.; Qi, L. Long-Term Distribution Patterns of Chlorophyll-a Concentration in China's Largest Freshwater Lake: MERIS Full-Resolution Observations with a Practical Approach. *Remote Sens.* **2014**, *7*, 275–299, doi:10.3390/rs70100275.
63. Hunter, P.D.; Tyler, A.N.; Carvalho, L.; Codd, G.A.; Maberly, S.C. Hyperspectral Remote Sensing of Cyanobacterial Pigments as Indicators for Cell Populations and Toxins in Eutrophic Lakes. *Remote Sens Environ* **2010**, *114*, 2705–2718, doi:10.1016/j.rse.2010.06.006.
64. Kallio, K.; Kutser, T.; Hannonen, T.; Koponen, S.; Pulliainen, J.; Vepsäläinen, J.; Pyhälahti, T. Retrieval of Water Quality from Airborne Imaging Spectrometry of Various Lake Types in Different Seasons. *Sci. Total Environ.* **2001**, *268*, 59–77, doi:10.1016/S0048-9697(00)00685-9.
65. Kutser, T.; Pierson, D.C.; Kallio, K.Y.; Reinart, A.; Sobek, S. Mapping Lake CDOM by Satellite Remote Sensing. *Remote Sens Environ* **2005**, *94*, 535–540, doi:10.1016/j.rse.2004.11.009.
66. Singh, K.P.; Basant, N.; Gupta, S. Support Vector Machines in Water Quality Management. *Anal. Chim. Acta* **2011**, *703*, 152–162, doi:10.1016/j.aca.2011.07.027.
67. Song, K.; Li, L.; Tedesco, L.P.; Li, S.; Duan, H.; Liu, D.; Hall, B.E.; Du, J.; Li, Z.; Shi, K.; et al. Remote Estimation of Chlorophyll-a in Turbid Inland Waters: Three-Band Model versus GA-PLS Model. *Remote Sens Environ* **2013**, *136*, 342–357, doi:10.1016/j.rse.2013.05.017.
68. Gong, Z.; Zhong, P.; Yu, Y.; Hu, W.; Li, S. A CNN with Multiscale Convolution and Diversified Metric for Hyperspectral Image Classification. *IEEE Trans. Geosci. Remote Sens.* **2019**, *57*, 3599–3618, doi:10.1109/TGRS.2018.2886022.

69. Peterson, K.; Sagan, V.; Sidike, P.; Cox, A.; Martinez, M. Suspended Sediment Concentration Estimation from Landsat Imagery along the Lower Missouri and Middle Mississippi Rivers Using an Extreme Learning Machine. *Remote Sens.* **2018**, *10*, 1503, doi:10.3390/rs10101503.
70. Kirk, J.T.O. *Light and Photosynthesis in Aquatic Ecosystems*; 2nd ed.; Cambridge University Press: Cambridge, UK, 1994;
71. Dekker, A.G.; Brando, V.E.; Anstee, J.M.; Pinnel, N.; Kutser, T.; Hoogenboom, E.J.; Peters, S.; Pasterkamp, R.; Vos, R.; Olbert, C.; et al. Imaging Spectrometry of Water. In *Imaging Spectrometry*; Meer, F.D. van der, Jong, S.M.D., Eds.; Remote Sensing and Digital Image Processing; Springer Netherlands: Dordrecht, The Netherlands, 2002; Vol. 4, pp. 307–359 ISBN 978-1-4020-0194-9.
72. Gómez, J.A.D.; Alonso, C.A.; García, A.A. Remote Sensing as a Tool for Monitoring Water Quality Parameters for Mediterranean Lakes of European Union Water Framework Directive (WFD) and as a System of Surveillance of Cyanobacterial Harmful Algae Blooms (SCyanoHABs). *Environ. Monit. Assess.* **2011**, *181*, 317–334, doi:10.1007/s10661-010-1831-7.
73. Sharaf El Din, E.; Zhang, Y. Estimation of Both Optical and Nonoptical Surface Water Quality Parameters Using Landsat 8 OLI Imagery and Statistical Techniques. *J. Appl. Remote Sens.* **2017**, *11*, 1, doi:10.1117/1.JRS.11.046008.
74. Torbick, N.; Hession, S.; Hagen, S.; Wiangwang, N.; Becker, B.; Qi, J. Mapping Inland Lake Water Quality across the Lower Peninsula of Michigan Using Landsat TM Imagery. *Int J Remote Sens* **2013**, *34*, 7607–7624, doi:10.1080/01431161.2013.822602.
75. Toming, K.; Kutser, T.; Laas, A.; Sepp, M.; Paavel, B.; Nõges, T. First Experiences in Mapping Lake Water Quality Parameters with Sentinel-2 MSI Imagery. *Remote Sens.* **2016**, *8*, 640, doi:10.3390/rs8080640.
76. Svirčev, Z.; Simeunović, J.; Subakov-Simić, G.; Krstić, S.; Pantelić, D.; Dulić, T. Cyanobacterial Blooms and Their Toxicity in Vojvodina Lakes, Serbia. *Int J Environ Res* **2013**, *7*, doi:10.22059/ijer.2013.654.
77. Paerl, H.W.; Huisman, J. Climate Change: A Catalyst for Global Expansion of Harmful Cyanobacterial Blooms. *Environ. Microbiol. Rep.* **2009**, *1*, 27–37, doi:10.1111/j.1758-2229.2008.00004.x.
78. Gower, J.F.R.; Brown, L.; Borstad, G.A. Observation of Chlorophyll Fluorescence in West Coast Waters of Canada Using the MODIS Satellite Sensor. *Can. J. Remote. Sens.* **2004**, *30*, 17–25, doi:10.5589/m03-048.

79. Harrington, J.; Repic, R. Hyperspectral and Video Remote Sensing of Oklahoma Lakes. In Proceedings of the Applied Geography Conferences; Denton, TX, USA, 1995; Vol. 18, pp. 79–86.
80. Giardino, C.; Brando, V.E.; Dekker, A.G.; Strömbeck, N.; Candiani, G. Assessment of Water Quality in Lake Garda (Italy) Using Hyperion. *Remote Sens Environ* **2007**, *109*, 183–195, doi:10.1016/j.rse.2006.12.017.
81. Giardino, C.; Bresciani, M.; Valentini, E.; Gasperini, L.; Bolpagni, R.; Brando, V.E. Airborne Hyperspectral Data to Assess Suspended Particulate Matter and Aquatic Vegetation in a Shallow and Turbid Lake. *Remote Sens Environ* **2015**, *157*, 48–57, doi:10.1016/j.rse.2014.04.034.
82. Gilerson, A.A.; Gitelson, A.A.; Zhou, J.; Gurlin, D.; Moses, W.; Ioannou, I.; Ahmed, S.A. Algorithms for Remote Estimation of Chlorophyll-a in Coastal and Inland Waters Using Red and near Infrared Bands. *Opt. Express* **2010**, *18*, 24109, doi:10.1364/OE.18.024109.
83. Gitelson, A.A.; Gurlin, D.; Moses, W.J.; Barrow, T. A Bio-Optical Algorithm for the Remote Estimation of the Chlorophyll-a Concentration in Case 2 Waters. *Environ. Res. Lett.* **2009**, *4*, 045003, doi:10.1088/1748-9326/4/4/045003.
84. Dall'Olmo, G.; Gitelson, A.A. Effect of Bio-Optical Parameter Variability and Uncertainties in Reflectance Measurements on the Remote Estimation of Chlorophyll-a Concentration in Turbid Productive Waters: Modeling Results. *Appl. Opt.* **2006**, *45*, 3577, doi:10.1364/AO.45.003577.
85. Gitelson, A.A.; Dall'Olmo, G.; Moses, W.; Rundquist, D.C.; Barrow, T.; Fisher, T.R.; Gurlin, D.; Holz, J. A Simple Semi-Analytical Model for Remote Estimation of Chlorophyll-a in Turbid Waters: Validation. *Remote Sens Environ* **2008**, *112*, 3582–3593, doi:10.1016/j.rse.2008.04.015.
86. Le, C.; Li, Y.; Zha, Y.; Sun, D.; Huang, C.; Lu, H. A Four-Band Semi-Analytical Model for Estimating Chlorophyll a in Highly Turbid Lakes: The Case of Taihu Lake, China. *Remote Sens Environ* **2009**, *113*, 1175–1182, doi:10.1016/j.rse.2009.02.005.
87. Boucher, J.; Weathers, K.C.; Norouzi, H.; Steele, B. Assessing the Effectiveness of Landsat 8 Chlorophyll *a* Retrieval Algorithms for Regional Freshwater Monitoring. *Ecological Applications* **2018**, *28*, 1044–1054, doi:10.1002/eap.1708.
88. Keith, D.J.; Milstead, B.; Walker, H.; Snook, H.; Szykman, J.; Wusk, M.; Kagey, L.; Howell, C.; Mellanson, C.; Drueke, C. Trophic Status, Ecological Condition, and

Cyanobacteria Risk of New England Lakes and Ponds Based on Aircraft Remote Sensing. *J. Appl. Remote Sens.* **2012**, *6*, 063577–1, doi:10.1117/1.JRS.6.063577.

89. Moses, W.J.; Gitelson, A.A.; Perk, R.L.; Gurlin, D.; Rundquist, D.C.; Leavitt, B.C.; Barrow, T.M.; Brakhage, P. Estimation of Chlorophyll-a Concentration in Turbid Productive Waters Using Airborne Hyperspectral Data. *Water Res.* **2012**, *46*, 993–1004, doi:10.1016/j.watres.2011.11.068.
90. Song, K.; Wang, Z.; Blackwell, J.; Zhang, B.; Li, F.; Zhang, Y.; Jiang, G. Water Quality Monitoring Using Landsat Themate Mapper Data with Empirical Algorithms in Chagan Lake, China. *J. Appl. Remote Sens.* **2011**, *5*, 5, doi:10.1117/1.3559497.
91. Flores-Anderson, A.I.; Griffin, R.; Dix, M.; Romero-Oliva, C.S.; Ochaeta, G.; Skinner-Alvarado, J.; Ramirez Moran, M.V.; Hernandez, B.; Cherrington, E.; Page, B.; et al. Hyperspectral Satellite Remote Sensing of Water Quality in Lake Atitlán, Guatemala. *Front. Environ. Sci.* **2020**, *8*, 7, doi:10.3389/fenvs.2020.00007.
92. Soomets, T.; Uudeberg, K.; Jakovels, D.; Brauns, A.; Zagars, M.; Kutser, T. Validation and Comparison of Water Quality Products in Baltic Lakes Using Sentinel-2 MSI and Sentinel-3 OLCI Data. *Sensors* **2020**, *20*, 742, doi:10.3390/s20030742.
93. Thiemann, S.; Kaufmann, H. Lake Water Quality Monitoring Using Hyperspectral Airborne Data—A Semiempirical Multisensor and Multitemporal Approach for the Mecklenburg Lake District, Germany. *Remote Sens Environ* **2002**, *81*, 228–237, doi:10.1016/S0034-4257(01)00345-5.
94. Blix, K.; Pálffy, K.; Tóth, V.; Eltoft, T. Remote Sensing of Water Quality Parameters over Lake Balaton by Using Sentinel-3 OLCI. *Water* **2018**, *10*, 1428, doi:10.3390/w10101428.
95. Wu, M.; Zhang, W.; Wang, X.; Luo, D. Application of MODIS Satellite Data in Monitoring Water Quality Parameters of Chaohu Lake in China. *Environ. Monit. Assess.* **2009**, *148*, 255–264, doi:10.1007/s10661-008-0156-2.
96. Alparslan, E.; Coskun, H.G.; Alganci, U. Water Quality Determination of Küçükçekmece Lake, Turkey by Using Multispectral Satellite Data. *The Sci. World J.* **2009**, *9*, 1215–1229, doi:10.1100/tsw.2009.135.
97. Sudheer, K.P.; Chaubey, I.; Garg, V. Lake Water Quality Assessment from Landsat Thematic Mapper Data Using Neural Network: An Approach to Optimal Band Combination Selection. *J Am Water Resour Assoc* **2006**, *42*, 1683–1695, doi:10.1111/j.1752-1688.2006.tb06029.x.

98. Mancino, G.; Nolè, A.; Urbano, V.; Amato, M.; Ferrara, A. Assessing Water Quality by Remote Sensing in Small Lakes: The Case Study of Monticchio Lakes in Southern Italy. *iForest* **2009**, *2*, 154–161, doi:10.3832/ifor0507-002.
99. Allee, R.J.; Johnson, J.E. Use of Satellite Imagery to Estimate Surface Chlorophyll a and Secchi Disc Depth of Bull Shoals Reservoir, Arkansas, USA. *Int J Remote Sens* **1999**, *20*, 1057–1072, doi:10.1080/014311699212849.
100. Chao Rodríguez, Y.; el Anjoumi, A.; Domínguez Gómez, J.A.; Rodríguez Pérez, D.; Rico, E. Using Landsat Image Time Series to Study a Small Water Body in Northern Spain. *Environ. Monit. Assess.* **2014**, doi:10.1007/s10661-014-3634-8.
101. Giardino, C.; Pepe, M.; Brivio, P.A.; Ghezzi, P.; Zilioli, E. Detecting Chlorophyll, Secchi Disk Depth and Surface Temperature in a Sub-Alpine Lake Using Landsat Imagery. *Sci. Total Environ.* **2001**, *268*, 19–29, doi:10.1016/S0048-9697(00)00692-6.
102. Wang, F.; Han, L.; Kung, H. -T.; Van Arsdale, R.B. Applications of Landsat-5 TM Imagery in Assessing and Mapping Water Quality in Reelfoot Lake, Tennessee. *International Journal of Remote Sensing* **2006**, *27*, 5269–5283, doi:10.1080/01431160500191704.
103. Mansaray, A.S.; Dzialowski, A.R.; Martin, M.E.; Wagner, K.L.; Gholizadeh, H.; Stoodley, S.H. Comparing PlanetScope to Landsat-8 and Sentinel-2 for Sensing Water Quality in Reservoirs in Agricultural Watersheds. *Remote Sens.* **2021**, *13*, 1847, doi:10.3390/rs13091847.
104. Menken, K.D.; Brezonik, P.L.; Bauer, M.E. Influence of Chlorophyll and Colored Dissolved Organic Matter (CDOM) on Lake Reflectance Spectra: Implications for Measuring Lake Properties by Remote Sensing. *Lake Reserv Manag* **2006**, *22*, 179–190, doi:10.1080/07438140609353895.
105. Havens, K.E. Submerged Aquatic Vegetation Correlations with Depth and Light Attenuating Materials in a Shallow Subtropical Lake. *Hydrobiologia* **2003**, *493*, 173–186, doi:10.1023/A:1025497621547.
106. Abdelmalik, K.W. Role of Statistical Remote Sensing for Inland Water Quality Parameters Prediction. *Egypt. J. Remote. Sens. Space Sci.* **2018**, *21*, 193–200, doi:10.1016/j.ejrs.2016.12.002.
107. Hicks, B.J.; Stichbury, G.A.; Brabyn, L.K.; Allan, M.G.; Ashraf, S. Hindcasting Water Clarity from Landsat Satellite Images of Unmonitored Shallow Lakes in the Waikato Region, New Zealand. *Environ. Monit. Assess.* **2013**, *185*, 7245–7261, doi:10.1007/s10661-013-3098-2.

108. Ma, Y.; Song, K.; Wen, Z.; Liu, G.; Shang, Y.; Lyu, L.; Du, J.; Yang, Q.; Li, S.; Tao, H.; et al. Remote Sensing of Turbidity for Lakes in Northeast China Using Sentinel-2 Images with Machine Learning Algorithms. *IEEE J. Sel. Top. Appl. Earth Observations Remote Sensing* **2021**, *14*, 9132–9146, doi:10.1109/JSTARS.2021.3109292.
109. Mushtaq, F.; Nee Lala, M.G. Remote Estimation of Water Quality Parameters of Himalayan Lake (Kashmir) Using Landsat 8 OLI Imagery. *Geocarto International* **2017**, *32*, 274–285, doi:10.1080/10106049.2016.1140818.
110. Papoutsa, C.; Retalis, A.; Toulios, L.; Hadjimitsis, D.G. Defining the Landsat TM/ETM+ and CHRIS/PROBA Spectral Regions in Which Turbidity Can Be Retrieved in Inland Waterbodies Using Field Spectroscopy. *Int J Remote Sens* **2014**, *35*, 1674–1692, doi:10.1080/01431161.2014.882029.
111. González-Márquez, L.C.; Torres-Bejarano, F.M.; Torregroza-Espinosa, A.C.; Hansen-Rodríguez, I.R.; Rodríguez-Gallegos, H.B. Use of LANDSAT 8 Images for Depth and Water Quality Assessment of El Guájaro Reservoir, Colombia. *J South Am Earth Sci* **2018**, *82*, 231–238, doi:10.1016/j.jsames.2018.01.004.
112. He, W.; Chen, S.; Liu, X.; Chen, J. Water Quality Monitoring in a Slightly-Polluted Inland Water Body through Remote Sensing — Case Study of the Guanting Reservoir in Beijing, China. *Front. Environ. Sci. Engin. China* **2008**, *2*, 163–171, doi:10.1007/s11783-008-0027-7.
113. Teubner, K.; Teubner, I.; Pall, K.; Kabas, W.; Tolotti, M.; Ofenböck, T.; Dokulil, M.T. New Emphasis on Water Transparency as Socio-Ecological Indicator for Urban Water: Bridging Ecosystem Service Supply and Sustainable Ecosystem Health. *Front. Environ. Sci.* **2020**, *8*, 573724, doi:10.3389/fenvs.2020.573724.
114. Bowers, D.G.; Roberts, E.M.; Hoguane, A.M.; Fall, K.A.; Massey, G.M.; Friedrichs, C.T. Secchi Disk Measurements in Turbid Water. *J. Geophys. Res. Oceans* **2020**, *125*, doi:10.1029/2020JC016172.
115. Maciel, D.A.; Novo, E.M.L.D.M.; Barbosa, C.C.F.; Martins, V.S.; Flores Júnior, R.; Oliveira, A.H.; Sander De Carvalho, L.A.; Lobo, F.D.L. Evaluating the Potential of CubeSats for Remote Sensing Reflectance Retrieval over Inland Waters. *Int. J. Remote Sens.* **2020**, *41*, 2807–2817, doi:10.1080/2150704X.2019.1697003.
116. Keller, S.; Maier, P.; Riese, F.; Norra, S.; Holbach, A.; Börsig, N.; Wilhelms, A.; Moldaenke, C.; Zaake, A.; Hinz, S. Hyperspectral Data and Machine Learning for Estimating CDOM, Chlorophyll a, Diatoms, Green Algae and Turbidity. *Int. J. Environ. Res. Public Health* **2018**, *15*, 1881, doi:10.3390/ijerph15091881.

117. Olmanson, L.G.; Bauer, M.E.; Brezonik, P.L. A 20-Year Landsat Water Clarity Census of Minnesota's 10,000 Lakes. *Remote Sens Environ* **2008**, *112*, 4086–4097, doi:10.1016/j.rse.2007.12.013.
118. Matthews, M.W.; Bernard, S.; Winter, K. Remote Sensing of Cyanobacteria-Dominant Algal Blooms and Water Quality Parameters in Zeekoevlei, a Small Hypertrophic Lake, Using MERIS. *Remote Sens Environ* **2010**, *114*, 2070–2087, doi:10.1016/j.rse.2010.04.013.
119. Isenstein, E.M.; Park, M.-H. Assessment of Nutrient Distributions in Lake Champlain Using Satellite Remote Sensing. *J Environ Sci (China)* **2014**, *26*, 1831–1836, doi:10.1016/j.jes.2014.06.019.
120. Sriwongsitanon, N.; Surakit, K.; Thianpopirug, S. Influence of Atmospheric Correction and Number of Sampling Points on the Accuracy of Water Clarity Assessment Using Remote Sensing Application. *J. Hydrol.* **2011**, *401*, 203–220, doi:10.1016/j.jhydrol.2011.02.023.
121. Allan, M.G.; Hicks, B.J.; Brabyn, L. *Remote Sensing of Water Quality in the Rotorua Lakes*; Environment Bay of Plenty: Whakatāne, New Zealand, 2007; p. 27;.
122. Osinska-Skotak, K.; Kruk, M.; Mróz, M. The Spatial Diversification of Lake Water Quality Parameters in Mazurian Lakes in Summertime. In Proceedings of the 26th EARSeL Symposium on New Developments and Challenges in Remote Sensing; Millpress: Warsaw, Poland, 2007; pp. 591–602.
123. Ekercin, S. Water Quality Retrievals from High Resolution IKONOS Multispectral Imagery: A Case Study in Istanbul, Turkey. *Water Air Soil Pollut.* **2007**, *183*, 239–251, doi:10.1007/s11270-007-9373-5.
124. Koponen, S.; Pulliainen, J.; Kallio, K.; Hallikainen, M. Lake Water Quality Classification with Airborne Hyperspectral Spectrometer and Simulated MERIS Data. *Remote Sens Environ* **2002**, *79*, 51–59, doi:10.1016/S0034-4257(01)00238-3.
125. Smith, W.L.; Knuteson, R.O.; Revercomb, H.E.; Feltz, W.; Howell, H.B.; Menzel, W.P.; Nalli, N.R.; Brown, O.; Brown, J.; Minnett, P.; et al. Observations of the Infrared Radiative Properties of the Ocean–Implications for the Measurement of Sea Surface Temperature via Satellite Remote Sensing. *Bulletin of the American Meteorological Society* **1996**, *77*, 41–52.
126. Vesecky, J.F.; Onstott, R.G.; Wang, N.-Y.; Lettvin, E.; Slawski, J.; Shuchman, R.A. Water Surface Temperature Estimates Using Active and Passive Microwave Remote Sensing: Preliminary Results from an Outdoor Wind-Wave Tank. In Proceedings of the

IGARSS ’94 - 1994 IEEE International Geoscience and Remote Sensing Symposium; IEEE: Pasadena, CA, USA, 1994; Vol. 2, pp. 1021–1023.

127. Sima, S.; Ahmadalipour, A.; Tajrishy, M. Mapping Surface Temperature in a Hyper-Saline Lake and Investigating the Effect of Temperature Distribution on the Lake Evaporation. *Remote Sens Environ* **2013**, *136*, 374–385, doi:10.1016/j.rse.2013.05.014.
128. Wloczyk, C.; Richter, R.; Borg, E.; Neubert, W. Sea and Lake Surface Temperature Retrieval from Landsat Thermal Data in Northern Germany. *Int J Remote Sens* **2006**, *27*, 2489–2502, doi:10.1080/01431160500300206.
129. Politi, E.; Cutler, M.E.J.; Rowan, J.S. Using the NOAA Advanced Very Highresolution Radiometer to Characterise Temporal and Spatial Trends in Watertemperature of Large European Lakes. *Remote Sens Environ* **2012**, *126*, 1–11, doi:10.1016/j.rse.2012.08.004.
130. Reinart, A.; Reinhold, M. Mapping Surface Temperature in Large Lakes with MODIS Data. *Remote Sens Environ* **2008**, *112*, 603–611, doi:10.1016/j.rse.2007.05.015.
131. Lotfi, S.; Ranjbar, S.; Amani, M.; Zarei, A. Lake Urmia Water Salinity Mapping Using Sentinel-2 Multi-Spectral Imagery. In Proceedings of the 2022 10th International Conference on Agro-geoinformatics (Agro-Geoinformatics); IEEE: Quebec City, QC, Canada, July 11 2022; pp. 1–5.
132. Bayati, M.; Danesh-Yazdi, M. Mapping the Spatiotemporal Variability of Salinity in the Hypersaline Lake Urmia Using Sentinel-2 and Landsat-8 Imagery. *Journal of Hydrology* **2021**, *595*, 126032, doi:10.1016/j.jhydrol.2021.126032.
133. Elachi, C.; Van Zyl, J.J. *Introduction to the Physics and Techniques of Remote Sensing*; John Wiley & Sons: New York, NY, USA, 2021; Vol. 28;.
134. Hu, C.; Chen, Z.; Clayton, T.D.; Swarzenski, P.; Brock, J.C.; Muller–Karger, F.E. Assessment of Estuarine Water-Quality Indicators Using MODIS Medium-Resolution Bands: Initial Results from Tampa Bay, FL. *Remote Sens Environ* **2004**, *93*, 423–441, doi:10.1016/j.rse.2004.08.007.
135. United States Environmental Protection Agency Conductivity Available online: https://archive.epa.gov/water/archive/web/html/vms59.html (accessed on 12 July 2023).
136. Hayashi, M.; Vogt, T.; Mächler, L.; Schirmer, M. Diurnal Fluctuations of Electrical Conductivity in a Pre-Alpine River: Effects of Photosynthesis and Groundwater Exchange. *J. Hydrol.* **2012**, *450–451*, 93–104, doi:10.1016/j.jhydrol.2012.05.020.
137. Mohamed, H.M.; Khalil, M.T.; El-Kafrawy, S.B.; El-Zeiny, A.M.; Khalifa, N.; Emam, W.W.M. Can Statistical Remote Sensing Aid in Predicting the Potential Productivity of

Inland Lakes? Case Study: Lake Qaroun, Egypt. *Stoch Environ Res Risk Assess* **2022**, *36*, 3221–3238, doi:10.1007/s00477-022-02189-z.

138. Brezonik, P.; Menken, K.D.; Bauer, M. Landsat-Based Remote Sensing of Lake Water Quality Characteristics, Including Chlorophyll and Colored Dissolved Organic Matter (CDOM). *Lake Reserv Manag* **2005**, *21*, 373–382, doi:10.1080/07438140509354442.
139. Chen, J.; Zhu, W.-N.; Tian, Y.Q.; Yu, Q. Estimation of Colored Dissolved Organic Matter from Landsat-8 Imagery for Complex Inland Water: Case Study of Lake Huron. *IEEE Trans. Geosci. Remote Sens.* **2017**, *55*, 2201–2212, doi:10.1109/TGRS.2016.2638828.
140. Dekker, A.G. Detection of Optical Water Quality Parameters for Eutrophic Waters by High Resolution Remote Sensing. PhD Thesis, Vrije Universiteit Amsterdam: Amsterdam, The Netherlands, 1993.
141. Li, J.; Chen, X.; Tian, L.; Huang, J.; Feng, L. Improved Capabilities of the Chinese High-Resolution Remote Sensing Satellite GF-1 for Monitoring Suspended Particulate Matter (SPM) in Inland Waters: Radiometric and Spatial Considerations. *ISPRS J. Photogramm. Remote Sens.* **2015**, *106*, 145–156, doi:10.1016/j.isprsjprs.2015.05.009.
142. Oppelt, N.; Scheiber, R.; Gege, P.; Wegmann, M.; Taubenböck, H.; Berger, M. Fundamentals of Remote Sensing for Terrestrial Applications: Evolution, Current State-of-the-Art and Future Possibilities. In *Remotely Sensed Data Characterization, Classification, and Accuracies*; Thenkabail, P.S., Ed.; CRC Press: Boca Raton, FL, USA, 2015; p. 24 ISBN 978-0-429-08939-8.
143. Pyo, J.; Ligaray, M.; Kwon, Y.; Ahn, M.-H.; Kim, K.; Lee, H.; Kang, T.; Cho, S.; Park, Y.; Cho, K. High-Spatial Resolution Monitoring of Phycocyanin and Chlorophyll-a Using Airborne Hyperspectral Imagery. *Remote Sens.* **2018**, *10*, 1180, doi:10.3390/rs10081180.
144. Chang, N.-B.; Vannah, B.W.; Yang, Y.J.; Elovitz, M. Integrated Data Fusion and Mining Techniques for Monitoring Total Organic Carbon Concentrations in a Lake. *Int J Remote Sens* **2014**, *35*, 1064–1093, doi:10.1080/01431161.2013.875632.
145. Cillero Castro, C.; Domínguez Gómez, J.A.; Delgado Martín, J.; Hinojo Sánchez, B.A.; Cereijo Arango, J.L.; Cheda Tuya, F.A.; Díaz-Varela, R. An UAV and Satellite Multispectral Data Approach to Monitor Water Quality in Small Reservoirs. *Remote Sens.* **2020**, *12*, 1514, doi:10.3390/rs12091514.
146. Rowan, G.S.L.; Kalacska, M. A Review of Remote Sensing of Submerged Aquatic Vegetation for Non-Specialists. *Remote Sens.* **2021**, *13*, 623, doi:10.3390/rs13040623.

147. Lo, Y.; Fu, L.; Lu, T.; Huang, H.; Kong, L.; Xu, Y.; Zhang, C. Medium-Sized Lake Water Quality Parameters Retrieval Using Multispectral UAV Image and Machine Learning Algorithms: A Case Study of the Yuandang Lake, China. *Drones* **2023**, *7*, 244, doi:10.3390/drones7040244.
148. Specim AISA Systems Available online: https://www.specim.com/aisa/ (accessed on 21 June 2024).
149. NASA CASI Available online: https://impact.earthdata.nasa.gov/casei/instrument/CASI (accessed on 21 June 2024).
150. NASA Airborne Imagery Available online: https://ntrs.nasa.gov/api/citations/20030001734/downloads/20030001734.pdf (accessed on 21 June 2024).
151. NASA HyMap Available online: https://airbornescience.nasa.gov/instrument/HyMap (accessed on 21 June 2024).
152. Sea Bird HyperOCR Radiometer Available online: https://www.seabird.com/hyperocr-radiometer/product?id=60762467730 (accessed on 21 June 2024).
153. Bianchi, R.; Marino, C.M.; Pignatti, S. Airborne Hyperspectral Remote Sensing in Italy.; Chavez, Jr., P.S., Marino, C.M., Schowengerdt, R.A., Eds.; Rome, Italy, December 21 1994; pp. 29–37.
154. ESA MERIS Available online: https://earth.esa.int/eogateway/instruments/meris (accessed on 21 June 2024).
155. Earth Resources Observation and Science (EROS) Center USGS EROS Archive - Earth Observing One (EO-1) - Hyperion Available online: https://www.usgs.gov/centers/eros/science/usgs-eros-archive-earth-observing-one-eo-1-hyperion#overview (accessed on 21 June 2024).
156. Maxar Ikonos Available online: https://resources.maxar.com/data-sheets/ikonos (accessed on 21 June 2024).
157. Landsat Landsat 5 Available online: https://landsat.gsfc.nasa.gov/satellites/landsat-5/ (accessed on 21 June 2024).
158. NASA LANDSAT 7 Available online: https://landsat.gsfc.nasa.gov/satellites/landsat-7/ (accessed on 21 June 2024).
159. NASA LANDSAT 8 Available online: https://landsat.gsfc.nasa.gov/satellites/landsat-8/ (accessed on 21 June 2024).
160. NOAA AVHRR Available online: https://coastwatch.noaa.gov/cwn/instruments/avhrr.html (accessed on 21 June 2024).

161. Planet PlanetScope Available online: https://developers.planet.com/docs/data/planetscope/ (accessed on 21 June 2024).
162. ESA CHRIS Available online: https://earth.esa.int/eogateway/instruments/chris (accessed on 21 June 2024).
163. ESA Copernicus: Sentinel-2 Available online: https://www.eoportal.org/satellite-missions/copernicus-sentinel-2 (accessed on 21 June 2024).
164. ESA Copernicus: Sentinel-3 Available online: https://www.eoportal.org/satellite-missions/copernicus-sentinel-3 (accessed on 21 June 2024).
165. NASA ASTER Available online: https://asterweb.jpl.nasa.gov/index.asp (accessed on 21 June 2024).
166. NASA MODIS Available online: https://modis.gsfc.nasa.gov/ (accessed on 21 June 2024).
167. Maxar WorldView-2 Available online: https://resources.maxar.com/data-sheets/worldview-2 (accessed on 21 June 2024).
168. Stipaničev, D.; Šerić, L.; Braović, M. *Uvod u umjetnu inteligenciju*; 1st ed.; Faculty of Electrical Engineering, Mechanical Engineering and Naval Architecture, Split: Split, Croatia, 2021; ISBN 978-953-290-108-5.
169. Wang, K.; Wan, Z.; Wang, P.; Sparrow, M.; Liu, J.; Zhou, X.; Haginoya, S. Estimation of Surface Long Wave Radiation and Broadband Emissivity Using Moderate Resolution Imaging Spectroradiometer (MODIS) Land Surface Temperature/Emissivity Products. *J. Geophys. Res.* **2005**, *110*, 110, doi:10.1029/2004JD005566.
170. Hou, P.; Chang, F.; Duan, L.; Zhang, Y.; Zhang, H. Seasonal Variation and Spatial Heterogeneity of Water Quality Parameters in Lake Chenghai in Southwestern China. *Water* **2022**, *14*, 1640, doi:10.3390/w14101640.
171. IPCC *Climate Change 2023: Synthesis Report. Contribution of Working Groups I, II and III to the Sixth Assessment Report of the Intergovernmental Panel on Climate Change [Core Writing Team, H. Lee and J. Romero (Eds.)]*; First.; IPCC, Geneva, Switzerland, pp. 1-34, doi: https://doi.org/10.59327/IPCC/AR6-9789291691647.001, 2023; pp. 1–34;.
172. Li, Z.; Zhang, Z.; Xiong, S.; Zhang, W.; Li, R. Lake Surface Temperature Predictions under Different Climate Scenarios with Machine Learning Methods: A Case Study of Qinghai Lake and Hulun Lake, China. *Remote Sens.* **2024**, *16*, 3220, doi:10.3390/rs16173220.

173. Wu, Q.; Xia, X.; Li, X.; Mou, X. Impacts of Meteorological Variations on Urban Lake Water Quality: A Sensitivity Analysis for 12 Urban Lakes with Different Trophic States. *Aquat. Sci.* **2014**, *76*, 339–351, doi:10.1007/s00027-014-0339-6.
174. Rezaee, A.; Mosaedi, A.; Beheshti, A.; Zarrin, A. Using Wavelet Transform to Analyze the Dynamics of Climatic Variables; to Assess the Status of Available Water Resources in Iran (1961–2020). *Earth Sci. Inf.* **2024**, doi:https://doi.org/10.1007/s12145-024-01433-0.
175. Vasistha, P.; Ganguly, R. Assessment of Spatio-Temporal Variations in Lake Water Body Using Indexing Method. *Environ. Sci. Pollut. Res.* **2020**, *27*, 41856–41875, doi:10.1007/s11356-020-10109-3.
176. Uslu, A.; Dugan, S.T.; El Hmaidi, A.; Muhammetoglu, A. Comparative Evaluation of Spatiotemporal Variations of Surface Water Quality Using Water Quality Indices and GIS. *Earth Sci. Inf.* **2024**, doi:10.1007/s12145-024-01389-1.
177. Gautam, R.; Shrestha, S.M. Hydrogeochemical Evaluation and Characterization of Water Quality in the Phewa Lake, Pokhara, Nepal. *Environ. Sci. Pollut. Res.* **2024**, *31*, 60568–60586, doi:10.1007/s11356-024-35213-6.
178. Horvat, Z.; Horvat, M.; Pastor, K. Assessment of Spatial and Temporal Water Quality Distribution in Shallow Lakes: Case Study for Lake Ludas, Serbia. *Environ. Earth Sci.* **2022**, *82*.
179. Jácome, G.; Valarezo, C.; Yoo, C. Assessment of Water Quality Monitoring for the Optimal Sensor Placement in Lake Yahuarcocha Using Pattern Recognition Techniques and Geographical Information Systems. *Environ. Monit. Assess.* **2018**, *190*, 259, doi:10.1007/s10661-018-6639-x.
180. İlhan, N.; Demir Yetiş, A.; Yeşilnacar, M.İ.; Atasoy, A.D.S. Predictive Modelling and Seasonal Analysis of Water Quality Indicators: Three Different Basins of Şanlıurfa, Turkey. *Environ. Dev. Sustainability* **2022**, *24*, 3258–3292.
181. Ding, W.; Zhao, J.; Qin, B.; Wu, T.; Zhu, S.; Li, Y.; Xu, S.; Ruan, S.; Wang, Y. Exploring and Quantifying the Relationship between Instantaneous Wind Speed and Turbidity in a Large Shallow Lake: Case Study of Lake Taihu in China. *Environ. Sci. Pollut. Res.* **2021**, *28*, 16616–16632, doi:10.1007/s11356-020-11544-y.
182. Kang, J.; Yang, F.; Wang, J.; Liu, Y.; Fang, D.; Jiang, C. Spatial-Temporal Evolution of Habitat Quality in Tropical Monsoon Climate Region Based on "Pattern–Process–Quality" – a Case Study of Cambodia. *Open Geosci.* **2025**, *17*, 20220748, doi:10.1515/geo-2022-0748.

183. Wang, R.; Pan, L.; Niu, W.; Li, R.; Zhao, X.; Bian, X.; Yu, C.; Xia, H.; Chen, T. Monitoring the Spatiotemporal Dynamics of Surface Water Body of the Xiaolangdi Reservoir Using Landsat-5/7/8 Imagery and Google Earth Engine. *Open Geosci.* **2021**, *13*, 1290–1302, doi:10.1515/geo-2020-0305.
184. Wilkinson, A.A.; Hondzo, M.; Guala, M. Vertical Heterogeneities of Cyanobacteria and Microcystin Concentrations in Lakes Using a Seasonal In Situ Monitoring Station. *Global Ecol. Conserv.* **2020**, *21*, e00838, doi:10.1016/j.gecco.2019.e00838.
185. Bayable, G.; Cai, J.; Mekonnen, M.; Legesse, S.A.; Ishikawa, K.; Sato, S.; Kuwahara, V.S. Spatiotemporal Variability of Lake Surface Water Temperature and Water Quality Parameters and Its Interrelationship with Water Hyacinth Biomass in Lake Tana, Ethiopia. *Environ. Sci. Pollut. Res.* **2024**, *31*, 45929–45953, doi:10.1007/s11356-024-34212-x.
186. Khouni, I.; Louhichi, G.; Ghrabi, A. Use of GIS Based Inverse Distance Weighted Interpolation to Assess Surface Water Quality: Case of Wadi El Bey, Tunisia. *Environ. Technol. Innovation* **2021**, *24*, 101892, doi:10.1016/j.eti.2021.101892.
187. Vasistha, P.; Ganguly, R. Water Quality Assessment in Two Lakes of Panchkula, Haryana, Using GIS: Case Study on Seasonal and Depth Wise Variations. *Environ. Sci. Pollut. Res.* **2022**, *29*, 43212–43236, doi:10.1007/s11356-022-18635-y.
188. Murphy, R.R.; Curriero, F.C.; Ball, W.P. Comparison of Spatial Interpolation Methods for Water Quality Evaluation in the Chesapeake Bay. *J. Environ. Eng.* **2010**, *136*, 160–171, doi:10.1061/(ASCE)EE.1943-7870.0000121.
189. Khan, M.; Almazah, M.M.A.; EIlahi, A.; Niaz, R.; Al-Rezami, A.Y.; Zaman, B. Spatial Interpolation of Water Quality Index Based on Ordinary Kriging and Universal Kriging. *Geomatics Nat. Hazards Risk* **2023**, *14*, 2190853, doi:10.1080/19475705.2023.2190853.
190. Vujović, F.; Ćulafić, G.; Valjarević, A.; Brđanin, E.; Durlević, U. Comparative Geomorphometric Analysis of Drainage Basin Using Aw3d30 Model in ArcGIS and QGIS Environment: Case Study of the Ibar River Drainage Basin, Montenegro. *Agric. For.* **2024**, *70*, doi:10.17707/AgricultForest.70.1.15.
191. Oseke, F.I.; Anornu, G.K.; Adjei, K.A.; Eduvie, M.O. Assessment of Water Quality Using GIS Techniques and Water Quality Index in Reservoirs Affected by Water Diversion. *Water-Energy Nexus* **2021**, *4*, 25–34, doi:10.1016/j.wen.2020.12.002.
192. Aleksova, B.; Lukić, T.; Milevski, I.; Spalević, V.; Marković, S.B. Modelling Water Erosion and Mass Movements (Wet) by Using GIS-Based Multi-Hazard Susceptibility

Assessment Approaches: A Case Study—Kratovska Reka Catchment (North Macedonia). *Atmosphere* **2023**, *14*, 1139, doi:10.3390/atmos14071139.

193. Durlević, U. Assessment of Torrential Flood and Landslide Susceptibility of Terrain: Case Study - Mlava River Basin (Serbia). *Glas. Srp. geogr. drus.* **2021**, *101*, 49–75, doi:10.2298/GSGD2101049D.
194. Antonakos, A.; Lambrakis, N. Spatial Interpolation for the Distribution of Groundwater Level in an Area of Complex Geology Using Widely Available GIS Tools. *Environ. Process.* **2021**, *8*, 993–1026, doi:10.1007/s40710-021-00529-9.
195. Boumpoulis, V.; Michalopoulou, M.; Depountis, N. Comparison between Different Spatial Interpolation Methods for the Development of Sediment Distribution Maps in Coastal Areas. *Earth Sci. Inf.* **2023**, *16*, 2069–2087, doi:10.1007/s12145-023-01017-4.
196. Ouabo, R.E.; Sangodoyin, A.Y.; Ogundiran, M.B. Assessment of Ordinary Kriging and Inverse Distance Weighting Methods for Modeling Chromium and Cadmium Soil Pollution in E-Waste Sites in Douala, Cameroon. *Journal of Health and Pollution* **2020**, *10*, 200605, doi:10.5696/2156-9614-10.26.200605.
197. Reimann, C.; Filzmoser, P. Normal and Lognormal Data Distribution in Geochemistry: Death of a Myth. Consequences for the Statistical Treatment of Geochemical and Environmental Data. *Environ. Geol.* **2000**, *39*, 1001–1014, doi:10.1007/s002549900081.
198. Vuković, N.; Alegro, A.; Koletić, N.; Rimac, A.; Šegota, V. Analysis of Macrophytes in Vransko Lake from 2010 to 2019 as Part of Change We Care Project (in Croatian) 2020.
199. Trbojević, I.; Šinžar Sekulić, J.; Subakov Simić, G.; Milovanović, V.; Ćuže Denona, M.; Fressel, N.; Rogić, D. *Monitoring of Algae from the Characeae Family in 2022*; University of Belgrade, Faculty of Biology (in Serbian), 2022;
200. Šiljeg, A. Digital Terrain Model in the Analysis of Geomorphometrical Parameters – the Example of Nature Park Lake Vrana. Doctoral Thesis, University of Zadar (in Croatian): Zadar, Croatia, 2013.
201. Public Institution Vransko Jezero Nature Park Management Plan for the Nature Park and Special Ornithological Reserve Vransko Lake and Its Associated Ecological Network Areas (PU 6163) 2023 – 2032 (in Croatian) 2022.
202. Kurt, O. Model-Based Prediction of Water Levels for the Great Lakes: A Comparative Analysis. *Earth Sci. Inf.* **2024**, doi:10.1007/s12145-024-01341-3.

203. Croatian Geological Survey *Vrana Lake - Hydrogeological Research*; Croatian Geological Survey, Department of Hydrogeology and Engineering Geology (in Croatian), 2012;
204. Batina, A.; Cukrov, N.; Ćuže Denona, M. Assessing Water Quality Dynamics in Vrana Lake [Dataset] 2024.
205. Rubinić, J.; Katalinić, A. Water Regime of Vrana Lake in Dalmatia (Croatia): Changes, Risks and Problems. *Hydrol. Sci. J.* **2014**, *59*, 1908–1924, doi:10.1080/02626667.2014.946417.
206. Musić, V.; Šikoronja, M.; Tomas, D.; Varat, M. *Report on the State of Surface Waters in 2021*; Hrvatske vode (in Croatian), 2023;
207. Planet Team Planet Application Program Interface: In Space for Life on Earth 2022.
208. Li, J.; Meng, Y.; Li, Y.; Cui, Q.; Yang, X.; Tao, C.; Wang, Z.; Li, L.; Zhang, W. Accurate Water Extraction Using Remote Sensing Imagery Based on Normalized Difference Water Index and Unsupervised Deep Learning. *J. Hydrol.* **2022**, *612*, 128202, doi:10.1016/j.jhydrol.2022.128202.
209. American Public Health Association *Standard Methods for the Examination of Water and Wastewater*; 17th ed.; American Public Health Association: Washington, DC, USA, 1989;
210. Xylem EXO User Manual 2020.
211. Zolfaghari, K.; Wilkes, G.; Bird, S.; Ellis, D.; Pintar, K.D.M.; Gottschall, N.; McNairn, H.; Lapen, D.R. Chlorophyll-a, Dissolved Organic Carbon, Turbidity and Other Variables of Ecological Importance in River Basins in Southern Ontario and British Columbia, Canada. *Environ. Monit. Assess.* **2020**, *192*, 1–16, doi:10.1007/s10661-019-7800-x.
212. "Understanding geostatistical analysis" Available online: https://pro.arcgis.com/en/pro-app/latest/help/analysis/geostatistical-analyst/understanding-geostatistical-analysis.htm (accessed on 17 December 2023).
213. "Exploratory Interpolation (Geostatistical Analyst)" Available online: https://pro.arcgis.com/en/pro-app/latest/tool-reference/geostatistical-analyst/exploratory-interpolation.htm (accessed on 17 December 2023).
214. "Using cross validation to assess interpolation results" Available online: https://pro.arcgis.com/en/pro-app/latest/help/analysis/geostatistical-analyst/performing-cross-validation-and-validation.htm (accessed on 24 April 2024).

215. Hengl, T. Finding the Right Pixel Size. *Computers & Geosciences* **2006**, *32*, 1283–1298, doi:10.1016/j.cageo.2005.11.008.
216. Pandžić, K.; Likso, T.; Biondić, R.; Biondić, B. A Review of the Contribution of Satellite Altimetry and Tide Gauge Data to Evaluate Sea Level Trends in the Adriatic Sea within a Mediterranean and Global Context. *GeoHazards* **2024**, *5*, 112–141, doi:10.3390/geohazards5010006.
217. Van Alphen, J.; Haasnoot, M.; Diermanse, F. Uncertain Accelerated Sea-Level Rise, Potential Consequences, and Adaptive Strategies in The Netherlands. *Water* **2022**, *14*, 1527, doi:10.3390/w14101527.
218. Holgerson, M.A.; Richardson, D.C.; Roith, J.; Bortolotti, L.E.; Finlay, K.; Hornbach, D.J.; Gurung, K.; Ness, A.; Andersen, M.R.; Bansal, S.; et al. Classifying Mixing Regimes in Ponds and Shallow Lakes. *Water Resour. Res.* **2022**, *58*, e2022WR032522, doi:10.1029/2022WR032522.
219. Girdner, S.; Mack, J.; Buktenica, M. Impact of Nutrients on Photoacclimation of Phytoplankton in an Oligotrophic Lake Measured with Long-Term and High-Frequency Data: Implications for Chlorophyll as an Estimate of Phytoplankton Biomass. *Hydrobiologia* **2020**, *847*, 1817–1830, doi:10.1007/s10750-020-04213-1.
220. Ye, R.; Shan, K.; Gao, H.; Zhang, R.; Xiong, W.; Wang, Y.; Qian, X. Spatio-Temporal Distribution Patterns in Environmental Factors, Chlorophyll-a and Microcystins in a Large Shallow Lake, Lake Taihu, China. *Int. J. Environ. Res. Public Health* **2014**, *11*, 5155–5169, doi:10.3390/ijerph110505155.
221. Leidonald, R.; Muhtadi, A.; Lesmana, I.; Harahap, Z.A.; Rahmadya, A. Profiles of Temperature, Salinity, Dissolved Oxygen, and pH in Tidal Lakes. *IOP Conf. Ser.: Earth Environ. Sci.* **2019**, *260*, 012075, doi:10.1088/1755-1315/260/1/012075.
222. Degermendzhy, A.G.; Zadereev, E.S.; Rogozin, D.Yu.; Prokopkin, I.G.; Barkhatov, Y.V.; Tolomeev, A.P.; Khromechek, E.B.; Janse, J.H.; Mooij, W.M.; Gulati, R.D. Vertical Stratification of Physical, Chemical and Biological Components in Two Saline Lakes Shira and Shunet (South Siberia, Russia). *Aquat. Ecol.* **2010**, *44*, 619–632, doi:10.1007/s10452-010-9336-6.
223. Kong, X.; Seewald, M.; Dadi, T.; Friese, K.; Mi, C.; Boehrer, B.; Schultze, M.; Rinke, K.; Shatwell, T. Unravelling Winter Diatom Blooms in Temperate Lakes Using High Frequency Data and Ecological Modeling. *Water Res.* **2021**, *190*, 116681, doi:10.1016/j.watres.2020.116681.

224. The Official Gazette *Official Gazette of the Republic of Croatia "Narodne novine."* 2023, pp. 1-51 (in Croatian).
225. Dominović, I.; Dutour-Sikirić, M.; Marguš, M.; Bakran-Petricioli, T.; Petricioli, D.; Geček, S.; Iglenečki, I. Deoxygenation and Stratification Dynamics in a Coastal Marine Lake. *Estuarine Coastal Shelf Sci.* **2023**, *291*, 108420, doi:10.1016/j.ecss.2023.108420.
226. Fondriest Environmental, Inc. Turbidity, Total Suspended Solids and Water Clarity. Available online: https://www.fondriest.com/environmental-measurements/parameters/water-quality/turbidity-total-suspended-solids-water-clarity/ (accessed on 14 March 2024).
227. Silva, F.L.D.; Stefani, M.S.; Smith, W.; Schiavone, D.C.; Cunha-Santino, M.B.D.; Bianchini Jr, I. An Applied Ecological Approach for the Assessment of Anthropogenic Disturbances in Urban Wetlands and the Contributor River. *Ecol. Complexity* **2020**, *43*, 100852, doi:10.1016/j.ecocom.2020.100852.
228. Anamunda, A.; Lamtane, H.A. Relationship between Physicochemical Parameters and the Abundance of Zooplankton in Lake Mweru-Wantipa, Zambia. *Int. J. Bonorowo Wetlands* **2022**, *12*, doi:10.13057/bonorowo/w120104.
229. Wang, Y.; Tao, J.; Zhao, L.; Qin, S.; Xiao, H.; Wang, Y.; Sheng, D.; Zhang, Y. Investigating Long-Term Changes in Surface Water Temperature of Dongting Lake Using Landsat Imagery, China. *Environ. Sci. Pollut. Res.* **2024**, *31*, 41167–41181, doi:10.1007/s11356-024-33878-7.
230. Saturday, A.; Lyimo, T.J.; Machiwa, J.; Pamba, S. Spatial and Temporal Variations of Phytoplankton Composition and Biomass in Lake Bunyonyi, South-Western Uganda. *Environ. Monit. Assess.* **2022**, *194*, 288, doi:10.1007/s10661-022-09954-1.
231. Fondriest Environmental, Inc. Dissolved Oxygen Available online: https://www.fondriest.com/environmental-measurements/parameters/water-quality/dissolved-oxygen/ (accessed on 24 February 2024).
232. Allesson, L.; Valiente, N.; Dörsch, P.; Andersen, T.; Eiler, A.; Hessen, D.O. Drivers and Variability of CO2:O2 Saturation along a Gradient from Boreal to Arctic Lakes. *Sci. Rep.* **2022**, *12*, 18989, doi:10.1038/s41598-022-23705-9.
233. Paerl, H.W.; Huisman, J. Blooms Like It Hot. *Science* **2008**, *320*, 57–58, doi:10.1126/science.1155398.
234. Davraz, A.; Varol, S.; Sener, E.; Sener, S.; Aksever, F.; Kırkan, B.; Tokgözlü, A. Assessment of Water Quality and Hydrogeochemical Processes of Salda Alkaline Lake

(Burdur, Turkey). *Environ Monit Assess* **2019**, *191*, 701, doi:10.1007/s10661-019-7889-y.

235. Moss, B. Allied Attack: Climate Change and Eutrophication. *IW* **2011**, *1*, 101–105, doi:10.5268/IW-1.2.359.
236. Chidiac, S.; El Najjar, P.; Ouaini, N.; El Rayess, Y.; El Azzi, D. A Comprehensive Review of Water Quality Indices (WQIs): History, Models, Attempts and Perspectives. *Rev Environ Sci Biotechnol* **2023**, *22*, 349–395, doi:10.1007/s11157-023-09650-7.
237. Syeed, M.M.M.; Hossain, M.S.; Karim, M.R.; Uddin, M.F.; Hasan, M.; Khan, R.H. Surface Water Quality Profiling Using the Water Quality Index, Pollution Index and Statistical Methods: A Critical Review. *Environmental and Sustainability Indicators* **2023**, *18*, 100247, doi:10.1016/j.indic.2023.100247.
238. Kothari, V.; Vij, S.; Sharma, S.; Gupta, N. Correlation of Various Water Quality Parameters and Water Quality Index of Districts of Uttarakhand. *Environmental and Sustainability Indicators* **2021**, *9*, 100093, doi:10.1016/j.indic.2020.100093.
239. Subramaniam, P.; Ahmed, A.N.; Fai, C.M.; Abdul Malek, M.; Kumar, P.; Huang, Y.F.; Sherif, M.; Elshafie, A. Integrated GIS and Multivariate Statistical Approach for Spatial and Temporal Variability Analysis for Lake Water Quality Index. *Cogent Engineering* **2023**, *10*, 2190490, doi:10.1080/23311916.2023.2190490.
240. Talukdar, S.; Shahfahad; Ahmed, S.; Naikoo, M.W.; Rahman, A.; Mallik, S.; Ningthoujam, S.; Bera, S.; Ramana, G.V. Predicting Lake Water Quality Index with Sensitivity-Uncertainty Analysis Using Deep Learning Algorithms. *Journal of Cleaner Production* **2023**, *406*, 136885, doi:10.1016/j.jclepro.2023.136885.
241. Ryan, S.; Nimick, E. Multi-Criteria Decision Analysis and GIS (accessed on 28 February 2025).
242. Nikolić, G.; Vujović, F.; Golijanin, J.; Šiljeg, A.; Valjarević, A. Modelling of Wildfire Susceptibility in Different Climate Zones in Montenegro Using GIS-MCDA. *Atmosphere* **2023**, *14*, 929, doi:10.3390/atmos14060929.
243. Pileggi, S.F. Is the World Becoming a Better or a Worse Place? A Data-Driven Analysis. *Sustainability* **2019**, *12*, 88, doi:10.3390/su12010088.
244. Ho, W.; Ma, X. The State-of-the-Art Integrations and Applications of the Analytic Hierarchy Process. *European Journal of Operational Research* **2018**, *267*, 399–414, doi:10.1016/j.ejor.2017.09.007.
245. Deb, D.; Majumder, M.; Chakraborty, T.; Khobragade, P.D.; Tripura, K. Surface Water Quality Assessment and Determination of Drinking Water Quality Index by Adopting

Multi Criteria Decision Analysis Techniques. In *Intelligent Computing and Optimization*; Vasant, P., Zelinka, I., Weber, G.-W., Eds.; Advances in Intelligent Systems and Computing; Springer International Publishing: Cham, 2021; Vol. 1324, pp. 907–921 ISBN 978-3-030-68153-1.

246. Alamanos, A.; Mylopoulos, N.; Loukas, A.; Gaitanaros, D. An Integrated Multicriteria Analysis Tool for Evaluating Water Resource Management Strategies. *Water* **2018**, *10*, 1795, doi:10.3390/w10121795.
247. Wang, H.; Cai, Y.; Tan, Q.; Zeng, Y. Evaluation of Groundwater Remediation Technologies Based on Fuzzy Multi-Criteria Decision Analysis Approaches. *Water* **2017**, *9*, 443, doi:10.3390/w9060443.
248. Ghosh, M.; Gope, D. Hydro-Morphometric Characterization and Prioritization of Sub-Watersheds for Land and Water Resource Management Using Fuzzy Analytical Hierarchical Process (FAHP): A Case Study of Upper Rihand Watershed of Chhattisgarh State, India. *Appl Water Sci* **2021**, *11*, 17, doi:10.1007/s13201-020-01340-x.
249. Lagogiannis, S.; Papadopoulos, A.; Dimitriou, E. Development of an Automatic Water Monitoring Network by Using Multi-Criteria Analysis and a GIS-Based Fuzzy Process. *Environ. Process.* **2024**, *11*, 36, doi:10.1007/s40710-024-00714-6.
250. Theochari, A.-P.; Feloni, E.; Bournas, A.; Baltas, E. Hydrometeorological - Hydrometric Station Network Design Using Multicriteria Decision Analysis and GIS Techniques. *Environ. Process.* **2021**, *8*, 1099–1119, doi:10.1007/s40710-021-00527-x.
251. Saltelli, A.; Chan, K.; Scott, E.M. *Sensitivity Analysis*; Wiley, 2009; ISBN 0-470-74382-4.
252. Seifi, A.; Dehghani, M.; Singh, V.P. Uncertainty Analysis of Water Quality Index (WQI) for Groundwater Quality Evaluation: Application of Monte-Carlo Method for Weight Allocation. *Ecological Indicators* **2020**, *117*, 106653, doi:10.1016/j.ecolind.2020.106653.
253. de Rocquigny, E.; Devictor, N.; Tarantola, S. *Uncertainty in Industrial Practice A Guide to Quantitative Uncertainty Management*; Wiley, 2008; ISBN 0-470-77074-0.
254. Romero, J.R.; Kagalou, I.; Imberger, J.; Hela, D.; Kotti, M.; Bartzokas, A.; Albanis, T.; Evmirides, N.; Karkabounas, S.; Papagiannis, J.; et al. Seasonal Water Quality of Shallow and Eutrophic Lake Pamvotis, Greece: Implications for Restoration. *Hydrobiologia* **2002**, *474*, 91–105, doi:https://doi.org/10.1023/A:1016569124312.
255. Umwali, E.D.; Kurban, A.; Isabwe, A.; Mind'je, R.; Azadi, H.; Guo, Z.; Udahogora, M.; Nyirarwasa, A.; Umuhoza, J.; Nzabarinda, V.; et al. Spatio-Seasonal Variation of Water

Quality Influenced by Land Use and Land Cover in Lake Muhazi. *Sci Rep* **2021**, *11*, 17376, doi:https://doi.org/10.1038/s41598-021-96633-9.

256. Armstrong, D.S.; Savoie, J.G.; DeSimone, L.A.; Laabs, K.L.; Carey, R.O. *Surface-Water-Quality Data to Support Implementation of Revised Freshwater Aluminum Water-Quality Criteria in Massachusetts, 2018–19*; Scientific Investigations Report; U.S. Geological Survey: Reston, VA, USA, 2022; p. 85;.
257. Schuwirth, N.; Honti, M.; Logar, I.; Stamm, C. Multi-Criteria Decision Analysis for Integrated Water Quality Assessment and Management Support. *Water Research X* **2018**, *1*, 100010, doi:10.1016/j.wroa.2018.100010.
258. Chen, X.; Liu, X.; Li, B.; Peng, W.; Dong, F.; Huang, A.; Wang, W.; Cao, F. Water Quality Assessment and Spatial–Temporal Variation Analysis in Erhai Lake, Southwest China. *Open Geosciences* **2021**, *13*, 1643–1655, doi:10.1515/geo-2020-0326.
259. Rubinić, J.; Radišić, M.; Bušelić, G.; Ćuže Denona, M. Kriptodepresije Jezerskih Sustava Na Području Hrvatskog Priobalja – Hidrološko Stanje i Rizici Od Neželjenih Promjena. In Proceedings of the 7. hrvatska konferencija o vodama; Hrvatske vode, 2019; pp. 301–309.
260. Holeček, P. Fuzzy AHP [Software] Available online: https://fuzzyahp.holecekp.eu/ (accessed on 28 February 2025).
261. Malczewski, J.; Rinner, C. *Multicriteria Decision Analysis in Geographic Information Science*; Advances in geographic information science; Springer: New York, Heidelberg, 2015; ISBN 978-3-540-74756-7.
262. Hamed, M.A.R. Multi Criteria Framework for Surface Water Quality Management. *JEP* **2019**, *10*, 1032–1042, doi:10.4236/jep.2019.108061.
263. Serbu, R.; Marza, B.; Borza, S. A Spatial Analytic Hierarchy Process for Identification of Water Pollution with GIS Software in an Eco-Economy Environment. *Sustainability* **2016**, *8*, 1208, doi:10.3390/su8111208.
264. Wang, T.; Yan, J.; Ma, J.; Li, F.; Liu, C.; Cai, Y.; Chen, S.; Zeng, J.; Qi, Y. A Fuzzy Comprehensive Assessment and Hierarchical Management System for Urban Lake Health: A Case Study on the Lakes in Wuhan City, Hubei Province, China. *IJERPH* **2018**, *15*, 2617, doi:10.3390/ijerph15122617.
265. Dersseh; Kibret; Tilahun; Worqlul; Moges; Dagnew; Abebe; Melesse Potential of Water Hyacinth Infestation on Lake Tana, Ethiopia: A Prediction Using a GIS-Based Multi-Criteria Technique. *Water* **2019**, *11*, 1921, doi:10.3390/w11091921.

266. Zhang, H.; Huang, G.H. Assessment of Non-Point Source Pollution Using a Spatial Multicriteria Analysis Approach. *Ecological Modelling* **2011**, *222*, 313–321, doi:10.1016/j.ecolmodel.2009.12.011.
267. European Environment Agency CORINE Land Cover 2018 (Raster 100 m), Europe, 6-Yearly - Version 2020_20u1, May 2020 2019.
268. Institute for Environmental and Nature Protection Registar Onečišćavanja Okoliša Available online: https://roo.azo.hr/ (accessed on 23 October 2024).
269. Avram, S.; Cipu, C.; Corpade, A.-M.; Gheorghe, C.A.; Manta, N.; Niculae, M.-I.; Pascu, I.S.; Szép, R.E.; Rodino, S. GIS-Based Multi-Criteria Analysis Method for Assessment of Lake Ecosystems Degradation—Case Study in Romania. *IJERPH* **2021**, *18*, 5915, doi:10.3390/ijerph18115915.
270. C3S ERA5 Hourly Data on Single Levels from 1940 to Present 2024.
271. Karbasi Ahvazi, A.; Ebadi, T.; Zarghami, M.; Hashemi, S.H. Application of Multi-Criteria Group Decision-Making for Water Quality Management. *Environ Monit Assess* **2024**, *196*, 683, doi:10.1007/s10661-024-12839-0.
272. Suresh, K.; Tang, T.; Van Vliet, M.T.H.; Bierkens, M.F.P.; Strokal, M.; Sorger-Domenigg, F.; Wada, Y. Recent Advancement in Water Quality Indicators for Eutrophication in Global Freshwater Lakes. *Environ. Res. Lett.* **2023**, *18*, 063004, doi:10.1088/1748-9326/acd071.
273. Esri Distance Accumulation (Spatial Analyst) Available online: https://pro.arcgis.com/en/pro-app/3.4/tool-reference/spatial-analyst/distance-accumulation.htm (accessed on 3 July 2025).
274. Fondriest Environmental, Inc. Conductivity, Salinity and Total Dissolved Solids. Available online: https://www.fondriest.com/environmental-measurements/parameters/water-quality/conductivity-salinity-tds/ (accessed on 14 March 2024).
275. Fondriest Environmental, Inc. Water Temperature. Available online: https://www.fondriest.com/environmental-measurements/parameters/water-quality/water-temperature/ (accessed on 14 March 2024).
276. Bisimwa, A.M.; Amisi, F.M.; Bamawa, C.M.; Muhaya, B.B.; Kankonda, A.B. Water Quality Assessment and Pollution Source Analysis in Bukavu Urban Rivers of the Lake Kivu Basin (Eastern Democratic Republic of Congo). *Environmental and Sustainability Indicators* **2022**, *14*, 100183, doi:10.1016/j.indic.2022.100183.

277. Batina, A.; Šiljeg, A.; Pedić, G. Salinity Dynamics in Vrana Lake, Croatia: Seasonal Variations and Spatial Distribution. In Proceedings of the Book of Abstracts of the 2nd International Scientific Symposium Interdisciplinary Approach to the Scientific Research of the Adriatic Sea – InspireAdriatic 2025; Ruđer Bošković Institute: Zagreb, Croatia, 2025; p. 45.
278. Ma, X.; Wang, Z.; Yin, Z.; Koenig, A. Nitrogen Flow Analysis in Huizhou, South China. *Environmental Management* **2008**, *41*, 378–388, doi:10.1007/s00267-007-9053-7.
279. Mathenge, C.; Mureithi, S.; Midingoyi, S.-K.; Nyilitya, B.; Kironchi, G.; Masso, C. Unveiling the Determinants of the Spatial Variability of Nitrogen Sources Use in the Lake Victoria Basin, East Africa. *Environmental and Sustainability Indicators* **2024**, *24*, 100484, doi:10.1016/j.indic.2024.100484.
280. Han, Y.; Bu, H. The Impact of Climate Change on the Water Quality of Baiyangdian Lake (China) in the Past 30 Years (1991–2020). *Science of The Total Environment* **2023**, *870*, 161957, doi:10.1016/j.scitotenv.2023.161957.
281. Keskin, M.; Dogru, A.O.; Balcik, F.B.; Goksel, C.; Ulugtekin, N.; Sozen, S. Comparing Spatial Interpolation Methods for Mapping Meteorological Data in Turkey. In *Energy Systems and Management*; Bilge, A.N., Toy, A.Ö., Günay, M.E., Eds.; Springer Proceedings in Energy; Springer International Publishing: Cham, 2015; pp. 33–42 ISBN 978-3-319-16023-8.
282. Gigović, L.; Pamučar, D.; Lukić, D.; Marković, S. GIS-Fuzzy DEMATEL MCDA Model for the Evaluation of the Sites for Ecotourism Development: A Case Study of "Dunavski Ključ" Region, Serbia. *Land Use Policy* **2016**, *58*, 348–365, doi:10.1016/j.landusepol.2016.07.030.
283. Ramík, J.; Korviny, P. Inconsistency of Pair-Wise Comparison Matrix with Fuzzy Elements Based on Geometric Mean. *Fuzzy Sets and Systems* **2010**, *161*, 1604–1613, doi:10.1016/j.fss.2009.10.011.
284. Fotsing Metegam, I.F. A GIS-Based on Application of Monte Carlo and Multi-Criteria Decision-Making Approach for Site Suitability Analysis of Solar-Hydrogen Production: Case of Cameroon. *Heliyon* **2025**, *11*, e41541, doi:10.1016/j.heliyon.2024.e41541.
285. Nasr, M.; Orwin, J.F. A Geospatial Approach to Identifying and Mapping Areas of Relative Environmental Pressure on Ecosystem Integrity. *Journal of Environmental Management* **2024**, *370*, 122445, doi:10.1016/j.jenvman.2024.122445.
286. Marić, I.; Peer, M.; Čipak, A.; Kobaš, K.; Šiljeg, A.; Krvavica, N. Integrated Coastal Vulnerability Index for Coastal Flooding: A Case Study of the Croatian Coast.

Environmental and Sustainability Indicators **2024**, *24*, 100514, doi:10.1016/j.indic.2024.100514.

287. Xiaojing, W.; Honglin, H.; Li, Z.; Lili, F.; Xiaoli, R.; Weihua, L.; Changxin, Z.; Naifeng, L. Spatial Sampling Design Optimization of Monitoring Network for Terrestrial Ecosystem in China. *Science of The Total Environment* **2022**, *847*, 157397, doi:10.1016/j.scitotenv.2022.157397.
288. Romanelli, A.; Esquius, K.S.; Massone, H.E.; Escalante, A.H. GIS-Based Pollution Hazard Mapping and Assessment Framework of Shallow Lakes: Southeastern Pampean Lakes (Argentina) as a Case Study. *Environ Monit Assess* **2013**, *185*, 6943–6961, doi:10.1007/s10661-013-3077-7.
289. Capon, S.J.; Stewart-Koster, B.; Bunn, S.E. Future of Freshwater Ecosystems in a 1.5°C Warmer World. *Front. Environ. Sci.* **2021**, *9*, doi:10.3389/fenvs.2021.784642.
290. Sidle, R.C.; Gomi, T. Hydrological Systems. In *Wetzel's Limnology*; Elsevier, 2024; pp. 57–73 ISBN 978-0-12-822701-5.
291. Paule-Mercado, Ma.C.; Rabaneda-Bueno, R.; Porcal, P.; Kopacek, M.; Huneau, F.; Vystavna, Y. Climate and Land Use Shape the Water Balance and Water Quality in Selected European Lakes. *Sci Rep* **2024**, *14*, doi:10.1038/s41598-024-58401-3.
292. Selak, L.; Marković, T.; Pjevac, P.; Orlić, S. Microbial Marker for Seawater Intrusion in a Coastal Mediterranean Shallow Lake, Lake Vrana, Croatia. *Science of The Total Environment* **2022**, *849*, 157859, doi:10.1016/j.scitotenv.2022.157859.
293. Andrzej Urbanski, J.; Wochna, A.; Bubak, I.; Grzybowski, W.; Lukawska-Matuszewska, K.; Łącka, M.; Śliwińska, S.; Wojtasiewicz, B.; Zajączkowski, M. Application of Landsat 8 Imagery to Regional-Scale Assessment of Lake Water Quality. *International Journal of Applied Earth Observation and Geoinformation* **2016**, *51*, 28–36, doi:10.1016/j.jag.2016.04.004.
294. Kuhn, C.; De Matos Valerio, A.; Ward, N.; Loken, L.; Sawakuchi, H.O.; Kampel, M.; Richey, J.; Stadler, P.; Crawford, J.; Striegl, R.; et al. Performance of Landsat-8 and Sentinel-2 Surface Reflectance Products for River Remote Sensing Retrievals of Chlorophyll-a and Turbidity. *Remote Sens. Environ.* **2019**, *224*, 104–118, doi:10.1016/j.rse.2019.01.023.
295. Kayastha, P.; Dzialowski, A.R.; Stoodley, S.H.; Wagner, K.L.; Mansaray, A.S. Effect of Time Window on Satellite and Ground-Based Data for Estimating Chlorophyll-a in Reservoirs. *Remote Sensing* **2022**, *14*, 846, doi:10.3390/rs14040846.

296. Deng, Y.; Zhang, Y.; Pan, D.; Yang, S.X.; Gharabaghi, B. Review of Recent Advances in Remote Sensing and Machine Learning Methods for Lake Water Quality Management. *Remote Sensing* **2024**, *16*, 4196, doi:10.3390/rs16224196.
297. Sun, X.; Zhang, Y.; Shi, K.; Zhang, Y.; Li, N.; Wang, W.; Huang, X.; Qin, B. Monitoring Water Quality Using Proximal Remote Sensing Technology. *Science of The Total Environment* **2022**, *803*, 149805, doi:10.1016/j.scitotenv.2021.149805.
298. Pizani, F.M.C.; Maillard, P.; Ferreira, A.F.F.; De Amorim, C.C. Estimation of Water Quality in a Reservoir from Sentinel-2 MSI and Landsat-8 OLI Sensors. *ISPRS Ann. Photogramm. Remote Sens. Spatial Inf. Sci.* **2020**, *V-3–2020*, 401–408, doi:10.5194/isprs-annals-V-3-2020-401-2020.
299. Parida, B.R.; Tiwari, S.; Dwivedi, C.S.; Pandey, A.C.; Singh, B.; Behera, M.D.; Kumar, N. Comparative Assessment of Satellite-Based Models through Planetscope and Landsat-8 for Determining Physico-Chemical Water Quality Parameters in Varuna River (India). *Appl Water Sci* **2025**, *15*, 55, doi:10.1007/s13201-025-02367-8.
300. Pan, Y.; Bélanger, S.; Huot, Y. Evaluation of Atmospheric Correction Algorithms over Lakes for High-Resolution Multispectral Imagery: Implications of Adjacency Effect. *Remote Sensing* **2022**, *14*, 2979, doi:10.3390/rs14132979.
301. Zhu, W.; Xia, W. Effects of Atmospheric Correction on Remote Sensing Statistical Inference in an Aquatic Environment. *Remote Sensing* **2023**, *15*, 1907, doi:10.3390/rs15071907.
302. Ivanda, A.; Šerić, L.; Braović, M. Exploring Applications of Convolutional Neural Networks in Analyzing Multispectral Satellite Imagery: A Systematic Review. *Big Data Min. Anal.* **2025**, *8*, 407–429, doi:10.26599/bdma.2024.9020086.
303. Ansper, A.; Alikas, K. Retrieval of Chlorophyll a from Sentinel-2 MSI Data for the European Union Water Framework Directive Reporting Purposes. *Remote Sens.* **2018**, *11*, 64, doi:10.3390/rs11010064.
304. Nguyen, U.N.T.; Pham, L.T.H.; Dang, T.D. An Automatic Water Detection Approach Using Landsat 8 OLI and Google Earth Engine Cloud Computing to Map Lakes and Reservoirs in New Zealand. *Environ. Monit. Assess.* **2019**, *191*, 235, doi:10.1007/s10661-019-7355-x.
305. Qu, K. Research on Linear Regression Algorithm. *MATEC Web Conf.* **2024**, *395*, 01046, doi:10.1051/matecconf/202439501046.
306. Liu, S.; Dobriban, E. Ridge Regression: Structure, Cross-Validation, and Sketching 2019.

307. Salman, H.A.; Kalakech, A.; Steiti, A. Random Forest Algorithm Overview. *Babylonian Journal of Machine Learning* **2024**, *2024*, 69–79, doi:10.58496/BJML/2024/007.
308. Natekin, A.; Knoll, A. Gradient Boosting Machines, a Tutorial. *Front. Neurorobot.* **2013**, *7*, doi:10.3389/fnbot.2013.00021.
309. Chen, T.; Guestrin, C. XGBoost: A Scalable Tree Boosting System. In Proceedings of the Proceedings of the 22nd ACM SIGKDD International Conference on Knowledge Discovery and Data Mining; ACM: San Francisco California USA, August 13 2016; pp. 785–794.
310. Basak, D.; Pal, S.; Patranabis, D. Support Vector Regression. *Neural Information Processing – Letters and Reviews* **2007**, *11*, 203–224.
311. Chen, G.; Ma, J.; Fattahi, S. RANSAC Revisited: An Improved Algorithm for Robust Subspace Recovery under Adversarial and Noisy Corruptions 2025.
312. Srisuradetchai, P.; Suksrikran, K. Random Kernel K-Nearest Neighbors Regression. *Front. Big Data* **2024**, *7*, 1402384, doi:10.3389/fdata.2024.1402384.
313. Yang, S.; Berdine, G. Poisson Regression. *SW Resp Crit Care Chron* **2015**, *3*, 61, doi:10.12746/swrccc.v3i9.191.
314. Villota-González, F.H.; Sulbarán-Rangel, B.; Zurita-Martínez, F.; Gurubel-Tun, K.J.; Zúñiga-Grajeda, V. Assessment of Machine Learning Models for Remote Sensing of Water Quality in Lakes Cajititlán and Zapotlán, Jalisco—Mexico. *Remote Sensing* **2023**, *15*, 5505, doi:10.3390/rs15235505.
315. Chicco, D.; Warrens, M.J.; Jurman, G. The Coefficient of Determination R-Squared Is More Informative than SMAPE, MAE, MAPE, MSE and RMSE in Regression Analysis Evaluation. *PeerJ Computer Science* **2021**, *7*, e623, doi:10.7717/peerj-cs.623.
316. Farhadpour, S.; Warner, T.A.; Maxwell, A.E. Selecting and Interpreting Multiclass Loss and Accuracy Assessment Metrics for Classifications with Class Imbalance: Guidance and Best Practices. *Remote Sensing* **2024**, *16*, 533, doi:10.3390/rs16030533.
317. Fawcett, T. An Introduction to ROC Analysis. *Pattern Recognition Letters* **2006**, *27*, 861–874, doi:10.1016/j.patrec.2005.10.010.
318. Niroumand-Jadidi, M.; Bovolo, F.; Bruzzone, L.; Gege, P. Physics-Based Bathymetry and Water Quality Retrieval Using PlanetScope Imagery: Impacts of 2020 COVID-19 Lockdown and 2019 Extreme Flood in the Venice Lagoon. *Remote Sensing* **2020**, *12*, 2381, doi:10.3390/rs12152381.
319. Di Francesco, S.; Biondi, F.; Casentini, B.; Fazi, S.; Amalfitano, S.; D'Eugenio, M.; Todisco, F.; Casadei, S.; Giannone, F. Sentinel-2 and Planet-Scope as Reliable Tools for

Water Quality Monitoring of Small Reservoirs. *The Egyptian Journal of Remote Sensing and Space Sciences* **2025**, *28*, 713–723, doi:10.1016/j.ejrs.2025.11.002.

320. Kramer, G.; Filho, W.P.; De Carvalho, L.A.S.; Trindade, P.M.P.; Da Rosa, C.N.; Dezordi, R. Performance and Validation of Water Surface Temperature Estimates from Landsat 8 of the Itaipu Reservoir, State of Paraná, Brazil. *Environ Monit Assess* **2023**, *195*, 137, doi:10.1007/s10661-022-10677-6.
321. Wong, W.Y.; Ibrahim Al-Ani, A.K.; Hasikin, K.; Mohd Khairuddin, A.S.; Razak, S.A.; Hizaddin, H.F.; Mokhtar, M.I.; Azizan, M.M. Water Quality Index Using Modified Random Forest Technique: Assessing Novel Input Features. *Computer Modeling in Engineering & Sciences* **2022**, *132*, 1011–1038, doi:10.32604/cmes.2022.019244.
322. Keith, D.J.; Schaeffer, B.A.; Lunetta, R.S.; Gould, R.W.; Rocha, K.; Cobb, D.J. Remote Sensing of Selected Water-Quality Indicators with the Hyperspectral Imager for the Coastal Ocean (HICO) Sensor. *Int J Remote Sens* **2014**, *35*, 2927–2962, doi:10.1080/01431161.2014.894663.
323. Moses, W.J.; Gitelson, A.A.; Berdnikov, S.; Povazhnyy, V. Satellite Estimation of Chlorophyll-a Concentration Using the Red and NIR Bands of MERIS—The Azov Sea Case Study. *IEEE Geosci. Remote Sensing Lett.* **2009**, *6*, 845–849, doi:10.1109/LGRS.2009.2026657.
324. Ruddick, K.G.; Gons, H.J.; Rijkeboer, M.; Tilstone, G. Optical Remote Sensing of Chlorophyll a in Case 2 Waters by Use of an Adaptive Two-Band Algorithm with Optimal Error Properties. *Appl. Opt.* **2001**, *40*, 3575, doi:10.1364/AO.40.003575.
325. Peña-Martínez, R.; Ruiz-Verdú, A.; Domínguez-Gómez, J.A. Mapping of Photosynthetic Pigments in Spanish Inland Waters Using MERIS Imagery. In Proceedings of the 2004 Envisat & ERS Symposium; Salzburg, Austria, September 6 2004.
326. Le, C.; Hu, C.; Cannizzaro, J.; English, D.; Muller-Karger, F.; Lee, Z. Evaluation of Chlorophyll-a Remote Sensing Algorithms for an Optically Complex Estuary. *Remote Sens Environ* **2013**, *129*, 75–89, doi:10.1016/j.rse.2012.11.001.
327. Ruiz-Verdú, A.; Domínguez-Gómez, J.-A.; Peña-Martínez, R. Use of CHRIS for Monitoring Water Quality in Rosarito Reservoir. In Proceedings of the 3rd CHRIS/Proba Workshop; Frascati, Italy, March 21 2005; p. 26.
328. Han, L.; Jordan, K.J. Estimating and Mapping Chlorophyll-*a* Concentration in Pensacola Bay, Florida Using Landsat ETM+ Data. *Int J Remote Sens* **2005**, *26*, 5245–5254, doi:10.1080/01431160500219182.

329. Zhang, C.; Han, M. Mapping Chlorophyll-a Concentration in Laizhou Bay Using Landsat 8 OLI Data. In Proceedings of the 36th IAHR World Congress; Hague, The Netherlands, 2015.
330. Hadjimitsis, D.G.; Clayton, C. Assessment of Temporal Variations of Water Quality in Inland Water Bodies Using Atmospheric Corrected Satellite Remotely Sensed Image Data. *Environ. Monit. Assess.* **2009**, *159*, 281–292, doi:10.1007/s10661-008-0629-3.
331. Osińska-Skotak, K.; Kruk, M.; Mróz, M.; Szumilo, M. Chris/Proba Superspectral Data for Inland Water Quality Studies. In Proceedings of the 4th EARSeL Workshop on Imaging Spectroscopy; Warsaw, Poland, 2005; pp. 317–325.
332. George, D.G. The Airborne Remote Sensing of Phytoplankton Chlorophyll in the Lakes and Tarns of the English Lake District. *Int J Remote Sens* **1997**, *18*, 1961–1975, doi:10.1080/014311697217972.
333. Dekker, A.G.; Peters, S.W.M. The Use of the Thematic Mapper for the Analysis of Eutrophic Lakes: A Case Study in the Netherlands. *Int J Remote Sens* **1993**, *14*, 799–821, doi:10.1080/01431169308904379.
334. Mannheim, S.; Segl, K.; Heim, B.; Kaufmann, H. Monitoring of Lake Water Quality Using Hyperspectral CHRIS/Proba Data. In Proceedings of the 2nd CHRIS/Proba Workshop; Frascati, Italy, April 28 2004.
335. Bhatti, A.M.; Rundquist, D.; Schalles, J.; Ramirez, L. Application of Hyperspectral Remotely Sensed Data for Water Quality Monitoring: Accuracy and Limitation. In Proceedings of the 9th International Symposium on Spatial Accuracy Assessment in Natural Resources and Environmental Sciences; International Spatial Accuracy Research Association (ISARA): Leicester, UK, July 20 2010; pp. 349–352.
336. González-Márquez, L.C.; Torres-Bejarano, F.M.; Rodríguez-Cuevas, C.; Torregroza-Espinosa, A.C.; Sandoval-Romero, J.A. Estimation of Water Quality Parameters Using Landsat 8 Images: Application to Playa Colorada Bay, Sinaloa, Mexico. *Appl Geomat* **2018**, *10*, 147–158, doi:10.1007/s12518-018-0211-9.
337. Sawaya, K.E.; Olmanson, L.G.; Heinert, N.J.; Brezonik, P.L.; Bauer, M.E. Extending Satellite Remote Sensing to Local Scales: Land and Water Resource Monitoring Using High-Resolution Imagery. *Remote Sens Environ* **2003**, *88*, 144–156, doi:10.1016/j.rse.2003.04.006.
338. Kloiber, S.M.; Brezonik, P.L.; Olmanson, L.G.; Bauer, M.E. A Procedure for Regional Lake Water Clarity Assessment Using Landsat Multispectral Data. *Remote Sens Environ* **2002**, *82*, 38–47, doi:10.1016/S0034-4257(02)00022-6.

339. Powell, R.; Brooks, C.; French, N.; Shuchman, R. *Remote Sensing of Lake Clarity*; Michigan Tech Research Institute: Ann Arbor, MI, USA, 2008;
340. Kloiber, S.M.; Brezonik, P.L.; Bauer, M.E. Application of Landsat Imagery to Regional-Scale Assessments of Lake Clarity. *Water Res.* **2002**, *36*, 4330–4340, doi:10.1016/S0043-1354(02)00146-X.
341. Olmanson, L.G.; Brezonik, P.L.; Finlay, J.C.; Bauer, M.E. Comparison of Landsat 8 and Landsat 7 for Regional Measurements of CDOM and Water Clarity in Lakes. *Remote Sens Environ* **2016**, *185*, 119–128, doi:10.1016/j.rse.2016.01.007.
342. Fisher, J.; Mustard, J.F. High Spatial Resolution Sea Surface Climatology from Landsat Thermal Infrared Data. *Remote Sens Environ* **2004**, *90*, 293–307, doi:10.1016/j.rse.2004.01.008.
343. Thomas, A.; Byrne, D.; Weatherbee, R. Coastal Sea Surface Temperature Variability from Landsat Infrared Data. *Remote Sens Environ* **2002**, *81*, 262–272, doi:10.1016/S0034-4257(02)00004-4.
344. Ahn, Y.-H.; Shanmugam, P.; Lee, J.-H.; Kang, Y.Q. Application of Satellite Infrared Data for Mapping of Thermal Plume Contamination in Coastal Ecosystem of Korea. *Mar. Environ. Res.* **2006**, *61*, 186–201, doi:10.1016/j.marenvres.2005.09.001.
345. Simon, R.N.; Tormos, T.; Danis, P.-A. Retrieving Water Surface Temperature from Archive LANDSAT Thermal Infrared Data: Application of the Mono-Channel Atmospheric Correction Algorithm over Two Freshwater Reservoirs. *Int J Appl Earth Obs Geoinf* **2014**, *30*, 247–250, doi:10.1016/j.jag.2014.01.005.
346. Brando, V.E.; Braga, F.; Zaggia, L.; Giardino, C.; Bresciani, M.; Matta, E.; Bellafiore, D.; Ferrarin, C.; Maicu, F.; Benetazzo, A.; et al. High-Resolution Satellite Turbidity and Sea Surface Temperature Observations of River Plume Interactions during a Significant Flood Event. *Ocean Sci.* **2015**, *11*, 909–920, doi:10.5194/os-11-909-2015.
347. Syariz, M.A.; Jaelani, L.M.; Subehi, L.; Pamungkas, A.; Koenhardono, E.S.; Sulisetyono, A. Retrieval of Sea Surface Temperature over Poteran Island Water of Indonesia with Landsat 8 Tirs Image: A Preliminary Algorithm. *Int. Arch. Photogramm. Remote Sens. Spat. Inf. Sci. - ISPRS Arch.* **2015**, *XL-2/W4*, 87–90, doi:10.5194/isprsarchives-XL-2-W4-87-2015.
348. Alcântara, E.H.; Stech, J.L.; Lorenzzetti, J.A.; Bonnet, M.P.; Casamitjana, X.; Assireu, A.T.; Novo, E.M.L. de M. Remote Sensing of Water Surface Temperature and Heat Flux over a Tropical Hydroelectric Reservoir. *Remote Sens Environ* **2010**, *114*, 2651–2665, doi:10.1016/j.rse.2010.06.002.

349. Dewidar, Kh.; Khedr, A.A. Remote Sensing of Water Quality for Burullus Lake, Egypt. *Geocarto International* **2005**, *20*, 43–49, doi:10.1080/10106040508542354.
350. Mitchell, D.E. Identifying Salinization through Multispectral Band Analysis: Lake Urmia, Iran 2014.
351. Mallick, J.; Hasan, M.A.; Alashker, Y.; Ahmed, M. Bathymetric and Geochemical Analysis of Lake Al-Saad, Abha, Kingdom of Saudi Arabia Using Geoinformatics Technology. *J. geogr. inf. syst.* **2014**, *06*, 440–452, doi:10.4236/jgis.2014.65038.
352. Ferdous, J.; Rahman, M.T.U. Developing an Empirical Model from Landsat Data Series for Monitoring Water Salinity in Coastal Bangladesh. *J. Environ. Manage.* **2020**, *255*, 109861, doi:10.1016/j.jenvman.2019.109861.

Appendices

Appendix 1

Integrating Remote Sensing Methods for Monitoring Lake Water Quality: A Comprehensive Review – *Supplementary materials*

Analysis of Water Quality Parameters Using Satellite Sensors and Spectral Bands.

Table A1. Selected remotely measurements of chl-a using various sensors and spectral bands, band combinations, and band equations (R in band combinations represents the reflectance at a certain wavelength).

Band Combination	Sensor	Band/Equation	Reference
Ratio between green and red	Landsat-5 TM	B3 (630-690 nm)/B2 (520-600 nm)	[98,102]
	PROBA-CHRIS	R_{706}/R_{561}	[122]
Ratio between NIR and red	AISA	$R_{699-705}/R_{670-677}$	[64]
	AISA	$(R_{700}-R_{781})/(R_{662}-R_{781})$	[124]
	AISA	R_{710}/R_{670}	[63]
	AISA	$(1/R_{666}-1/R_{704})*R_{723}$	[89]
	AISA	R_{704}/R_{666}	[89]
	CASI	R_{705}/R_{678}	[93]
	CASI-2	R_{710}/R_{670}	[63]
	HICO	$(1/R_{686}-1/R_{703})*R_{735}$	[322]
	HyMap	R_{705}/R_{678}	[93]
	HyperOCR	$(1/R_{672}-1/R_{712})*R_{749}$	[88]
	Envisat MERIS	$(1/R_{660–670}-1/R_{700–730})*R_{740–760}$	[85]
	Envisat MERIS	$(1/R_{660–670}-1/R_{703.75–713.75})*R_{750–757.5}$	[83]
	Envisat MERIS	$(1/R_{665}-1/R_{708})*R_{753}$	[82,323]
	Envisat MERIS	R_{708}/R_{665}	[82,323]
	Envisat MERIS	R_{672}/R_{704}	[324]
	Envisat MERIS	R_{708}/R_{664}	[118]
	Envisat MERIS	$(1/R_{660}-1/R_{692})*R_{740}$	[86]
	Envisat MERIS	$(1/R_{622}-1/R_{693})*(1/R_{740}-1/R_{705})$	[86]
	Envisat MERIS	B9 (703.75-713.75 nm)/B7 (660-670 nm)	[325]
	Envisat MERIS	R_{709}/R_{665}	[326]
	Envisat MERIS	(B9 (703.75-713.75 nm)-B7 (660-670 nm))*(B9 (703.75-713.75 nm)+B7 (660-670 nm))	[72]
	Terra MODIS	$R_{743–753}/R_{662–672}$	[83,85]
	Terra MODIS	R_{665}/R_{748}	[324]
	Terra MODIS	R_{700}/R_{670}	[104]
	PROBA-CHRIS	R_{706}/R_{672}	[327]
	Sentinel-2 MSI	R_{705}/R_{665}	[92]
	Sentinel-3 OLCI	$(1/R_{665}–1/R_{705}) \times R_{752}$	[67]

		Sentinel-3 OLCI	R_{665}/R_{709}	[92]
Ratio between green and blue		EO-1 Hyperion	R_{490}/R_{550}	[80]
		EO-1 Hyperion	R_{467}/R_{559}	[91]
		Landsat-5 TM	B2 (520-600 nm)/ B1 (450-520 nm)	[100]
		Envisat MERIS	(B5 (555-565 nm)-B2 (437.5-447.5 nm))*(B5 (555-565 nm)+B2 (437.5-447.5 nm))	[72]
		WorldView-2	B1 (400-450 nm)/B3 (510-580 nm)	[42]
Ratio between blue and red		Landsat-7 ETM+	B1 (450-515 nm)/B3 (630-690 nm)	[121,328]
		Landsat-8 OLI	$(R_{630-680}-R_{433-453})/(R_{630-680}+R_{433-453})$	[329]
Single band	Blue	Landsat-5 TM	B1 (450-520 nm)	[330]
		MIVIS	R_{440}	[81]
		Terra MODIS	B8 (405-420 nm)	[95]
	Red	PROBA-CHRIS	$R_{650-690}$	[331]
	Green	Daedalus ATM	B3 (520-600 nm)	[332]
		Landsat-5 TM	B2 (520-600 nm)	[333]
		Terra MODIS	B11 (526-536 nm)	[95]
		Terra MODIS	B4 (545-565 nm)	[95]
	NIR	Terra MODIS	B2 (840-876 nm)	[95]
Multiple bands		PROBA-CHRIS	B8 (581.345-596.935 nm), B9 (613.7-627.1 nm), B10 (641.27-656.25 nm), B11 (661.44-672.12 nm), B12 (672.15-683.21 nm)	[334]
		Ikonos OSA	B1 (450–530 nm), B2 (520–610 nm), B3 (640–720 nm), B4 (770–880 nm)	[123]
		Landsat-5 TM	B1 (450-520 nm), B2 (520-600 nm), B3 (630-690 nm), B5 (1550-1750 nm), B6 (10400-12500 nm)	[112]
		Landsat-5 TM	B1 (450-520 nm), B2 (520-600 nm)	[97]
		Landsat-5 TM	B1 (450-520 nm), B3 (630-690 nm)	[74,101,138]
		Landsat-5 TM	B1 (450-520 nm), B2 (520-600 nm), B3 (630-690 nm)	[90,138]
		Landsat-5 TM	B1 (450-520 nm), B3 (630-690 nm), B4 (760-900 nm)	[138]
		Landsat-5 TM	B1 (450-520 nm), B2 (520-600 nm), B3 (630-690 nm), B4 (760-900 nm)	[97]
		Landsat-5 TM	B1 (450-520 nm), B2 (520-600 nm), B3 (630-690 nm), B4 (760-900 nm), B5 (1550-1750 nm), B7 (2080-2350 nm)	[96]
		Landsat-8 OLI	B5 (850-880 nm), B6 (1570-1650 nm), B7 (2110-2290 nm)	[103]
		Landsat-8 OLI	B1 (433–453 nm), B2 (450-515 nm), B3 (525-600 nm), B4 (630-680 nm)	[87]
		Envisat MERIS	B7 (664 nm), B8 (680.5 nm), B9 (708 nm)	[53]
		Terra MODIS	B1 (645 nm), B2 (859 nm), B3 (469 nm), B4 (555 nm)	[60]

	Terra MODIS	B1 (620-670 nm), B4 (545-565 nm)	[95]
	PlanetScope	B2 (465-515 nm), B4 (547-583 nm), B6 (650-680 nm), B8 (845-885 nm)	[103]
	Sentinel-2 MSI	B4 (649.6-679.6 nm), B5 (697.1-711.1 nm), B6 (733.5-747.5 nm), B11 (1568.7-1658.7 nm), B12 (2115.4-2289.4)	[103]
	Sentinel-3 OLCI	B1 (392.5-407.5 nm), B4 (485-495 nm), B6 (555-565 nm), B8 (660-670 nm), B9 (670-677.5 nm)	[94]

Table A2. Sensor data for various waterbodies including waterbody type, country, study area, mean depth, study duration, method for retrieval of chl-a based on satellite imagery, range of measured chl-a values (minimum and maximum), and a correlation coefficient (R^2) between satellite imagery and chl-a in situ *values.*

Sensor	Waterbody type	Waterbody	Country	Study area [km^2]	Surface area category	Mean depth [m]	Mean depth category	Study Duration	Method	Chl-a min [µg/L]	Chl-a max [µg/L]	R^2	Reference
Landsat-5 TM	Lakes	Küçükçekmece Lake	Turkey	15.22	large	~10	shallow	1 month	multiple regression	0.62	3.99	0.513	[96]
Landsat-5 TM	Reservoirs	Beaver Reservoir	Arkansas, USA	103	very large	18	deep	9 months in 4 years (throughout)	ANN	1.4	10	0.53	[97]
EO Hyperion-1	Lakes	Garda Lake	Italy	368	very large	133	deep	1 month	analytical	0.5	12	0.59	[80]
Terra MODIS	Lakes	Chaohu Lake	China	780	very large	2.5	very shallow	4 months	NN	5.2	33.9	0.632	[95]
Landsat-7 ETM+	Estuary	Pensacola Bay	Florida, USA	373	very large	6	shallow	1 month	regression	1.14	23.23	0.67	[328]
Landsat-5 TM	Lakes	Reelfoot Lake	Tennessee, USA	296.4	very large	1.5	very shallow	1 month	regression	66	188.59	0.705	[102]
EO Hyperion-1	Lakes	Atitlán Lake	Guatemala	132	very large	188	deep	3 months	semi-empirical	1.01	10.91	0.7054	[91]
MIVIS	Lakes	Trasimeno Lake	Italy	124	very large	4.5	shallow	1 month	analytical	0.75	4.3	0.71	[81]

Landsat-5 TM	Lakes	Piccolo Lake	Italy	0.14	small	18	deep	1 month	multiple regression	1.11	4.57	0.72	[98]
Landsat-5 TM	Lakes	Grande Lake	Italy	0.41	small	9	shallow	1 month	multiple regression	4.63	11.35	0.72	[98]
Envisat MERIS	Lakes	Taihu Lake	China	2338	very large	1.9	very shallow	5 months in 2005 for calibration and 1 month in 2007	semi-analytical	1	89	0.8	[86]
PROBA-CHRIS	Reservoirs	Rosarito	Spain	14.75	large	5.8	shallow	5 months	regression	0	100	0.8	[327]
Landsat-5 TM	Lakes	Arreo Lake	Spain	0.07	small	5.3	shallow	6 years (throughout)	-	0.4	20	0.82	[100]
Sentinel-3 OLCI	Lakes	Balaton Lake	Hungary	596	very large	3.5	shallow	6 months	ML, NN	2	55	0.83	[94]
Landsat-5 TM	Reservoirs	Bull Shoals Reservoir	Arkansas, USA	~400	very large	20	deep	4 months in 2 years (July, December, February, and July)	regression	1	7	0.84	[99]
Envisat MERIS	Lakes	Balaton Lake	Hungary	596	very large	3.5	shallow	5 years (throughout)	NN	0.016	120	0.87	[53]
Envisat MERIS	Estuary	Tampa Bay	Florida, USA	~1000	very large	4	shallow	9 sessions in 13 years (throughout)	non-linear regression	2	80	0.88	[326]
CASI HyMap	Lakes	Wumm Lake	Germany	1.2	medium	max 36 m	deep	4 months in 3 years (May-September)	semi-empirical	1	3	0.89	[93]
CASI HyMap	Lakes	Bramin Lake	Germany	0.75	small	max 3 m	very shallow	4 months in 3 years (May-September)	semi-empirical	50	100	0.89	[93]

Envisat MERIS	Lakes	Zeekoevlei Lake	South Africa	2.58	medium	1.9	very shallow	1 month	empirical	61	247.4	0.964	[118]
Landsat-5 TM	Lakes	Chagan Lake	China	0.37	small	1.5	very shallow	1 month	empirical, NN	5	30	0.98	[90]
Ikonos OSA	Estuary	Golden Horn	Turkey	28	large	max 35 m	deep	1 month	multiple regression	2.32	53.77	0.992	[123]
Landsat-5 TM	Lakes	Iseo Lake	Italy	61	large	124	deep	1 month	empirical	5.5	7.7	0.999	[101]
CASI-2 AISA	Lakes	Loch Leven & Esthwaite Water	UK	1-13.3	small-large	3.9-6.4	shallow	2 months	empirical, semi-analytical	3.85	56.7	0.863	[63]
Sentinel-2 MSI Sentinel-3 OLCI	Lakes	4 lakes	Latvia, Estonia	40-270	large-very large	1.6 - 7	very shallow-shallow	8 months	semi-empirical	6.3	120	0.84	[92]
Sentinel-3 OLCI	Lakes Reservoirs River	9 waterbodies	USA, Australia, China	2250	very large	2	very shallow	6 years (throughout)	ML	2.8	285.5	0.91	[67]
PROBA-CHRIS	Lakes Reservoirs	10 Mazurian lakes	Poland	0.05-11	small-large	1-14	very shallow-shallow	1 month	empirical	0	55	0.89	[122]
AISA	Lakes	11 lakes	Finland	1-111	small-very large	2-85	very shallow-deep	3 years	regression	0	100	0.937	[124]
AISA	Lakes	11 lakes	Finland	1-111	small-very large	2-85	very shallow-deep	4 months in 3 years (May, August)	empirical	1	100	0.91	[64]
Sentinel-2 MSI	Lakes	9 small and 2 large lakes	Estonia	1-47800	medium-very large	2.2-11.9	very shallow-shallow	3 sessions in 1 month	semi-empirical	3.6	72.9	0.83	[75]
Sentinel-2 MSI	Reservoirs	13 reservoirs	Oklahoma, USA	4-188	medium-very large	4-20	shallow-deep	3 years	empirical	0.6	540	0.85	[103]

Terra MODIS	Lakes	15 lakes	Minnesota, USA	6-410 ha	small-medium	2-9	very shallow-shallow	1 month	nonlinear regression	1.8	397	0.99	[104]
Landsat-7 ETM+	Lakes	12 Rotorua lakes and Lake Taupo	New Zealand	0.3-80.6	small-large	7-60	shallow-deep	2 months	empirical	6	136	0.91	[121]

Table A3. Selected remotely measurements of turbidity using various sensors and spectral bands, band combinations, and band equations (R in band combinations represents the reflectance at a certain wavelength).

Band Combination		Sensor	Band/Equation	Reference
Ratio between green and red		Landsat-5 TM	B3 (630-690 nm)/B2 (520-600 nm)	[102]
Ratio between NIR and red		AISA	R_{850}/R_{550}	[335]
Single band	NIR	AISA	R_{714}	[124]
		AISA	$R_{705-714}$	[64]
		Landsat-7 ETM+	B4 (770-900 nm)	[107]
		PROBA-CHRIS	B31(706-712 nm)	[110]
	Red	HICO	R_{646}	[322]
		Landsat-5 TM	B3 (630-690 nm)	[330]
		Landsat-5 TM	B3 (630-690 nm)	[110]
		Landsat-7 ETM+	B3 (630-690 nm)	[330]
		Landsat-7 ETM+	B3 (630-690 nm)	[110]
Multiple bands		Terra ASTER	B1 (520-600 nm), B2 (630-690 nm), B3 (780-860 nm)	[106]
		Terra ASTER	B1 (520-600 nm), B2 (630-690 nm), B3 (780-860 nm)	[106]
		Landsat-5 TM	B2 (520-600 nm), B3 (630-690 nm), B6 (10400-12500 nm), B7 (2080-2350 nm)	[112]
		Landsat-5 TM	B1 (450-520 nm), B3 (630-690 nm)	[138]
		Landsat-5 TM	B1 (450-520 nm), B3 (630-690 nm), B4 (760-900 nm)	[138]
		Landsat-5 TM	B2 (520-600 nm), B3 (630-690 nm)	[138]
		Landsat-5 TM	B1 (450-520 nm), B3 (630-690 nm), B4 (760-900 nm)	[90]
		Landsat-5 TM	B1 (450-520 nm), B2 (520-600 nm), B3 (630-690 nm), B4 (760-900 nm), B5 (1550-1750 nm), B7 (2080-2350 nm)	[96]
		Landsat-8 OLI	B4 (630-670 nm), B5 (850-880 nm)	[109,111]
		Landsat-8 OLI	B2 (450-510 nm), B4 (630-670 nm)	[336]

	Landsat-8 OLI	B3 (525-600 nm), B4 (630-680 nm), B5 (850-880 nm), B7 (2110-2290 nm)	[103]
	PlanetScope	B4 (547-583 nm), B6 (650-680 nm), B8 (845-885 nm)	[103]
	Sentinel-2 MSI	B2 (460.2-525.2 nm), B4 (649.6-679.6 nm), B8 (780.3-885.3 nm), B12 (2115.4-2289.4)	[103]
	Sentinel-2 MSI	B3 (542.3-577.3 nm), B4 (649.6-679.6 nm), B5 (697.1-711.1 nm), B12 (2115.4-2289.4)	[108]

Table A4. Sensor data for various waterbodies including waterbody type, country, study area, mean depth, study duration, method for retrieval of turbidity based on satellite imagery, range of measured turbidity values (minimum and maximum), and a correlation coefficient (R^2) between satellite imagery and turbidity in situ *values.*

Sensor	Waterbody type	Waterbody	Country	Study area [km^2]	Surface area category	Mean depth [m]	Mean depth category	Study Duration	Method	Turb. min [NTU]	Turb. max [NTU]	R^2	Reference
Landsat-5 TM	Lakes	Reelfoot Lake	Tennessee, USA	296	very large	1.5	very shallow	1 month	regression	4.1	20	0.537	[102]
Landsat-8 OLI	Reservoirs	El Guájaro Reservoir	Columbia	116	very large	5	shallow	1 month	empirical	13.5	117	0.6419	[111]
Landsat-5 TM	Lakes	Küçükçekmece Lake	Turkey	15	large	~10	shallow	1 month	multiple regression	2.9	33.5	0.822	[96]
Landsat-5 TM Landsat-7 ETM+	Reservoirs	Asprokremmos Reservoir	Cyprus	2590	very large	~50	deep	6 months (April-October 2010)	regression	7.94	26.3	0.85	[110]
PROBA-CHRIS	Reservoirs	Asprokremmos Reservoir	Cyprus	2590	very large	~50	deep	6 months (April-October 2010)	regression	7.94	26.3	0.9	[110]
Landsat-5 TM	Reservoirs	Guanting Reservoir	China	253	very large	7.1	shallow	2 times in 1 month	empirical	2.133	142	0.937	[112]

Landsat-5 TM	Lakes	Chagan Lake	China	0.4	small	1.5	very shallow	1 month	empirical, NN	5	180	0.98	[90]
Terra ASTER	Lakes	Qaroun Lake	Egypt	200	very large	8	shallow	2 months	empirical	0	85	0.998	[106]
PlanetScope	Reservoirs	13 reservoirs	Oklahoma, USA	4-188	medium-very large	4-20 m	shallow-deep	3 years	empirical	0	966	0.79	[103]
Landsat-7 ETM+	Lakes	34 shallow lakes in the Waikato region	New Zealand	0.05 - 34	small-large	max 1.8 - 8.7 m	very shallow-shallow	6 sessions during summer in 10 years	empirical	75	275	0.924	[107]

Table A5. Selected remotely measurements of SDD using various sensors and spectral bands, band combinations, and band equations (R in band combinations represents the reflectance at a certain wavelength).

Band Combination		Sensor	Band/Equation	Reference
Ratio between red and green		Landsat-5 TM	B3 (630-690 nm)/B2 (520-600 nm)	[98,102]
Ratio between NIR and red		AISA	$(R_{670-677}-R_{747-755})/(R_{699-705}-R_{747-755})$	[64]
		Envisat MERIS	R_{708}/R_{664}	[118]
Ratio between NIR and green		AISA	$(R_{521}-R_{781})/(R_{700}-R_{781})$	[124]
Ratio between blue and red		Landsat-7 ETM+	B1 (450-515 nm)/B3 (630-690 nm)	[121]
		PROBA-CHRIS	$(R_{410}+R_{651})/R_{680}$	[122]
Ratio between blue and green		Landsat-5 TM	B1 (450-520 nm)/B2 (520-600 nm)	[101]
		PlanetScope	B2 (465-515 nm)/B3 (513-549 nm)	[115]
Single band	Red	Landsat-5 TM	B3 (630-690 nm)	[99,333]
		Terra MODIS	B1 (620-670 nm)	[95]
	NIR	Terra MODIS	R_{710}	[104]
Multiple bands		Ikonos OSA	B1 (450–530 nm), B2 (520–610 nm), B3 (640–720 nm)	[123]
		Ikonos OSA	B1 (445-516 nm), B3 (632-698 nm)	[337]
		Landsat-5 MSS	B1 (500-600 nm), B2 (600-700 nm)	[338]
		Landsat-5 TM	B1 (450-520 nm), B2 (520-600 nm), B3 (630-690 nm)	[98,339]
		Landsat-5 TM	B1 (450-520 nm), B2 (520-600 nm)	[100]

	Landsat-5 TM	B1 (450-520 nm), B3 (630-690 nm)	[74,117,120,138,337,338,340]
	Landsat-5 TM	B1 (450-520 nm), B4 (760-900 nm)	[138]
	Landsat-5 TM	B1 (450-520 nm), B2 (520-600 nm), B4 (760-900 nm)	[138]
	Landsat-7 ETM+	B1 (450-515 nm), B3 (630-690 nm)	[107,341]
	Landsat-7 ETM+	B3 (630-690 nm), B7 (2090-2350 nm)	[119]
	Landsat-8 OLI	B1 (433-453 nm), B2 (450-515 nm), B4 (630-680 nm)	[341]
	Landsat-8 OLI	B2 (450-515 nm), B4 (630-680 nm)	[341]
	Landsat-8 OLI	B3 (525-600 nm), B4 (630-680 nm), B5 (845-885 nm)	[103]
	PlanetScope	B2 (465-515 nm), B6 (650-680 nm), B8 (845-885 nm)	[103]
	Sentinel-2 MSI	B3 (542.3-577.3 nm), B4 (649.6-679.6 nm), B7 (773.3-792.3 nm), B12 (2115.4-2289.4)	[103]

Table A6. Sensor data for various waterbodies including waterbody type, country, study area, mean depth, study duration, method for retrieval of SDD based on satellite imagery, range of measured SDD values (minimum and maximum), and a correlation coefficient (R^2) between satellite imagery and SDD in situ *values.*

Sensor	Waterbody type	Waterbody	Country	Study area [km^2]	Surface area category	Mean depth [m]	Mean depth category	Study Duration	Method	SDD min [m]	SDD max [m]	R^2	Reference
Landsat-5 TM	Lakes	Reelfoot Lake	Tennessee, USA	296.40	very large	1.5	very shallow	1 month	regression	0.16	0.33	0.588	[102]
Terra MODIS	Lakes	Chaohu Lake	China	780	very large	2.5	very shallow	4 months	NN	0.25	1.2	0.628	[95]
Landsat-5 TM	Lakes	Arreo Lake	Spain	0.06	small	5.3	shallow	6 years	-	1.33	7.53	0.63	[100]
Landsat-7 ETM+	Lakes	Champlain Lake	Canada-USA	1269	very large	19.5	deep	3 months in summer	empirical	0	3	0.8	[119]
Envisat MERIS	Lakes	Zeekoevlei Lake	South Africa	2.58	medium	1.9	very shallow	1 month	empirical	0.23	0.39	0.801	[118]

Landsat-5 TM	Lakes	Grande Lake	Italy	0.4	small	9	shallow	1 month	multiple regression	0.25	1	0.82	[98]
Landsat-5 TM	Lakes	Piccolo Lake	Italy	0.14	small	18	deep	1 month	multiple regression	3	3.75	0.82	[98]
Landsat-5 TM	Lakes	Iseo Lake	Italy	61	large	124	deep	1 month	empirical	4.6	6.8	0.852	[101]
Landsat-5 TM	Lakes	Bung Boraphet Lake	Thailand	148	very large	1.2	very shallow	3 sessions in spring in 2 months	linear regression	0.2	2.5	0.929	[120]
Landsat-5 TM	Reservoirs	Bull Shoals Reservoir	Arkansas, USA	~400	very large	20	deep	4 months in 2 years	regression	1.2	5	0.96	[99]
Ikonos OSA	Estuary	Golden Horn	Turkey	28	large	max 35 m	deep	1 month	multiple regression	0.8	6.5	0.989	[123]
PlanetScope	Lakes	2 lakes in Lower Amazon Floodplain	Brazil	984-1600	very large	1.6-4	very shallow-shallow	1 month	empirical	0.6	1.94	0.816	[115]
PROBA-CHRIS	Lakes Reservoirs	10 Masurian lakes	Poland	5-1100 ha	small-large	1-14	very shallow-shallow	1 month	empirical	0	6	0.95	[122]
AISA	Lakes	11 lakes	Finland	1-111	small-very large	max 2-85 m	very shallow-deep	3 years	regression	0.3	7	0.926	[124]
AISA	Lakes	11 lakes	Finland	1-111	small-very large	max 2-85 m	very shallow-deep	4 months in 3 years	empirical	0.4	7	0.86	[64]
Landsat-7 ETM+	Lakes	12 Rotorua lakes and Lake Taupo	New Zealand	0.3-80.6	small-large	7-60	shallow-deep	2 months	empirical	0.78	4.23	0.82	[121]
Sentinel-2 MSI	Reservoirs	13 reservoirs	Oklahoma, USA	4-188 km^2	medium-very large	4-20	shallow-deep	3 years	empirical	0.08	4	0.8	[103]

Terra MODIS	Lakes	15 lakes	Minnesota, USA	6-410 ha	small-medium	2-9	very shallow-shallow	1 month	nonlinear regression	0.2	6.1	0.52	[104]
Landsat-7 ETM+	Lakes	34 lakes in the Waikato region	New Zealand	0.05 – 34.4	small-large	max 1.8 - 8.7 m	very shallow-shallow	6 sessions during summer in 10 years	empirical	0.05	3.04	0.67	[107]

Table A7. Selected remotely measurements of WT using various sensors and spectral bands, band combinations, and band equations.

Band Combination		Sensor	Band/Equation	Reference
Single band	TIR	Landsat-5 TM	B6 (10400-12500 nm)	[100,101,342–344]
		Landsat-7 ETM+	B6 (10400-12500 nm)	[128,345]
		Landsat-8 TIRS	B10 (10600-11190 nm)	[346]
Multiple bands		Terra ASTER	B8 (2295-2365 nm), B10 (8125-8475 nm), B11 (8475-8825 nm), B13 (10250-10950 nm)	[106]
		Landsat-8 TIRS	B10 (10600-11190 nm), B11 (11500-12510 nm)	[347]
		Terra MODIS	B31 (10780-11280 nm), B32 (11770-12270 nm)	[127,348]
		Terra MODIS	B31 (10780-11280 nm), B32 (11770-12270 nm)	[130]
		NOAA-9, -11, -12, -14, -16, -17, -19 AVHRR	B4 (1030-1130 nm), B5 (1150–1250 nm)	[129]

Table A8. Sensor data for various waterbodies including waterbody type, country, study area, mean depth, study duration, method for retrieval of WT based on satellite imagery, range of measured WT values (minimum and maximum), and a correlation coefficient (R^2) between satellite imagery and WT in situ *values.*

Sensor	Waterbody type	Waterbody	Country	Study area [km^2]	Surface area category	Mean depth [m]	Mean depth category	Study Duration	Method	WT min [°C]	WT max [°C]	R^2	Reference
Terra ASTER	Lakes	Qaroun Lake	Egypt	200	very large	8	shallow	2 months	empirical	29.7	31.2	0.535	[106]

Terra MODIS	Lakes	Urmia Lake	Iran	2366	very large	7	shallow	46 sessions in 4 years	empirical	3.5	32	0.92	[127]
Landsat-7 ETM+ Landsat-5 TM	Lakes	Stechlin Lake	Germany	4.52	medium	max 70	deep	9 sessions in 10 months (February-November 2000)	empirical	2.5	21.5	0.921	[128]
Terra MODIS	Lakes	2 lakes	Sweden	5650 - 1912	very large	28 - 41	deep	23 sessions in 2 years between April and October (2002-2003)	empirical	1	22	0.9928	[130]
NOAA AVHRR	Lakes	4 lakes	Switzerland-France, Hungary, Sweden & Finland	580 - 1900	very large	3 - 153	shallow-deep	120 sessions in 6 years for 4 lakes (2 x 3 years)	linear regression	1	29	0.792	[129]

Table A9. Selected remotely measurements of salinity using various sensors and spectral bands, band combinations, and band equations.

Band Combination	Sensor	Band/Equation	Reference
Ratio between SWIR 2 and SWIR 1	Landsat-5 TM	B7 (2080-2350 nm)/B5 (1550-1750 nm)	[349]
Multiple bands	Terra ASTER	B3 (780-860 nm), B5 (2145-2185 nm), B7 (2235-2285 nm)	[106]
	Landsat-5 TM	B1 (450-520 nm), B4 (*760-900 nm*), B6 (10400-12500 nm)	[350]
	Landsat-8 OLI	B2 (450-515 nm), B3 (525-600 nm), B4 (630-680 nm)	[132]
	Landsat-8 OLI	B2 (450-515 nm), B5 (850-880 nm), B10 (10600-11190 nm), B11 (11500-12510 nm)	[350]
	Sentinel-2 MSI	B2 (460.2-525.2 nm), B3 (542.3-577.3 nm), B4 (649.6-679.6 nm), B6 (733.5-747.5 nm), B7 (773.3-792.3 nm), B8 (780.3-885.3 nm)	[131]
	Sentinel-2 MSI	B2 (460.2-525.2 nm), B3 (542.3-577.3 nm), B4 (649.6-679.6 nm)	[132]

Table A10. Sensor data for various waterbodies including waterbody type, country, study area, mean depth, study duration, method for retrieval of salinity based on satellite imagery, range of measured salinity values (minimum and maximum), and a correlation coefficient (R^2) between satellite imagery and salinity in situ *values.*

Sensor	Waterbody type	Waterbody	Country	Study area [km^2]	Surface area category	Mean depth [m]	Mean depth category	Study Duration	Method	SS min	SS max	R^2	Reference
Sentinel-2 MSI	Lakes	Urmia Lake	Iran	2917	very large	7	shallow	4 sessions in 3 months (2xApril, June and July 2021)	ML	30.7	36.1	0.657	[131]
Sentinel-2 MSI	Lakes	Urmia Lake	Iran	2917	very large	7	shallow	2 months (April and June 2019)	ANN	6.5	32	0.94	[132]

Table A11. Selected remotely measurements of EC using various sensors and spectral bands, band combinations, and band equations.

Band Combination		Sensor	Band/Equation	Reference
Ratio between green and red		Landsat-8 OLI	B3 (525-600 nm)/B4 (630-680 nm)	[137]
Single band	Red	Landsat-8 OLI	B4 (630-680 nm)	[109]
	Blue	WorldView-2	B2 (450-510 nm)	[351]
Multiple bands		Terra ASTER	B3 (780-860 nm), B4 (1600-1700 nm), B8 (2295-2365 nm)	[106]
		Landsat-5 TM	B1 (450-520 nm), B2 (520-600 nm), B3 (630-690 nm)	[352]
		Landsat-8 OLI	B2 (450-510 nm), B3 (525-600 nm), B4 (630-680 nm)	[352]
		Landsat-8 OLI	B2 (450-510 nm), B3 (525-600 nm), B4 (630-680 nm), B6 (1570-1650 nm)	[111]
		Landsat-8 OLI	B1 (430-450 nm), B2 (450-510 nm), B3 (525-600 nm), B5 (850-880 nm), B6 (1570-1650 nm)	[336]

Table A12. Sensor data for various waterbodies including waterbody type, country, study area, mean depth, study duration, method for retrieval of EC based on satellite imagery, range of measured EC values (minimum and maximum), and a correlation coefficient (R^2) between satellite imagery and EC in situ *values.*

Sensor	Waterbody type	Waterbody	Country	Study area [km^2]	Surface area category	Mean depth [m]	Mean depth category	Study Duration	Method	EC min [mS/cm]	EC max [mS/cm]	R^2	Reference
Landsat-8 OLI	Lakes	Wular Lake, Kashmir	India	189	very large	5.8	shallow	1 month	empirical	0.014	0.3	0.615	[109]
Landsat-8 OLI	Reservoirs	El Guájaro Reservoir	Columbia	116	very large	5	shallow	1 month	empirical	0.54	1.82	0.6994	[111]
Landsat-8 OLI	Lakes	Qaroun Lake	Egypt	200	very large	8	shallow	1 month	stepwise regression	42.86	52.55	0.87	[137]

Appendix 2

Spatiotemporal Water Quality Analysis of Vrana Lake, Croatia
Supplementary information.
Table A13. Historical meteorological and water level data for Vrana Lake from 1990 to 2023.

Type	Year	AT [°C]	PP [mm]	WL [m]
Historical data	1990	15.27	635	0.28
	1991	14.30	779	0.65
	1992	15.30	890	0.74
	1993	14.90	948	0.90
	1994	15.90	725	1.06
	1995	14.70	965	0.69
	1996	14.70	1024	0.96
	1997	14.90	524	0.81
	1998	15.28	753	0.91
	1999	15.10	846	1.07
	2000	15.60	834	1.06
	2001	15.10	710	1.32
	2002	15.40	840	0.59
	2003	15.70	612	0.91
	2004	14.90	1021	1.09
	2005	14.30	1123	1.09
	2006	14.90	664	1.21
	2007	15.70	516	0.49
	2008	15.70	634	0.32
	2009	15.50	1083	1.08
	2010	14.90	1036	1.09
	2011	15.90	436	0.56
	2012	15.73	700	0.31
	2013	15.63	1076	1.17
	2014	16.18	1269	1.39
	2015	15.99	849	1.13
	2016	15.87	791	0.94
	2017	15.70	829	0.63
	2018	16.39	1011	1.21
	2019	16.28	882	0.66
	2020	16.16	703	0.76
	2021	15.91	850	0.86
	2022	16.65	646	0.64
	2023	16.80	1007	1.12
Trends	**Annually**	+0.05°C/a	+ 2.28 mm/a	+3.12 mm/a
	Total	+1.54°C	77.50 mm	+106.20 mm

Table A14. Meteorological and water level data for Vrana Lake for research period.

Representative month	**Measurement date**	**AT [°C]**	**WS [Beaufort number]**	**RH [%]**	**AP [hPa]**	**WL [m]**	**PP [mm]**	**PP [mm] – cube root transformation**	**SH [h]**
Jul-23	17.07.2023	29.4	1.7	53	1015.5	1.12	0	0	13.7
Aug-23	18.08.2023	26.5	2.0	64	1013.3	0.90	0	0	12.4
Sep-23	27.09.2023	24.4	2.3	46	1015.4	0.75	11	2.22398	10.2
Oct-23	13.10.2023	19.3	1.7	85	1020.2	0.69	0	0	8.4
Nov-23	04.12.2023	5.8	1.7	56	1019.7	0.97	9	2.06456	5.6
Dec-23	19.12.2023	9.3	1.0	87	1022.5	1.15	0	0	7.8
Jan-24	11.01.2024	3.3	1.3	69	1021.2	1.15	0	0	8.3
Feb-24	19.02.2024	11.6	1.7	66	1022.3	1.29	0	0	2.4
Mar-24	14.03.2024	11.0	1.7	77	1017.1	1.42	35	3.27418	10.6
Apr-24	29.04.2024	17.9	2.0	60	1019.4	1.19	4	1.58740	13.2
May-24	24.05.2024	20.8	2.0	64	1017.4	0.99	0	0	12.5
Jun-24	17.06.2024	23.8	1.7	62	1015.3	0.86	0	0	14.4
Test for normality	Observations	12	12	12	12	12	12	12	12
	Sample Skewness	-0.1879	-0.4154	0.4254	-0.0772	0.0077	2.7150	1.1895	-0.7619
	Sample Kurtosis	-1.2709	1.1101	-0.2546	-1.2572	-0.6469	7.8832	-0.0187	0.0946
	JB Test Statistic	0.8782	0.9613	0.3943	0.8022	0.2093	45.8148	2.8301	1.1654
	p-value	**0.64462**	**0.61837**	**0.82106**	**0.66960**	**0.90062**	*0.00000*	**0.24292**	**0.55840**

Table A15. A list of sampling stations and statistical values (mean, minimum, maximum, median, and a range of values) for measured parameters using YSI EXO2 probe.

Representative month		**Jul-23**	**Aug-23**	**Sep-23**	**Oct-23**	**Nov-23**	**Dec-23**	**Jan-24**	**Feb-24**	**Mar-24**	**Apr-24**	**May-24**	**Jun-24**	∑
Measurement date		17.07. 2023	18.08. 2023	27.09. 2023	13.10. 2023	04.12. 2023	19.12. 2023	11.01. 2024	19.02. 2024	14.03. 2024	29.04. 2024	24.05. 2024	17.06. 2024	**12**
Measured stations		3-21	2-21	2-13	2-21	2-21	2-21	2-5, 7-21	2-21	2-21	2-21	2-21	2-21	**230**
Parameter	Statistics													
Chl-a [µg/L]	Mean	0.55	0.90	1.53	1.15	1.62	0.97	1.09	0.81	1.06	0.46	0.59	0.82	0.94
	Min	0.35	0.65	1.10	0.88	1.38	0.68	0.85	0.60	0.67	0.15	0.44	0.52	0.15
	Max	0.82	1.16	1.99	1.97	2.39	1.67	1.76	1.20	1.60	0.78	0.87	1.49	2.39
	Median	0.49	0.90	1.49	1.09	1.55	0.94	1.04	0.78	1.10	0.44	0.58	0.81	0.90
	Range	0.47	0.51	0.89	1.09	1.01	0.99	0.91	0.60	0.93	0.93	0.93	0.93	2.24
	St. Dev.	0.17	0.13	0.29	0.23	0.22	0.20	0.20	0.15	0.23	0.14	0.12	0.24	0.39
	MAD	0.14	0.07	0.25	0.12	0.07	0.10	0.07	0.11	0.18	0.09	0.07	0.17	0.24
EC [dS/m]	Mean	4.53	4.58	4.59	4.60	4.64	4.35	4.15	3.69	3.39	3.08	3.10	3.09	3.96
	Min	3.59	4.21	4.51	4.41	4.12	4.18	3.71	3.33	3.00	2.67	2.70	2.66	2.66
	Max	4.68	4.73	4.64	4.65	4.80	4.52	4.25	3.81	3.51	3.22	3.18	3.16	4.80
	Median	4.50	4.65	4.60	4.61	4.72	4.34	4.19	3.76	3.45	3.12	3.15	3.14	4.19
	Range	1.09	0.52	0.13	0.24	0.68	0.34	0.54	0.48	0.51	0.51	0.51	0.51	2.14
	St. Dev.	0.25	0.14	0.03	0.05	0.19	0.11	0.12	0.14	0.14	0.14	0.13	0.12	0.65
	MAD	0.18	0.04	0.02	0.02	0.06	0.09	0.04	0.05	0.03	0.09	0.01	0.01	0.49
Turbidity [FNU]	Mean	1.71	14.43	10.59	9.51	9.63	2.11	3.13	2.63	6.06	3.25	4.00	3.71	5.76
	Min	0.73	13.47	9.43	8.89	9.18	1.47	1.78	2.09	4.47	2.90	3.56	3.11	0.73
	Max	2.75	15.93	11.55	10.15	10.27	3.07	4.93	3.02	7.83	4.10	4.43	4.56	15.93
	Median	1.47	14.55	10.74	9.51	9.63	2.03	2.98	2.62	6.16	3.20	3.95	3.76	3.85
	Range	2.02	2.46	2.12	1.26	1.09	1.60	3.15	0.93	3.36	3.36	3.36	3.36	15.20
	St. Dev.	0.53	0.66	0.59	0.39	0.31	0.35	0.76	0.25	1.14	0.30	0.25	0.36	3.96
	MAD	0.31	0.61	0.18	0.35	0.27	0.17	0.56	0.19	1.07	0.13	0.20	0.18	1.63
Salinity	Mean	2.42	2.44	2.46	2.46	2.49	2.31	2.20	1.96	1.79	1.62	1.62	1.61	2.10

	Min	1.90	2.23	2.42	2.36	2.19	2.23	1.95	1.75	1.57	1.39	1.40	1.37	1.37
	Max	2.50	2.53	2.49	2.49	2.58	2.41	2.25	2.02	1.85	1.70	1.66	1.64	2.58
	Median	2.40	2.48	2.46	2.47	2.53	2.31	2.22	2.00	1.82	1.64	1.64	1.63	2.22
	Range	0.60	0.30	0.07	0.13	0.39	0.18	0.30	0.27	0.28	0.28	0.28	0.28	1.21
	St. Dev.	0.14	0.08	0.02	0.03	0.11	0.06	0.06	0.08	0.08	0.08	0.07	0.07	0.36
	MAD	0.10	0.02	0.01	0.01	0.03	0.05	0.02	0.02	0.02	0.05	0.01	0.01	0.28
WT [ºC]	Mean	29.25	25.11	18.93	21.51	8.52	6.64	5.24	10.96	12.74	16.72	23.21	25.75	16.98
	Min	28.37	24.37	18.59	20.79	7.76	6.37	4.47	10.74	12.35	15.94	22.82	25.38	4.47
	Max	30.22	26.23	19.42	22.17	9.17	7.27	6.07	11.40	13.31	17.50	23.70	26.31	30.22
	Median	29.09	25.03	18.91	21.57	8.47	6.64	5.28	10.91	12.74	16.71	23.12	25.68	17.16
	Range	1.85	1.86	0.83	1.38	1.41	0.90	1.60	0.66	0.96	0.96	0.96	0.96	25.75
	St. Dev.	0.53	0.55	0.25	0.37	0.35	0.23	0.38	0.19	0.27	0.44	0.27	0.29	7.87
	MAD	0.45	0.39	0.13	0.23	0.26	0.19	0.16	0.12	0.19	0.32	0.20	0.18	7.33
DO [mg/L]	Mean	9.24	8.65	9.09	9.94	11.33	12.01	12.36	10.85	10.44	10.46	9.73	9.38	10.33
	Min	8.29	7.60	8.70	9.30	10.80	11.10	12.00	10.70	10.10	10.20	9.40	8.80	7.60
	Max	10.80	9.50	9.30	10.40	11.60	12.20	12.60	10.90	10.70	11.00	10.40	10.50	12.60
	Median	9.17	8.65	9.15	9.95	11.35	12.05	12.40	10.90	10.50	10.40	9.70	9.30	10.35
	Range	2.51	1.90	0.60	1.10	0.80	1.10	0.60	0.20	0.60	0.60	0.60	0.60	5.00
	St. Dev.	0.63	0.37	0.16	0.29	0.20	0.22	0.18	0.07	0.13	0.18	0.26	0.40	1.15
	MAD	0.45	0.15	0.10	0.18	0.15	0.05	0.10	0.00	0.10	0.10	0.20	0.20	0.85
SO [%]	Mean	122.34	106.20	99.47	114.26	98.29	99.56	98.85	99.54	99.67	108.67	114.86	116.21	106.70
	Min	108.75	94.75	95.04	106.61	94.09	93.46	97.07	98.04	97.30	106.30	111.28	110.46	93.46
	Max	143.28	119.55	101.12	120.87	99.46	100.48	99.79	100.51	102.73	114.99	122.63	130.73	143.28
	Median	121.08	105.68	99.94	114.28	98.78	99.94	99.14	99.55	99.72	108.23	114.09	114.73	103.64
	Range	34.53	24.80	6.08	14.26	5.37	7.02	2.72	2.47	5.43	5.43	5.43	5.43	49.82
	St. Dev.	8.11	4.62	1.59	3.41	1.13	1.48	0.74	0.58	1.21	2.02	2.98	4.70	8.85
	MAD	6.10	2.03	0.75	1.85	0.27	0.35	0.40	0.28	0.88	1.25	1.61	1.94	4.95

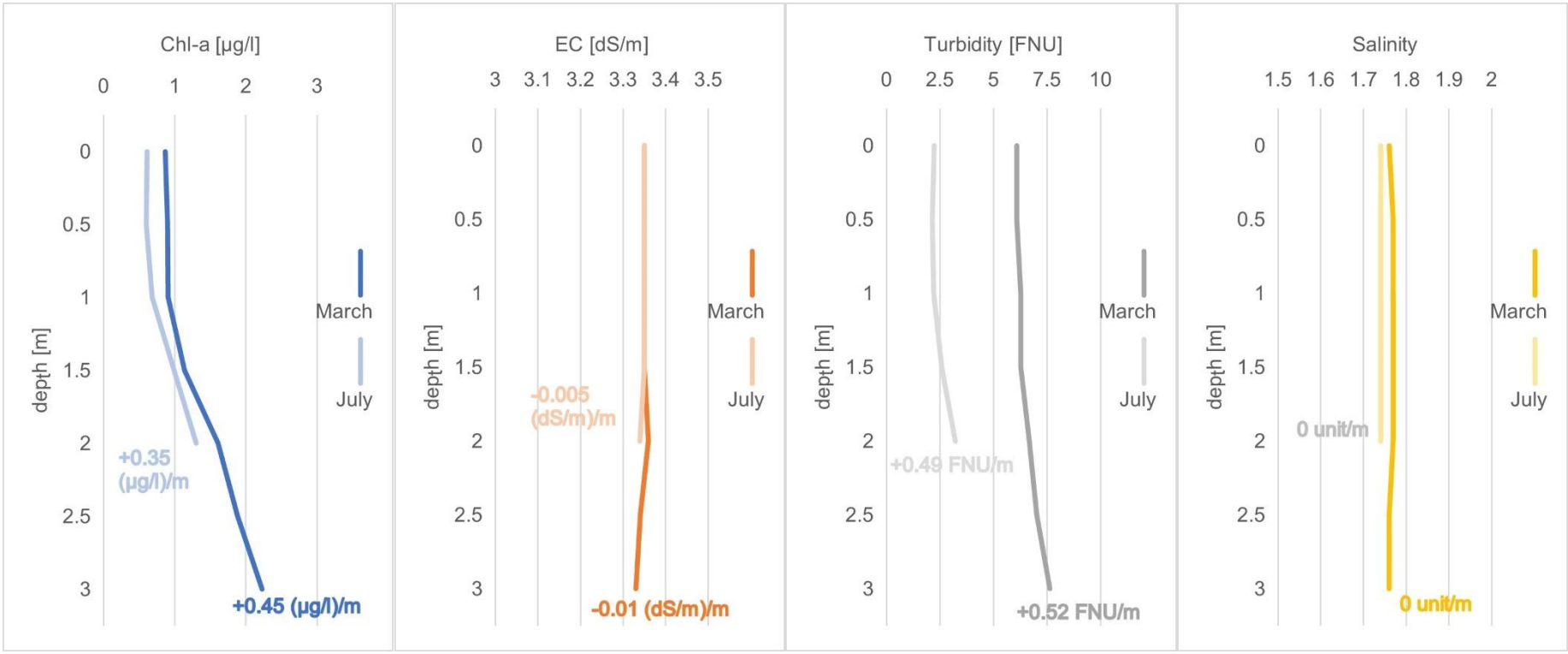
Chl-a [µg/l]
0 1 2 3
depth [m]
0 0.5 1 1.5 2 2.5 3
March
July
+0.35 (µg/l)/m
+0.45 (µg/l)/m
EC [dS/m]
3 3.1 3.2 3.3 3.4 3.5
depth [m]
0 0.5 1 1.5 2 2.5 3
March
July
-0.005 (dS/m)/m
-0.01 (dS/m)/m
Turbidity [FNU]
0 2.5 5 7.5 10
depth [m]
0 0.5 1 1.5 2 2.5 3
March
July
+0.49 FNU/m
+0.52 FNU/m
Salinity
1.5 1.6 1.7 1.8 1.9 2
depth [m]
0 0.5 1 1.5 2 2.5 3
March
July
0 unit/m
0 unit/m

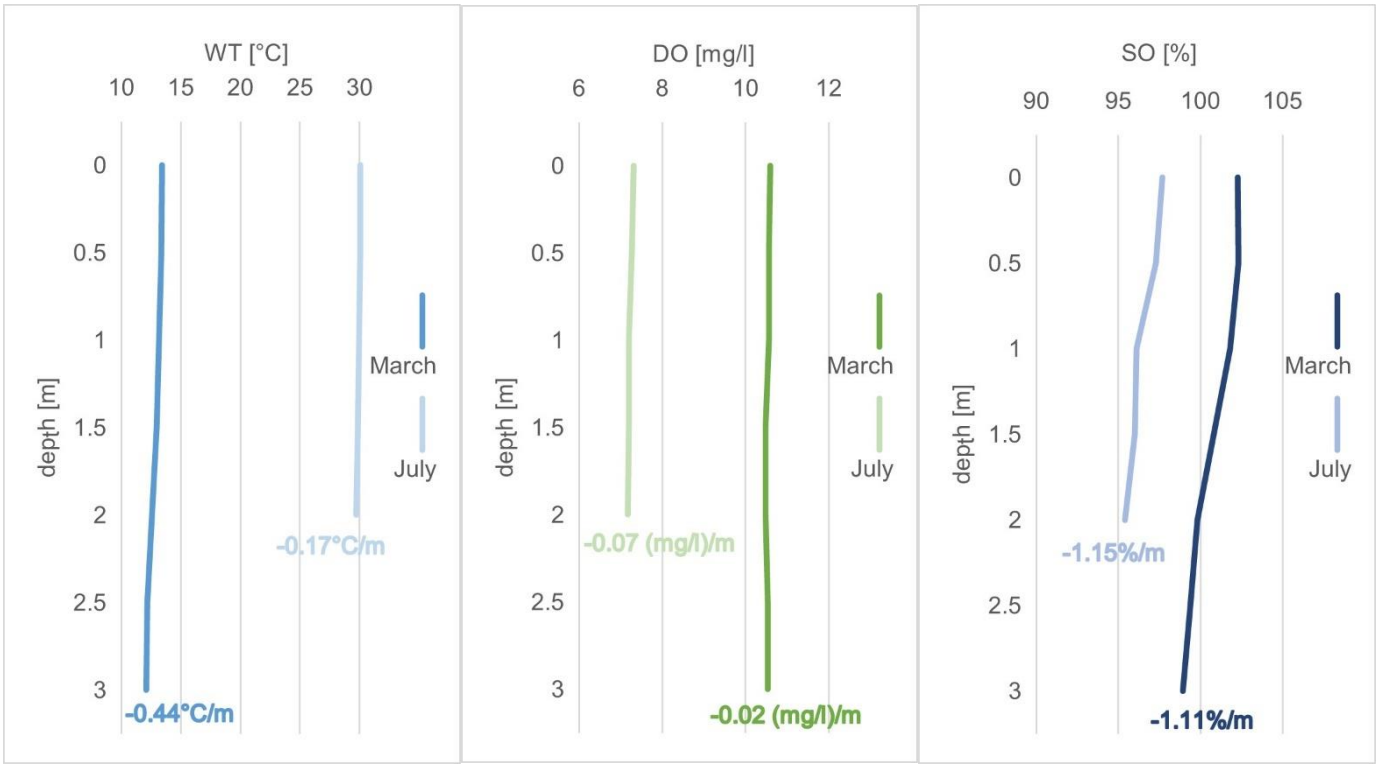

Figure A1. Vertical profiles of average parameter values measured every 30 minutes in March and July.

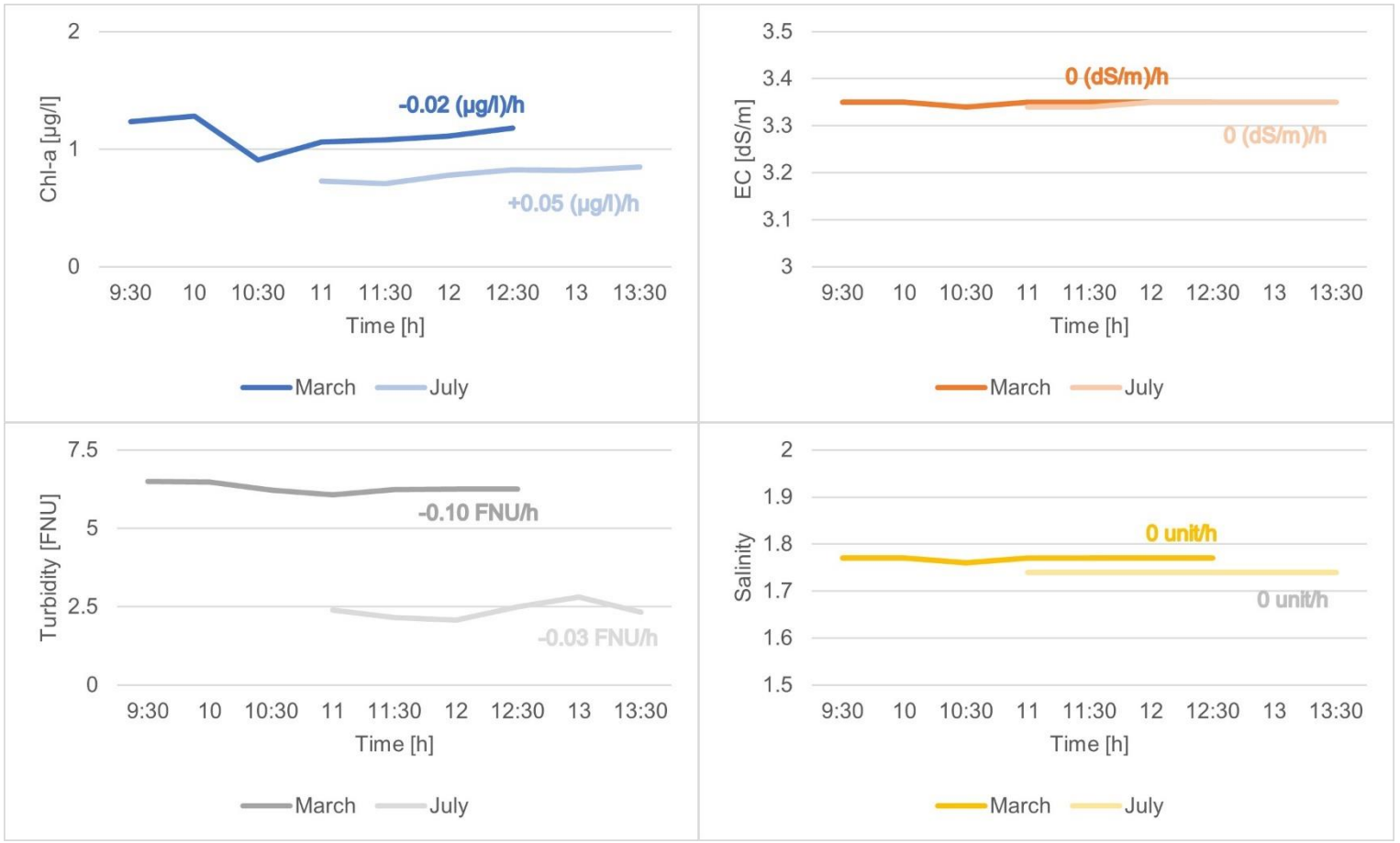
Chl-a [µg/l]
2
1
0
-0.02 (µg/l)/h
+0.05 (µg/l)/h
9:30 10 10:30 11 11:30 12 12:30 13 13:30
Time [h]
March
July
EC [dS/m]
3.5
3.4
3.3
3.2
3.1
3
0 (dS/m)/h
0 (dS/m)/h
9:30 10 10:30 11 11:30 12 12:30 13 13:30
Time [h]
March
July
Turbidity [FNU]
7.5
5
2.5
0
-0.10 FNU/h
-0.03 FNU/h
9:30 10 10:30 11 11:30 12 12:30 13 13:30
Time [h]
March
July
Salinity
2
1.9
1.8
1.7
1.6
1.5
0 unit/h
0 unit/h
9:30 10 10:30 11 11:30 12 12:30 13 13:30
Time [h]
March
July

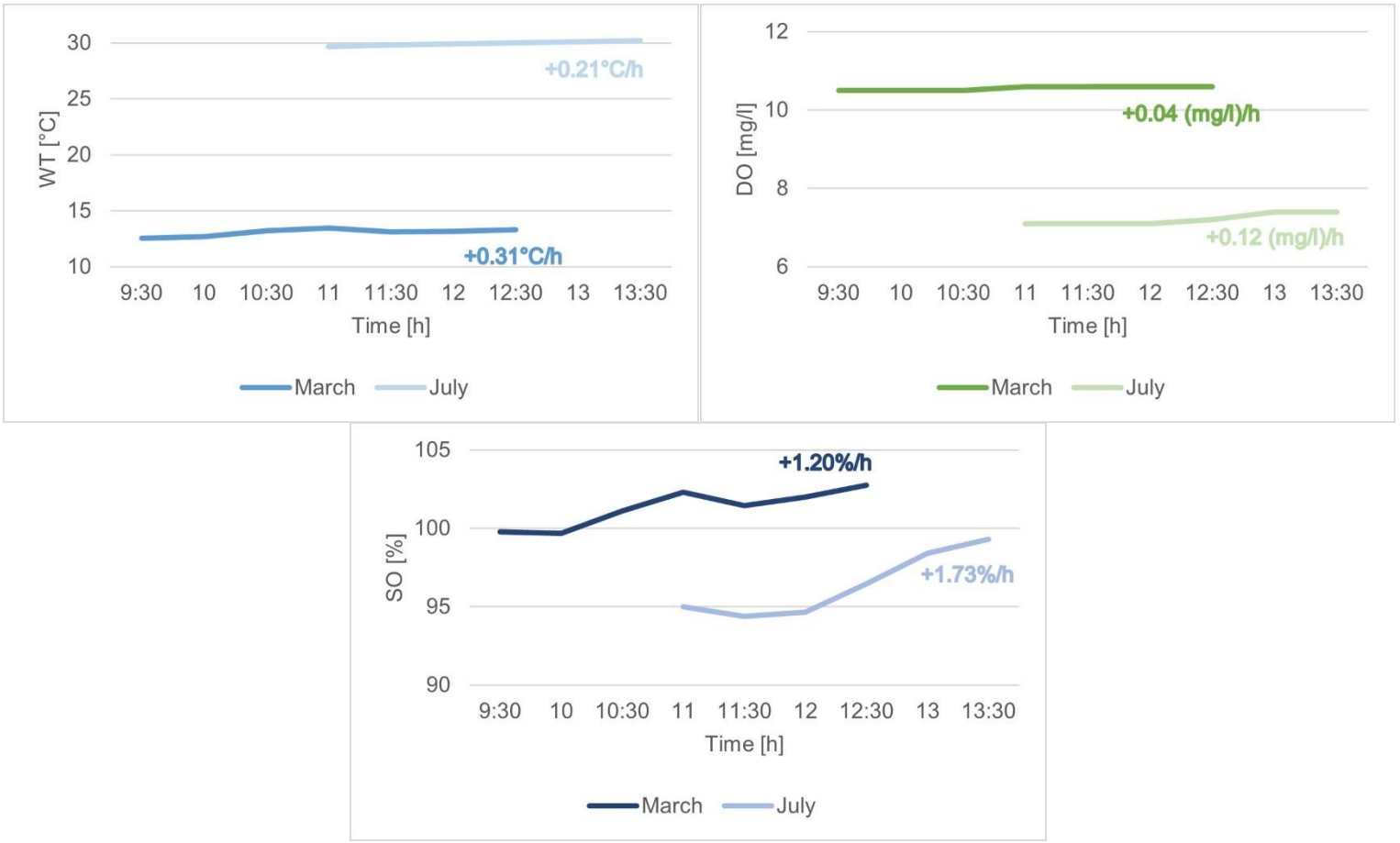

Figure A2. Temporal variation of median parameter values measured every 30 minutes in March and July.

Table A16. Comparison of interpolation methods using RMSE and ME as accuracy measures for each parameter.

	Chl-a		EC		Turbidity		Salinity		WT		DO		SO	
Interpolation Method	RMSE	ME	RMSE	ME	RMSE	ME	RMSE	ME	RMSE	ME	RMSE	ME	RMSE	ME
Simple Kriging – Trend	0.36873	0.00003	0.65718	0.00010	3.99575	0.00048	0.36696	0.00006	7.97592	-0.00008	1.16632	0.00001	8.96418	-0.00038
Global Polynomial Interpolation – Second order	**0.36807**	-0.00006	0.66400	0.00004	4.04828	-0.00009	0.37078	0.00002	8.08375	0.00069	1.18081	-0.00020	9.08129	-0.00043
Simple Kriging – Optimized	0.37460	0.00730	**0.65134**	0.00737	3.96147	-0.01939	**0.36365**	0.00596	7.87438	0.10378	**1.15401**	0.02554	**8.85096**	-0.12312
Inverse Distance Weighted – Optimized	0.38833	0.00000	0.70634	0.00000	4.31279	0.00000	0.39443	0.00000	8.61556	0.00000	1.25279	0.00000	9.58389	0.00000
Inverse Distance Weighted – Default	0.38833	0.00000	0.70634	0.00000	4.31279	0.00000	0.39443	0.00000	8.61556	0.00000	1.25279	0.00000	9.58389	0.00000
Simple Kriging – Default	0.37503	0.00668	0.65265	0.00919	3.96681	-0.02673	0.36416	0.00651	**7.87438**	0.10365	1.15417	0.02567	8.86481	-0.13253
Global Polynomial Interpolation – Third order	0.37299	0.00002	0.67532	0.00007	4.11955	0.00029	0.37711	0.00004	8.23039	0.00066	1.19815	-0.00025	9.21398	-0.00057
Kernel (Local Polynomial Interpolation)	0.36993	0.00751	0.66294	-0.01139	4.04559	-0.01352	0.37018	-0.00629	8.07800	-0.00899	1.17784	0.00830	9.04910	0.09793
Empirical Bayesian	0.38833	0.00000	0.70634	0.00000	4.31279	0.00000	0.39443	0.00000	8.61556	0.00000	1.25279	0.00000	9.58389	0.00000

Kriging – Default														
Simple Kriging – Trend and transformation	0.36877	-0.00539	0.65769	0.02556	3.99621	-0.06077	0.36713	0.01060	7.97869	0.21052	1.16671	0.03023	8.96623	0.21883
Empirical Bayesian Kriging – Advanced	0.36850	0.01554	0.66932	0.07600	**3.95395**	0.06313	0.37346	0.03038	7.91331	0.41442	1.15447	-0.00826	8.94164	-0.43145
Ordinary Kriging – Optimized	0.37383	0.01752	0.67946	-0.01007	4.16955	-0.20150	0.37942	-0.00543	8.30816	-0.77938	1.21378	0.10919	9.26311	-0.58006
Ordinary Kriging – Default	0.37419	0.01610	0.68043	-0.01932	4.16955	-0.20150	0.37994	-0.01050	8.30816	-0.77938	1.21378	0.10919	9.26354	-0.57031
Universal Kriging – Optimized	0.39513	0.00407	0.72338	0.03318	4.46958	0.08133	0.40397	0.01904	8.71592	-0.12613	1.27897	0.01056	9.63265	-0.08465
Universal Kriging – Default	0.39513	0.00407	0.72326	0.03118	4.47018	0.07428	0.40397	0.01904	8.71592	-0.12613	1.28679	0.03514	9.66442	-0.02252

Figure A3. Visualisation of RMSE (columns) and ME (lines) for various GIS spatial interpolation methods (SK – Simple Kriging, OK – Ordinary Kriging, UK – Universal Kriging, EBK – Empirical Bayesian Kriging, LPI – Local Polynomial Interpolation, IDW – Inverse Distance Weighted,

GPI – Global Polynomial Interpolation) across different parameters: (A) Chl-a, (B) electrical conductivity, (C) turbidity, (D) salinity, (E) water temperature, (F) dissolved oxygen, and (G) oxygen saturation.

Table A17. Comparison of interpolation methods ranked by RMSE and ME accuracy measures.

Interpolation Method	Average Rank	Highest Accuracy Rank (RMSE)	Lowest Bias Rank (ME)
Simple Kriging – Trend	4.3	3.6	5.0
Global Polynomial Interpolation – Second order	5.4	5.9	4.9
Simple Kriging – Optimized	5.7	2.4	9.0
Inverse Distance Weighted – Optimized	6.0	11.0	1.0
Inverse Distance Weighted – Default	6.0	11.0	1.0
Simple Kriging – Default	6.4	3.1	9.6
Global Polynomial Interpolation – Third order	6.4	7.7	5.1
Kernel (Local Polynomial Interpolation)	7.2	5.6	8.9
Empirical Bayesian Kriging – Default	7.3	11.6	3.0
Simple Kriging – Trend and transformation	7.9	4.6	11.3
Empirical Bayesian Kriging – Advanced	8.1	3.7	12.4
Ordinary Kriging – Optimized	10.6	8.7	12.6
Ordinary Kriging – Default	11.2	9.3	13.1
Universal Kriging – Optimized	12.4	14.1	10.7
Universal Kriging – Default	12.6	14.6	10.7

Appendix 3

SIGMaL: An Integrated Framework for Water Quality Monitoring in a Coastal Shallow Lake

The WQI applied in this study was originally developed and fully described by Batina and Šiljeg (2025) [26]. For the purpose of methodological transparency and self-description, this appendix presents a concise summary of the WQI formulation, including the criteria set, weighting approach, aggregation method, and validation framework. The complete methodological details and extended analyses are available in the original reference.

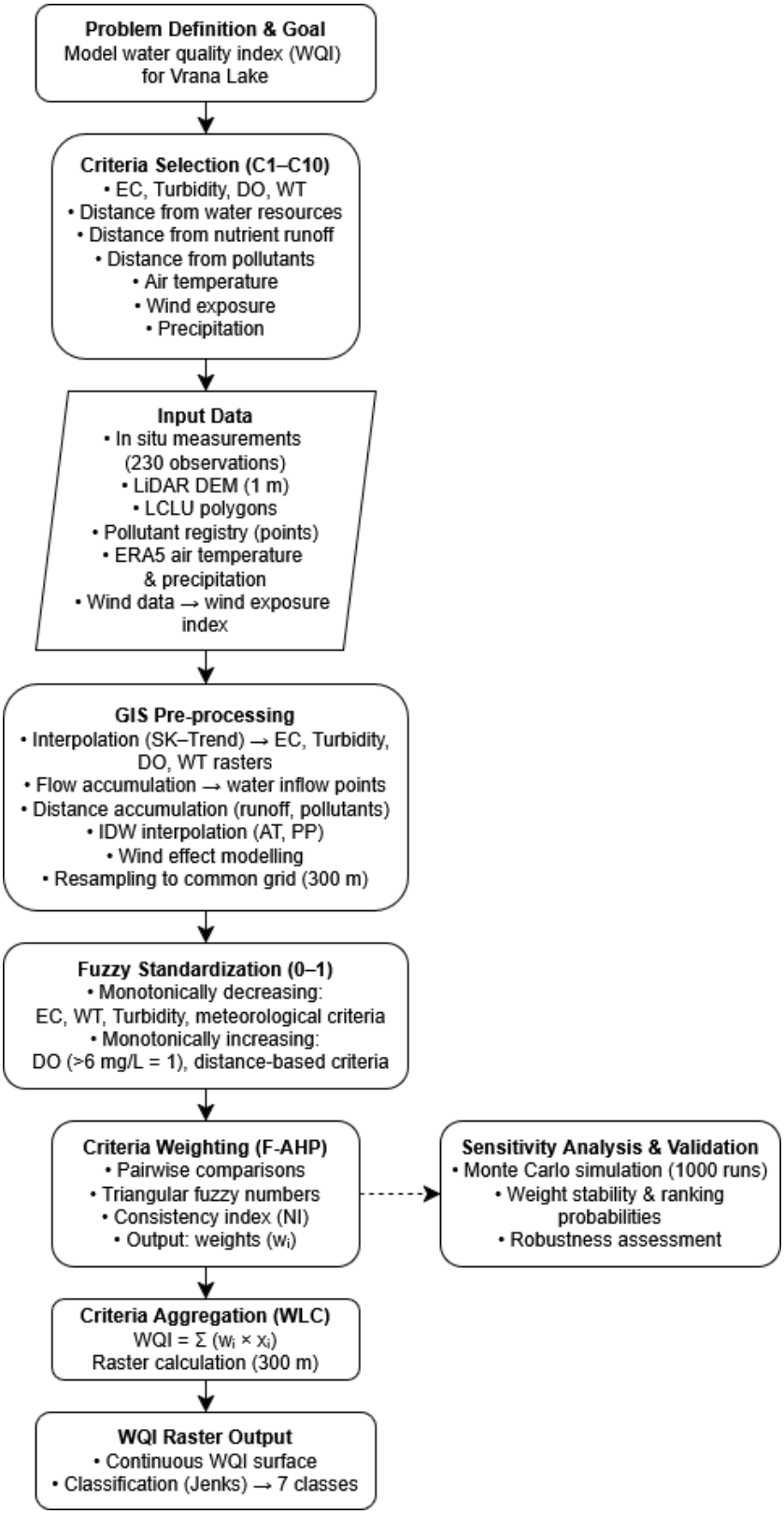

Figure A4. Workflow of the GIS–MCDA-based WQI model, showing criteria selection, spatial data preparation, fuzzy standardization, F-AHP weighting, WLC aggregation, and sensitivity analysis.

List of Figures

Figure 2.1. Number of publications retrieved from Elsevier Scopus on the search topic "(remote sensing) lake water quality" 13
Figure 2.2. A map showing the literature count per country of origin based on the bibliometric analysis 14
Figure 2.3. Schematic overview of the path of electromagnetic spectrum from the sun to a waterbody and a sensor 19
Figure 2.4. Workflow proposal for monitoring and assessment of water quality parameters in lakes using remote sensing methods 38
Figure 3.1. An overview of (a) Vrana Lake position and in situ stations, (b) preparation for measuring vertical profiles, and (c) and (d) in situ monitoring 45
Figure 3.2. Comparison of AT, PP, and WL data for the research period of 2023/24 against historical averages 46
Figure 3.3. Flowchart illustrating the study's methodology 47
Figure 3.4. Annual average and trends of AT, PP, and WL during 1990-2023 52
Figure 3.5. Median values of water quality parameters from the dataset (Chl-a, EC, turbidity, salinity, WT, DO, SO) 55
Figure 3.6. Spearman's coefficient of determination between: (a) WL, meteorological (AT, WS, RH, AP, PP, SH), and water quality parameters (Chl-a, EC, turbidity, salinity, WT, DO, SO) and (b) in-between water quality parameters (Chl-a, EC, turbidity, salinity, WT, DO, SO) ..56
Figure 3.7. SK – Trend interpolation showing parameter distributions: (a) Chl-a, (b) EC, (c) turbidity, (d) salinity, (e) WT, (f) DO, and (g) SO 57
Figure 4.1. Overview of Vrana Lake's geospatial features and in situ monitoring stations 66
Figure 4.2. Maps of (a) stream lengths and environmental pollutants, (b) total nitrogen export capacity of land, and (c) wind rose 73
Figure 4.3. Maps of standardized criteria and the aggregation per cluster. *Abbreviations alphabetically: AT – Air temperature, C1 – Electrical conductivity criterion, C2 – Turbidity criterion, C3 – Dissolved oxygen criterion, C4 – Water temperature criterion, C5 – Distance from water resource criterion, C6 – Distance from land nutrient runoff criterion, C7 – Distance from environmental pollutants criterion, C8 – Air temperature criterion, C9 - Wind criterion, C10 – Precipitation criterion, Dist. – Distance, PP – Precipitation, Turb. – Turbidity 79

Figure 4.4. Aggregation of the final water quality map using weighted linear combination of all criteria (green colour represents higher water quality, while yellow and light orange represent lower water quality) 83
Figure 4.5. Histograms of normalized weights for each criterion based on 1000 Monte Carlo simulations 84
Figure 4.6. Violin plot of rank distributions based on 1000 Monte Carlo simulations 85
Figure 4.7. Map showing water quality regions, along with the locations of existing in situ stations and optimized monitoring stations 86
Figure 4.8. Allocation of monitoring stations per water quality class of (a) existing 20 in situ stations and (b) optimized 7 stations 87
Figure 5.1. Vrana Lake with monitoring stations and main hydrological features 95
Figure 5.2. Calibration of the YSI EXO2 multiparameter probes 97
Figure 5.3. Water quality raster of Vrana Lake derived from MCDA and its use for dataset densification. (a) Continuous raster surface classified into seven WQI classes. (b) Discretized raster with 318 extracted samples shown together with 20 in situ monitoring stations 101
Figure 5.4. Integrated SIGMaL workflow combining in situ data, GIS-MCDA, satellite imagery, and ML for WQI prediction 107
Figure 5.5. Confusion matrices showing WQI classification performance for Sentinel-2 spectral and temporal models 113
Figure 5.6. Training and validation accuracy and loss curves for the Sentinel-2 CNN spectral and temporal models 114
Figure 5.7. Confusion matrices showing WQI classification performance for Landsat 8–9 spectral and temporal models 115
Figure 5.8. Training and validation accuracy and loss curves for the Landsat 8–9 CNN spectral and temporal models 116
Figure 5.9. Confusion matrices showing WQI classification performance for PlanetScope spectral and temporal models 117
Figure 5.10. Training and validation accuracy and loss curves for the PlanetScope CNN spectral and temporal models 118
Figure 5.11. Predicted spatial distribution of WQI classes in Vrana Lake for the 12-month period following field measurements, based on CNN models using Sentinel-2, Landsat 8–9, and PlanetScope imagery under spectral and temporal modelling scenarios 119

Figure A1. Vertical profiles of average parameter values measured every 30 minutes in March and July. 188
Figure A2. Temporal variation of median parameter values measured every 30 minutes in March and July. 190
Figure A3. Visualisation of RMSE (columns) and ME (lines) for various GIS spatial interpolation methods (SK – Simple Kriging, OK – Ordinary Kriging, UK – Universal Kriging, EBK – Empirical Bayesian Kriging, LPI – Local Polynomial Interpolation, IDW – Inverse Distance Weighted, GPI – Global Polynomial Interpolation) across different parameters: (A) Chl-a, (B) electrical conductivity, (C) turbidity, (D) salinity, (E) water temperature, (F) dissolved oxygen, and (G) oxygen saturation. 193
Figure A4. Workflow of the GIS–MCDA-based WQI model, showing criteria selection, spatial data preparation, fuzzy standardization, F-AHP weighting, WLC aggregation, and sensitivity analysis. 196

List of Tables

Table 2.1. WFD lakes typology [51,52] 15
Table 2.2. Overview of satellite and airborne sensors commonly used in aquatic environments 30
Table 3.1. Summary of the dataset and probe specifications 48
Table 3.2. List of GIS interpolation methods 50
Table 4.1. Summary of GIS-MCDA criteria with corresponding codes, formats, spatial resolutions, data sources, and membership functions 68
Table 4.2. F-AHP matrix using triangular fuzzy elements 81
Table 4.3. Criteria weighting and consistency 82
Table 4.4. Summary of mean ranks, standard deviations, and probabilities for the criteria based on 1000 Monte Carlo simulations 85
Table 5.1. Comparison of Sentinel-2 MSI, Landsat 8–9 OLI/TIRS, and PlanetScope sensor specifications 99
Table 5.2. Overview of dates of in situ measurements, corresponding satellite acquisitions, temporal offsets, and number of measured stations 100
Table 5.3. Benchmark results of regression models for each target variable for Sentinel-2 . 108
Table 5.4. Benchmark results of regression models for each target variable for Landsat 8–9 109
Table 5.5. Benchmark results of regression models for each target variable for PlanetScope 110
Table 5.6. Performance of ML models for WQI classification across satellite sensors, based on spectral and temporal analyses 112

Table A1. Selected remotely measurements of chl-a using various sensors and spectral bands, band combinations, and band equations (R in band combinations represents the reflectance at a certain wavelength). 169
Table A2. Sensor data for various waterbodies including waterbody type, country, study area, mean depth, study duration, method for retrieval of chl-a based on satellite imagery, range of measured chl-a values (minimum and maximum), and a correlation coefficient (R^2) between satellite imagery and chl-a in situ values. 171

Table A3. Selected remotely measurements of turbidity using various sensors and spectral bands, band combinations, and band equations (R in band combinations represents the reflectance at a certain wavelength). 174
Table A4. Sensor data for various waterbodies including waterbody type, country, study area, mean depth, study duration, method for retrieval of turbidity based on satellite imagery, range of measured turbidity values (minimum and maximum), and a correlation coefficient (R^2) between satellite imagery and turbidity in situ values. 175
Table A5. Selected remotely measurements of SDD using various sensors and spectral bands, band combinations, and band equations (R in band combinations represents the reflectance at a certain wavelength). 176
Table A6. Sensor data for various waterbodies including waterbody type, country, study area, mean depth, study duration, method for retrieval of SDD based on satellite imagery, range of measured SDD values (minimum and maximum), and a correlation coefficient (R^2) between satellite imagery and SDD in situ values. 177
Table A7. Selected remotely measurements of WT using various sensors and spectral bands, band combinations, and band equations. 179
Table A8. Sensor data for various waterbodies including waterbody type, country, study area, mean depth, study duration, method for retrieval of WT based on satellite imagery, range of measured WT values (minimum and maximum), and a correlation coefficient (R^2) between satellite imagery and WT in situ values. 179
Table A9. Selected remotely measurements of salinity using various sensors and spectral bands, band combinations, and band equations. 180
Table A10. Sensor data for various waterbodies including waterbody type, country, study area, mean depth, study duration, method for retrieval of salinity based on satellite imagery, range of measured salinity values (minimum and maximum), and a correlation coefficient (R^2) between satellite imagery and salinity in situ values. 181
Table A11. Selected remotely measurements of EC using various sensors and spectral bands, band combinations, and band equations. 181
Table A12. Sensor data for various waterbodies including waterbody type, country, study area, mean depth, study duration, method for retrieval of EC based on satellite imagery, range of measured EC values (minimum and maximum), and a correlation coefficient (R^2) between satellite imagery and EC in situ values. 182
Table A13. Historical meteorological and water level data for Vrana Lake from 1990 to 2023. 183

Table A14. Meteorological and water level data for Vrana Lake for research period. 184
Table A15. A list of sampling stations and statistical values (mean, minimum, maximum, median, and a range of values) for measured parameters using YSI EXO2 probe. 185
Table A16. Comparison of interpolation methods using RMSE and ME as accuracy measures for each parameter.....191
Table A17. Comparison of interpolation methods ranked by RMSE and ME accuracy measures.....194

CV

Anja Batina was born on August 23, 1991, in Split, Croatia. She completed her primary and secondary education in Split. She enrolled at the Faculty of Geodesy, University of Zagreb, where she completed both the Bachelor's and Master's studies in the field of geodesy and geoinformatics, graduating in 2015 with the academic title of Master of Engineering in Geodesy and Geoinformatics.

Following her graduation, she began her professional career as a GIS specialist at the company Prehnit Ltd., where she worked on projects related to geospatial analysis, environmental monitoring, and spatial data management. In 2018, she was appointed Technical Director of the GIS Department, a position she held until 2023, with responsibilities including project management, consulting, education, and the development of geospatial solutions.

In 2018, she enrolled in the doctoral study programme in the field of geodesy and geoinformatics at the Faculty of Geodesy, University of Zagreb. Since 2024, she has been employed as a research assistant at the Center for Geospatial Technologies, University of Zadar, where she participates in international and interdisciplinary research activities, including the SMART-Water project.

Her doctoral research focuses on the development of a geospatial multi-sensor approach for lake water quality monitoring and assessment. As part of her doctoral work, she has authored and co-authored several scientific papers published in international journals and conference proceedings and has presented her research at international scientific conferences. She is fluent in Croatian and English and has basic knowledge of the German language.

List of Papers Published in Scientific Journals

1. Batina, Anja; Šiljeg, Ante; Krtalić, Andrija; Šerić, Ljiljana. SIGMaL: An Integrated Framework for Water Quality Monitoring in a Coastal Shallow Lake // Remote sensing, 18 (2026), 2; 312, 29. doi: 10.3390/rs18020312
2. Batina, Anja; Šiljeg, Ante. Enhancing water quality monitoring in a coastal shallow lake using GIS and multi-criteria decision analysis // Environmental and sustainability indicators, 28 (2025), 100881, 14. doi: 10.1016/j.indic.2025.100881
3. Batina, Anja; Šiljeg, Ante; Pedić, Gloria; Parać, Marija. Utilizing Sentinel-2 Remote Sensing for Water Quality Monitoring in Deran Lake, Bosnia and Herzegovina // The international archives of the photogrammetry, remote sensing and spatial information sciences, XLVIII-4/W13-202, 2025. str. 65-72. doi: 10.5194/isprs-archives-xlviii-4-w13-2025-65-2025
4. Batina, Anja; Cukrov, Neven; Ćuže Denona, Maja. Spatiotemporal water quality analysis of Vrana Lake, Croatia // Open Geosciences, 17 (2025), 1; -, 15. doi: 10.1515/geo-2025-0817
5. Batina, Anja; Krtalić, Andrija. Integrating Remote Sensing Methods for Monitoring Lake Water Quality: A Comprehensive Review // Hydrology, 11 (2024), 7; 92, 28. doi: 10.3390/hydrology11070092

List of Papers Published in Scientific Conference Proceedings

1. Butorac, Ksenija; Maurer, Dubravka; Batina, Anja. Geographic Profiling – Environmental and Offenders' Behavior Patterns of Robbery Characteristics // Investigating and Proving Contemporary Forms of Crime: Scientific Approaches / Simović, Darko; Gnjatović, Milan; Spasić, Danijela et al. (ur.). Beograd: University of Criminal Investigation and Police Studies, 2025. str. 459-475
2. Batina, Anja; Roland, Vlatko; Tasić, Dragan. Digitalizacija podataka, modeliranje terena i 3D vizualizacija objekata za potrebe planiranja pametnog grada // Prvih 600

godina Metkovića (1422. - 2022), 2. dio / Gluščević, Smiljan; Vekić, Denis (ur.). Metković: Sveučilište u Zadru; Grad Metković; Sveučilište u Dubrovniku, 2024. str. 477-487

3. Batina, Anja. Data Cubes – A Modern Approach for Handling Earth Observation Data // 2023 International Conference on Earth Observation and Geo-Spatial Information (ICEOGI) / Radja, Kheddam (ur.). Piscataway (NJ): Institute of Electrical and Electronics Engineers (IEEE), 2023. str. 1-6. doi: 10.1109/iceogi57454.2023.10292958
4. Roland, Vlatko; Šiljeg, Ante; Batina, Anja. Obrada LiDAR podataka i stvaranje GIS baze pomoću Ortosky alata na primjeru Skradinskog buka // Zbornik radova Vizija i izazovi upravljanja zaštićenim područjima prirode u Republici Hrvatskoj - Aktivna zaštita i održivo upravljanje u Nacionalnom parku "Krka". Šibenik, 2017. str. 978-993